Optimising Translational Aspects of Physiologically-based Pharmacokinetic Modelling and Simulation to Aid Precision Dosing in Liver Cirrhosis

A thesis submitted to the University of Manchester for the degree of Doctor of Philosophy
in the Faculty of Biology, Medicine and Health

2021

EMAN M. EL-KHATEEB

School of Health Sciences
Division of Pharmacy & Optometry

Contents

Word Count: 50,489

List of figures

List of tables

Abbreviations and Acronyms

%	**Percent**
ABC	Adenosine triphosphate-binding cassette
ADH	Alcohol Dehydrogenases
ADME	Absorption, Distribution, Metabolism, and Excretion
ALDH	Aldehyde Dehydrogenase
AOX	Aldehyde Oxidase
ATP1A1	Sodium/Potassium-Transporting ATPase
AUC	Area Under the Plasma Concentration Time Curve
AUCR	Ratio of AUC in Diseased Population to AUC in Healthy Population
BCA	Bicinchoninic Acid
BCRP	Breast Cancer Resistant Protein
BSEP	Bile Salt Export Pump
CES	Carboxyestrase
CI	Confidence Interval
CL	Clearance
C_{max}	Maximum Concentration
CP	Child-Pugh Score
CPPGL	Cytosolic Protein Per Gram Liver
CV	Coefficient of Variation
CYP	Cytochrome P450
DDI	Drug-Drug Interaction
DDT	Dithiothreitol
DME&T or DMET	Drug-Metabolising Enzymes and Drug Transporters
DMEs	Drug-Metabolising Enzymes
EMA	European Medicine Agency
EPHX	Epoxide Hydrolase
ER	Extraction Ratio
FA	Formic Acid
FASP	Filter Aided Sample Preparation
FDA	US food and Drug Administration

FMO	Flavin-containing Monooxygenase
g	Gram
g	Gravity
GUI	Graphical User Interface
HI	Hepatic Impairment
Hi3	High Three Ion Intensity Approach
HLM	Human Liver Microsomes
HomPPGL	Homogenate Protein Per Gram Liver
iBAQ	Intensity-Based Absolute Quantification
IVIVE	In Vitro-in Vivo Extrapolation
kDa	Kilo Dalton
Kp	Partition Coefficient
LC-MS	Liquid chromatography – Mass spectrometry
LysC	Lysine C
M&S	Modelling and Simulations
m/z	Mass to Charge Ratio
MATE	Multidrug and Toxin Extrusion
MCT	Monocarboxylate Transporter
MDR	Multidrug Resistance Protein
MetCAT	Metabolic Enzymes QconCAT (CYP450 and UGTs)
MGST	Microsomal Glutathione S-transferase
min	Minute
MPPGL	Microsomal Protein Per Gram Liver
MRP	Multidrug Resistance Like Protein
NAFLD	Non-alcoholic Fatty Liver Disease
NAT	N-acetyltransferase
NNOP	Non-naturally Occurring Peptide
NTCP	Sodium Taurocholate- Co-transporting Polypeptide
NuncCAT	Non-UGT Non-CYP Metabolic Enzymes QconCAT
OAT	Organic Anion Transporter
OATP	Organic Anion Transporting Polypeptide
OCT	Organic Cation Transporter

OST	Oligosaccharyltransferase
PBC	primary Biliary Cholangitis
PBPK	Physiologically-Based Pharmacokinetics
P-gp	P-glycoprotein
PK	Pharmacokinetics
pmol	Picomoles
PSC	primary Sclerosing cholangitis
QC	Quality Control
QconCAT	Concatenated Peptides for Protein Quantification
rpm	Revolutions Per Minute
SD	Standard Deviation
SLC	Solute Carrier Family
SLCO	Sloute Carrier Organic Anion Transporter Family
SULT	Sulfotransferase
TFA	Triflouroacetic Acid
TPA	Total Protein Approach
TPMT	Thiopurine Methyltransferase
TransCAT	Transporters QconCAT
UGT	Uridine 5′-Diphospho-Glucuronosyltransferase
µM	Micro-molar

Amino Acid Abbreviations

Amino Acid	Abbreviation	
	Three Letters	One Letter
Alanine	Ala	A
Arginine	Arg	R
Asparagine	Asn	N
Aspartic Acid	Asp	D
Cysteine	Cys	C
Glutamic Acid	Glu	E
Glutamine	Gln	Q
Glycine	T	G
Histidine	His	H
Isoleucine	Ile	I
Leucine	Leu	L
Lysine	Lys	K
Methionine	Met	M
Phenylalanine	Phe	F
Proline	Pro	P
Serine	Ser	S
Threonine	Thr	T
Tryptophan	Trp	W
Tyrosine	Tyr	Y
Valine	Val	V

Abstract

Background: Cirrhosis is a chronic illness that reduces liver functions including drug metabolism. Many drugs that are available in the market lack dosage guidance for hepatic impairment patients. Including those patients in the early phases of clinical trials can be risky if safe doses were not used. Whilst precision medicine is not a new concept, optimising *in silico* modelling such as physiologically-based pharmacokinetic (PBPK) modelling and simulation (M&S), can assist in informing drug labelling. This area is quickly growing over the last years, especially for special patient populations. ***Methods***: Literature reviews were performed to understand the current situation with drug dosing in hepatic impairment, the quality of current PBPK models, and identify the gaps. Experimentally, scaling factors for converting clearance data from *in vitro* to *in vivo* in cirrhosis were determined. LC-MS/MS-based targeted proteomics were implemented to quantify the abundances of 51 drug-metabolising enzymes and transporters (DME&T) in 32 liver samples from cirrhosis patients at different degrees of disease severity compared to 14 normal control samples. ***Results***: Microsomal and cytosolic protein contents decreased in cirrhosis relative to control samples and varied according to associated liver pathologies. Disease perturbation factor (DPF) reconciled differences in absolute abundances between various proteomic data analysis methods. Specifically designed heavy-labelled concatenated unique peptides from target proteins showed good performances as internal standards with the samples. Abundances of most DME&T per gram liver were lower by 30-50% in mild, 40-70% in moderate, and 50-98% in severe cirrhosis groups compared to controls. DPF, used as a scalar for protein abundances in PBPK models for repaglinide, dabigatran etexilate, and zidovudine, helped to enhance models' predictive performance. ***Conclusion:*** This thesis, to our knowledge, provides the first comprehensive quantification of relevant DME&T in all stages of liver cirrhosis. This helps the development of existing *in silico*

cirrhosis models to inform drug labelling and recommends dose adjustments in scenarios that have not been studied clinically.

Declaration

No portion of the work referred to in the thesis has been submitted in support of an application for another degree of qualification of this or any other university or other institute of learning.

Copyright statement

Dedication

To Mum, Dad, and My Lovely Daughter Sara!

Acknowledgments

First and foremost, I would like to praise and thank God, the almighty, who has granted patience, knowledge, power, and countless blessings to me, so that I have been finally able to accomplish the thesis.

The funding for this PhD project came from the Egyptian missions sector of the Egyptian government, to whom I am very grateful.

During the course of this project, I have had the great pleasure of working alongside a dedicated and enthusiastic team of researchers within the Centre for Applied Pharmacokinetics Research (CAPKR). Of these, I would like to express my foremost appreciation to my supervisors, Professor Amin Rostami-Hodjegan, Dr Jill Barber, and Dr Adam Darwich and research collaborators Dr Varinder Athwal and Dr Venkatesh Pilla Reddy for their invaluable insights, expertise, and support. Thank you for the opportunity to complete a PhD at the University of Manchester. I am also grateful to Dr Brahim Achour, Dr Zubida Al-Majdoub, and Dr Daniel Scotcher for their support and guidance throughout my PhD on many different aspects of the project, from method optimisation to data analysis and everything in-between.

I would like to thank Cambridge University Tissue Bank for providing the invaluable liver samples that made this project possible.

Thank you to the team in the Biological Mass Spectrometry Core Research Facility, University of Manchester; Stacey Warwood, Emma-Jayne Keevill, Jullian Selley, and David Knight, for the use of vital equipment and software.

Thank you to my colleagues, lab mates, and friends Areti Maria Vasilogianni and Sarah Alrubia for a cherished time spent together in the lab, and in social settings from the start of this PhD.

Last but not least, I would like to thank my family and friends for their endless love, encouragement, and support. You have all shaped who I am today; I could not have done this without you!

In this thesis the journal format (Formerly known as the alternative format) was used. This format was chosen as the core elements of the work formed nine separate but linked chapters. Apart from the "General Introduction", "Aims and Objectives", and the "General Discussion" chapters, this format allows the incorporation of six other chapters that have already been published (2 chapters), submitted (2 chapters), or to be considered for publication (2 chapters) in peer-reviewed journals. Another two articles that I have managed to publish during my PhD are summarised and cited in the "General Introduction" and the "General Discussion" chapters as they have some elements related to PBPK modelling and drug dosing in hepatic impairment populations. This format also maximised the research output in the form of publications over the course of the study.

A declaration at the start of each chapter highlights the contribution of each author. The thesis, in general, aims to apply proteomic lab-based data using human liver tissue along with *in silico* modelling and simulations of drug pharmacokinetics to aid precision dosing in hepatic impairment populations. Each chapter has its own "References" and "Supplementary Material" sections. References cited in the Supplementary Material section are included in the same bibliography of its relevant chapter.

The chapters were not ordered according to publication dates (for already published or submitted parts), but according to the flow of the whole story in a more logical order.

The first chapter represents a general introduction setting the scene and giving the background to the research and identifies knowledge gaps. It also shows the trends in physiologically-based pharmacokinetic (PBPK) models over the last two decades and how research on disease population models are growing according to a recent survey that I have published in the Journal of *Biopharmaceutics and Drug Disposition*.

The second chapter illustrates the aims and objectives of the whole thesis.

In the third chapter, I tried to address the need for predicting drug clearance and its exposure levels as well as identifying the optimum dose for special populations, specifically for hepatic impairment patients. It also identifies the obstacles with the current classification system, the gaps in the current PBPK models, and methods proposed to fill in these gaps.

Chapter four represents the experimentally-defined, cirrhosis-specific scaling factors required for the extrapolation from microsomal or cytosolic *in vitro* systems to liver tissue before being included in PBPK models. These scalars can help in predicting drug clearance and selection of dosage regimens for cirrhosis populations. Attempts to consider potential changes have been empirical and ignored the potential impact of the disease cause. We obtained experimental values for these scalars for the first time and assessed their impact on predicted exposure to various substrate drugs using physiologically-based pharmacokinetic simulations. This chapter has been published in the Drug Metabolism and Disposition Journal.

To fill in the gap related to the abundances of drug-metabolising enzymes and drug transporters (DME&T) in cirrhosis, a review on different LC-MS proteomic methods and their applications in drug development has been published in the Journal of Pharmacology and Therapeutics and represents the **fifth chapter** of this thesis.

For the experimental investigation of the use of proteomics in determining the abundance of DME&T in diseased and control samples, I have designed a novel and specific standard protein for the quantification of the most important non-CYP, non-UGT metabolising enzymes. This QconCAT, along with the previously designed QconCATs (MetCAT and TransCAT), covers most of the proteins that play a key role in drug metabolism. The design and quality control checks of this new standard are described in the sixth paper (**Chapter Six**).

Chapter Seven is related to the experimental design and the choice of the best quantification method and how differences among all methods can be reconciled using a set of control

samples as a proof-of-concept. Cirrhosis pooled samples were used to verify the utility of disease perturbation factor as a scalar for proteomic data instead of the absolute abundance levels.

Method optimisations and proteomic tools discussed in the previous two chapters were invested in the next chapter **(Chapter Eight)** which covers the absolute abundances of different DME&T in individual human liver microsomal samples from cirrhosis patients and how these proteomic data can be applied into PBPK models to achieve better predictions of drug exposure.

Chapter Nine is a general discussion and conclusions chapter that summarises the overall findings of the research, how the data generated can optimise future PBPK models, and how these models should be applied in drug development. An example to this urgent application was in COVID crisis where verified PBPK models of different promising drugs were used to substitute the "guess work" in scenarios were clinical data are not available as in organ impairment populations. I participated in the latter research in collaboration with AstraZeneca® and Certara ® with a paper published in the *British Journal of Clinical Pharmacology.* Moreover, it highlights the future outlook and areas that require more investigations.

1 Chapter One

General Introduction

Declaration

This chapter illustrates the current situation in dosing of patients with hepatic impairment, the current strategies in drug development, and the need for evidence-based approaches in the absence of clinically-based drug labelling. It also explains the trends in PBPK modelling and simulation applications over the last two decades and the increased interest in using these tools for drug dosing in hepatic impairment. Moreover, it identifies the current gaps in this area and how this thesis can help to fill in these gaps.

1.1. Current strategy for drug development

In drug development, new molecular entities pass through pre-clinical followed by three phases of clinical trials to assess drug efficacy and safety in both healthy volunteers and patients who are diseased with the disease for which this drug was designed (Umscheid, et al., 2011). The enrolment of patients in these clinical trials is based on a list of inclusion criteria and usually a longer list of exclusion criteria that in most cases include organ impaired patients such as hepatic and renal impairment. This is mainly to avoid the risk of inappropriate dosing in those patients (Duma, et al., 2019). However, it is also recommended to have dedicated studies later on for these special patient populations in order to assess the change in drug exposure in those patients (FDA, 2016). However, most of the drugs that have been approved in 2013 and 2014 lack clinically-based information on dosing of special disease populations in their labels (Jadhav, et al., 2015). In this project we have followed the same survey criteria (In Chapter 3) and realised that this situation is still the same for at least hepatic impairment populations. Therefore, those patients will be treated with these drugs without appropriate dosage guidance in their label which might expose them to the risk of toxicity or drug ineffectiveness if the dose was outside the therapeutic range.

1.2. Physiologically based Pharmacokinetic modelling and simulations in human

Over the last 2 decades mathematical and computational modelling progressed massively in the form of what is called “Physiologically Based Pharmacokinetic Modelling and Simulations” or “PBPK M&S”. This approach implements system (drug independent parameters) that divides the human body into different organs each has its own distribution, blood flow, and other pharmacokinetic related characteristics. These parameters are combined with drug-specific parameters (physicochemical properties of the drug, protein binding, elimination pathways, etc) and study design parameters (route of administration, dose and

dosing regimen, proportion of female to male subjects, etc) to predict the drug exposure in human. Most of these system or physiological parameters are affected by intrinsic factors (including the disease condition such as hepatic impairment) and extrinsic factors (alcohol, diet, polypharmacy, smoking, etc). Therefore, these modelling approaches seem to be promising in replacing the guess work or what is called "*in cerebro*" dosing with more evidence-based "*in silico*" dosing in scenarios where clinical data are scarce or lacking. There is no doubt that to achieve this purpose, these models have to be robust and verified with the currently available clinical data for this specific drug and the population under investigation.

1.3. Development of PBPK M&S tools and applications over the years

More interest was paid to PBPK models in the last decade as evident from the growth rate in PBPK M&S publications which was massively higher in the last decade compared to the previous decade (43 fold). Whereas, the increase in publications for the overall science and general pharmacokinetic studies was nearly three folds over the last two decades (El-Khateeb, et al., 2020). PBPK M&S include many applications such as clinical study design, formulation impact on drug exposure, metabolic drug-drug interactions (DDIs), changes in exposures in special populations such as disease (e.g. Hepatic, renal impairments), paediatrics, pregnancy, and geriatrics.

According to a recent update by the FDA that highlights the application of PBPK models included in regulatory submissions, some areas such as metabolic DDIs were highly mature and showed high level of confidence, while for organ impairment populations, there is still a limited experience and a low confidence of using these model to predict the drug in these populations (Grimstein, et al., 2019). Interestingly, the highest increase in studies, by academia, industry, and regulatory agencies, collectively over the last decade according to a recent publication, was in the area of special populations (mainly disease populations of more than 8

fold increase). This indicates the growing interest in this area and the urgent need to develop robust and reliable PBPK models for those populations (El-Khateeb, et al., 2020). Hepatic impairment is especially well represented in the study of special populations. Although hepatic impairment can arise from several diseases, cirrhosis is a major player. This is predicted to be reflected in the future as a higher number of new drug submissions to the regulators using PBPK models in organ impairment.

PBPK M&S tools are used by academia, pharmaceutical industry as well as regulatory authorities. Some of them are commercial tools and others are free, however based on the same publication analysis, graphical user-interface based tools (Simcyp, Gastroplus, and PKsim) were the most commonly used by all organisations relative to bespoke software or scripting tools. Therefore, throughout this thesis, I applied the generated experimental and optimised data to Simcyp® software, but of course, it can be implemented into other PBPK models irrespective of the used tool.

Cirrhosis population library have been generated based on previous publications (Edginton & Willmann, 2008; Johnson, et al., 2010) and classified virtual patients according to Child-Pugh scoring system. Although many drug models have illustrated that the current set-up and parameters in those population libraries were useful to predict drug exposure within 2 fold range of the observed clinical data, some other situations did not show good predictions. According to a recent publication from the QI consortium using Simcyp simulator to predict the exposure of nearly 60 drugs in cirrhosis populations, 30% of the simulated scenarios were outside the 2-fold range (Heimbach, et al., 2020). Moreover, most of these investigated drugs were of low hepatic extraction ratio and therefore the degree of changes in the expression of metabolising enzymes and drug transporters (DME&T) might need to be revisited.

1.4. Current gaps in cirrhosis populations PBPK models

Predicted exposure profiles using PBPK models in cirrhosis are showing over-estimation of the disease impact on the drug clearance for some drugs especially in the moderate and severe stage of cirrhosis. Therefore parameters related intrinsic clearance predictions such as *in vitro-in vivo* scaling factors and the changes in DME&T expressions have to be disease-specific, accurately determined and updated with the gold standard techniques in the field.

The changes in the expression of many enzymes did not use the current gold standard protein quantification method such as LC-MS/MS and rely either on immunoblotting, immune-histochemical analysis and correcting the available *in vitro* and *in vivo* activity studies for only a limited number of target proteins. Many other non-CYP enzymes have not been implemented into the models because of the lack of sufficient data in all stages of cirrhosis disease severity.

1.5. References

Duma, N, Kothadia, SM, Azam, TU, Yadav, S, Paludo, J, Vera Aguilera, J, Gonzalez Velez, M, Halfdanarson, TR, Molina, JR, Hubbard, JM, Go, RS, Mansfield, AS, and Adjei, AA. (2019). Characterization of Comorbidities Limiting the Recruitment of Patients in Early Phase Clinical Trials. *Oncologist*, 24(1), 96–102.

Edginton, AN, and Willmann, S. (2008). Physiology-based simulations of a pathological condition: Prediction of pharmacokinetics in patients with liver cirrhosis. *Clin. Pharmacokinet.*, 47(11), 743–752.

El-Khateeb, E, Burkhill, S, Murby, S, Amirat, H, Rostami-Hodjegan, A, and Ahmad, A. (2020). Physiological-based pharmacokinetic modeling trends in pharmaceutical drug development over the last 20-years; In-depth analysis of applications, organizations, and platforms. *Biopharm. Drug Dispos.*, bdd.2257.

Grimstein, M, Yang, Y, Zhang, X, Grillo, J, Huang, S-M, Zineh, I, and Wang, Y. (2019). Physiologically Based Pharmacokinetic Modeling in Regulatory Science: An Update From the U.S. Food and Drug Administration's Office of Clinical Pharmacology. *J. Pharm. Sci.*, 108(1), 21–25.

Heimbach, T, Chen, Y, Chen, J, Dixit, V, Parrott, N, Peters, SA, Poggesi, I, Sharma, P, Snoeys, J, Shebley, M, Tai, G, Tse, S, Upreti, V V., Wang, Y, Tsai, A, Xia, B, Zheng, M, … Hall, S. (2020). Physiologically-Based Pharmacokinetic Modeling in Renal and Hepatic Impairment Populations: A Pharmaceutical Industry Perspective. *Clin. Pharmacol. Ther.*, cpt.2125.

Jadhav, PR, Cook, J, Sinha, V, Zhao, P, Rostami-Hodjegan, A, Sahasrabudhe, V, Stockbridge, N, and Powell, JR. (2015). A proposal for scientific framework enabling specific population drug dosing recommendations. *J. Clin. Pharmacol.*, 55(10), 1073–1078.

Johnson, TN, Boussery, K, Rowland-Yeo, K, Tucker, GT, and Rostami-Hodjegan, A. (2010). A semi-mechanistic model to predict the effects of liver cirrhosis on drug clearance. *Clin. Pharmacokinet.*, 49(3), 189–206.

Umscheid, CA, Margolis, DJ, and Grossman, CE. (2011). Key Concepts of Clinical Trials: A Narrative Review. *Postgrad. Med.*, 123(5), 194–204.

2 Chapter Two

Aims and Objectives

2.1. The ultimate aim

The overall aim of this thesis is to optimise and qualify the currently available physiologically-based pharmacokinetic (PBPK) models for the purpose of predicting the exposure and the most appropriate dose (Safe and at the same time effective) for liver cirrhosis patients. Part of this is thought to be achieved by revisiting and updating different translational aspects related to *in vitro in vivo* extrapolation before coupling these data with PBPK models in liver cirrhosis virtual populations.

Each subsequent chapter satisfies one or more of the following objectives related to the above mentioned overall aim.

2.2. Objectives

1- Identifying and criticising the current situation related to dosing and classification of adult liver cirrhosis patients, needs and the gaps in this area (Chapter 3).

2- Estimation of disease specific-scaling factors for extrapolating *in vitro* clearance data to *in vivo* to be fed into PBPK models (Chapter 4).

3- Understanding the experimental work flow and the differences among LC-MS proteomic methods as a gold standard tool for the quantification of biological proteins and its applications in drug development (Chapter 5).

4- Design and quality control assessment of new standard proteins to be used in the proteomic experiment for the quantification of various metabolising enzymes simultaneously in the same sample (Chapter 6).

5- Comparing the performance of different proteomic data analysis methods for the purpose of quantifying metabolising proteins in health and disease and ways to reconcile differences among these methods (Chapter 7).
6- Comprehensive absolute quantification of DME&T in liver samples from adult cirrhotic patients at different grades of disease severity and various disease aetiologies (chapter 8).
7- Applying the generated proteomic data into PBPK models for some drugs (Chapter 8).

3 Chapter Three

Time to Revisit Child-Pugh Score as the Basis for Predicting Drug Clearance in Hepatic Impairment

Declaration

This chapter constitutes an article submitted for publication to the Alimentary Pharmacology and Therapeutics Journal

El-Khateeb, E., Darwich, AS., Achour, B., Athwal, V., & Rostami-Hodjegan, A. (n.d). Time to revisit Child-Pugh score as the basis for predicting drug clearance in hepatic impairment. *Alimentary Pharmacology & Therapeutics*. Under review.

I carried out the literature search, collation of data and wrote the manuscript. Dr Brahim Achour reviewed and edited the section on Future Directions, Dr Adam Darwich, Dr Varinder Athwal and Prof Amin Rostami-Hodjegan edited the manuscript. I retained final editorial control

3.1. Abstract

Background

Prescription information for many available drugs, particularly at the time of entering the market, lacks dosage guidance for hepatic impairment (HI). Dedicated studies for assessing the fate of drugs in HI commonly use Child-Pugh (CP) score for stratifying patients. CP is a prognostic clinical score but it has many limitations in reflecting capacity to eliminate drugs.

Aims

To demonstrate the need for better drug-dosing approaches in HI, summarise the current status, identify knowledge gaps regarding parameters defining the changes in drug disposition in HI, propose solutions for predicting the impact of HI on drug exposure, and discuss barriers to improving dosing guidance in HI population.

Methods

Relevant reports on dosage adjustment in HI patients were reviewed and analysed regarding the prediction of the effects of impairment on drug kinetics, particularly when using physiologically-based pharmacokinetic (PBPK) modelling.

Results

PBPK models are suggested as a potential framework to understand drug clearance changes in HI. However, quantifying the changes in abundance and activity of drug-metabolising enzymes and drug transporters, understanding the impact of shunting, and accounting for variations on drug absorption in each individual, outside the frame of CP score, could be considered as key elements for extending the success of HI PBPK models.

Conclusions

Many physiological changes in HI determining drug disposition do not necessarily correlate with CP scores. Quantifying these changes in individual patient is essential in future HI studies. CP scores were never intended for anything beyond the clinical assessment of HI patients.

3.2. Introduction

Liver metabolism is responsible for the elimination for many drugs. The liver has impressive functional hepatic reserve and consequently significant hepatic impairment (HI) has to occur before changes in drug metabolism occur. Unlike renal impairment (RI), there is currently no surrogate markers to estimate HI and limited evidence to guide drug dose adjustment (Davenport, et al., 2011). HI can be defined as any acute or chronic liver injury that affects liver functional capacity. Dose adjustment in HI population is challenging as the impact of the disease on drugs clearance varies depending on the drug characteristics as well as individual patient factors (Delcò, et al., 2005).

Cirrhosis is a significant and increasing burden of disease worldwide (Sepanlou, et al., 2020). It is the common end-point of most chronic fibrotic liver diseases and the point at which hepatic reserve has been exhausted. Consequently, decline in hepatic function is evident with progressive cirrhosis. Multiple interacting factors determine the behaviour of drugs in cirrhosis, making drug dose adjustment a challenge. Under or over dosing could have significant clinical consequences. Therefore, given the prevalence of disease and the importance of optimal drug dosing, it is essential to predict drug metabolism. In this review we focus on strategies for drug dosing in liver cirrhosis.

In cirrhosis, the absorption and disposition kinetics of most drugs are affected. It changes not only the metabolic function of the liver, but it also has an impact also on parameters such as liver blood flow, binding to plasma proteins, and biliary and renal excretion. These all potentially influence drug pharmacokinetics at different degrees depending on the drug and the severity of the disease in the patient (Verbeeck & Horsmans, 1998). This in turns may lead to significant alterations in the exposure to many drugs, necessitating dosage adjustment to avoid drug toxicity.

Dedicated pharmacokinetic studies for HI patients are part of many drug development programs and there is a regulatory guidance on the conduct of such studies and interpretation of the results. This is with a view to providing information to prescribers in the drug label. However, many drug regulatory authorities may approve drugs prior to availability of complete dosage guidance in sub-groups of patients, such as those with HI (Jadhav, et al., 2015). This raises the need for evidence-based approaches to guide clinicians to the best course of action regarding any dose adjustment of drugs in HI until clinical evidence is established. Physiologically-based pharmacokinetic (PBPK) modelling and simulations have been used for this purpose. However optimisation is still required to increase the predictive performance of these models. This review summarises key requirements for developing PBPK models for hepatic impairment populations; the current scoring systems implemented into these models; their limitations; and potential to enhance model predictability.

3.3. Cirrhosis epidemiology, causes, and classification

Cirrhosis is a global health burden, accounting for over 1 million deaths per annum, and 4.9% to 9.5% of the global population are believed to have some level of cirrhosis (Blachier, et al., 2013; Mokdad, et al., 2014; Sarin SK, 2016). Alcohol, hepatitis C, hepatitis B, and non-alcoholic steatohepatitis (NASH) are among the most common causes of cirrhosis worldwide (Schuppan & Afdhal, 2008). Different classification systems have been used for categorisation of cirrhosis, among which Child-Pugh classification is the most common.

3.3.1. Child-Pugh system

Liver cirrhosis is routinely classified based on disease progression into Child-Pugh (CP) grades, CP-A (mild), CP-B (moderate), and CP-C (severe) (Child & Turcotte, 1964)**.** Although this classification is widely used clinically and can give an indication of the severity of liver disease, it does not express quantitative changes in hepatic metabolic function responsible for

drug clearance (Schuppan, et al., 2008). Scores in this classification are calculated based on encephalopathy, ascites degree (absent, moderate/controlled or severe/refractory), serum bilirubin and albumin levels, as well as prothrombin time or the international normalised ratio (INR) (Tsoris & Marlar, 2021).

3.3.2. Other classification systems

Apart from CP score, several models exist for grading the severity of liver disease. The Model for End Stage Liver Disease (MELD) score depends on three readily available laboratory variables; serum creatinine, serum bilirubin, and INR (Wiesner, et al., 2003).

The MELD score was developed and validated to predict mortality in patients with portal hypertension undergoing placement of transjugular intrahepatic portosystemic shunts, but it is now more commonly used to predict survival in cirrhosis and for prioritisation of patients for liver transplant (Kamath, 2001; Malinchoc, et al., 2000).

Another system to assess HI specifically in oncology patients was developed by the National Cancer Institute (NCI) Organ Dysfunction Working Group (ODWG) to guide dosing for chemotherapeutics (Patel, et al., 2004). The NCI classification system (NCIc) uses two biochemical parameters to grade hepatic dysfunction: total bilirubin and aspartate aminotransferase (Elmeliegy, et al., 2021).

Other classification systems for cirrhosis are available but are not frequently used. Most of these correlate with the CP classification, including Maddrey's discriminant function (df) (Maddrey, et al., 1978) (using prothrombin time and total serum bilirubin), and the Mayo Survival Model for primary biliary cirrhosis (Dickson, et al., 1989).

Using specific markers of metabolic activity has been an alternative approach. Monoethylglycinexylidide (MEGX) is a lignocaine metabolite (via cytochrome P450 (CYP) 3A) and a biomarker for the assessment of oxidative enzymes activity (Testa, et al., 1997). Indocyanine green clearance has been validated as a tool for pre-operative assessment of liver

function and also gives indication of hepatic blood flow (Figg, et al., 1995). Consequently, it has been assessed as a tool for measuring hepatic function for drug metabolism (Gasperi, et al., 2016). Galactose single point (GSP) is a simple test that can be used to define clearance of both highly metabolised drugs and drugs which are eliminated without undergoing metabolism in the liver (Tang and Hu, 1992). GSP was originally reported in 1995 and further validation studies are awaited (Hu, et al., 1995). Overall, despite promising results, the lack of routine availability limits clinical utility of all these tests.

3.3.3. Limitations of the CP scoring system for drug dosing

Although the CP score is the most commonly used classification system for patients with cirrhosis, it has some limitations that can be explained as follows:

1) *Subjective scoring*: Two elements in CP classification are clinical parameters. These are ascites and encephalopathy scores. They are subjective according to clinical judgement and can also be confused with other disorders (Kok & Abraldes, 2019). For example, a patient with liver cirrhosis and diabetes can experience diabetic coma that can be mistakenly diagnosed as hepatic encephalopathy. Similarly, a patient with a brain tumour along with cirrhosis can show symptoms that may be confused with hepatic dysfunction or disorder. Metabolic encephalopathy can be also precipitated by sepsis or renal insufficiency (Kunze, 2002). Ascites severity is also a subjective assessment and may be exacerbated by non-cirrhotic factors, including heart failure, cancer, and infectious diseases (Carrier, et al., 2014). Careful clinical diagnosis is required to rule out other causes and reduce the subjective nature of these parameters. Other scoring systems such as MELD and NCI scores include only biochemical laboratory tests to overcome this subjectivity in CP scoring.

2) *Not accounting for renal function*: Although RI is common with cirrhosis, this scoring system does not consider changes in renal function. For drugs that are mainly eliminated by the kidney, CP classification does not help in clinical predictions or correlate with drug

kinetics. Other scoring systems, such as MELD score, were developed to overcome this limitation by including creatinine levels as one of its components.

3) *Not distinguishing between different causes of cirrhotic liver disease*: Different reports have indicated discrepancies between different causes of cirrhosis in relation to enzyme and transporter expression, inflammatory mediators, speed of progression, and control by certain drugs, such as ursodeoxycholic acid (UDCA). Scoring systems (i.e. MELD) consider cholestatic and alcoholic cirrhosis as lower risk than other underlying causes in the formula score, but it is uncertain if these aetiologies have better hepatic function compared to other disease aetiologies for the same biochemistry (Cholongitas, et al., 2005).

4) *Correlation with liver metabolic capacity is not well established:* CP classification was not created to assess liver metabolic function and it utilises assays attributable to synthetic state, function and clinical status. However, it is not possible to separate the main contributor to CP grade from these three elements. For example, a patient with normal metabolic and synthetic liver function that has refractory ascites or encephalopathy might be scored in the same class as a patient with deteriorated functions and normal clinical measures. Those two patients may require completely different treatment options and drug doses as the metabolic capacity of their livers are widely different. Therefore, the use of markers like serum albumin, prothrombin time and bilirubin is encouraged and abnormalities in these parameters may be better related to drug elimination capacity than other components of the CP classification, e.g. encephalopathy and ascites as recommended by the European Medicine Agency (EMA) (EMA, 2005).

In spite of all the limitations discussed above, CP scoring system is still the most widely used in drug development. This scoring system is recommended by the US Food and Drug Administration (FDA) and the EMA owing to its reproducibility, low cost, classification of cirrhosis into only 3 main categories (simplicity of interpretation), and incorporation of routinely measured parameters for hepatically-impaired patients. Ninety five percent of

pharmacokinetic studies dedicated for HI populations in drug development use CP classification to categorise patients at different stages of disease severities by contrast less than 2% use NCI or MELD score exclusively (Talal, et al., 2017).

3.4. Methods proposed to overcome limitations of the CP scoring system

Several attempts have been made to correlate CP score with NCI, MELD and other scoring systems (Patel, et al., 2004), or to use other non-invasive metabolic scoring systems such as:

Disease severity index (DSI): This test uses metabolism of oral and intravenous radioactive cholates that account for the changes in first-pass metabolism and the effect of shunting (Helmke, et al., 2015). This score showed good correlation with CP score but not with the MELD score. Although it seems to be a promising non-invasive method, its applicability in routine clinical practice and in clinical trials have yet to be investigated.

Changing the cut-off points for key biomarkers: The current cut-off points for several biomarkers included in the CP scoring system shown in Table 3.1 were not previously validated, and therefore this scoring system has shown some shortcomings in predicting the five-year survival of patients with different aetiologies. A retrospective study was performed to refine these cut-off levels for bilirubin, albumin and INR and to introduce creatinine levels into the classification system (Kaplan, et al., 2016). Although these changes reflected better predictive performance for intermediate and long-term survival, they have not yet been investigated against the metabolic capacity of the liver for different drugs.

Table 3.1. Parameters used in the calculation of the Child-Pugh score

Parameter	**Points Scored for Observed Findings**		
	1	**2**	**3**
Encephalopathy grade †	None	1 or 2	3 or 4
Ascites	Absent	Slight	Moderate

Serum bilirubin, mg/dl	<2	2-3	>3
Serum albumin, g/dl	>3.5	2.8-3.5	<2.8
Prothrombin time, sec prolonged INR (international normalised ratio)	<4 <1.7	4-6 1.7-2.3	>6 >2.3

†Grade 0: normal consciousness, personality, neurological examination, and electroencephalogram.
Grade 1: restless, sleep disturbed, irritable/agitated, tremor, impaired handwriting, 5 cps waves
Grade 2: lethargic, time-disoriented, inappropriate, asterixis, ataxia, slow tri-phasic waves.
Grade 3: somnolent, stuporous, place-disoriented, hyperactive reflexes, rigidity, slower waves.
Grade 4: unarousable coma, no personality/behaviour, decerebrate, slow 2-3 cps delta activity.
5-6 points; mild or CP-A, 7-9 points; moderate or CP-B, 10-15 points; Severe or CP-C (Child & Turcotte, 1964).

Imaging techniques: Liver stiffness measurements such as transient elastography, are linked to the deposition of extracellular matrix and can be used to identify patients with cirrhosis and predict progression to decompensated disease (Talal, et al., 2017). Computed tomography has also been used as a tool to scale-up enzyme abundance and activity data by measuring the functional hepatocyte volume as a direct reflection of the functional reserve of the organ and correlating these values with changes in the CP score (Edginton & Willmann, 2008; Johnson, et al., 2010). The simulation outputs for different drugs were in agreement with the biologically determined scalars using microsomal and cytosolic protein contents (El-Khateeb, et al., 2020). These technologies offer promise but more studies are required to investigate the change in the activities of different drug-metabolising enzymes and drug transporters (DME&T) against image-related measures.

3.5. Regulatory perspective on drug development in hepatic impairment

Drug dosing is moving from a "one dose fits all" dosing strategy to "personalised medicine", individualised tailoring of drug dosing to optimise efficacy and minimise harm has become a key focus of investigation. The united states' FDA guidance recommends pharmacokinetic (PK) studies in patients with impaired hepatic function if the hepatic metabolism and/or excretion accounts for a substantial portion of the elimination of the parent drug or its active metabolite (>20% of absorbed dose is eliminated by the liver). The guidance also recommends a HI study even if the drug and/or its active metabolite are eliminated to a lesser extent by the liver when they have a narrow therapeutic index. In the case of drugs that are intended only for single-dose administration, a HI study will generally not be necessary unless clinical concerns suggest otherwise (FDA, 2003).

These PK studies determine the plasma concentrations of the parent drug and sufficiently important active metabolites and calculate PK parameters, such as the area under the concentration-time curve (AUC), terminal half-life ($t_{1/2}$), maximum plasma concentration (C_{max}), and apparent clearance for the parent compound (CL/F). For multiple dose studies, trough concentration (C_{min}) and fluctuation should be taken into account. When possible, both unbound and total concentrations are used to express these parameters. Generally, dose reduction is required if the change in the AUC in HI exceeds a two-fold increase relative to healthy volunteers (FDA, 2003). Usually, doses are reduced if the liver disease has resulted in a clinically significant impairment in the clearance of the drug except for prodrugs, in which doses may be increased or the frequency of administration may be decreased. In some cases, the drug may be classified as contraindicated in severe liver impairment, depending on the drug's therapeutic window and the impact on the clearance of the drug. In the case of lack of data supporting drug labelling, the drug may be classified as "used with extreme caution"

(Pena, et al., 2016). To ensure equitable access to patients with cirrhosis to potentially safe and efficacious medication, it is critical that drugs are appropriately scrutinised in HI.

3.6. The need for dose adjustment in hepatic impairment

Around 50-80% of new molecular entities (NMEs) approved in the United States between the years 2013 and 2014 did not include clinical studies that inform dosage recommendations in RI and HI, irrespective of whether these clinical trials were required (Jadhav, et al., 2015). The percentage of drugs which did not have dosing recommendations for mild and moderate HI at initial approval was ~30% and 50%, respectively, in both of the years 2013 and 2014. However, for severe HI, this proportion was close to 80% in 2013 and ~60% in 2014, as shown by the left part of Figure 3.1 derived from data published by Jadhav and co-workers (Jadhav, et al., 2015).

We followed the same strategy and found that a similar trend persisted in subsequent years in the period 2016 to 2019 (Supplementary Table 3.1). Biologics were not included in this survey. In 2016, about 53%, 60%, and 60% of the NMEs lacked study-based label guidance for mild (CP-A), moderate (CP-B), and severe (CP-C) cirrhosis, respectively. In the following two years (2018-2019), the situation remained similar with a gradual rise in the percentage of drugs without label guidance, mainly in the severe stage of cirrhosis, as shown in Figure 3.1. These drugs are now available in the market without any labelling guidance regarding their dose levels in this special patient population.

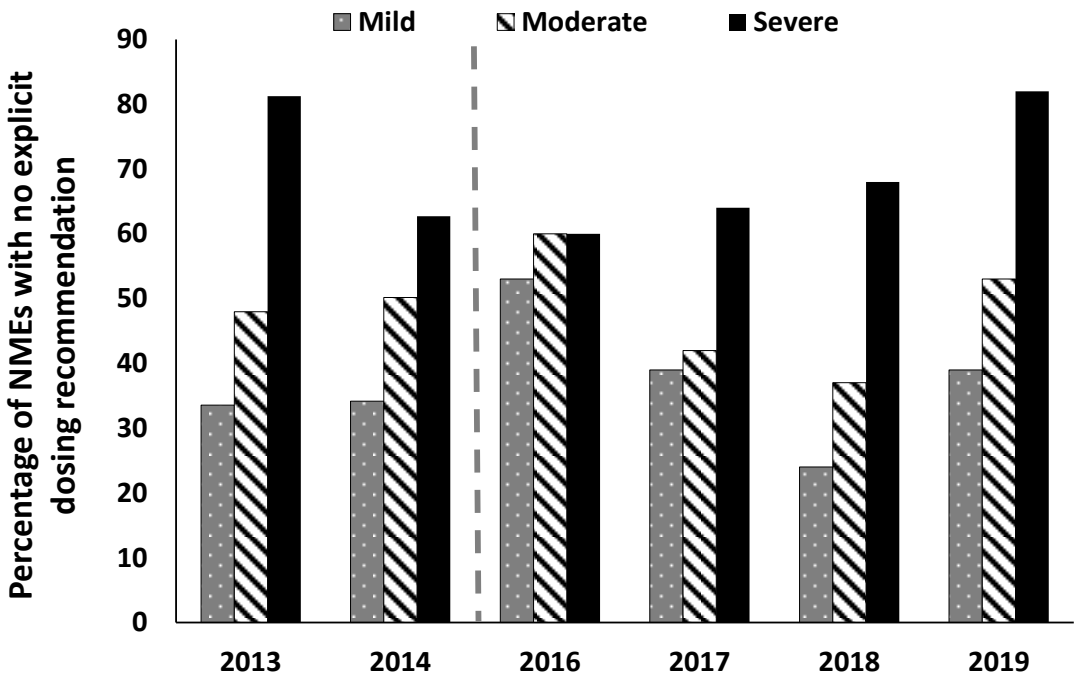

Figure 3.1. The percentage of new molecular entities (NMEs) approved without explicit dosing recommendations in hepatic impairment population on their initial approval from 2013 to 2019 (Data for the first two years are derived from Jadhav et al, (2015) while the rest represents data from the current review for the period from 2016 to 2019).

During the different phases of clinical trials, patients are recruited and treated by the investigational drug to test its safety and efficacy. Many special patient populations are excluded during these phases to avoid subjecting those individuals to any risks of unexpected side effects due to inappropriate dosing. However, extensive narrowing of the inclusion criteria or expansion of the exclusion criteria without an obvious aim may influence the inference and usefulness of clinical trials with respect to different issues. First, a large number of patients may miss the opportunity to participate in such trials that may be clinically beneficial. Second, trial results will be less likely to capture the diversity in patient populations that might be exposed to this therapy after being released onto the market. The study population may in fact only represent a small fraction of the market population. Third, extensive time wastage in the

recruitment of patients can occur with “restricted” criteria in all phases of clinical studies (Kim, et al., 2017).

Ironically, when we examine the exclusion criteria related to organ dysfunction, one can find that these exclusions are based on liver function tests (LFTs) and CP scores in the case of hepatic dysfunction. Unlike renal dysfunction, where creatinine clearance can be a reliable measure of renal clearance, neither LFTs nor CP score accurately reflect the drug-metabolising efficiency of the liver. The upper limits of normal (ULN) range for LFTs, such as aspartate transaminase (AST) and alanine transaminase (ALT), is around 40 IU/L (Yin & Tong, 2009). These can vary between populations according to sex, age and weight of the patient as well as between laboratories (Giannini, 2005). Some patients with mild and moderate hepatic impairment may have LFTs between 5 and 20 folds the ULN; however, they can still tolerate the approved doses without any symptoms or complications. Thus, for drugs metabolised by the liver, a total exclusion of patients with liver enzymes above 2-3 fold ULN is not logical and the lack of more metabolic-reflective measures is an urgent issue (Lichtman, et al., 2017).

Due to the aforementioned reasons, the American Society of Clinical Oncology (ASCO) adopted a suggestion to modify the eligibility criteria in cancer research clinical trials to be more inclusive of patients with organ dysfunction as long as the dose is suitably adjusted based on evidence-based data (Masters & Wiernik, 2018). After this recommendation, the FDA published a guidance document for broadening eligibility criteria to increase diversity in enrolment and to include more patients from underrepresented populations (FDA, 2020).

3.7. Can physiologically-based pharmacokinetic modelling help in filling the gap in dedicated clinical trials?

Physiologically based pharmacokinetics (PBPK) is an ‘in silico’ modelling approach that has been advanced over the last decades and has been supported by regulatory agencies such as

EMA and the FDA to be used for informing drug labelling (Rostami-Hodjegan, 2012; Younis, et al., 2017). It mathematically integrates physiochemical and biochemical drug-related data parameters along with physiological/system specific parameters such as blood flow, organ volume/weight, and protein concentration to simulate the expected pharmacokinetics of individuals within a population (Jones & Rowland-Yeo, 2013) (Figure 3.2). This distinct advantage of incorporating variability in physiological parameters is particularly valuable in disease states (such as HI) where these parameters may be altered from healthy subjects. PBPK models can also account for the compounding effects of changes to other compartments/organs and the drug dosing regimen (Rostami-Hodjegan, 2012).

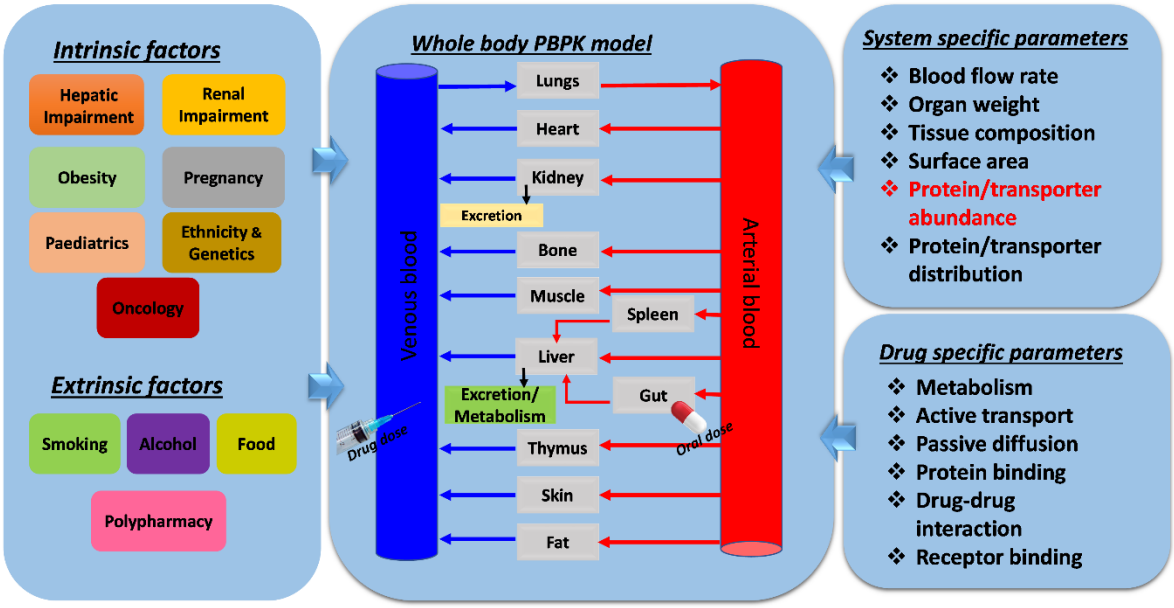

Figure 3.2. The Components of physiologically based pharmacokinetic (PBPK) models (drug-specific and system-specific parameters) with the intrinsic and extrinsic factors that can affect drug exposure. Adapted from (Zhao, et al., 2011).

Although PBPK modelling may inform regulatory approval for many drugs and in different situations with more confidence in relation to drug-drug interactions and paediatric applications, only a small number of FDA submissions use PBPK for predicting drug exposure in hepatic impairment (Wagner, et al., 2015). Different physiological changes in cirrhosis with

disease progression were reported to impact on drug exposure, such as changes in blood flow to gut, liver, kidneys, and other organs, plasma protein levels, haematocrit level, liver size, DME&T expression and activity both in the liver and the gut, renal function, and liver circulation, including shunting (Edginton, et al., 2008; Johnson, et al., 2010). Although the application of these changes in models produced good predictions (within 2-fold in predicted versus observed data), poor predictive performance of these models have been reported in other scenarios which have shown under-prediction of the clearance of the modelled drugs, especially in moderate and severe stages of cirrhosis (Figure 3.3 and Supplementary Table 3.2). No single factor can be the source of these biases, as they are not related to common features of the drugs. For example, some models for CYP2D6 substrates showed good performance with moderate HI populations as in the case of eliglustat, while others such as atomoxetine did not (Huang, et al., 2017; Li, et al., 2020).

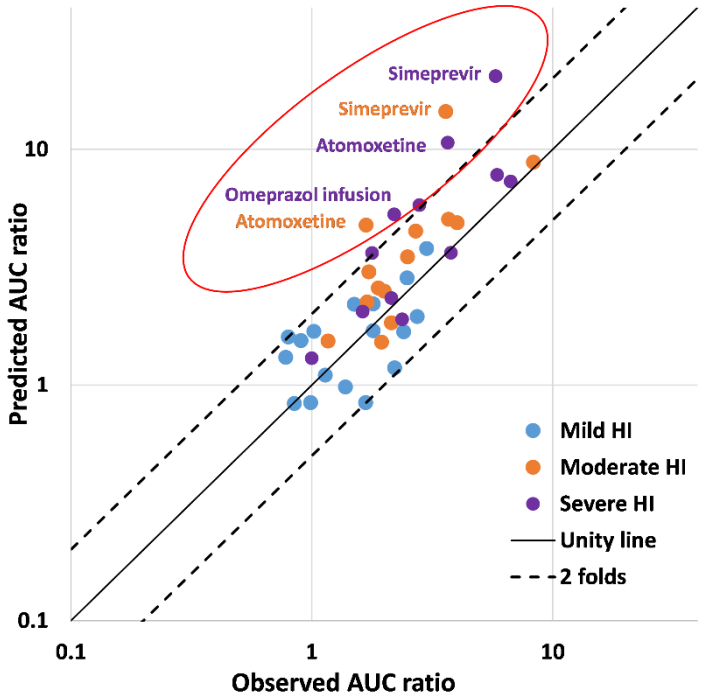

Figure 3.3. The predictive performance of published models for 20 different drugs in hepatic impairment populations with different severities (mild, moderate, and severe cirrhosis). Data were obtained from 14 studies (Chiney, et al., 2020; Huang, et al., 2017; Johnson, et al.,

2010; Li, et al., 2020, 2015; Morcos, et al., 2018; Ogawa, et al., 2020; Ono, et al., 2017; Prasad, et al., 2018; Rasool, et al., 2019, 2017; Snoeys, et al., 2017; Tortorici, et al., 2011; Tse, et al., 2020).

However, some of these studies used different software tools and different model structures. Therefore, IQ consortium has recently conducted a comprehensive PBPK modelling and simulation research with fixed physiological parameters on nearly 60 drugs and concluded that about 70% of the predicted performance was within two-fold difference (Heimbach, et al., 2020). Similar to previous studies, most of the 30% outliers were observed in moderate and severe HI populations. More knowledge and understanding of these pathophysiological changes, a proper classification system of HI patients that correlates with liver metabolic capacity, and availability of clinical data for validation might help in improving the predictive performance of these models and increase their robustness and reliability. The use of PBPK modelling in drug development has grown over the years to inform doses, optimise clinical study design, shorten the duration of clinical studies, and simulate untested scenarios (such as steady state exposure, drug-drug interactions, or different doses and/or formulations) (Zhang, et al., 2020).

3.8. Current gaps and challenges for PBPK modelling in hepatic impairment populations

3.8.1. The heterogeneous nature of the disease and the scoring system

As pointed out earlier, chronic liver disease is progressive and different grades and classifications are available with different scoring systems. The mild grade of CP classification is variable with widely different survival rates depending on whether the disease is associated with portal hypertension or not (Vilar-Gomez, et al., 2018). Other scoring systems do not correlate well with CP score making the use of these systems interchangeably very difficult. Moreover, the level of change in the expression and activity of different DME&T is not the

same across scores and is also affected by the aetiology of the disease and its surrounding environment (Drozdzik, et al., 2019; El-Khateeb, et al., 2020). This can be partly attributed to the fact that the liver is actually not 'well-stirred' as usually assumed in different models. The well-stirred model assumes that the liver is a single well-stirred compartment and that the unbound drug concentration in the emergent blood is in equilibrium with the unbound drug within the liver (Pang & Rowland, 1977). Some preclinical evidence has shown that inter-zonal and inter-lobar differences in the distribution of enzymes and transporters as well as the location and degree of liver disease can have a key role in predicting the pharmacokinetic outcome (Berasain & Avila, 2014; George, et al., 1995a; Gougelet, et al., 2014). Therefore, designing a dedicated study using the most common scoring system, such as CP scoring, with all its limitations with regard to assessment of hepatic metabolic capacity, makes dosage adjustment for those patients and extrapolation of PBPK models for liver disease more challenging.

3.8.2. Information on abundance and activity of drug-metabolising enzymes and transporters (DME&T)

3.8.2.1. Drug-metabolising enzymes

Xenobiotic detoxification process in the liver rely on the presence of metabolic enzymes. Within the hepatocyte, transforming enzymes are primarily located in the microsomes (small vesicles) of the endoplasmic reticulum and the soluble fraction of the cytoplasm (cytosol). The impact of impairment on drug clearance varies depending on the metabolic reaction involved to clear this drug and the functional reserve of these enzymes in the liver. Phase I metabolism is usually known to be significantly affected by the severity of hepatic dysfunction to a higher degree than phase II conjugation reactions. The difference between phase I and phase II biotransformation in response to HI supports the oxygen limitation theory (Yang, et al., 2003). This theory is based on the assumption of reduced oxygen transfer from blood to hepatocytes

by capillarisation of sinusoids and cirrhotic tissue development. It relies on the observation that oxidative Phase I reactions are substantially reduced in liver disease, while Phase II (conjugative) metabolic reactions are preserved until end-stage liver disease is reached (Palatini & De Martin, 2016). For example, theophylline clearance, which depends mainly on CYP450 oxidative metabolism, was shown to be reduced by 37% in cirrhotic rats and activity was restored to normal values by oxygen supplementation (Hickey, et al., 1995).

Some clinical studies showed that glucuronidation does not appear to be altered except when hepatic cell mass is reduced abruptly, while others found that some patients with severe hepatic disease exhibited an increase in enzyme activities (Larson, et al., 2009; Rowland & Tozer, 2011; Verbeeck, 2008). Debinski and coworkers (1995) demonstrated upregulation of UDP-glucuronosyltransferase (UGT) enzymes in the remaining viable human hepatocytes of diseased livers, as observed using immunohistochemical staining (Supplementary Table 3.4). Impaired glucuronidation is observed for drugs, such as morphine, lamotrigine, lometazepam, zidovudine, and mycophenolate mofetil, especially in advanced stages of cirrhosis (Verbeeck, 2008).

Clinical studies have also shown that the biotransformation of CYP3A4 substrates, such as midazolam or erythromycin, is significantly reduced in severe HI, while for CYP2C, the situation is different as the expression trends of these enzymes are highly variable (ranging from no change in liver disease to about 34-72% of that in healthy control subjects). Murray and co-workers recently concluded that CYP2C protein expression is not impaired in cirrhotic livers by studying selective drug substrates (Murray, et al., 2018).

Studies using immunochemical quantification reported variability in the microsomal levels of different CYP isoforms with different sensitivities toward disease progression as shown in Figure 3.4 and Supplementary Table 3.3 (George, et al., 1995b; Guengerich & Turvy, 1991; Lown, et al., 1992). This wide variation in the response of enzymes to hepatic injury is most

probably linked to the disease stage and its severity as proposed by Frye *et al* who suggested a "sequential progressive model of hepatic dysfunction", leading finally to a decrease in the activity of most CYP450 enzymes in end-stage liver disease (Frye, et al., 2006). Moreover, a doubling in CYP2E1 activity and depletion in glutathione levels were revealed in chronic alcohol ingestion, leading to lower protection against paracetamol, isoniazid, methotrexate and other substrates of this enzyme (Verbeeck, 2008).

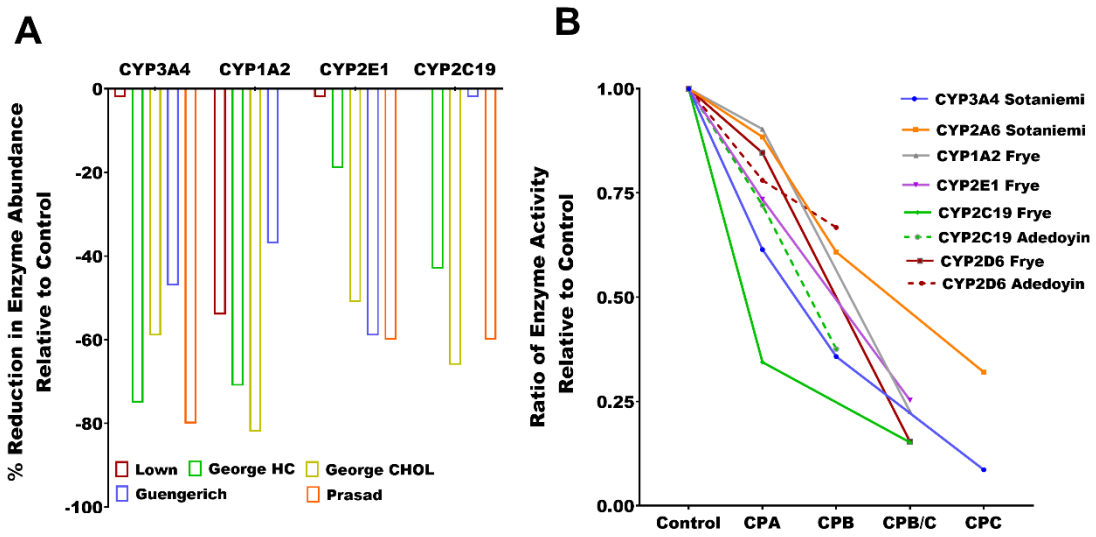

Figure 3.4. Changes in the abundances (A) and activities (B) of different CYP450 isoforms in cirrhotic liver disease relative to control, as reported in the literature (Adedoyin, et al., 1998; Frye, et al., 2006; George, et al., 1995a; Guengerich, et al., 1991; Lown, et al., 1992; Prasad, et al., 2018; Sotaniemi, et al., 1995). Activities are assessed in vivo using selective probes at different stages of disease progression. Abundances were measured my immunoblotting, immunohistochemistry or proteomics per milligram liver microsomes obtained from either control or cirrhosis livers. HC; Hepatocellular liver disease, CHOL; Cholestatic liver disease, CPA; Child-Pugh score A, CPB; Child-Pugh score B, CPC; Child-Pugh score C.

There are several methods for assessing metabolic enzyme activity and expression in cirrhotic patients and comparing them to healthy control subjects. One of these methods is the

measurement of tissue-specific mRNA expression either through reverse transcription (RT)-quantitative polymerase chain reaction (PCR) or microarrays (Heikkinen, et al., 2015; Nakai, et al., 2008). In spite of the utility of this approach, many limitations have been reported, including:

- Providing a relative quantification between tissues.
- mRNA does not always correlate with protein abundances such as the weak correlation for most CYP450s and UGTs (George, et al., 1995a; Izukawa, et al., 2009).
- Dependence on mRNA synthesis and degradation rather than protein turnover.

Another commonly used approach is the use of selective probe drugs for a limited number of enzymes (Table 3.2). These probes should have a high degree of enzyme selectivity either *in vitro* or *in vivo* (Adedoyin, et al., 1998; Frye, et al., 2006; Sotaniemi, et al., 1995). However, this technique has the limitation of small sample size (limited number of patients) in addition to the interference of other factors that may affect the study results, such as other elimination pathways (*e.g.,* renal elimination), inaccuracy in metabolic ratio calculations for complex pathways, and the effect of genotype differences (Prasad, et al., 2018; Tucker, et al., 1998).

Table 3.2. Activity studies for different CYP450 isoforms at different degrees of disease severity with the applied indices and probes.

Study	Stage of liver disease	CYP isoform	Probe	Cause of cirrhosis (number of patients)	Measure/index for activity
Sotaniemi (Sotaniemi, et al., 1995)	Mild, Moderate, and Severe	CYP3A4 CYP2A6	Lignocaine (i.v.) Coumarine (P.O)	All are alcoholic (26)	- Plasma concentration of MEGX metabolite in the 15 min post injection - Urine recovery of the hydroxyl metabolite after 2, 4 and 24 h from the oral dose.
Frye (Frye, et al., 2006)	Mild and Moderate-to-severe	- CYP1A2 - CYP2C19 - CYP2D6 - CYP2E1	- Caffeine - Mephenytoin - Debrisoquin - Chlorzoxozone	HCV (14), HBV (1), chemical (1), alcoholic (2), PSC (1), cryptogenic (1).	- $\frac{Cp\ of\ Paraxanthine}{Cp\ of\ caffeine}$ in the 8 h post dose sample - Urinary recovery of hydroxyl metabolite/ (urine recovery of parent (mephenytoin)+metabolite) - Urinary recovery of hydroxyl metabolite/ (urine recovery of parent (debrisoquin)+metabolite) - $\frac{Cp\ of\ hydroxymetabolite}{Cp\ pf\ the\ parent\ (Chlorzoxazone)}$ in the 4 h post dose sample
Adedoyin (Adedoyin, et al., 1998)	Mild and moderate	- CYP2C19 - CYP2D6	- S-mephenytoin - Debrisoquin	Not specified	Urine was collected over 192 hours - Urinary recovery of 4-hydroxymephenytoin - Urinary excretion ratio of the hydroxydebrisoquin relative to (debrisoquin+ hydroxydebrisoquin urine recoveries)

i.v.: intravenous dosing, P.O: Per oral dosing, MEGX: monoethylglycinexylidide (lignocaine metabolite), HCV and HBV: hepatitis C and B virus infections respectively, *Cp*: Plasma concentration.

Apart from relative quantification, absolute quantification of protein abundances is relatively recent with limited studies available (Supplementary Table 3.3 and Supplementary Table 3.4). It provides the possibility of measuring absolute and direct protein amounts for incorporation into PBPK models and bridging between studies without the necessity of correlation to a reference sample. Different techniques have been used for protein quantification, such as immunoblotting as well as label-free and isotope-labelling proteomic techniques. The choice of suitable methodology depends on the sample under study, the number and nature of the target proteins being quantified, whether discrimination of isoforms of the same subfamily is required and the overall cost (El-Khateeb, et al., 2019; Heikkinen, et al., 2015).

According to Prasad et al, (Prasad, et al., 2018) the changes in abundance of CYPs, UGTs and other drug-metabolising enzymes in cirrhotic livers is not only dependent on the enzyme but also the origin or cause of cirrhosis. For example, there is an evidence of more extensive reduction in drug-metabolising enzyme abundance in alcoholic cirrhosis than hepatitis C-induced cirrhosis (Prasad, et al., 2018). However, this study did not assess changes in enzyme abundances for mild and moderate cirrhosis patients or zonal differences in these abundances across the liver. Moreover, some of the enzymes, such as CYP2B6, CYP3A5, UGT2B17, and UGT1A1, were below the detection limit of the analytical method.

3.8.2.2. Transporters

Drug transporters are membrane-bound proteins present in organs, such as the intestine, liver, and kidneys, and they play a key role in the absorption and elimination of drugs and their metabolites. Figure 3.5 shows the most important transporters in drug disposition within the liver. Drug transporters are categorised either functionally into two superfamilies: uptake transporters or phase 0 proteins and efflux transporters or phase III proteins, or structurally mainly into solute carriers (SLC) and ATP-binding cassette (ABC) transporters (Döring & Petzinger, 2014; Nigam, 2015).

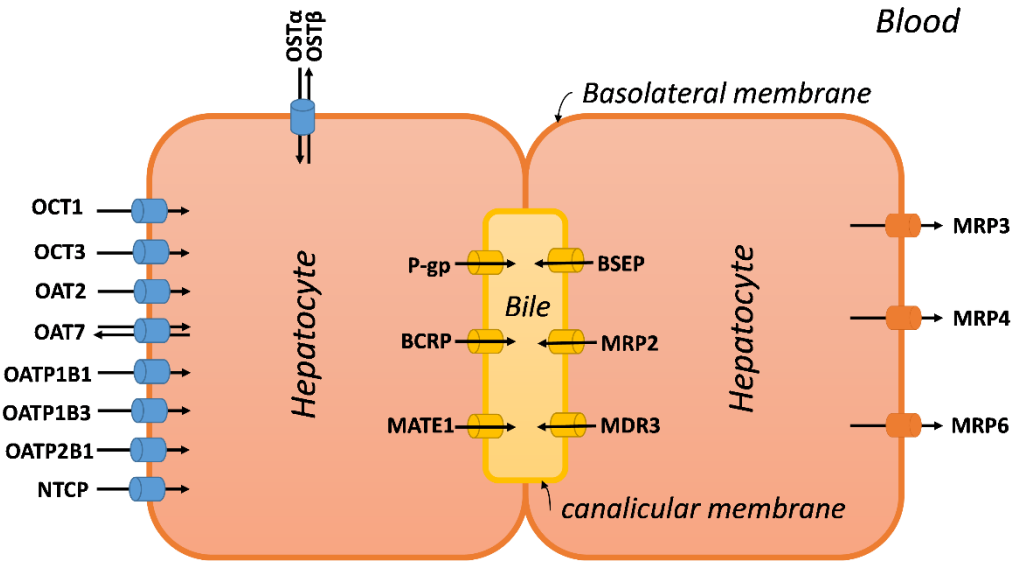

Figure 3.5. Location of clinically relevant drug transporters expressed in human hepatocytes. Uptake transporters located in the basolateral membrane include members of the SLC superfamily, such as OCT1, OCT3, OAT2, OAT7, OATP1B1, OATP1B3, OATP2B1, and NTCP. Efflux transporters located in the basolateral membrane include members of the ABC transporters superfamily, such as MRP3, MRP4, and MRP6. Efflux transporters are also located in the canalicular membrane and include BCRP, BSEP, MATE 1, MDR3, MRP2, and P-gp.

Relative transporter mRNA levels have previously been measured by quantitative PCR at different stages of HCV liver disease (Nakai, et al., 2008). NTCP and OCT1 showed a significant rise in mild F1 fibrosis relative to normal control (~75% and 38%, respectively), while later stages showed a non-significant difference in NTCP expression relative to healthy subjects and a significant reduction, by 38%, in OCT1 levels in severe cirrhosis. On the other hand, OATP-C transporters showed a gradual reduction of 16%, 20%, and 60% with F1, F2, to F3 fibrosis scores, respectively.

Ogasawara et al, (2010) also investigated the effect of HCV-related cirrhosis on 17 different hepatic drug transporters and observed that the expression of most of these transporters (OCT1,

OATP1B1, OATP1B3, MATE1, MRP4, MRP5 and BCRP) decreased by approximately 50% in cirrhosis. This does not only affect the hepatic uptake of drugs *via* these transporters but also biliary excretion was also noticeably reduced.

More and co-workers studied transporter mRNA (using QuantiGene Plex 2.0 assay) as well as relative transporters protein expression (using Western blotting) in human liver tissues with steatosis (with no cirrhosis), alcoholic cirrhosis, or diabetic alcoholic cirrhosis compared to normal livers (More, et al., 2013). A summary of the results of the study is shown in Table 3.3. This study did not assess the activity at different stages of disease severity, and did not measure OATP1B1/1B3 because of lack of commercially available high-quality specific antibodies for these transporters at the time of the study. Moreover, the results are not scalable to liver tissue levels, which limits their usefulness in modelling. Recent studies assessed changes in transporter abundances per unit mass of tissue using LC-MS proteomic techniques in samples with different causes of cirrhosis and reported progressive reduction of most key transporters with disease progression (Drozdzik, et al., 2020; Wang, et al., 2016).

In spite of the impact of cirrhosis aetiology on enzyme expressions, hepatocyte uptake and biliary excretion, the current CP classification does not differentiate between the different causes of the disease as previously indicated.

Table 3.3. Transporter mRNA and protein expression in cirrhotic livers with different aetiologies.

Cause of Cirrhosis	No change from control (↔)	Decreased compared to control (↓ %)	Increased compared to control (↑ %)
Transporter mRNA expression			
Alcohol †	SLCO1B1, ABCC2, ABCC3, ABCC6	SLCO1B3 (78%)	SLCO2B1 (51%), ABCC1 (38.44%), ABCC4 (58%), ABCC5 (34%), ABCG2 (194%)

Alcohol and diabetes mellitus †	SLCO1B1, SLCO1B3, SLCO2B1, ABCG2, ABCC1, ABCC2, ABCC4, ABCC5, ABCC6, ABCC2	ABCC3 (88%)	
Transporters protein expression			
Alcohol and diabetes mellitus †	ABCC2	ABCC6 (~30-40%)	ABCC1 (1.5-2 folds) ABCC3 (2-3 folds) ABCC5 (~20-30%) ABCC4 (~ 2 folds) ABCG2 (~50%)
Alcohol ‡	SLC47A1, ABCC2, ABCB1, SLCO2B1	SLC10A1 (35%), SLCO1B1 (55%), SLCO1B3 (87%), SLC22A1 (73%), ABCG2 (50%), ABCB11 (36%)	ABCC3 (38%)
Alcohol §	--	SLC10A1 (24%), SLCO1B1 (39%), SLCO1B3 (21%), SLC22A7 (74%), ABCC2 (70%), and OATP2B1 (27%)	--
Chronic hepatitis C ‡	ABCG2, ABCC3, SLCO1B1	ABCB11, ABCC2, SLCO10A1, SLCO1B3, SLC22A1, ABCB1 (32-56%)	SLC47A1 (46%)
Chronic hepatitis C §	--	ABCB11 (53%), SLCO2B1 (26%)	--
Cholestatic liver disease §	--	--	ABCB1 (~3.5 folds), ABCC4 (~3 folds)
Autoimmune hepatitis §	--	ABCC2 (82%)	ABCB1 (~4folds), ABCC4 (~2.5 folds)

Data derived from †(More, et al., 2013), ‡(Wang, et al., 2016), §(Drozdzik, et al., 2020)

3.8.1. Small sample size in dedicated clinical studies

In clinical studies dedicated to HI, which are designed to developing dosage recommendations, subjects are stratified based on CP score with at least six subjects per arm (FDA, 2003). Although the guidance states that for pathways known to exhibit genetic polymorphism (such as CYP2D6 and CYP2C19) the number increases and should include no less than eight subjects per arm, this still might not be enough to represent the whole population and allow accurate prediction of drug exposure changes in HI. Other causes of differences can be age, weight, smoking, concomitantly administered drugs and other disease states that are not completely reported for every patient. Moreover, most of these dedicated studies do not enrol all classes of liver impairment (Figure 3.1). In some situations, reduced (in terms of the acceptable number of enrolled patients) clinical trials are accepted when the oral clearance of the drug shows a negative correlation with the progression of the disease. In that case, the findings in the moderate category would be applied to patients with a mild CP category, and dosing in the severe category would generally be contraindicated (FDA, 2003). However, dosage adjustment in moderate HI cannot be generalised or extrapolated to mild or less severe conditions and the drug can be still useful in severe stages with appropriate dosage adjustment.

3.8.2. Accounting for the change in plasma protein binding in HI patients

Plasma protein concentrations mainly albumin and α1 acid glycoprotein are known to decline with progress of HI severity (Li, et al., 2018). The fraction unbound of a drug is the proportion that is responsible for therapeutic effect and available for systemic metabolism and elimination which can be calculated in HI from Equation 1. Scaling with this equation was shown to have high predictive performance especially for albumin bound drugs (Li, et al., 2018).

$$f_{u,HI} = \frac{1}{1+\frac{[P]_{HI}}{[P]_{normal}} \times \frac{1-f_{u,normal}}{f_{u,normal}}} \quad \text{..... (1)}$$

Where $f_{u,normal}$ and $f_{u,HI}$ denote free drug fraction in plasma in normal and hepatic impairment subjects, respectively. $[P]_{normal}$ and $[P]_{HI}$ are the plasma protein concentrations in normal and hepatic disease, respectively. Although the prediction of the absolute value of *fu* was good, the authors did not assess the predictive performance based on the relative changes of *fu* (by comparing the observed and predicted changes of different drugs in various HI populations).

When doses are intended to be adjusted in cirrhotic patients, $CL/F_{unbound}$ and $AUC_{unbound}$ are the parameters that should be taken into account rather than the total parameters; CL/F_{total} and AUC_{total} (bound and unbound) as the latter are deceiving. For instance, the AUC_{total} may not change or, on the contrary, may decrease, while the unbound value, which is more clinically relevant, increases. This conclusion has been recommended by many studies and was observed for different drugs, such as naproxen, (Williams, et al., 1984) carvedilol, (Rasool, et al., 2017) and quinine (Orlando, et al., 2009). The decrease in $CL/F_{unbound}$ is obscured by the increase in the unbound fraction of the drug in the blood f_{ub} as can be deduced from the following equation:

$$CL/F_{unbound} = \frac{CL/F_{total}}{fub} \quad \text{..... (2)}$$

Therefore, the net result may be unchanged total CL/F_{total} as in the case of naproxen in cirrhotic patients compared to that in healthy controls, or a worse result as in the case of quinine, which showed an increase in CL/F_{total} for cirrhotic patients relative to healthy individuals. This may lead to a major error in dose adjustment. This factor will mainly affect the systemic clearance of low clearance or low extraction ratio drugs (T'jollyn, et al., 2018).

It is also important to note that differences in protein binding obtained from *in vitro* experiments and *in vivo* situations can be observed, and this can contribute to the poor predictive performance for some drugs in HI populations (Yim, 2019; Zeitlinger, et al., 2011).

3.8.3. The shunting effect

Due to the progressively developing portal hypertension with increasing cirrhosis severity, spontaneous porto-systemic shunts (SPSS) are formed to vent the increased portal pressure

(Nardelli, et al., 2020). Unfortunately, although this mechanism seems to be compensating for deterioration during cirrhosis, complications such as hepatic encephalopathy, variceal bleeding, portal vein thrombosis, and deterioration of liver function start to appear (Simón-Talero, et al., 2018). Concerning pharmacokinetics of administered drugs, these SPSS as well as surgically implemented transjugular intrahepatic portosystemic shunts (TIPS) constitute a challenge to the predictive performance of different models. TIPS can lead to a reduction in gut CYP3A4 levels as well as levels of hepatic enzymes (Chalasani, et al., 2001). Therefore, changes in the mesenteric blood flow and CYP3A4 should be accounted for in the models based on the presence or absence of these shunts, their severities, and the stage of cirrhosis (Johnson, et al., 2010; Neal, et al., 1979). Computed tomography images can help in visualisation and identification of SPSS. It should be highlighted that the MELD score fails to capture severity of portal hypertension, while CP does reflect this to an extent, but neither of these scoring systems addresses the presence or severity of spontaneous portosystemic shunting.

3.8.4. Impact of hepatic impairment on drug absorption is not well understood

As pointed out earlier, the degree of shunting and the corresponding changes in mesenteric blood flow and intestinal enzyme abundances and activities in HI can affect oral drug bioavailability (Chalasani, et al., 2001; Verbeeck, 2008). The bioavailability of drugs such as morphine, meperidine, verapamil, metoprolol, clomethiazole, labetalol, carvedilol and midazolam may increase to double their values in cirrhosis because they escape extensive first-pass metabolism.

One of the changes that may occur in severe hepatic impairment is the change in the gastric emptying time. In a PBPK modelling and simulation study that compared the residence times of metformin in the elderly and young populations with and without hepatic impairment, a 40-50% increase in gastric emptying time was suggested in patients with CP-C compared to their

healthy control counterparts (Rhee, et al., 2017). Although these findings have not been validated by clinical data, this change may not only cause a slight delay in T_{max} (time to C_{max}) or the rate of absorption but may also play a role, to some degree, in alteration of the extent of absorption in these populations.

3.9. Future directions

Given the limitations in the classification systems of HI, it is clear that there is no magic number that can be applied to all drugs in all patients with HI. Strategies using CP score or other tests of disease severity and inter-individual variation cannot reliably predict differences with regard to exposure to therapeutic drugs. Genotyping is one of the methods that have been used to individualise patient's therapy, however there are still variabilities among patients with the same genotype. Liver biopsy is an invasive and impractical approach to the characterisation of individual patients by direct measurement of the expression of metabolising enzymes and transporters or their activities. Therefore, newly developed liquid biopsy and multi-omic techniques are proposed as a minimally invasive alternative to tissue biopsies by measuring plasma biomarkers that reflect the liver's metabolic capacity (Achour, et al., 2021). The link between liquid biopsy and tissue is predicated on the continuous shedding into the bloodstream of exosomes that contain a sample from the intracellular bimolecular pool of liver tissue. This technology has recently been applied to the characterisation of various hepatic enzymes and transporters at baseline and after drug treatment in healthy controls and liver cancer patients (Achour, et al., 2021; Aslanis, et al., 2019). The technique has the potential of monitoring not only markers of hepatic elimination of drugs but also biomarkers of disease severity and progression. However, the use of this technique for the highlighted application requires further assessment in liver disease to demonstrate its applicability in clinical practice.

3.10. Conclusion

There is unmet clinical need for dose adjustment in HI populations especially for drugs that have been released to the market and are lacking appropriate guidance in liver disease patients. PBPK modelling and simulations were proposed as tools to fill in this gap. Dedicated pharmacokinetic clinical studies required for dosage adjustment in HI and for the validation of PBPK models use CP system for patients' stratification which has shown a lot of limitations. Other scoring systems, DSI, and imaging techniques, and the emerging liquid biopsy can be introduced to overcome some of CP pitfalls. Whilst it is unlikely that CP score will be replaced by an alternative stratification system when it comes to dose adjustment in HI, ongoing efforts should be encouraged in light of the evidence of poor performance of CP scoring as an indication for changes to drug clearance, a task that the CP system was never designed for.

3.11. References

Achour, B, Al-Majdoub, ZM, Grybos-Gajniak, A, Lea, K, Kilford, P, Zhang, M, Knight, D, Barber, J, Schageman, J, and Rostami-Hodjegan, A. (2021). Liquid Biopsy Enables Quantification of the Abundance and Interindividual Variability of Hepatic Enzymes and Transporters. *Clin. Pharmacol. Ther.*, 109(1), 222–232.

Adedoyin, A, Arns, PA, Richards, WO, Wilkinson, GR, and Branch, RA. (1998). Selective effect of liver disease on the activities of specific metabolizing enzymes: Investigation of cytochromes P450 2C19 and 2D6. *Clin. Pharmacol. Ther.*, 64(1), 8–17.

Aslanis, V, Umehara, K, Huth, F, Ouatas, T, Bharathy, S, Butler, AA, Zhou, W, and Gadbaw, B. (2019). Multiple administrations of fluconazole increase plasma exposure to ruxolitinib in healthy adult subjects. *Cancer Chemother. Pharmacol.*, 84(4), 749–757.

Berasain, C, and Avila, MA. (2014). Deciphering liver zonation: New insights into the β-catenin, Tcf4, and HNF4α triad. *Hepatology*, 59(6), 2080–2082.

Blachier, M, Leleu, H, Peck-Radosavljevic, M, Valla, D-C, and Roudot-Thoraval, F. (2013). The burden of liver disease in Europe: A review of available epidemiological data. *J. Hepatol.*, 58(3), 593–608.

Carrier, P, Jacques, J, Debette-Gratien, M, Legros, R, Sarabi, M, Vidal, E, Sautereau, D, Bezanahary, H, Ly, KH, and Loustaud-Ratti, V. (2014). L'ascite non liée à la cirrhose : physiopathologie, diagnostic et étiologies. *La Rev. Médecine Interne*, 35(6), 365–371.

Chalasani, N, Gorski, JC, Patel, NH, Hall, SD, and Galinsky, RE. (2001). Hepatic and intestinal cytochrome P450 3A activity in cirrhosis: Effects of transjugular intrahepatic

portosystemic shunts. *Hepatology*, 34(6), 1103–1108.

Child, CG, and Turcotte, JG. (1964). Surgery and portal hypertension. *Major Probl. Clin. Surg.*, 1, 1–85.

Chiney, MS, Ng, J, Gibbs, JP, and Shebley, M. (2020). Quantitative Assessment of Elagolix Enzyme-Transporter Interplay and Drug–Drug Interactions Using Physiologically Based Pharmacokinetic Modeling. *Clin. Pharmacokinet.*, 59(5), 617–627.

Cholongitas, E, Papatheodoridis, G, Vangeli, M, Terreni, N, Patch, D, and Burroughs, AK. (2005). Systematic review: the model for end-stage liver disease - should it replace Child-Pugh's classification for assessing prognosis in cirrhosis? *Aliment. Pharmacol. Ther.*, 22(11–12), 1079–1089.

Congiu, M, Mashford, ML, Slavin, JL, and Desmond, P V. (2002). UDP Glucuronosyltransferase mRNA Levels in Human Liver Disease. *Drug Metab. Dispos.*, 30(2), 129–134.

Davenport, A, Cholongitas, E, Xirouchakis, E, and Burroughs, AK. (2011). Pitfalls in assessing renal function in patients with cirrhosis--potential inequity for access to treatment of hepatorenal failure and liver transplantation. *Nephrol. Dial. Transplant.*, 26(9), 2735–2742.

Debinski, HS, Lee, CS, Danks, JA, Mackenzie, PI, and Desmond, P V. (1995). Localization of uridine 5′-diphosphate-glucuronosyltransferase in human liver injury. *Gastroenterology*, 108(5), 1464–1469.

Delcò, F, Tchambaz, L, Schlienger, R, Drewe, J, and Krähenbühl, S. (2005). Dose Adjustment in Patients with Liver Disease. *Drug Saf.*, 28(6), 529–545.

Dickson, ER, Grambsch, PM, Fleming, TR, Fisher, LD, and Langworthy, A. (1989). Prognosis in primary biliary cirrhosis: Model for decision making. *Hepatology*, 10(1), 1–7.

Döring, B, and Petzinger, E. (2014). Phase 0 and phase III transport in various organs: combined concept of phases in xenobiotic transport and metabolism. *Drug Metab. Rev.*, 46(3), 261–282.

Drozdzik, M, Busch, D, Lapczuk, J, Müller, J, Ostrowski, M, Kurzawski, M, and Oswald, S. (2019). Protein Abundance of Clinically Relevant Drug Transporters in the Human Liver and Intestine: A Comparative Analysis in Paired Tissue Specimens. *Clin. Pharmacol. Ther.*, 105(5), 1204–1212.

Drozdzik, M, Szelag-Pieniek, S, Post, M, Zeair, S, Wrzesinski, M, Kurzawski, M, Prieto, J, and Oswald, S. (2020). Protein Abundance of Hepatic Drug Transporters in Patients With Different Forms of Liver Damage. *Clin. Pharmacol. Ther.*, 107(5), 1138–1148.

Edginton, AN, and Willmann, S. (2008). Physiology-based simulations of a pathological condition: Prediction of pharmacokinetics in patients with liver cirrhosis. *Clin. Pharmacokinet.*, 47(11), 743–752.

El-Khateeb, E, Achour, B, Scotcher, D, Al-Majdoub, ZM, Athwal, V, Barber, J, and Rostami-Hodjegan, A. (2020). Scaling Factors for Clearance in Adult Liver Cirrhosis. *Drug Metab. Dispos.*, 48(12), 1271–1282.

El-Khateeb, E, Vasilogianni, A-M, Alrubia, S, Al-Majdoub, ZM, Couto, N, Howard, M, Barber, J, Rostami-Hodjegan, A, and Achour, B. (2019). Quantitative mass spectrometry-

based proteomics in the era of model-informed drug development: Applications in translational pharmacology and recommendations for best practice. *Pharmacol. Ther.*, 203, 107397.

Elekima, OTL, Mills, CO, Ahmad, A, Skinner, GRB, Ramsden, DB, Bown, J, Young, TW, and Elias, E. (2000). Reduced hepatic content of dehydroepiandrosterone sulphotransferase in chronic liver diseases. *Liver*, 20(1), 45–50.

Elmeliegy, M, Yang, DZ, Salama, E, Parivar, K, and Wang, DD. (2021). Discordance Between Child-Pugh and National Cancer Institute Classifications for Hepatic Dysfunction: Implications on Dosing Recommendations for Oncology Compounds. *J. Clin. Pharmacol.*, 61(1), 105–115.

EMA. (2005). Guideline on the Evaluation of the Pharmacokinetics of Medicinal Products in Patients With Impaired Hepatic Function. *Ema*, 1-10 CPMP/EWP/2339/02. https://www.ema.europa.eu/en/documents/scientific-guideline/guideline-evaluation-pharmacokinetics-medicinal-products-patients-impaired-hepatic-function_en.pdf

FDA. (2003). Pharmacokinetics in patients with impaired hepatic function: study design, data analysis, and impact on dosing and labelling. *FDA Guid.* https://www.fda.gov/regulatory-information/search-fda-guidance-documents/pharmacokinetics-patients-impaired-hepatic-function-study-design-data-analysis-and-impact-dosing-and

FDA. (2020). Enhancing the Diversity of Clinical Trial Populations—Eligibility Criteria, Enrollment Practices, and Trial Designs Guidance for Industry. *Guid. Doc.* https://www.fda.gov/regulatory-information/search-fda-guidance-documents/enhancing-diversity-clinical-trial-populations-eligibility-criteria-enrollment-practices-and-trial

Figg, WD, Dukes, GE, Lesesne, HR, Carson, SW, Songer, SS, Pritchard, JF, Hermann, DJ, Powell, JR, and Hak, LJ. (1995). Comparison of Quantitative Methods to Assess Hepatic Function: Pugh's Classification, Indocyanine Green, Antipyrine, and Dextromethorphan. *Pharmacother. J. Hum. Pharmacol. Drug Ther.*, 15(6), 693–700.

Frye, RF, Zgheib, NK, Matzke, GR, Chaves-Gnecco, D, Rabinovitz, M, Shaikh, OS, and Branch, RA. (2006). Liver disease selectively modulates cytochrome P450-mediated metabolism. *Clin. Pharmacol. Ther.*, 80(3), 235–245.

Gasperi, A De, Mazza, E, and Prosperi, M. (2016). Indocyanine green kinetics to assess liver function: Ready for a clinical dynamic assessment in major liver surgery? *World J. Hepatol.*, 8(7), 355.

George, J, Liddle, C, Murray, M, Byth, K, and Farrell, GC. (1995a). Pre-translational regulation of cytochrome P450 genes is responsible for disease-specific changes of individual P450 enzymes among patients with cirrhosis. *Biochem. Pharmacol.*, 49(7), 873–881.

George, J, Murray, M, Byth, K, and Farrell, GC. (1995b). Differential alterations of cytochrome P450 proteins in livers from patients with severe chronic liver disease. *Hepatology*, 21(1), 120–128.

Giannini, EG. (2005). Liver enzyme alteration: a guide for clinicians. *Can. Med. Assoc. J.*, 172(3), 367–379.

Gougelet, A, Torre, C, Veber, P, Sartor, C, Bachelot, L, Denechaud, P-D, Godard, C, Moldes, M, Burnol, A-F, Dubuquoy, C, Terris, B, Guillonneau, F, Ye, T, Schwarz, M, Braeuning,

A, Perret, C, and Colnot, S. (2014). T-cell factor 4 and β-catenin chromatin occupancies pattern zonal liver metabolism in mice. *Hepatology*, 59(6), 2344–2357.

Guengerich, FP, and Turvy, CG. (1991). Comparison of levels of several human microsomal cytochrome P-450 enzymes and epoxide hydrolase in normal and disease states using immunochemical analysis of surgical liver samples. *J. Pharmacol. Exp. Ther.*, 256(3), 1189–1194.

Heikkinen, AT, Lignet, F, Cutler, P, and Parrott, N. (2015). The role of quantitative ADME proteomics to support construction of physiologically based pharmacokinetic models for use in small molecule drug development. *PROTEOMICS - Clin. Appl.*, 9(7–8), 732–744.

Heimbach, T, Chen, Y, Chen, J, Dixit, V, Parrott, N, Peters, SA, Poggesi, I, Sharma, P, Snoeys, J, Shebley, M, Tai, G, Tse, S, Upreti, V V., Wang, Y, Tsai, A, Xia, B, Zheng, M, … Hall, S. (2020). Physiologically-Based Pharmacokinetic Modeling in Renal and Hepatic Impairment Populations: A Pharmaceutical Industry Perspective. *Clin. Pharmacol. Ther.*, cpt.2125.

Helmke, S, Colmenero, J, and Everson, GT. (2015). Noninvasive assessment of liver function. *Curr. Opin. Gastroenterol.*, 31(3), 199–208.

Hickey, PL, Angus, PW, Mclean, AJ, and Morgan, DJ. (1995). Oxygen supplementation restores theophylline clearance to normal in cirrhotic rats. *Gastroenterology*, 108(5), 1504–1509.

Hu, OY, Tang, H-S, and Chang, C-L. (1995). Novel Galactose Single Point Method as a Measure of Residual Liver Function: Example of Cefoperazone Kinetics in Patients with Liver Cirrhosis. *J. Clin. Pharmacol.*, 35(3), 250–258.

Huang, W, Nakano, M, Sager, J, Ragueneau-Majlessi, I, and Isoherranen, N. (2017). Physiologically based pharmacokinetic model of the CYP2D6 probe atomoxetine: Extrapolation to special populations and drug-drug interactions. *Drug Metab. Dispos.*, 45(11), 1156–1165.

Iqbal, S, Vickers, C, and Elias, E. (1990). Drug metabolism in end-stage liver disease. *J. Hepatol.*, 11(1), 37–42.

Izukawa, T, Nakajima, M, Fujiwara, R, Yamanaka, H, Fukami, T, Takamiya, M, Aoki, Y, Ikushiro, S, Sakaki, T, and Yokoi, T. (2009). Quantitative Analysis of UDP-Glucuronosyltransferase (UGT) 1A and UGT2B Expression Levels in Human Livers. *Drug Metab. Dispos.*, 37(8), 1759–1768.

Jadhav, PR, Cook, J, Sinha, V, Zhao, P, Rostami-Hodjegan, A, Sahasrabudhe, V, Stockbridge, N, and Powell, JR. (2015). A proposal for scientific framework enabling specific population drug dosing recommendations. *J. Clin. Pharmacol.*, 55(10), 1073–1078.

Johnson, TN, Boussery, K, Rowland-Yeo, K, Tucker, GT, and Rostami-Hodjegan, A. (2010). A semi-mechanistic model to predict the effects of liver cirrhosis on drug clearance. *Clin. Pharmacokinet.*, 49(3), 189–206.

Jones, H, and Rowland-Yeo, K. (2013). Basic Concepts in Physiologically Based Pharmacokinetic Modeling in Drug Discovery and Development. *CPT Pharmacometrics Syst. Pharmacol.*, 2(8), 63.

Kamath, P. (2001). A model to predict survival in patients with end-stage liver disease. *Hepatology*, 33(2), 464–470.

Kaplan, DE, Dai, F, Skanderson, M, Aytaman, A, Baytarian, M, D'Addeo, K, Fox, R, Hunt, K, Knott, A, Mehta, R, Pedrosa, M, Pocha, C, Valderrama, A, and Taddei, T. (2016). Recalibrating the Child–Turcotte–Pugh Score to Improve Prediction of Transplant-Free Survival in Patients with Cirrhosis. *Dig. Dis. Sci.*, 61(11), 3309–3320.

Kim, TH, Shin, S, Bulitta, JB, Youn, YS, Yoo, SD, and Shin, BS. (2017). Development of a Physiologically Relevant Population Pharmacokinetic in Vitro-in Vivo Correlation Approach for Designing Extended-Release Oral Dosage Formulation. *Mol. Pharm.*, 14(1), 53–65.

Kok, B, and Abraldes, J. (2019). Child–Pugh Classification: Time to Abandon? *Semin. Liver Dis.*, 39(01), 096–103.

Kunze, K. (2002). Metabolic encephalopathies. *J. Neurol.*, 249(9), 1150–1159.

Larson, AM, Kaplan, MM, and Bonis, PAL. (2009). Drugs and the liver: Metabolism and mechanisms of injury. *UpToDate, Waltham, MA.(Last Accessed Sept. 4th, 2015.)*.

Li, G-F, Yu, G, Li, Y, Zheng, Y, Zheng, Q-S, and Derendorf, H. (2018). Quantitative Estimation of Plasma Free Drug Fraction in Patients With Varying Degrees of Hepatic Impairment: A Methodological Evaluation. *J. Pharm. Sci.*, 107(7), 1948–1956.

Li, J, Chen, J, Kanamaluru, V, Gaemers, SJM, Peterschmitt, MJ, Hou, AW, Xue, Y, Turpault, S, and Rudin, D. (2020). Impact of hepatic and renal impairment on the pharmacokinetics and tolerability of eliglustat therapy for Gaucher disease type 1. *Mol. Genet. Metab.*, 129(2), 117–124.

Li, R, Barton, H, and Maurer, T. (2015). A Mechanistic Pharmacokinetic Model for Liver Transporter Substrates Under Liver Cirrhosis Conditions. *CPT Pharmacometrics Syst. Pharmacol.*, 4(6), 338–349.

Lichtman, SM, Harvey, RD, Damiette Smit, M-A, Rahman, A, Thompson, MA, Roach, N, Schenkel, C, Bruinooge, SS, Cortazar, P, Walker, D, and Fehrenbacher, L. (2017). Modernizing Clinical Trial Eligibility Criteria: Recommendations of the American Society of Clinical Oncology–Friends of Cancer Research Organ Dysfunction, Prior or Concurrent Malignancy, and Comorbidities Working Group. *J. Clin. Oncol.*, 35(33), 3753–3759.

Lown, K, Kolars, J, Turgeon, K, Merion, R, Wrighton, SA, and Watkins, PB. (1992). The erythromycin breath test selectively measures P450IIIA in patients with severe liver disease. *Clin. Pharmacol. Ther.*, 51(3), 229–238.

Maddrey, WC, Boitnott, JK, Bedine, MS, Weber, FL, Mezey, E, and White, RI. (1978). Corticosteroid therapy of alcoholic hepatitis. *Gastroenterology*, 75(2), 193–199.

Malinchoc, M, Kamath, PS, Gordon, FD, Peine, CJ, Rank, J, and ter Borg, PCJ. (2000). A model to predict poor survival in patients undergoing transjugular intrahepatic portosystemic shunts. *Hepatology*, 31(4), 864–871.

Masters, JC, and Wiernik, PH. (2018). Are We Ready to Include Organ-Impaired Patients in Oncology Trials? A Clinical Pharmacology Perspective on Recent Recommendations. *J. Clin. Pharmacol.*, 58(6), 701–703.

Mokdad, AA, Lopez, AD, Shahraz, S, Lozano, R, Mokdad, AH, Stanaway, J, Murray, CJ, and Naghavi, M. (2014). Liver cirrhosis mortality in 187 countries between 1980 and 2010: a systematic analysis. *BMC Med.*, 12(1), 145.

Morcos, PN, Cleary, Y, Sturm-Pellanda, C, Guerini, E, Abt, M, Donzelli, M, Vazvaei, F, Balas, B, Parrott, N, and Yu, L. (2018). Effect of Hepatic Impairment on the Pharmacokinetics of Alectinib. *J. Clin. Pharmacol.*, 58(12), 1618–1628.

More, VR, Cheng, Q, Donepudi, AC, Buckley, DB, Lu, ZJ, Cherrington, NJ, and Slitt, AL. (2013). Alcohol Cirrhosis Alters Nuclear Receptor and Drug Transporter Expression in Human Liver. *Drug Metab. Dispos.*, 41(5), 1148–1155.

Murray, M, Gillani, TB, Ghassabian, S, Edwards, RJ, and Rawling, T. (2018). Differential effects of hepatic cirrhosis on the intrinsic clearances of sorafenib and imatinib by CYPs in human liver. *Eur. J. Pharm. Sci.*, 114, 55–63.

Nakai, K, Tanaka, H, Hanada, K, Ogata, H, Suzuki, F, Kumada, H, Miyajima, A, Ishida, S, Sunouchi, M, Habano, W, Kamikawa, Y, Kubota, K, Kita, J, Ozawa, S, and Ohno, Y. (2008). Decreased Expression of Cytochromes P450 1A2 , 2E1 , and 3A4 and Drug Transporters Na+ -Taurocholate-Cotransporting Polypeptide , Organic Cation Transporter 1 , and Organic Anion-Transporting Peptide-C Correlates with the Progression of Liver Fibrosis in. *Pharmacology*, 36(9), 1786–1793.

Nardelli, S, Riggio, O, Gioia, S, Puzzono, M, Pelle, G, and Ridola, L. (2020). Spontaneous porto-systemic shunts in liver cirrhosis: Clinical and therapeutical aspects. *World J. Gastroenterol.*, 26(15), 1726–1732.

Neal, EA, Meffin, PJ, Gregory, PB, and Blaschke, TF. (1979). Enhanced Bioavailability and Decreased Clearance of Analgesics in Patients with Cirrhosis. *Gastroenterology*, 77(1), 96–102.

Nigam, SK. (2015). What do drug transporters really do? *Nat. Rev. Drug Discov.*, 14(1), 29–44.

Ogasawara, K, Terada, T, Katsura, T, Hatano, E, Ikai, I, Yamaoka, Y, and Inui, K. (2010). Hepatitis C virus-related cirrhosis is a major determinant of the expression levels of hepatic drug transporters. *Drug Metab. Pharmacokinet.*, 25(2), 190–199.

Ogawa, S, Shimizu, M, and Yamazaki, H. (2020). Plasma concentrations of pemafibrate with co-administered drugs predicted by physiologically based pharmacokinetic modeling in virtual populations with renal/hepatic impairment. *Xenobiotica*, 50(9), 1023–1031.

Ono, C, Hsyu, P-H, Abbas, R, Loi, C-M, and Yamazaki, S. (2017). Application of Physiologically Based Pharmacokinetic Modeling to the Understanding of Bosutinib Pharmacokinetics: Prediction of Drug–Drug and Drug–Disease Interactions. *Drug Metab. Dispos.*, 45(4), 390–398.

Orlando, R, De Martin, S, Pegoraro, P, Quintieri, L, and Palatini, P. (2009). Irreversible CYP3A inhibition accompanied by plasma protein-binding displacement: A comparative analysis in subjects with normal and impaired liver function. *Clin. Pharmacol. Ther.*, 85(3), 319–326.

Pacifici, G, Viani, A, Franchi, M, Santerini, S, Temellini, A, Giuliani, L, and Carrai, M. (1990). Conjugation pathways in liver disease. *Br. J. Clin. Pharmacol.*, 30(3), 427–435.

Palatini, P, and De Martin, S. (2016). Pharmacokinetic drug interactions in liver disease: An update. *World J. Gastroenterol.*, 22(3), 1260–1278.

Pang, KS, and Rowland, M. (1977). Hepatic clearance of drugs. I. Theoretical considerations of a “well-stirred” model and a “parallel tube” model. Influence of hepatic blood flow,

plasma and blood cell binding, and the hepatocellular enzymatic activity on hepatic drug clearance. *J. Pharmacokinet. Biopharm.*, 5(6), 625–653.

Patel, H, Egorin, MJ, Remick, SC, Mulkerin, D, Takimoto, CHM, Doroshow, JH, Potter, D, Ivy, SP, Murgo, AJ, and Ramanathan, RK. (2004). Comparison of Child-Pugh (CP) criteria and NCI organ dysfunction working group (NCI-ODWG) criteria for hepatic dysfunction (HD): Implications for chemotherapy dosing. *J. Clin. Oncol.*, 22(14_suppl), 6051–6051.

Pena, MA, Horga, JF, and Zapater, P. (2016). Variations of pharmacokinetics of drugs in patients with cirrhosis. *Expert Rev. Clin. Pharmacol.*, 9(3), 441–458.

Prasad, B, Bhatt, DK, Johnson, K, Chapa, R, Chu, X, Salphati, L, Xiao, G, Lee, C, Hop, CECA, Mathias, A, Lai, Y, Liao, M, Humphreys, WG, Kumer, SC, and Unadkat, JD. (2018). Abundance of Phase 1 and 2 Drug-Metabolizing Enzymes in Alcoholic and Hepatitis C Cirrhotic Livers: A Quantitative Targeted Proteomics Study. *Drug Metab. Dispos.*, 46(7), 943–952.

Rasool, MF, Khalid, S, Majeed, A, Saeed, H, Imran, I, Mohany, M, Al-Rejaie, SS, and Alqahtani, F. (2019). Development and Evaluation of Physiologically Based Pharmacokinetic Drug–Disease Models for Predicting Rifampicin Exposure in Tuberculosis and Cirrhosis Populations. *Pharmaceutics*, 11(11), 578.

Rasool, MF, Khalil, F, and Läer, S. (2017). Optimizing the Clinical Use of Carvedilol in Liver Cirrhosis Using a Physiologically Based Pharmacokinetic Modeling Approach. *Eur. J. Drug Metab. Pharmacokinet.*, 42(3), 383–396.

Rhee, S, Chung, H, Yi, S, Yu, K-S, and Chung, J-Y. (2017). Physiologically Based Pharmacokinetic Modelling and Prediction of Metformin Pharmacokinetics in Renal/Hepatic-Impaired Young Adults and Elderly Populations. *Eur. J. Drug Metab. Pharmacokinet.*, 42(6), 973–980.

Rostami-Hodjegan, A. (2012). Physiologically based pharmacokinetics joined with in vitro-in vivo extrapolation of ADME: A marriage under the arch of systems pharmacology. *Clin. Pharmacol. Ther.*, 92(1), 50–61.

Rowland, M, and Tozer, TN. (2011). *Clinical pharmacokinetics/pharmacodynamics* (pp. 403–44). Lippincott Williams and Wilkins, a Wolters Kluwer business.

Sarin SK, RM. (2016). Global Burden Of Liver Disease: A True Burden on Health Sciences and Economies!! | World Gastroenterology Organisation. *Wgo*. https://www.worldgastroenterology.org/publications/e-wgn/e-wgn-expert-point-of-view-articles-collection/global-burden-of-liver-disease-a-true-burden-on-health-sciences-and-economies

Schuppan, D, and Afdhal, NH. (2008). Liver cirrhosis. *Lancet*, 371(9615), 838–851.

Sepanlou, SG, Safiri, S, Bisignano, C, Ikuta, KS, Merat, S, Saberifiroozi, M, Poustchi, H, Tsoi, D, Colombara, D V., Abdoli, A, Adedoyin, RA, Afarideh, M, Agrawal, S, Ahmad, S, Ahmadian, E, Ahmadpour, E, Akinyemiju, T, … Malekzadeh, R. (2020). The global, regional, and national burden of cirrhosis by cause in 195 countries and territories, 1990–2017: a systematic analysis for the Global Burden of Disease Study 2017. *Lancet Gastroenterol. Hepatol.*, 5(3), 245–266.

Simón-Talero, M, Roccarina, D, Martínez, J, Lampichler, K, Baiges, A, Low, G, Llop, E,

Praktiknjo, M, Maurer, MH, Zipprich, A, Triolo, M, Vangrinsven, G, Garcia-Martinez, R, Dam, A, Majumdar, A, Picón, C, Toth, D, … Botella, ER. (2018). Association Between Portosystemic Shunts and Increased Complications and Mortality in Patients With Cirrhosis. *Gastroenterology*, 154(6), 1694-1705.e4.

Snoeys, J, Beumont, M, Monshouwer, M, and Ouwerkerk-Mahadevan, S. (2017). Elucidating the Plasma and Liver Pharmacokinetics of Simeprevir in Special Populations Using Physiologically Based Pharmacokinetic Modelling. *Clin. Pharmacokinet.*, 56(7), 781–792.

Sotaniemi, E, Rautio, A, Backstrom, M, Arvela, P, and Pelkonen, O. (1995). CYP3A4 and CYP2A6 activities marked by the metabolism of lignocaine and coumarin in patients with liver and kidney diseases and epileptic patients. *Br. J. Clin. Pharmacol.*, 39(1), 71–76.

T'jollyn, H, Vermeulen, A, Van Bocxlaer, J, and Colin, P. (2018). A Physiologically Based Pharmacokinetic Perspective on the Clinical Utility of Albumin-Based Dose Adjustments in Critically Ill Patients. *Clin. Pharmacokinet.*, 57(1), 59–69.

Talal, AH, Venuto, CS, and Younis, I. (2017). Assessment of Hepatic Impairment and Implications for Pharmacokinetics of Substance Use Treatment. *Clin. Pharmacol. Drug Dev.*, 6(2), 206–212.

Testa, R, Caglieris, S, Risso, D, Arzani, L, Campo, N, Alvarez, S, Giannini, E, Lantieri, PB, and Celle, G. (1997). Monoethylglycinexylidide formation measurement as a hepatic function test to assess severity of chronic liver disease. *Am. J. Gastroenterol.*, 92(12 SUPPL.).

Tortorici, MA, Toh, M, Rahavendran, S V., LaBadie, RR, Alvey, CW, Marbury, T, Fuentes, E, Green, M, Ni, G, Hee, B, and Pithavala, YK. (2011). Influence of mild and moderate hepatic impairment on axitinib pharmacokinetics. *Invest. New Drugs*, 29(6), 1370–1380.

Tse, S, Dowty, ME, Menon, S, Gupta, P, and Krishnaswami, S. (2020). Application of Physiologically Based Pharmacokinetic Modeling to Predict Drug Exposure and Support Dosing Recommendations for Potential Drug-Drug Interactions or in Special Populations: An Example Using Tofacitinib. *J. Clin. Pharmacol.*, 60(12), 1617–1628.

Tsoris, A, and Marlar, CA. (2021). Use Of The Child Pugh Score In Liver Disease. In *StatPearls [Internet]*. http://www.ncbi.nlm.nih.gov/pubmed/31194448

Tucker, g. T, Rostami-hodjegan, A, and Jackson, p. R. (1998). Determination of drug-metabolizing enzyme activity in vivo : pharmacokinetic and statistical issues. *Xenobiotica*, 28(12), 1255–1273.

Verbeeck, RK. (2008). Pharmacokinetics and dosage adjustment in patients with hepatic dysfunction. *Eur. J. Clin. Pharmacol.*, 64(12), 1147.

Verbeeck, RK, and Horsmans, Y. (1998). Effect of hepatic insufficiency on pharmacokinetics and drug dosing. *Pharm. World Sci.*, 20(5), 183–192.

Vilar-Gomez, E, Calzadilla-Bertot, L, Wai-Sun Wong, V, Castellanos, M, Aller-de la Fuente, R, Metwally, M, Eslam, M, Gonzalez-Fabian, L, Alvarez-Quiñones Sanz, M, Conde-Martin, AF, De Boer, B, McLeod, D, Hung Chan, AW, Chalasani, N, George, J, Adams, LA, and Romero-Gomez, M. (2018). Fibrosis Severity as a Determinant of Cause-Specific Mortality in Patients With Advanced Nonalcoholic Fatty Liver Disease: A Multi-National Cohort Study. *Gastroenterology*, 155(2), 443-457.e17.

Wagner, C, Zhao, P, Pan, Y, Hsu, V, Grillo, J, Huang, SM, and Sinha, V. (2015). Application of Physiologically Based Pharmacokinetic (PBPK) Modeling to Support Dose Selection: Report of an FDA Public Workshop on PBPK. *CPT Pharmacometrics Syst. Pharmacol.*, 4(4), 226–230.

Wang, L, Collins, C, Kelly, EJ, Chu, X, Ray, AS, Salphati, L, Xiao, G, Lee, C, Lai, Y, Liao, M, Mathias, A, Evers, R, Humphreys, W, Hop, CECA, Kumer, SC, and Unadkat, JD. (2016). Transporter expression in liver tissue from subjects with alcoholic or hepatitis C cirrhosis quantified by targeted quantitative proteomics. *Drug Metab. Dispos.*, 44(11), 1752–1758.

Wiesner, R, Edwards, E, Freeman, R, Harper, A, Kim, R, Kamath, P, Kremers, W, Lake, J, Howard, T, Merion, RM, Wolfe, RA, and Krom, R. (2003). Model for end-stage liver disease (MELD) and allocation of donor livers. *Gastroenterology*, 124(1), 91–96.

Williams, RL, Upton, RA, Cello, JP, Jones, RM, Blitstein, M, Kelly, J, and Nierenburg, D. (1984). Naproxen disposition in patients with alcoholic cirrhosis. *Eur. J. Clin. Pharmacol.*, 27(3), 291–296.

Yang, LQ, Li, SJ, Cao, YF, Man, XB, Yu, WF, Wang, HY, and Wu, MC. (2003). Different alterations of cytochrome P450 3A4 isoform and its gene expression in livers of patients with chronic liver diseases. *World J. Gastroenterol.*, 9(2), 359–363.

Yim, D-S. (2019). Potency and plasma protein binding of drugs in vitro —a potentially misleading pair for predicting in vivo efficacious concentrations in humans. *Korean J. Physiol. Pharmacol.*, 23(4), 231.

Yin, LK, and Tong, KS. (2009). Elevated Alt and Ast in an Asymptomatic Person: What the primary care doctor should do? *Malaysian Fam. Physician Off. J. Acad. Fam. Physicians Malaysia*, 4(2–3), 98–99.

Younis, IR, Robert Powell, J, Rostami-Hodjegan, A, Corrigan, B, Stockbridge, N, Sinha, V, Zhao, P, Jadhav, P, Flamion, B, and Cook, J. (2017). Utility of Model-Based Approaches for Informing Dosing Recommendations in Specific Populations: Report From the Public AAPS Workshop. *J. Clin. Pharmacol.*, 57(1), 105-109 .

Zeitlinger, MA, Derendorf, H, Mouton, JW, Cars, O, Craig, WA, Andes, D, and Theuretzbacher, U. (2011). Protein binding: do we ever learn? *Antimicrob. Agents Chemother.*, 55(7), 3067–3074.

Zhang, X, Yang, Y, Grimstein, M, Fan, J, Grillo, JA, Huang, S, Zhu, H, and Wang, Y. (2020). Application of PBPK Modeling and Simulation for Regulatory Decision Making and Its Impact on US Prescribing Information: An Update on the 2018-2019 Submissions to the US FDA's Office of Clinical Pharmacology. *J. Clin. Pharmacol.*, 60, S160–S178.

Zhao, P, Zhang, L, Grillo, JA, Liu, Q, Bullock, JM, Moon, YJ, Song, P, Brar, SS, Madabushi, R, Wu, TC, Booth, BP, Rahman, NA, Reynolds, KS, Gil Berglund, E, Lesko, LJ, and Huang, S-M. (2011). Applications of Physiologically Based Pharmacokinetic (PBPK) Modeling and Simulation During Regulatory Review. *Clin. Pharmacol. Ther.*, 89(2), 259–267.

3.12. Supplementary Material

Supplementary Table 3.1. Drugs accepted as new molecular entities (NMEs) during 2016, 2017, 2018, and 2019 without label guidance related to their use in different stages of hepatic impairment (HI).

Year / Population	The number of NMEs with no explicit dosing recommendation in hepatic impairment population			
	2016	**2017**	**2018**	**2019**
Mild HI	7	13	10	15
Moderate HI	6	14	15	20
Severe HI	6	21	28	31
Total number of NMEs approved	15	33	41	38

Supplementary Table 3.2. Model performance of different drugs reported in the literature that have both observed and predicted AUC ratio; AUCR (diseased relative to healthy control) at different stages of hepatic impairment progression.

Drug	Predicted AUCR			Observed AUCR			Predicted / Observed			Reference
	Mild	Moderate	Severe	Mild	Moderate	Severe	Mild	Moderate	Severe	(Johnson, et al., 2010)
Omeprazole infusion	**2.2**	**2.5**	**5.3**	**1.5**	**2**	**2.2**	**1.5**	**1.3**	**2.4**	
Omeprazole oral	**1.7**	**3.5**	**5.8**	**1.8**	**2.5**	**2.8**	**0.9**	**1.4**	**2.1**	
Oral theophylline	**3.8**	N/A	**1.3**	**3**	N/A	**1**	**1.3**	**N/A**	**1.3**	
Carvedilol i.v.	N/A	N/A	**2.1**	N/A	N/A	**1.6**	N/A	N/A	**1.3**	(Rasool, et al., 2017)
Carvedilol oral	N/A	N/A	**7.8**	N/A	N/A	**5.9**	N/A	N/A	**1.3**	
Bosentan	**1.5**	N/A	N/A	**0.9**	N/A	N/A	**1.7**	N/A	N/A	(Li, et al., 2015)
Olmesartan	**1.1**	**1.5**	N/A	**1.1**	**1.2**	N/A	**1**	**1.3**	N/A	
Repaglinide	N/A	**4.9**	N/A	N/A	**4.0**	N/A	N/A	**1.2**	N/A	
Telmisartan	**1.95**	N/A	N/A	**2.7**	N/A	N/A	**0.7**	N/A	N/A	
Valsartan	**1.2**	**1.8**	N/A	**2.2**	**2.1**	N/A	**0.5**	**0.9**	N/A	
Bosutinib	**1.7**	**2.6**	**3.6**	**2.4**	**1.9**	**1.8**	**0.7**	**1.4**	**2**	(Ono, et al., 2017)
Atomoxetine	**N/A**	**4.8**	**10.7**	N/A	**1.7**	**3.7**	N/A	**2.8**	**2.9**	(Huang, et al., 2017)
Simeprevir	**N/A**	**14.5**	**20.5**	N/A	**3.6**	**5.8**	N/A	**4**	**3.5**	(Snoeys, et al., 2017)

Axitinib	**1.3**	**1.52**	N/A	**0.78**	**1.95**	N/A	**1.7**	**0.8**	N/A	(Tortorici, et al., 2011)
Zidavudine	N/A	N/A	**3.6**	N/A	N/A	**3.8**	N/A	N/A	**0.9**	(Prasad, et al., 2018)
Morphine	N/A	N/A	**1.9**	N/A	N/A	**2.4**	N/A	N/A	**0.8**	
Eliglustat	**2.85**	**8.84**	N/A	**2.49**	**8.33**	N/A	**1.1**	**1.1**	N/A	(Li, et al., 2020)
Elagolix	**1.6**	**4.5**	**7.3**	**0.8**	**2.7**	**6.7**	**2**	**1.7**	**1.1**	(Chiney, et al., 2020)
Alectinib	N/A	**2.25**	**2.34**	N/A	**1.7**	**2.14**	N/A	**1.3**	**1.1**	(Morcos, et al., 2018)
Pemafibrate	**2.21**	**5.05**	N/A	**1.8**	**3.7**	N/A	**1.2**	**1.4**	N/A	(Ogawa, et al., 2020)
Rifampicin Profile 1	**0.84**	N/A	N/A	**0.99**	N/A	N/A	**0.8**	N/A	N/A	(Rasool, et al., 2019)
Rifampicin Profile 2	**0.84**	N/A	N/A	**1.67**	N/A	N/A	**0.5**	**N/A**	**N/A**	
Rifampicin Profile 3	**0.83**	N/A	N/A	**0.85**	N/A	N/A	**1**	**N/A**	**N/A**	
Rifampicin Profile 4	**0.98**	N/A	N/A	**1.38**	N/A	N/A	**0.7**	**N/A**	**N/A**	
Tofacitinib	**1.69**	**3.02**	N/A	**1.02**	**1.73**	N/A	**1.7**	**1.7**	**N/A**	(Tse, et al., 2020)

N/A: no data available for the model validation. Grey cells: represents situations in which the predictive performance was poor (> 2 folds Predicted/observed ratio).

Supplementary Table 3.3. Changes in content/expression/abundances of different CYP enzymes in cirrhosis

Enzyme/ isoform	Significant change in Protein abundance level relative to control	Severity of the disease	Method used	Reference
CYP3A4	↓ to 25% in HC & 41% in CHOL	Mixed	Microsomal proteins using gel electrophoresis and immunochemical quantification	(George, et al., 1995b)
	↓ to 53%	Not specified	Microsomal proteins using gel electrophoresis and immunochemical staining	(Guengerich, et al., 1991)
	±	Moderate and severe	Microsomal levels using gel electrophoresis and immunochemical staining	(Lown, et al., 1992)
	↓ to <25%	Severe	LC-MS/MS quantification after isolation of S9 fractions	(Prasad, et al., 2018)
CYP1A2	↓ to 29% in HC & to 18% in CHOL	Mixed	Microsomal proteins using gel electrophoresis and immunochemical quantification	(George, et al., 1995b)
	↓ by 47%	Not specifies	Microsomal levels using gel electrophoresis and immunochemical staining	(Guengerich, et al., 1991)
	↓ to 46%	Moderate and severe	Microsomal levels using gel electrophoresis and immunochemical staining	(Lown, et al., 1992)
	↓ to <25%	Severe	LC-MS/MS quantification after isolation of S9 fractions	(Prasad, et al., 2018)
CYP1A4	↓ to <25%	Severe	LC-MS/MS quantification after isolation of S9 fractions	(Prasad, et al., 2018)
CYP1A6	↓ to <25%	Severe	LC-MS/MS quantification after isolation of S9 fractions	(Prasad, et al., 2018)

CYP2E1	↓ to 41%	Not specified	Microsomal protein content using gel electrophoresis and immunochemical staining	(Guengerich, et al., 1991)
	↓ to 81% in HC & to 49% in CHOL	Mixed	Microsomal proteins using gel electrophoresis and immunochemical quantification	(George, et al., 1995b)
	±	Moderate and severe	Microsomal levels using gel electrophoresis and immunochemical staining	(Lown, et al., 1992)
	↓ to 25-50%	Severe	LC-MS/MS quantification after isolation of S9 fractions	(Prasad, et al., 2018)
CYP2A6	↓ to 25-50%	Severe	LC-MS/MS quantification after isolation of S9 fractions	(Prasad, et al., 2018)
CYP2B7	↓ to <25%	Severe	LC-MS/MS quantification after isolation of S9 fractions	(Prasad, et al., 2018)
CYP2D6	±	Severe	LC-MS/MS quantification after isolation of S9 fractions	(Prasad, et al., 2018)
CYP2C19	±	Not specified	Microsomal proteins using gel electrophoresis and immunochemical staining	(Guengerich, et al., 1991)
	↓ to 57% in HC & 34% in CHOL	Mixed	Microsomal proteins using gel electrophoresis and immunochemical quantification	(George, et al., 1995b)
	↓ to 25-50%	Severe	LC-MS/MS quantification after isolation of S9 fractions	(Prasad, et al., 2018)
CYP2C8	↓ to 55%	Moderate and severe	Microsomal levels using gel electrophoresis and immunochemical staining	(Lown, et al., 1992)
CYP2C9	↓ to 47%	Moderate and severe	Microsomal levels using gel electrophoresis and immunochemical staining	(Lown, et al., 1992)

CYP: Cytochrome P450**, LC-MS**: Liquid Chromatography-Mass spectrometry, ± no change**,** ↓ Significant decrease relative to healthy control, HC: Hepatocellular cirrhosis, CHOL: Cirrhosis with cholestatic origin.

Supplementary Table 3.4. Changes in content/expression/ activities of different Phase II metabolising enzymes in cirrhosis

Enzyme	Significant change in activity	Method used for in-vitro activity	Significant change in abundance/ protein level	Method used for protein quantification	Reference
Glucuronidation (UGT)	--	--	↑ staining in the remaining hepatocytes	Semi-quantitative Immuno-chemical microsomal staining	(Debinski, et al., 1995)
	±	Activity towards 2-naphthol and ethinyloestradiol as substrates	--	--	(Pacifici, et al., 1990)
	±	Hepatic mRNA levels	--	--	(Congiu, et al., 2002)
UGT1A6,UGT1A4,UGT2B7,UGT2B15	± in alcoholic cirrhosis	Hepatic mRNA expression	--	--	(More, et al., 2013)
	--	--	↓ to <25% ↓to 40-50%	LC-MS/MS quantification after isolation of S9 fractions	(Prasad, et al., 2018)
Sulphation SULT	↓ Activity for • Lithocolate to ~45% • Estrone to ~28%	Lithocolate and estrone metabolism were determined in supernatant fractions from PBC patients	--	--	(Iqbal, et al., 1990)
	↓ Activity for • 2-naphthol to ~41% • Ethinylestradiol to ~47%	Activity towards 2-naphthol and ethinyloestradiol as substrates	--	--	(Pacifici, et al., 1990)
	--	--	↓ to (33% - 74%) based on the type of	Quantified DHEA ST in human liver cytosol using a semiquantitative gel	(Elekima, et al., 2000)

			cirrhosis and the method of quantification	electrophoresis (SDS-PAGE)/ immunoblotting method, and ELISA.	
Acetylation	↓ Activity to 22%	Activity towards *p*-aminobenzoic acid	--	--	(Pacifici, et al., 1990)
Glutathione conjugation	↓ Activity to 29%	Activity towards BPO as substrates	--	--	(Pacifici, et al., 1990)
Thiomethylation	↓ Activity to 25%	Activity towards mercaptoethanol	--	--	(Pacifici, et al., 1990)

± No significant change**,** ↓ Significant decrease relative to healthy control, ↑ significant increase relative to healthy control, **DHEA ST**: Dehydroepiandro-steronesulphotransferase, **SDS-PAGE**: sodium dodecyl sulphate/polyacrylamide gel electrophoresis, **ELISA**: enzyme-linked immunosorbent assay. **BPO**: 4,5-dihydro-benzo(a)-pyrene-4,5-oxide.

4 Chapter Four

Scaling Factors for Clearance in Adult Liver Cirrhosis

Declaration

This chapter constitutes a published article.

El-Khateeb, E., Achour, B., Scotcher, D., Al-Majdoub, Z. M., Athwal, V., Barber, J., & Rostami-Hodjegan, A. (**2020**). Scaling factors for clearance in adult liver cirrhosis. *Drug Metabolism and Disposition*, 48(12), 1271-1282.

I carried out the literature search, sourcing the samples, experimental and simulation work, data analysis, statistics and wrote the manuscript. Dr Brahim Achour and Dr Zubida M. Al-Majdoub were consulted on the experimental methodology and data analysis. Dr Daniel Scotcher was consulted on the modelling and simulation part. Dr Varinder Athwal participated in the clinical classification of the samples. Dr Jill Barber and Prof Amin Rostami-Hodjegan provided guidance on the study design and suggested edits to the manuscript. All co-authors edited the manuscript. I retained editorial control.

4.1. Abstract

In-vitro in-vivo extrapolation (IVIVE) enables prediction of *in vivo* clinical outcomes related to drug exposure in various populations from *in vitro* data. Prudent IVIVE requires scalars specific to the biological characteristics of the system in each population. This study determined experimentally, for the first time, scalars in liver samples from patients with varying degrees of cirrhosis. Microsomal and cytosolic fractions were extracted from 13 non-cirrhotic and 32 cirrhotic livers (6 mild, 13 moderate, and 13 severe, based on Child-Pugh Score). Fractional protein content was determined and cytochrome P450 reductase activity was used to correct for microsomal protein loss. Although the median microsomal protein per gram liver (MPPGL) in mild, moderate, and severe cirrhosis (26.2, 32.4, and 30.8 mg/g, respectively) seemed lower than control livers (36.6 mg/g), differences were not statistically significant (Kruskal-Wallis test, $p > 0.05$). Corresponding values for cytosolic protein per gram liver (CPPGL) were 88.2, 67.9, 62.2 and 75.4 (mg/g) for mild, moderate, sever cirrhosis and control livers, respectively, with statistically lower values for server *vs* controls (Mann-Whitney $p = 0.006$). Cirrhosis associated with cancer showed lower MPPGL (24.8 mg/g) than cirrhosis associated with cholestasis (38.3 mg/g, $p = 0.003$). Physiologically-based pharmacokinetic simulations with disease-specific scalars captured cirrhosis impact on exposure to afentanil, metoprolol, midazolam, and ethinylestradiol. These experimentally-determined scalars should alleviate the need for indirect scaling using functional liver volume. Scaling factors in cirrhosis might be a reflection of the aetiology rather than the disease severity. Hence, bundling various cirrhotic conditions under the same umbrella when predicting hepatic impairment impact should be revisited.

4.2. Introduction

Cirrhosis is a histological end-point of most chronic liver diseases. It is characterised by pathological deposition of extra-cellular matrix, fibrosis, and impairments of liver functions, including metabolic activity. Chronic liver disease can be secondary to different aetiologies, such as alcoholic and non-alcoholic fatty livers, chronic biliary disease, viral infections, and other causes. Moreover, most hepatocellular carcinomas arise within chronic liver cirrhosis (Kanda, et al., 2019; Schuppan & Afdhal, 2008). Liver cirrhosis is commonly classified using Child-Pugh Score ranging from A (least severe) to C (most severe), based on synthetic liver function (prothrombin time, albumin, and bilirubin serum levels) and clinical liver function (ascites and encephalopathy scores). This classification gives prognostic information on survival and assessment of disease severity. However, it is not predictive of metabolic capacity for drug hepatic elimination (EMA, 2005; Pugh, et al., 1973), and consequently, may not be useful in predicting the necessary drug dose changes in patients suffering from hepatic impairment.

Physiologically-based pharmacokinetic (PBPK) modelling offers the possibility of model-informed precision dosing (MIPD) in cases where drug label information is not provided for vulnerable patients (Darwich, et al., 2017). To achieve MIPD, PBPK modelling requires information on how systems' parameters change in these special patient populations along with drug-specific parameters. The prediction of *in vivo* hepatic clearance from *in-vitro* data using *in-vitro in-vivo* extrapolation (IVIVE) has been reported to considerably improve drug exposure predictions within PBPK modelling framework (Chen, et al., 2012).

Scaling from *in vitro* enriched sub-cellular fractions, such as microsomes or the cytosol, is common in IVIVE (Houston, 1994). In most cases, these scaling approaches rely on robust estimates of biologically-relevant scaling factors, including protein content of sub-cellular

fractions from the tissue of interest. Microsomal protein per gram liver (MPPGL) for healthy human liver ranges from 32 to 40 mg/g and is commonly used for IVIVE of drug metabolism data (Barter, et al., 2007). Factors such as age and sex that contribute to differences in MPPGL have been highlighted (Barter, et al., 2008). Additional variability in reported values originate from differences in specificities of the markers used for correction for protein loss during the preparation of subcellular fractions and in the design of these studies (Harwood, et al., 2014). Cytochrome P450 content and P450 reductase activity are frequently used as markers for microsomal protein loss (Barter, et al., 2008). Activities of glutathione-S-transferase or alcohol dehydrogenase can be used to estimate loss in cytosolic protein per gram liver, CPPGL (Cubitt, et al., 2011).

Although scaling factors have been reported in human liver samples obtained from healthy individuals and certain patient populations (Barter, et al., 2007; De Bock, et al., 2014), data are lacking for liver cirrhosis, particularly with reference to disease severity (Johnson, et al., 2010) and the cause of cirrhosis. Previous attempts to incorporate fractional protein content in severe cirrhosis compared to healthy livers did not consider any estimate of protein recovery and reported the values in milligrams of microsomal protein while assuming these recoveries to be similar between cirrhotic and non-cirrhotic tissue (Prasad, et al., 2018; Wang, et al., 2016).

Current practice of scaling *in vitro* data for prediction of hepatic clearance in cirrhosis population is based on functional liver mass (Edginton & Willmann, 2008; Johnson, et al., 2010; Prasad, et al., 2018). This empirical parameter is derived using a radio-ligand that binds to a surface antigen on viable cells (Miki, et al., 2001) along with some computed tomography (CT) image processing (Matsui, et al., 1996). It assumes that viable cells in diseased livers retain similar microsomal and cytosolic protein yields as viable healthy hepatocytes (intact cell theory), which has not been confirmed (Morgan & McLean, 1995). Moreover, this assumption does not account for changes in overall liver weight in cirrhosis relative to healthy liver

(Supplementary Table 4.1). At its best, this approach can be considered as an indirect way of estimating scaling factors with no differentiations for various sub-categories of cirrhosis.

Therefore, there is an urgent need for determining cirrhosis-specific MPPGL and CPPGL values that can serve as a biological mean for PBPK-based extrapolation from normal to diseased liver function, thereby enabling model informed dose adjustments for the cirrhosis population. To our knowledge, this is the first report to provide such experimental data which will facilitate accurate prediction of clearance and help in MIPD in cirrhosis populations. It also provides preliminary links between these scalars and disease severity as well as causes/associated diseases with cirrhosis. Applicability of the generated data is demonstrated in PBPK simulations using different probe drugs.

4.3. Methods

4.3.1. Liver Samples and Donor Characteristics

Liver samples, obtained from explanted livers from patients with cirrhosis undergoing liver transplantation or liver resection, were provided by Cambridge University Hospitals (CUH) tissue bank, Cambridge, UK. Cirrhotic (n = 32). Histologically non-cirrhotic/normal control liver tissues were obtained from tissue adjacent to metastatic tumours after surgical liver resection (n =13). Anonymised demographic and clinical data, are provided in Supplementary Table 4.2 and Supplementary Table 4.3. This study is covered by ethical Health Research Authority and Health and Care Research Wales Approval (Research Ethics Committees Reference 18/LO/1969).

The samples were categorised for severity of cirrhosis according to Child-Pugh system using clinical data extracted from the records related to each donor into Child-Pugh A for mild severity (CP-A, n = 6), Child-Pugh B for moderate severity (CP-B, n = 13), Child-Pugh C for severe stage (CP-C, n = 13) (see Supplementary Table 4.3 for details). The power of the study

(80%) had been estimated based on sample size of ≥10 per each group to detect at least a 12 mg/g difference in scalars values (confidence level 95%). The above difference deemed to be of adequate clinical significance. Post-hoc analysis of data (see Results section) indicated that the differences in many cases were lower than the level that we could statistically detect with the current sample size.

The number of cirrhosis liver samples was higher than the control, allowing assessment of hypothesis regarding the possible effect of the aetiology of the disease or co-existing liver conditions on the scalars. Using patient diagnosis data, the samples were further classified into the following groups: cirrhosis associated with cancer, biliary or cholestatic liver disease, and alcoholic and non-alcoholic fatty liver disease (NAFLD).

4.3.2. Preparation of Microsomal and Cytosolic Fractions

Microsomal fractions were isolated from control and cirrhotic liver samples using differential centrifugation (Graham, 2002) (Figure 4.1). Homogenisation of the liver tissue (50-380 mg) was performed on ice using a mechanical homogenizer (CamLab, Cambridge, UK) in potassium phosphate buffer (0.25 M, pH 7.25, and 1.15% KCl) at 10 ml buffer per gram of liver tissue. The homogenate was centrifuged with an Optima^{TM} L-100 ultracentrifuge (Beckman Coulter, Inc., Fullerton, CA) at 10,000 *g* for 20 min at 4°C, and the supernatant (S9 fraction) was retained and centrifuged at 100,000 *g* for 75 min at 4°C. The supernatant (cytosol) was retained and the microsomal pellet was suspended at 1 ml of storage buffer (0.25 M potassium phosphate, pH 7.25) per gram of liver tissue. Homogenate, cytosol and microsomal fractions from each sample were stored at -80°C.

4.3.3. Determination of the Total Protein Content

Protein content in all fractions was determined using bicinchoninic acid (BCA) assay (Pierce® Microplate BCA Protein Assay Kit – Reducing Agent Compatible). Each sample fraction was

assessed in triplicate and the mean of the three readings was calculated. The protein concentrations of each fraction were used to determine the amount of protein per gram liver, as described below.

4.3.4. NADPH Cytochrome P450 Reductase Activity

MPPGL was corrected for loss due to centrifugation based on cytochrome P450 reductase activity, a marker of microsomal membrane. The choice of the activity assay compatible with bilirubin was necessary because a subset of the samples were from patients with biliary disease. Bilirubin shows absorption at 453 nm (Vreman, et al., 2019), which interferes with the absorbance results of the dithionite difference method obtained at 450 nm (De Bock, et al., 2014). The NADPH cytochrome P450 reductase (NADPH-P450 reductase) method relies on measurement of absorbance at a different wavelength (550 nm) and was therefore preferred (Matsubara, et al., 1976; Omura & Sato, 1964), and was used as previously described (Achour, et al., 2011; Guengerich, et al., 2009). Briefly, microsomal or homogenate fraction from 1 mg of tissue was mixed in 1.5 ml cuvette with 80 µl of 0.5 mM oxidised equine cytochrome c (Sigma-Aldrich, Poole, UK), 900 µl of potassium phosphate buffer and 10 µl of 1 mM potassium cyanide. Baseline absorbance was measured at 550 nm using the kinetic mode of a Jenway 7315 UV-Visible spectrophotometer (Camlab Ltd., Cambridge, UK) every 20 seconds for 2 min The reaction was started by adding 10 µl of 10 mM NADPH and the absorbance (A) was measured every 20 seconds for 3 min. The activity of NADPH-P450 reductase represented in units per millilitre of the fraction (homogenate or microsome) was determined by calculating the slope of the linear phase of the curve after the addition of NADPH and applying the following equation.

$$\text{Units/mg tissue} = \frac{\Delta A_{550}/\min \times dil \times Reaction\ volume\ in\ ml}{21.1 \times Enzvol} \quad (1)$$

Where one unit will reduce 1 µmol of oxidised cytochrome c in the presence of 100 µM NADPH per minute at pH 7.8 at 25ºC; $\Delta A_{550}/min$ = the rate of change in the absorbance at 550 nm = $\Delta A_{sample} - \Delta A_{blank}$; *dil* is the dilution factor of the original enzyme sample; *Enzvol* is the volume of the sample equivalent to 1 mg of tissue (millilitre) and 21.1 is the extinction coefficient (ε^{mM}) for reduced cytochrome c.

The ratio of the microsomal slope to the homogenate slope per gram of tissue indicates the fraction of recovered microsomal protein and is used to correct MPPGL values for each individual liver sample (Eq. 2; Figure 4.1) (Barter, et al., 2008).

$$\text{MPPGL (mg/g)} = \frac{Protein\ content\ in\ mg\ per\ g\ of\ tissue}{Recovery\ factor} \qquad (2)$$

The ratio of the slopes of the microsomes and the homogenate per 1 mg total protein was used to calculate enrichment in the microsomal fraction.

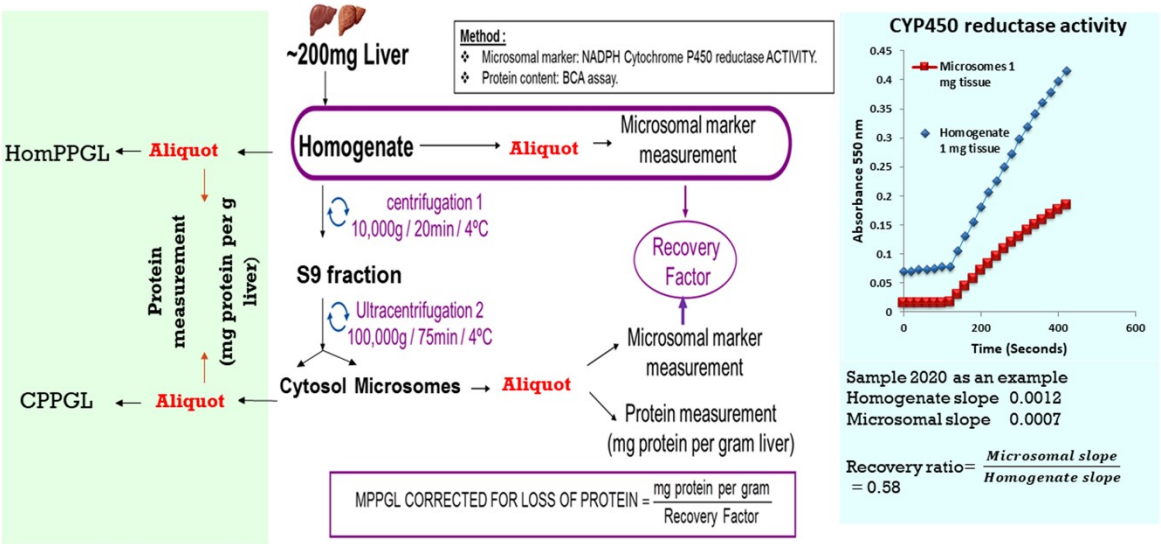

Figure 4.1. Preparation of sub-cellular fractions from liver tissue samples. Microsomal protein loss is estimated by cytochrome P450 reductase activity to correct microsomal protein per gram liver (MPPGL). CPPGL and HomPPGL are the uncorrected cytosol and homogenate protein contents per gram of liver, respectively.

4.3.5. Assessing the Effect of Disease Severity and Aetiology or Underlying Liver Conditions with Cirrhosis

The median values of the scalars (MPPGL, CPPGL, and homogenate protein per gram of liver/HomPPGL) from six mild, 13 moderate and 13 severe cirrhosis samples were compared with the control set (n = 13). Further, the cirrhotic samples were stratified according to co-existing liver diseases into four different groups: NAFLD (n = 8), hepatocellular carcinoma (HCC, n = 9), alcoholic liver injury (n = 2), and biliary disease or cholestasis (n = 13). The MPPGL and CPPGL values in these different groups were compared against one another and to normal controls.

4.3.6. Statistical Data Analysis

Statistical analysis of the data was carried out and graphs were created using GraphPad Prism version 7.0 (La Jolla, California USA). Shapiro-Wilk normality test was applied to assess normality of distribution of the data. Data sets with *p values* >0.05 were considered to be normally distributed.

For reporting NADPH-P450 reductase activities, mean ± SD was used as normal distribution was confirmed in all groups. For all other data, in the absence of normal distribution, non-parametric statistics were used, and results were presented as median and 95% confidence interval (CI). Equality of variance was assessed by a modified Levene's test (Brown-Forsythe test) at 0.05 significance level.

The differences in median values of MPPGL and CPPGL between the control group and the three levels of disease severity (mild, moderate, and severe) were assessed using Kruskal-Wallis ANOVA test with statistical significance level set at 0.05. If this test indicated statistically significant differences, post hoc Mann-Whitney test was performed for all pairwise comparisons with statistical significance considered after Bonferroni correction at $*p < 0.0085$

and $^{**}p < 0.0017$ (six iteration). Similarly, Kruskal-Wallis test and Mann-Whitney tests with Bonferroni correction were performed to compare the data for the control group and four different underlying disease states. For post hoc analysis in this case, $^{*}p < 0.005$ and $^{**}p < 0.001$ were considered statistically significant (10 iteration).

Mann-Whitney test was performed at a 0.05 significance level to compare MPPGL and CPPGL values between male and female donors within either control or disease groups. Correlation with age of the donors was assessed using Spearman correlation test.

4.3.7. PBPK Simulations to Assess the Impact of Scalars for Cirrhotic Liver

PBPK simulations were performed to assess the impact of the experimentally determined scalars on drug exposure. Substrates predominantly metabolised by the liver were selected. Three cytochrome P450 (CYP) substrates with different hepatic extraction ratios (ERs)- namely, alfentanil (low ER), metoprolol (high ER) and midazolam (intermediate ER)- were selected from the compound library in Simcyp® Simulator V18 Release 1 (Certara, Sheffield, UK) to compare the impact of three different methods of scaling on their predicted clearance and exposure. No modifications were made to metoprolol and midazolam compound files. However, for alfentanil, the full PBPK distribution model recently described and verified in healthy adults by Abduljalil et al., (2020) was used (See supplementary information for more details).Alfentanil is mainly metabolised by CYP3A4, midazolam is a substrate of CYP3A4 and uridine diphosphate (UDP)-glucuronosyltransferase (UGT) 1A4, whereas metoprolol is mainly metabolised by CYP3A4/2D6. All these enzymes are microsomal.

Firstly, the model was validated in healthy population then extrapolated to cirrhosis populations using three different methods of scaling (Figure 4.2).

Method 1 (CS; Cirrhosis-specific scalar, no liver size adjustment) uses cirrhosis-specific scaling factor values (MPPGL) from the current study and normal liver volume (1.65 L).

Method 2 (CS+SA; Cirrhosis-specific scalar +whole liver size adjustment) uses cirrhosis-specific scaling factor values (MPPGL) from the current study and the average liver volume corresponding to each Child-Pugh grade (1.04 fold of normal liver volume for CP-A, 0.87 of normal liver volume for CP-B, 0.68 of normal liver volume for CP-C) (Ozaki, et al., 2016).

Method 3 (EFLV; Empirical functional liver volume + scalars from healthy population) uses Equation 3 below from Barter et al., (2008) that describes relationship between MPPGL and age (in years) in healthy subjects, and accounts for the change in the functional hepatocyte volume as a reflection of the functional reserve of the liver (1.469 L for CP-A, 1.17 L for CP-B, and 0.94 L for CP-C). These functional hepatocyte volumes are implemented into the simulator according to unpublished meta-analysis of tissue imaging literature data (Li, 2003; Lin, et al., 1998; Reddy, et al., 2018; Shan, et al., 2005; Zhu, 1999).

$$\text{MPPGL (mg/g)} = 10^{(C0 + C1*age + C2*age^2 + C3*age^3)} \quad (3)$$

Where, *C0* = 1.407, *C1* = 0.0158, *C2* = -0.00038, *C3* = 0.0000024.

For Methods 1 and 2, the coefficients of variation (CV) in MPPGL for mild, moderate, and severe cirrhosis populations were calculated from the SD and mean for CP-A, and CP-B groups in this study; for Method 3, the CV was 26.9% (Barter, et al., 2008).

To assess the impact of change in the CPPGL on drug exposure, ethinylestradiol was selected from Simcyp compound files library as a substrate of both microsomal enzymes (mainly CYP3A4, 2C9, and 1A2 and UGT1A1), and a cytosolic sulfotransferase 1E1 (SULT1E1) (Zhang, et al., 2007). The compound file supplied with the software was altered to allow inclusion of cytosolic elimination (Supplementary Table 4.6). All hepatic intrinsic clearance other than those for CYPs and UGTs were assumed to be cytosolic (by SULT1E1). So, the additional human liver microsomal (HLM) clearance obtained from back-calculation from the intravenous clearance via the well-stirred liver model and reported by Ezuruike et al., (2018)

were converted to human liver cytosol (HLC) intrinsic clearance after the correction with relative ratio of healthy MPPGL to healthy CPPGL values.

The three cirrhosis scaling methods mentioned above were also applied for ethinylestradiol in addition to using the current study's median CPPGL and CV values corresponding to each CP group in Methods 1 and 2. The mean (CV) CPPGL for a healthy virtual population of 81.03 mg/g (21.47%) (Mallick, et al., 2020) was applied in the healthy population simulations and in scaling Method 3 for the cirrhosis populations.

The demographic, anatomic, and physiologic parameters that were used in the creation of virtual populations (healthy and disease) were based on Simcyp population libraries with no change apart from the scaling parameters illustrated above for the three methods (Supplementary Table 4.9). Simulations of virtual or mixed virtual populations were performed with 10 trials. The number of subjects in each trial, age range and proportion of females were consistent with clinical studies with the drugs from which observed data were derived (Supplementary Table 4.5). For all models, non-specific binding in microsomes or hepatocytes from diseased livers were assumed to be similar to healthy livers. In the case of ethinylestradiol, no clinical data were available for the cirrhosis groups; therefore, a trial design of 10 subjects per trial, age range 21-23 years, and 100% females was used. The arithmetic mean of plasma concentration-time profile for the 10 trials per simulation was plotted using Microsoft Excel. The average $AUC_{0\text{-}t}$ of the 10 simulation trials for each simulation method was calculated for each drug using the linear trapezoidal method. Average AUC_{∞} was used only for metoprolol to allow comparison with clinical data.

Predictions within 1.5-fold range of the observed AUC were considered acceptable for both healthy and cirrhosis simulations. The ratios of AUC in the cirrhosis population to the AUC in healthy population (AUCR) was reported for each scaling method. Then, the ratio of predicted

AUCR to the observed AUCR (AUCR_pred/AUCR_obs) was calculated to evaluate the ability of the model to capture the disease effect (Figure 4.2). Any difference in the predicted cirrhosis AUC values less than 25% between different scaling methods was considered negligible. Doses similar to those used in the corresponding clinical studies were chosen for alfentanil, metoprolol, and midazolam simulations (Supplementary Table 4.5). Input parameters for each drug are reported in Supplementary Table 4.6.

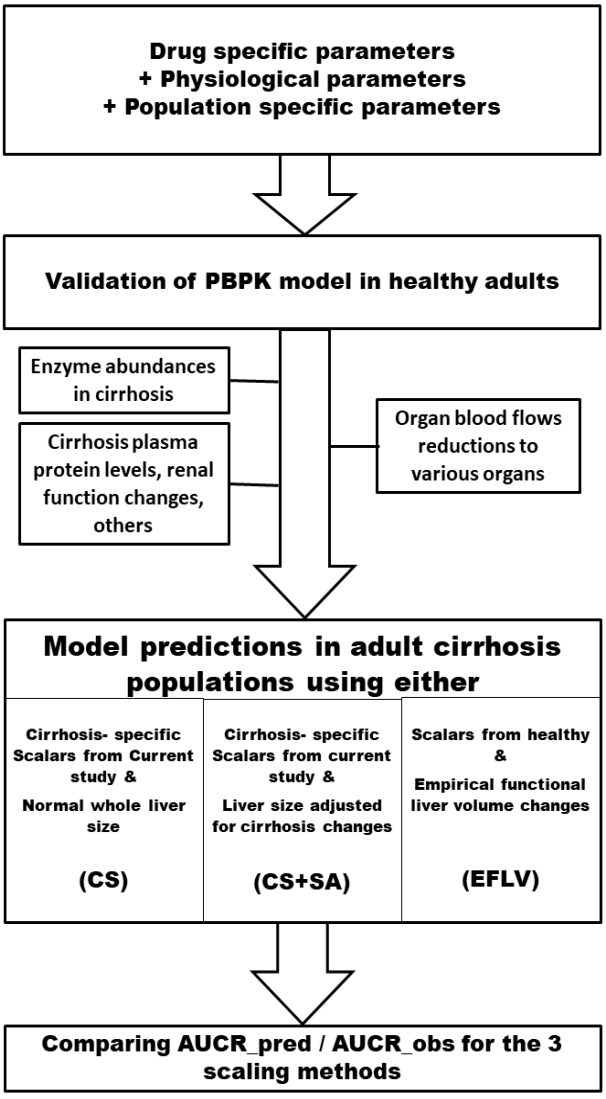

Figure 4.2. A Schematic illustration showing the workflow of PBPK simulations for alfentanil, midazolam, metoprolol and ethinylestradiol to validate the simulator's built-in model and extrapolate to cirrhosis populations using empirical scaling with functional liver

volume compared to scaling with current study cirrhosis-specific scalars (MPPGL/CPPGL). AUCR; ratio of area under the plasma concentration-time curve in cirrhosis relative to healthy population.

4.4. Results

In this study, homogenate, microsomal, and cytosol protein concentrations were measured in relevant fractions from healthy livers (n = 13) and in livers with varying degrees of cirrhosis (n = 32) (Supplementary Table 4.7). The median and range of the uncorrected protein contents per gram tissue for each fraction (microsomes, cytosol, and homogenate) in control and cirrhotic groups were calculated based on measured concentrations as shown in Supplementary Table 4.8.

4.4.1. Recovery and Enrichment of Microsomal Fractions

Cytochrome P450 reductase activity in homogenate and microsomal fractions were measured for each sample (Supplementary Table 4.4). Data for all groups (control as well as mild, moderate, and severe cirrhosis) showed normal distribution (p >0.05 with Shapiro-Wilk normality test). The mean ± SD of activity in homogenate fraction for the control group was 3.4 ± 1.13 units/mg of tissue, and it decreased in mild, moderate, and severe cirrhosis (2.3±0.34, 2.7±0.95, and 2±0.66 units/mg of tissue, respectively). The recovery and enrichment ratios were measured based on P450 reductase activity using the ratio of the slope associated with the microsomal fraction to the slope for the homogenate corresponding to 1 mg of tissue or 1 mg of total protein, respectively, for each individual sample. Recovery ratios ranged from 20 to 90% (mean of 50.8%), whereas the enrichment factor ranged from 1.6- to 9.0-fold (mean ~3.0-fold).

4.4.2. MPPGL and CPPGL Values for Control and Cirrhosis Samples

MPPGL values for the control group did not show normal distribution (Shapiro-Wilk test, $p = 0.005$). Similarly, CPPGL data for the CP-C group, NAFLD, and cholestasis-associated cirrhosis groups were not normally distributed ($p < 0.01$). Therefore, non-parametric statistics were applied for all comparisons. Using Brown-Forsythe test, MPPGL and CPPGL values among all groups with different Child-Pugh scores and causes of disease showed homogeneity of variance ($p > 0.05$), and accordingly, Kruskal-Wallis and post hoc Mann-Whitney tests were used for comparison between groups.

Although median MPPGL values in all three cirrhosis groups were lower compared to the control group (Figure 4.3), these were not statistically significant (Kruskal-Wallis test, $p = 0.054$).

Median MPPGL values in the disease sets were 26.2 (95% CI 12.9- 42.2 mg/g), 32.4 (95% CI 24.8- 42.4 mg/g), and 30.8 (95% CI 25.1- 38.3 mg/g) for mild, moderate, and severe cirrhosis, respectively, compared to 36.6 (95% CI 33- 49.5 mg/g) for the control group.

There was an apparent gradual decrease in median CPPGL with increasing disease severity. Kruskal-Wallis ANOVA test showed a significant difference among the four groups ($p = 0.008$). CPPGL median values were 88.2 (95% CI 61.4- 105.5 mg/g; $p = 0.28$) and 67.9 (95% CI 58.3- 76.9 mg/g; $p = 0.07$) in the mild and moderate cirrhosis groups, respectively, compared to 75.4 (95% CI 63.2- 89.5 mg/g) for the control group. The CPPGL median value for severe cirrhosis group was 62.2 (95% CI 58.1- 64.9 mg/g), which was significantly lower than the control group ($p = 0.006$ *). The CPPGL median values of the three groups of cirrhosis were not significantly different from each other ($p > 0.0085$).

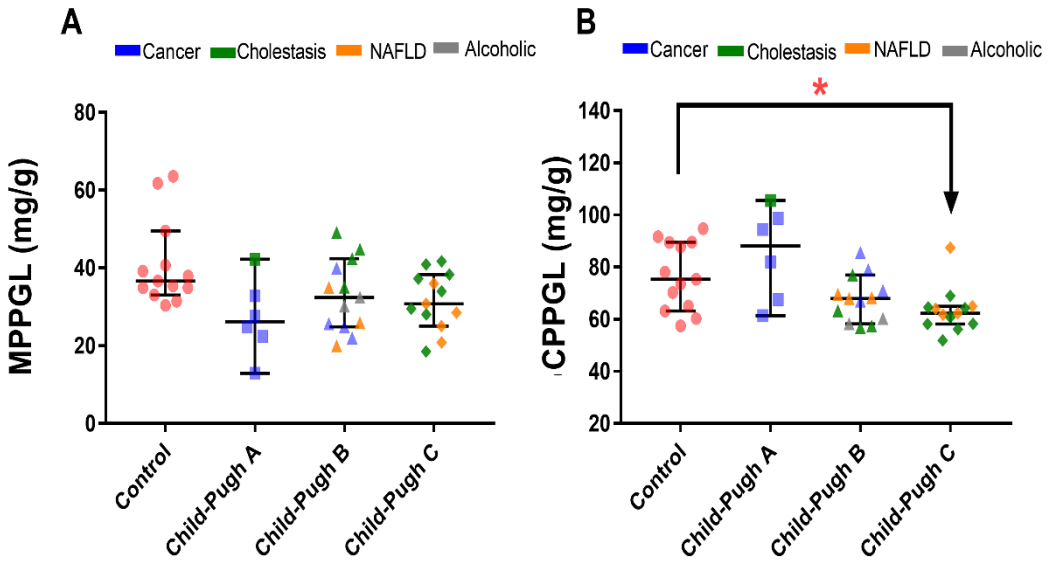

Figure 4.3. Protein content per gram of liver for microsomal (A) and cytosolic (B) fractions (MPPGL and CPPGL) for samples from control, mild cirrhosis (Child-Pugh A), moderate cirrhosis (Child-Pugh B), and severe cirrhosis (Child-Pugh C) groups. Horizontal lines represent median values, and error bars represent 95% confidence intervals. The asterisk (*) represents a statistically significant difference in the median of the severe cirrhotic group relative to control determined (Mann-Whitney test, p = 0.006). For cirrhosis groups, different symbols refer to different disease severities, and different colours refer to the primary concomitant liver disease. NAFLD, non-alcoholic fatty liver disease.

4.4.3. Effects of Underlying Liver Disease on Scaling Factors

MPPGL and CPPGL were compared for different groups of samples classified according to the most likely cause of liver cirrhosis and/or coexisting disease conditions related to cirrhosis (Figure 4.4). Kruskal-Wallis test showed significant differences in median MPPGL values among all groups ($p = 0.001$).

Cirrhosis groups associated with NAFLD and cancer showed significantly lower median MPPGL values of 27.2 (95% CI 20- 36 mg/g; p value of Mann-Whitney test compared to control = 0.003*), and 24.8 (95% CI 22- 32.8 mg/g; p = 0.0009 **), respectively (Figure

4.4 A), compared to control group median MPPGL at 36.6 (95% CI 33- 49.5 mg/g), whereas MPPGL for cirrhosis with cholestasis and alcoholic liver was comparable to the control groups with median values of 38.3 (95% CI 29.5- 42.4 mg/g; p = 0.96), and 31.3 mg/g (95% CI 30.2- 32.4 mg/g; p = 0.08), respectively.

Among cirrhosis groups, only cancer-associated cirrhosis showed statistically significant lower median MPPGL compared to cholestasis-cirrhosis group (p = 0.003*).

Although Kruskal-Wallis test showed p *value* = 0.009 (<0.05), Mann-Whitney pairwise comparisons with Bonferroni correction showed no significant differences in median CPPGL values among all groups. CPPGL median values for cirrhosis groups associated with cholestasis, NAFLD, alcoholic liver injury, and cancer were 60.7 (95% CI 56.7- 68.9 mg/g; p = 0.01), 66.4 (95% CI 61.7- 87.5 mg/g; p = 0.12), 59.3 (95% CI 58.3- 60.2 mg/g; p = 0.08), 78.9 (95% CI 66.9- 94.4 mg/g; p = 0.74), respectively (Figure 4.4 B), compared to the control group at 75.4 (95% CI 63.2- 89.5 mg/g).

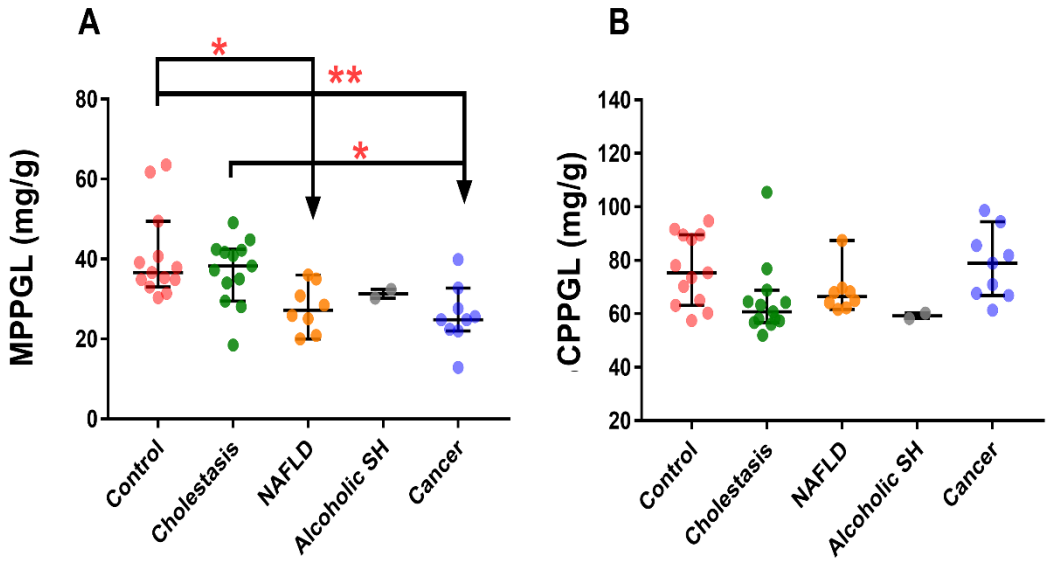

Figure 4.4. Differences in median MPPGL (A) and CPPGL (B) values between groups of cirrhotic livers with different underlying pathologies and associated diseases. Cholestasis,

cirrhosis with any biliary/cholestatic liver disease; NAFLD, cirrhosis with non-alcoholic fatty liver disease; Alcoholic SH, cirrhosis with alcoholic steatohepatitis; Cancer, cirrhosis with hepatocellular carcinoma. Horizontal lines represent median values and error bars represent 95% confidence intervals. *, and ** represent statistically significant differences between different groups at $p < 0.005$, and $p < 0.0025$, respectively.

4.4.4. Impact of Demographics on Scaling Factors

Among the 13 histologically normal liver samples, four were from female donors. The age range of all control liver donors was from 36 to 83 years, with a median age of 71 years. For the 32 cirrhosis livers, the median age of donors was 61 years (from 39 to 75 years), and 13 were females (Supplementary Table 4.2 and Supplementary Table 4.3).

Non-parametric Spearman correlation between age and MPPGL or CPPGL in both control and diseased groups was weak (Rs = -0.11 and -0.40 for the control group and 0.02 and 0.20 for the diseased group, respectively, $p > 0.05$). Differences in MPPGL and CPPGL values between males and females were not significant in control or disease groups (Mann-Whitney test, $p > 0.05$).

4.4.5. Comparison of Scaling in the Current Study with Previous Scaling Methods

Previous scaling methods (Edginton, et al., 2008; Johnson, et al., 2010; Prasad, et al., 2018) used the difference in functional liver volume because of unavailability of experimental MPPGL values for cirrhosis populations (Supplementary Table 4.1). For MPPGL-based scaling methods, the ratios of the scalars from the current study relative to control were comparable to corresponding ratios with the functional liver volume especially for moderate and severe cirrhosis populations (Table 4.1).

Table 4.1. Comparing MPPGL-based scaling factors for mild, moderate, and severe cirrhosis relative to control from the current study with empirical scaling methodology

Population	Scalar from the current study (MPPGL_Population × Total liver volume_Population*) Relative to healthy population	Empirical scalar (Healthy MPPGL × Functional liver volume_population) Relative to healthy population		
		(Johnson, et al., 2010)	Simcyp V18 & V19**	Simcyp V20**
Healthy	**1**	**1**	**1**	**1**
Cirrhosis Child-Pugh A	**0.74**	**0.81**	**0.89**	**0.86**
Cirrhosis Child-Pugh B	**0.77**	**0.65**	**0.71**	**0.71**
Cirrhosis Child-Pugh C	**0.57**	**0.53**	**0.61**	**0.59**

*From (Ozaki, et al., 2016), ** Unpublished meta-analyses of literature functional liver volume data from imaging techniques (Li, 2003; Lin, et al., 1998; Reddy, et al., 2018; Shan, et al., 2005; Zhu, 1999) via personal communication with Trevor Johnson, Simcyp, Sheffield, UK.

4.4.6. PBPK Simulations Using the Measured Scaling Factors

Figure 4.5 shows alfentanil simulations in healthy population and in mixed virtual cirrhosis populations (CP-A, one individual; CP-B, seven individuals; CP-C, three individuals). In cirrhosis simulations, the three scaling methods were applied and compared. The three methods showed average $AUC_{0\text{-}10h}$ within 1.5-fold of observed values obtained from a previous study (Ferrier, et al., 1985) (Figure 4.5, and Table 4.2). The relative difference in AUCR_pred/AUCR_obs ratio among all simulations with the three different scaling methods did not exceed 17% (Table 4.2).

Table 4.2. Measures of alfentanil model predictive performance in healthy and cirrhosis populations using three in-vitro in-vivo clearance scaling methods after a single 0.05 mg/kg intravenous bolus dose.

Population (method of scaling)	AUC_pred (ng.h/ml)	AUC_Obs (ng.h/ml)*	Model predictability of disease impact AUCR_pred /AUCR_obs
Healthy	296	269	NA

Cirrhosis A, B, and C (CS)	499	521	0.87
Cirrhosis A, B, and C (CS+SA)	545	521	0.95
Cirrhosis A, B, and C (EFLV)	586	521	1.02

A, B, and C refer to a mixed population with different Child-Pugh scores; AUCR_pred/AUCR_obs, A ratio representing model predictability of disease impact; CS, Cirrhosis population-specific scalar from current study and normal liver size; CS+SA, Cirrhosis population-specific scalar + liver size adjustment; EFLV, Empirical functional liver volume with scalars from healthy population; AUCR, $AUC_{cirrhosis}/AUC_{healthy}$; pred, Predicted value from the simulation. *The observed values were derived from (Ferrier, et al., 1985). NA; Not applicable.

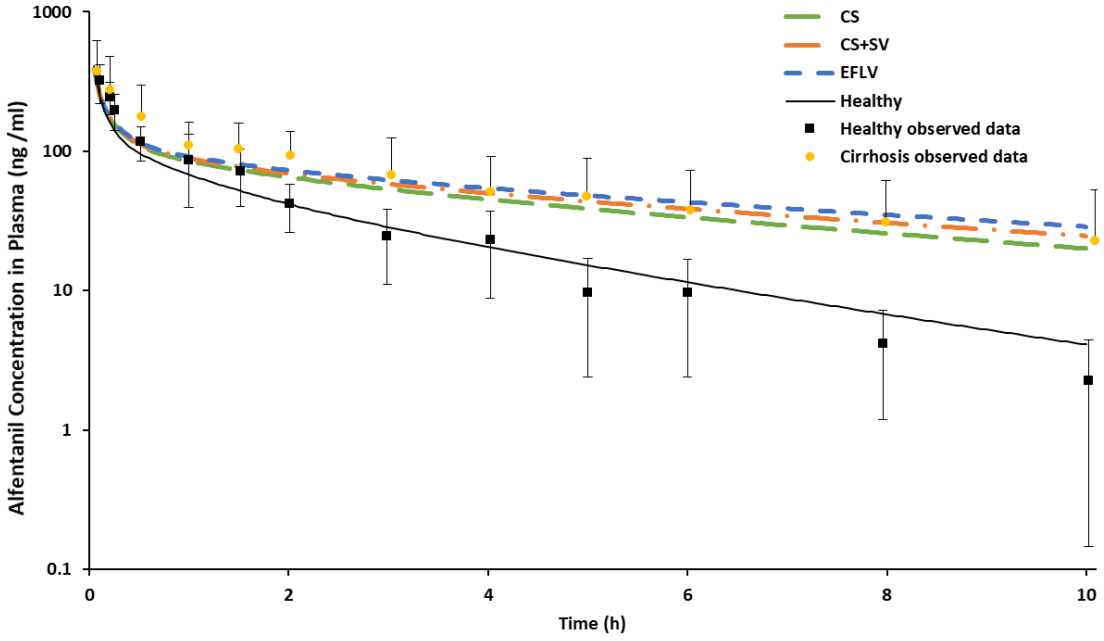

Figure 4.5. Alfentanil plasma concentration-time profile following a single 0.05 mg/kg intravenous bolus dose in healthy (black line) and cirrhosis populations (coloured dashed lines) with three different in-vitro in-vivo scaling methods (CS, Cirrhosis population-specific scalar from the current study + normal liver size; CS+SA, Cirrhosis population-specific scalar + liver size adjustment; EFLV, Empirical functional liver volume with scalars from healthy population). Symbols represent observed clinical data from healthy individuals and

cirrhosis patients (mixed CP-A, -B, and -C) (Ferrier, et al., 1985). Error bars represent the standard deviation from the mean observed data.

For metoprolol, the predicted $AUC_{0-\infty}$ for healthy populations was within 1.5 fold of the corresponding observed value from a previous study (Regårdh, et al., 1981). Regårdh, et al. also reported metoprolol pharmacokinetic data for patients with cirrhosis, although there were no specific data in this report on the Child-Pugh score for these cirrhotic individuals. Therefore, simulations for mild, moderate, and severe cirrhosis were performed separately with the three scaling methods, and each was compared with the clinical data of Regårdh, et al., (1981) (Figure 4.6). For the mild cirrhosis population only, the AUCR_pred/AUCR_obs ratio was close to unity; the difference in these ratios were less than 8% for the three methods of scaling (Table 4.3). For moderate and severe populations, the CS method showed modest deviations in relative disease impact factor from CS+SV (9% and 20%, respectively) and EFLV (19% and 25%, respectively) methods. Scaling with the CS+SA method showed comparable predictability to EFLV method, with differences within 15% in all degrees of the disease severity.

Table 4.3. Measures of metoprolol model predictive performance in healthy and cirrhosis populations using three in-vitro in-vivo clearance scaling methods after intravenous infusion with 20 mg metoprolol tartrate over 10 min.

Population/ method of scaling		**AUC_pred (ng.h/ml)**	**AUC_Obs* (ng.h/ml)**	**Model predictability of disease impact AUCR_pred/AUCR_obs**
Healthy		363	379	NA
Cirrhosis CP-A	CS	743	697	1.11
	CS+SA	725		1.09
	EFLV	689		1.03
Cirrhosis CP-B	CS	1056		1.58
	CS+SA	1148		1.72
	EFLV	1318		1.97
	CS	1907		2.85

Cirrhosis CP-C	CS+SA	2389		3.58
	EFLV	2538		3.8

AUCR, AUC_cirrhosis/AUC_healthy; pred, Predicted value from the simulation; AUCR_pred/AUCR_obs, A ratio representing model predictability of disease impact; * obs, The observed value for both healthy and cirrhosis groups (one value for all diseased groups as there was no information on the Child-Pugh grade) were derived from (Regårdh, et al., 1981); CS, Cirrhosis population-specific scalar from current study and normal liver size; CS+SA, Cirrhosis population-specific scalar + liver size adjustment; EFLV, Empirical functional liver volume with scalars from healthy population; NA, Not applicable.

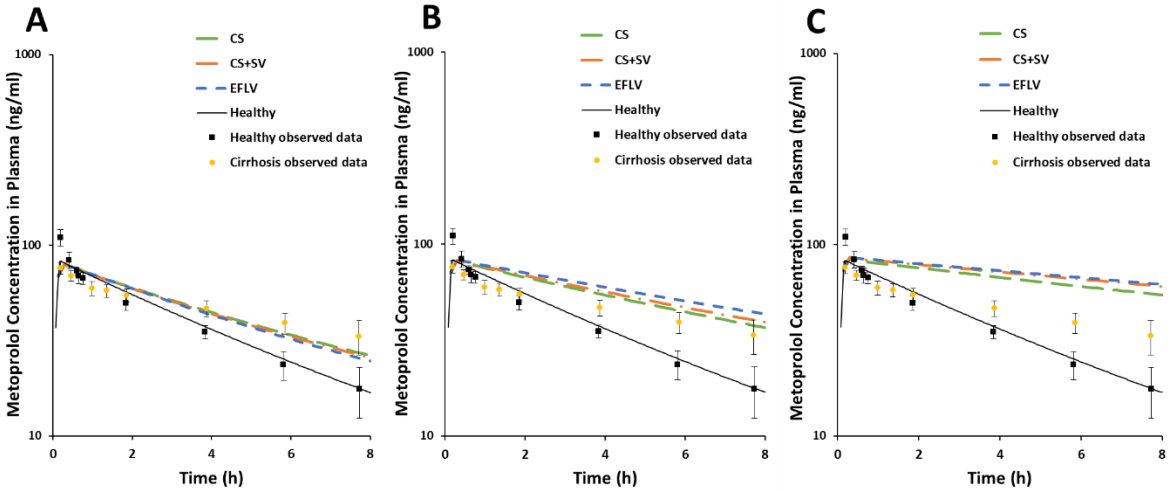

Figure 4.6. Metoprolol plasma concentration-time profiles after intravenous infusion in healthy (black line) versus (A) Child-Pugh A, (B) Child-Pugh B, (C) Child-Pugh C cirrhosis populations (coloured dashed lines) with three different in-vitro in-vivo scaling methods (CS, Cirrhosis population-specific scalar from current study and normal liver size; CS+SA, Cirrhosis population-specific scalar + liver size adjustment; EFLV, Empirical functional liver volume with scalars from healthy population). Symbols represent observed clinical data from healthy individuals and cirrhosis patients (Regårdh, et al., 1981). Error bars represent the standard deviation from the mean observed data.

Good predictive performance of the PBPK model was also noted for midazolam, in both healthy and cirrhosis populations (within 1.5 fold of the observed $AUC_{0\text{-}24h}$ values), for

intravenous and oral routes of administration (Figure 4.7). The clinical data derived from a previous study (Pentikäinen, et al., 1989) represented a mixed cirrhosis population consisting of both CP-B (n = 5) and CP-C (n = 2) patients. The differences in AUCR_pred/AUCR_obs among the three methods were within 20% for both intravenous and oral dosing (Table 4.4).

Table 4.4. Measures of midazolam model predictive performance in healthy and cirrhosis populations using three in-vitro in-vivo clearance scaling methods after single intravenous bolus and oral doses.

Population (method of scaling)	**Intravenous bolus (7.5 mg single dose)**			**Oral (15 mg single dose)**		
	AUC_pred (ng.h/ml)	AUC_Obs (ng.h/ml)	AUCR_pred /AUCR_obs	AUC_pred (ng.h/ml)	AUC_Obs (ng.h/ml)	AUCR_pred /AUCR_obs
Healthy	303	298	NA	347	362	NA
Cirrhosis CP-B & C (CS)	522	543	0.95	522	576	0.95
Cirrhosis CP-B & C (CS+SA)	589	543	1.07	621	576	1.12
Cirrhosis CP-B & C (EFLV)	631	543	1.14	629	576	1.14

AUCR, AUC_cirrhosis/AUC_healthy; pred, The predicted value from the simulation; obs, The observed value from the clinical study (Pentikäinen, et al., 1989); AUCR_pred/AUCR_obs, A ratio representing model predictability of disease impact; CS, Cirrhosis population-specific scalar from current study and normal liver size; CS+SA, Cirrhosis population-specific scalar + liver size adjustment; EFLV, Empirical functional liver volume with scalars from healthy population; NA, Not applicable.

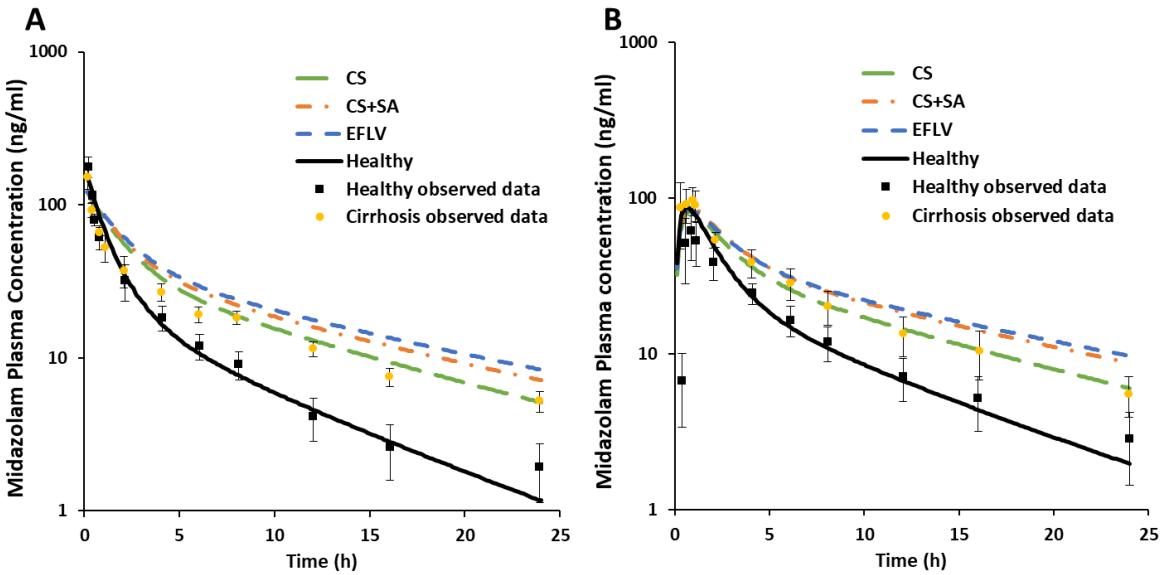

Figure 4.7. Intravenous (A) and oral (B) observed and simulated midazolam plasma concentration-time profiles in in healthy (black line) and cirrhosis populations (coloured dashed lines) with three different in-vitro in-vivo scaling methods (CS, Cirrhosis population-specific scalar from the current study and normal liver size; CS+SA, Cirrhosis population-specific scalar + liver size adjustment; EFLV, Empirical functional liver volume with scalars from healthy population). Symbols represent observed clinical data from healthy individuals and cirrhosis patients (mixed CP-B and -C) (Pentikäinen, et al., 1989). Error bars represent the standard deviation from the mean observed data.

Overall for MPPGL, at high severities of cirrhosis, the CS scaling method showed the highest predicted clearance compared to other scaling methods for all drugs evaluated, whereas EFLV showed the lowest predicted clearance. The CS+SV method was closer to EFLV scaling method than CS method in all scenarios. Nevertheless, these differences were effectively negligible (<25%).

For ethinylestradiol, simulations were run with a single oral dose (0.05 mg) in healthy and mild, moderate, and severe cirrhosis populations. In the healthy population, the predicted $AUC_{0\text{-}24}$ was within 1.5 fold of observed values derived from previous study (Back, et al., 1979). Predicted $AUC_{0\text{-}24}$ (AUC_pred) was 1.03 ng.h/ml (95% CI 1.01- 1.06 ng.h/ml).

AUC_obs in healthy populations was 1.048 ng.h/ml (95% CI 0.564- 1.53 ng.h/ml). Because of the lack of clinical data for single oral ethinylestradiol dosing in cirrhosis populations, only the simulations for the cirrhosis populations were presented in this study (Figure 4.8, and Table 4.5). The differences in the predicted AUCR for the CS and CS+SV methods of scaling relative to the EFLV method were 40% and 2% in mild, 8% and 1.4% in moderate, and 12.1% and 12.4% in severe cirrhosis (Figure 4.8, and Table 4.5). The exposures predicted by CS+SA and EFLV methods were comparable, with lower differences than the CS method in all cirrhosis populations (Table 4.5).

Table 4.5. Differences in the predicted impact of cirrhosis on ethinylestradiol exposure between three in-vitro in-vivo clearance scaling methods after 0.05 mg single oral dose.

Population /Method of scaling		**AUC_pred (ng.h/ml)**	**% difference in disease**
Healthy		1	NA
Cirrhosis CP-A	CS	2.2	40%
	CS+SA	1.6	2%
	EFLV	1.6	NA
Cirrhosis CP-B	CS	1.6	8%
	CS+SA	1.8	1%
	EFLV	1.8	NA
Cirrhosis CP-C	CS	37	12%
	CS+SA	51	12%
	EFLV	48	NA

AUCR, AUC_cirrhosis/AUC_healthy; pred, Predicted value from the simulation; CS, Cirrhosis population-specific scalar from current study and normal liver size; CS+SA, Cirrhosis population-specific scalar + liver size adjustment; EFLV, Empirical functional liver volume with scalars from healthy population; NA, Not applicable.

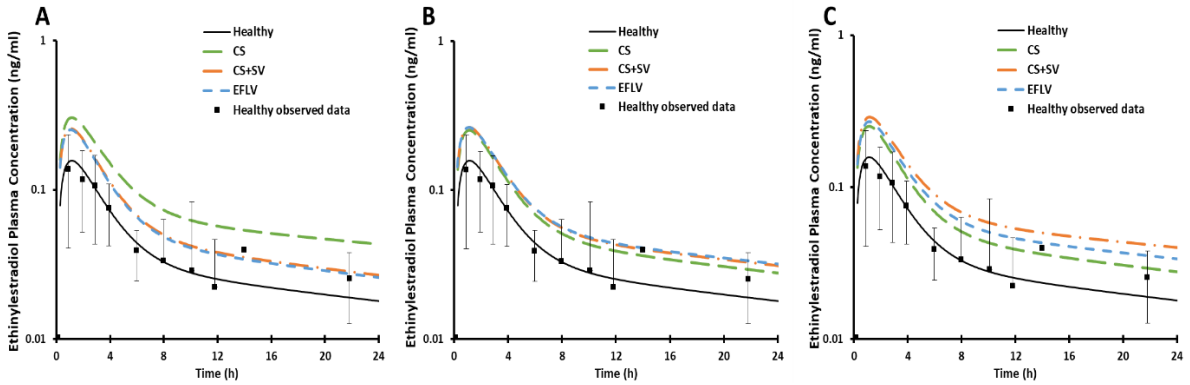

Figure 4.8. Simulated ethinylestradiol plasma concentration-time profiles following single 0.05 mg oral dose in healthy (black line) versus (A) Child-Pugh A, (B) Child-Pugh B, and (C) Child-Pugh C cirrhosis populations (coloured dashed lines) with three different in-vitro in-vivo scaling methods (CS, Cirrhosis population-specific scalar from current study and normal liver size; CS+SA, Cirrhosis population-specific scalar + liver size adjustment; EFLV, Empirical functional liver volume with scalars from healthy population). Black squares represent observed clinical data from healthy individuals (Back, et al., 1979). Error bars represent the standard deviation from the mean observed data.

4.5. Discussion

Subcellular fractions are frequently used in *in-vitro* studies to assess the activity or the expression of different hepatic enzymes, followed by IVIVE scaling based on protein content per unit liver mass (MPPGL and CPPGL) (Barter, et al., 2007). Cirrhosis is a chronic hepatic disorder characterised by impaired drug and xenobiotic metabolism (Prasad, et al., 2018). There are different classification systems for the degree of cirrhosis, with the Child-Pugh being the most widely used for diagnosis as well as clinical pharmacokinetic studies and dose adjustment recommendations (Talal, et al., 2017). Information on the effects of hepatic impairment associated with cirrhosis on IVIVE scaling factors is lacking. Therefore, this study aimed to investigate, for the first time, the impact of various cirrhosis conditions on MPPGL and CPPGL.

The average activity of P450 reductase in the control group (0.097 ± 0.029 units/mg microsomal protein) was in agreement with reported values (Mishin, et al., 2014). The median MPPGL for controls (36.6 mg/g) was within the reported range for healthy human liver (Barter, et al., 2007). Although CPPGL was not corrected for loss, no major loss in the cytosol (soluble fraction) is expected during preparation. The median value for the control group (75.4 mg/g) was within the reported range of 45-134 mg/g (Cubitt, et al., 2011), and close to the range reported using organelle-specific markers, 65-75 mg/g (Xu, et al., 2018).

Differences in MPPGL and CPPGL between male and female in both control and diseased groups were negligible, and correlation with age was weak, in agreement with published evidence from adult livers (Barter, et al., 2007, 2008). Moreover, the set of samples used in this study was obtained from the right lobe of the liver in order to allow comparison between scalar values; evaluation of any potential differences due to liver lobe heterogeneity were therefore beyond the scope of this study.

Fewer CP-A samples were acquired than intended based on the power analysis. Clinical sample acquisition and annotation is a commonly cited challenge for this type of research, frequently leading to apparently low sample sizes (Grizzle, et al., 2011); indeed, consensus paper that reported meta-analysis of 10 publications for healthy livers had 197 samples in total (i.e., average of nearly 20 samples per publication, some of them with only four samples) (Barter, et al., 2007).

We expected a decline in both MPPGL and CPPGL with the severity of cirrhosis to reflect the decrease in amounts of most metabolic proteins within hepatocytes as reported previously by Prasad et al., (Prasad, et al., 2018). However, there was no statistically significant differences in MPPGL among groups (Figure 4.3) which may be attributed to the following factors:

- First: the small sample size, especially in the case of mild cirrhosis, may have affected the confidence in the detection of small differences.
- Second, Child-Pugh classification is a clinical classification with some subjective elements, such as scoring ascites and encephalopathy, which are variable according to the physician's judgment, and patient compliance on diuretics and lactulose (Peng, et al., 2016),
- Third, this classification does not consider the cause of cirrhosis and is not directly related to liver metabolic function (Talal, et al., 2017). There seems to be a confounding effect by the accompanying disease of cirrhosis. For example, most of the mild cirrhosis samples were diagnosed with cancer and had the lowest MPPGL values. This, in turn, caused the median MPPGL to drop to a lower value than the severe group, most of which belong to cholestasis origin. Less subjective classification systems might be required such as National Cancer Institute (NCI), and Model for End-Stage Liver Disease (MELD) scores, but donors' data were not enough to calculate these scores.

Comparison of cirrhotic MPPGL ratios (relative to control) against ratios of functional liver volume showed very similar trends, especially after correction by the change in whole liver size (Table 4.1), lending more support to the observation of concomitant decrease in content and function associated with cirrhotic livers. This comparison was only confined to previous studies that have used MPPGL and functional liver volumes as scalars. Studies that have scaled the clearance using functional liver volume values reported based on single article and only one cause of the disease; alcoholic cirrhosis was not included (Edginton, et al., 2008).

The control group MPPGL values were mostly (11 samples out of 13) within the 95th confidence interval of age-matched predicted values using Equation 3 from Barter et al., (2008) (Supplementary Figure 4.1). The little bias observed might be attributed to the fact that the

control samples were from histologically normal samples from metastatic liver diseases and not from healthy volunteers (Supplementary Table 4.2).

Patients with cirrhosis tend to exhibit various concomitant liver diseases that are either likely to be a cause of cirrhosis or are developed as a result of cirrhosis progression (e.g. hepatocellular carcinoma). Some of these disorders were reflected in the samples used in this study. We could not confirm whether these associated diseases were the main cause of cirrhosis according to the clinical information provided by the tissue bank; however, diagnosis notes showed these as existing conditions at the time of sample collection.

A decrease in the expression of cytochrome P450 enzymes with increasing severity of fatty liver disease has been reported previously (Fisher, et al., 2009), and this could be a general trend for microsomal proteins. There were only two samples associated with alcoholic liver disease, which also showed lower levels of MPPGL relative to controls; however larger sample size might be recommended for future studies to asses any differences (Figure 4.4). Similarly for CPPGL, although previous proteomic and immuo-histochemical investigations reported changes in expression of various cytosolic proteins in alcohol-fed rats compared to normal control animals (Kim, et al., 2015), cytosolic protein contents did not show significant differences.

A statistical analysis of the subgroups with different coexisting diseases and according to Child-Pugh score was not possible due to the low sample size. The variations in scalars associated with co-existing conditions (especially in case of MPPGL) might assist in more specific scaling of *in vitro* data for the development of models in various cirrhosis populations with different underlying conditions instead of the conventional practice of averaging values from all cirrhotic livers.

The PBPK simulations compared different methods to recapitulate cirrhosis within IVIVE scaling. Very limited differences in alfentanil model's performance was noted between the methods (Figure 4.5, and Table 4.2), while for metoprolol and midazolam, late stages of cirrhosis showed modest differences between CS and EFLV methods (Figure 4.6, Figure 4.7, Table 4.3, and Table 4.4). These results indicate that changes in cirrhosis-specific MPPGL values correlate with changes in functional liver mass, especially when the former values were adjusted with actual whole liver volume at different cirrhosis populations. As the hepatic extraction ratio of the drug increased, the sensitivity to this whole liver volume adjustment increased. This can be attributed to the change in whole liver volume among the three methods of scaling leading to changes in liver blood flow and consequently variability in hepatic clearance of these drugs.

The ethinylestradiol model was developed to assess the simultaneous impact of cirrhosis-specific CPPGL and MPPGL values on the drug exposure. As intrinsic clearance per mg of cytosolic protein was used in the model, changes due to differences in the cytosolic enzyme expression or activity between healthy and cirrhosis populations were not considered in this model; the main variables influencing the overall hepatic clearance of the drug were CPPGL, MPPGL, liver volume, fraction unbound and liver blood flow changes. Similar to CYP450 specific substrates, the ethinylestradiol profile showed that CS+SV scalar method agreed with EFLV scalar in all stages of the disease.

Further studies might be required to validate current experimental scalars not only with already established PBPK models but also to assess the *in vivo* clearance of different probes using *in vitro* liver microsomal and cytosol fractions from cirrhosis patients. This is a common approach when a considerable amount of *in vitro* fractions are available and when the model is not yet defined for drugs in early stages of development (Obach, 1999; Obach, et al., 1997).

In conclusion, this study compared, for the first time, MPPGL and CPPGL scalars in livers with varying severity of cirrhosis relative to histologically normal livers. Cirrhosis associated with NAFLD and liver cancer showed the largest reduction in MPPGL. Simulations using experimentally-derived MPPGL and CPPGL values showed agreement with empirical methodology using functional liver volume especially when considering that whole liver volume changes with disease progression. However, the experimental and biologic nature of MPPGL and CPPGL values provided here offer more confidence to PBPK models for *a priori* dose adjustment in cirrhosis patients. This finding is in line with what was promoted by different reports (Jadhav, et al., 2015; Younis, et al., 2017) to achieve evidence-based dosage adjustment for special populations when there are no clinical data available (instead of the guess work or *in cerebro* modelling). It also helps in including cirrhosis patients into drug clinical trials with safe doses, as described in recent Food and Drug Administration guidance (FDA, 2020).

4.6. References

Abduljalil, K, Pan, X, Pansari, A, Jamei, M, and Johnson, TN. (2020). A Preterm Physiologically Based Pharmacokinetic Model. Part I: Physiological Parameters and Model Building. *Clin. Pharmacokinet.*, 59(4), 485–500.

Achour, B, Barber, J, and Rostami-Hodjegan, A. (2011). Cytochrome P450 pig liver pie: Determination of individual cytochrome P450 isoform contents in microsomes from two pig livers using liquid chromatography in conjunction with mass spectroscopy. *Drug Metab. Dispos.*, 39(11), 2130–2134.

Ando, H, Izawa, S, Hori, W, and Nakagawa, I. (2008). Utility of a single adjusting compartment: a novel methodology for whole body physiologically-based pharmacokinetic modelling. *Theor. Biol. Med. Model.*, 5(1), 19.

Back, DJ, Breckenridge, AM, Crawford, FE, MacIver, M, Orme, ML, Rowe, PH, and Watts, MJ. (1979). An investigation of the pharmacokinetics of ethynylestsadiol in women using badioimmunoassay. *Contraception*, 20(3), 263–273.

Barter, ZE, Bayliss, M, Beaune, P, Boobis, A, Carlile, D, Edwards, R, Brian Houston, J, Lake, B, Lipscomb, J, Pelkonen, O, Tucke, G, and Rostami-Hodjegan, A. (2007). Scaling Factors for the Extrapolation of In Vivo Metabolic Drug Clearance From In Vitro Data: Reaching a Consensus on Values of Human Micro-somal Protein and Hepatocellularity Per Gram of Liver. *Curr. Drug Metab.*, 8(1), 33–45.

Barter, ZE, Chowdry, JE, Harlow, JR, Snawder, JE, Lipscomb, JC, and Rostami-Hodjegan, A. (2008). Covariation of Human Microsomal Protein Per Gram of Liver with Age: Absence of Influence of Operator and Sample Storage May Justify Interlaboratory Data Pooling. *Drug Metab. Dispos.*, 36(12), 2405–2409.

Chen, Y, Jin, JY, Mukadam, S, Malhi, V, and Kenny, JR. (2012). Application of IVIVE and PBPK modeling in prospective prediction of clinical pharmacokinetics: strategy and approach during the drug discovery phase with four case studies. *Biopharm. Drug Dispos.*, 33(2), 85–98.

Cubitt, HE, Houston, JB, and Galetin, A. (2011). Prediction of Human Drug Clearance by Multiple Metabolic Pathways: Integration of Hepatic and Intestinal Microsomal and Cytosolic Data. *Drug Metab. Dispos.*, 39(5), 864–873.

Darwich, AS, Ogungbenro, K, Vinks, AA, Powell, JR, Reny, J-L, Marsousi, N, Daali, Y, Fairman, D, Cook, J, Lesko, LJ, McCune, JS, Knibbe, CAJ, de Wildt, SN, Leeder, JS, Neely, M, Zuppa, AF, Vicini, P, … Rostami-Hodjegan, A. (2017). Why Has Model-Informed Precision Dosing Not Yet Become Common Clinical Reality? Lessons From the Past and a Roadmap for the Future. *Clin. Pharmacol. Ther.*, 101(5), 646–656.

De Bock, L, Boussery, K, De Bruyne, R, Van Winckel, M, Stephenne, X, Sokal, E, and Van Bocxlaer, J. (2014). Microsomal protein per gram of liver (MPPGL) in paediatric biliary atresia patients. *Biopharm. Drug Dispos.*, 35(5), 308–312.

Edginton, AN, and Willmann, S. (2008). Physiology-based simulations of a pathological condition: Prediction of pharmacokinetics in patients with liver cirrhosis. *Clin. Pharmacokinet.*, 47(11), 743–752.

EMA. (2005). Guideline on the Evaluation of the Pharmacokinetics of Medicinal Products in Patients With Impaired Hepatic Function. *Ema*, 1-10 CPMP/EWP/2339/02. https://www.ema.europa.eu/en/documents/scientific-guideline/guideline-evaluation-pharmacokinetics-medicinal-products-patients-impaired-hepatic-function_en.pdf

Ezuruike, U, Humphries, H, Dickins, M, Neuhoff, S, Gardner, I, and Rowland Yeo, K. (2018). Risk-Benefit Assessment of Ethinylestradiol Using a Physiologically Based Pharmacokinetic Modeling Approach. *Clin. Pharmacol. Ther.*, 104(6), 1229–1239.

FDA. (2020). Enhancing the Diversity of Clinical Trial Populations—Eligibility Criteria, Enrollment Practices, and Trial Designs Guidance for Industry. *Guid. Doc.* https://www.fda.gov/regulatory-information/search-fda-guidance-documents/enhancing-diversity-clinical-trial-populations-eligibility-criteria-enrollment-practices-and-trial

Ferrier, C, Marty, J, Bouffard, Y, Haberer, JP, Levron, JC, and Duvaldestin, P. (1985). Alfentanil pharmacokinetics in patients with cirrhosis. *Anesthesiology*, 62(4), 480–484.

Fisher, CD, Lickteig, AJ, Augustine, LM, Ranger-Moore, J, Jackson, JP, Ferguson, SS, and Cherrington, NJ. (2009). Hepatic Cytochrome P450 Enzyme Alterations in Humans with Progressive Stages of Nonalcoholic Fatty Liver Disease. *Drug Metab. Dispos.*, 37(10), 2087–2094.

Graham, JM. (2002). Preparation of crude subcellular fractions by differential centrifugation. *ScientificWorldJournal.*, 2, 1638–1642.

Grizzle, WE, Bell, WC, and Sexton, KC. (2011). Issues in collecting, processing and storing human tissues and associated information to support biomedical research. *Cancer*

Biomarkers, 9(1–6), 531–549.

Guengerich, FP, Martin, M V., Sohl, CD, and Cheng, Q. (2009). Measurement of cytochrome P450 and NADPH–cytochrome P450 reductase. *Nat. Protoc.*, 4(9), 1245–1251.

Harwood, MD, Russell, MR, Neuhoff, S, Warhurst, G, and Rostami-Hodjegan, A. (2014). Lost in centrifugation: Accounting for transporter protein losses in quantitative targeted absolute proteomics. *Drug Metab. Dispos.*, 42(10), 1766–1772.

Houston, JB. (1994). Utility of in vitro drug metabolism data in predicting in vivo metabolic clearance. *Biochem. Pharmacol.*, 47(9), 1469–1479.

Jadhav, PR, Cook, J, Sinha, V, Zhao, P, Rostami-Hodjegan, A, Sahasrabudhe, V, Stockbridge, N, and Powell, JR. (2015). A proposal for scientific framework enabling specific population drug dosing recommendations. *J. Clin. Pharmacol.*, 55(10), 1073–1078.

Johnson, TN, Boussery, K, Rowland-Yeo, K, Tucker, GT, and Rostami-Hodjegan, A. (2010). A semi-mechanistic model to predict the effects of liver cirrhosis on drug clearance. *Clin. Pharmacokinet.*, 49(3), 189–206.

Kanda, T, Goto, T, Hirotsu, Y, Moriyama, M, and Omata, M. (2019). Molecular Mechanisms Driving Progression of Liver Cirrhosis towards Hepatocellular Carcinoma in Chronic Hepatitis B and C Infections: A Review. *Int. J. Mol. Sci.*, 20(6), 1358.

Kim, D, Lee, E-M, Do, S-H, Jeong, D-H, and Jeong, K-S. (2015). Changes of the Cytoplasmic Proteome in Response to Alcoholic Hepatotoxicity in Rats. *Int. J. Mol. Sci.*, 16(8), 18664–18682.

Li, Y-M. (2003). Evaluation of liver functional reserve by combining D-sorbitol clearance rate and CT measured liver volume. *World J. Gastroenterol.*, 9(9), 2092.

Lin, X-Z, Sun, Y-N, Liu, YH, Sheu, B-S, Cheng, BN, Chen, C-Y, Tsai, H-M, and Shen, CL. (1998). Liver volume in patients with or without chronic liver diseases. *Hepatogastroenterology.*, 45(22), 1069–1074.

Mallick, P, Moreau, M, Song, G, Efremenko, AY, Pendse, SN, Creek, MR, Osimitz, TG, Hines, RN, Hinderliter, P, Clewell, HJ, Lake, BG, and Yoon, M. (2020). Development and Application of a Life-Stage Physiologically Based Pharmacokinetic (PBPK) Model to the Assessment of Internal Dose of Pyrethroids in Humans. *Toxicol. Sci.*, 173(1), 86–99.

Matsubara, T, Koike, M, Touchi, A, Tochino, Y, and Sugeno, K. (1976). Quantitative determination of cytochrome P-450 in rat liver homogenate. *Anal. Biochem.*, 75(2), 596–603.

Matsui, Y, Tu, W, Kitade, H, Nakagawa, A, Kamiya, T, Kwon, A-H, Uetsuji, S, and Kamiyama, Y. (1996). Hepatocyte volume as an indicator of hepatic functional reserve in cirrhotic patients with liver tumours. *J. Gastroenterol. Hepatol.*, 11(6), 540–545.

Miki, K, Kubota, K, Inoue, Y, Vera, DR, and Makuuchi, M. (2001). Receptor measurements via Tc-GSA kinetic modeling are proportional to functiosal hepatocellular mass. *Gastroenterology*, 120(5), A548.

Mishin, V, Heck, DE, Laskin, DL, and Laskin, JD. (2014). Human Recombinant Cytochrome P450 Enzymes Display Distinct Hydrogen Peroxide Generating Activities During Substrate Independent NADPH Oxidase Reactions. *Toxicol. Sci.*, 141(2), 344–352.

Morgan, DJ, and McLean, a J. (1995). Clinical pharmacokinetic and pharmacodynamic considerations in patients with liver disease. An update. *Clin. Pharmacokinet.*, 29(5), 370–391.

Obach, RS. (1999). Prediction of human clearance of twenty-nine drugs from hepatic microsomal intrinsic clearance data: An examination of in vitro half-life approach and nonspecific binding to microsomes. *Drug Metab. Dispos.*, 27(11), 1350–1359.

Obach, RS, Baxter, JG, Liston, TE, Silber, BM, Jones, BC, MacIntyre, F, Rance, DJ, and Wastall, P. (1997). The prediction of human pharmacokinetic parameters from preclinical and in vitro metabolism data. *J. Pharmacol. Exp. Ther.*, 283(1), 46–58.

Omura, T, and Sato, R. (1964). The carbon monoxide-binding pigment of liver microsomes I. Evidence for its hemoprotein nature. *J. Biol. Chem.*, 239(7), 2370–2378.

Ozaki, K, Matsui, O, Kobayashi, S, Minami, T, Kitao, A, and Gabata, T. (2016). Morphometric changes in liver cirrhosis: aetiological differences correlated with progression. *Br. J. Radiol.*, 89(1059), 20150896.

Pentikäinen, PJ, Välisalmi, L, Himberg, J-J, and Crevoisier, C. (1989). Pharmacokinetics of Midazolam Following Intravenous and Oral Administration in Patients with Chronic Liver Disease and in Healthy Subjects. *J. Clin. Pharmacol.*, 29(3), 272–277.

Prasad, B, Bhatt, DK, Johnson, K, Chapa, R, Chu, X, Salphati, L, Xiao, G, Lee, C, Hop, CECA, Mathias, A, Lai, Y, Liao, M, Humphreys, WG, Kumer, SC, and Unadkat, JD. (2018). Abundance of Phase 1 and 2 Drug-Metabolizing Enzymes in Alcoholic and Hepatitis C Cirrhotic Livers: A Quantitative Targeted Proteomics Study. *Drug Metab. Dispos.*, 46(7), 943–952.

Pugh, RNH, Murray-Lyon, IM, Dawson, JL, Pietroni, MC, and Williams, R. (1973). Transection of the oesophagus for bleeding oesophageal varices. *Br. J. Surg.*, 60(8), 646–649.

Reddy, VP, Jones, BC, Colclough, N, Srivastava, A, Wilson, J, and Li, D. (2018). An Investigation into the Prediction of the Plasma Concentration-Time Profile and Its Interindividual Variability for a Range of Flavin-Containing Monooxygenase Substrates Using a Physiologically Based Pharmacokinetic Modeling Approach. *Drug Metab. Dispos.*, 46(9), 1259–1267.

Regårdh, C-G, Jordö, L, Ervik, M, Lundborg, P, Olsson, R, and Rönn, O. (1981). Pharmacokinetics of Metoprolol in Patients with Hepatic Cirrhosis. *Clin. Pharmacokinet.*, 6(5), 375–388.

Rodgers, T, and Rowland, M. (2006). Physiologically based pharmacokinetic modelling 2: Predicting the tissue distribution of acids, very weak bases, neutrals and zwitterions. *J. Pharm. Sci.*, 95(6), 1238–1257.

Rowland Yeo, K, Jamei, M, Yang, J, Tucker, GT, and Rostami-Hodjegan, A. (2010). Physiologically based mechanistic modelling to predict complex drug–drug interactions involving simultaneous competitive and time-dependent enzyme inhibition by parent compound and its metabolite in both liver and gut—The effect of diltiazem on the time-c. *Eur. J. Pharm. Sci.*, 39(5), 298–309.

Schuppan, D, and Afdhal, NH. (2008). Liver cirrhosis. *Lancet*, 371(9615), 838–851.

Shan, Y-S, Hsieh, Y-H, Sy, ED, Chiu, N-T, and Lin, P-W. (2005). The influence of spleen size

on liver regeneration after major hepatectomy in normal and early cirrhotic liver. *Liver Int.*, 25(1), 96–100.

Talal, AH, Venuto, CS, and Younis, I. (2017). Assessment of Hepatic Impairment and Implications for Pharmacokinetics of Substance Use Treatment. *Clin. Pharmacol. Drug Dev.*, 6(2), 206–212.

Vreman, HJ, Kourula, S, Jašprová, J, Ludvíková, L, Klán, P, Muchová, L, Vítek, L, Cline, BK, Wong, RJ, and Stevenson, DK. (2019). The effect of light wavelength on in vitro bilirubin photodegradation and photoisomer production. *Pediatr. Res.*, 85(6), 865–873.

Wang, L, Collins, C, Kelly, EJ, Chu, X, Ray, AS, Salphati, L, Xiao, G, Lee, C, Lai, Y, Liao, M, Mathias, A, Evers, R, Humphreys, W, Hop, CECA, Kumer, SC, and Unadkat, JD. (2016). Transporter expression in liver tissue from subjects with alcoholic or hepatitis C cirrhosis quantified by targeted quantitative proteomics. *Drug Metab. Dispos.*, 44(11), 1752–1758.

Xu, M, Saxena, N, Vrana, M, Zhang, H, Kumar, V, Billington, S, Khojasteh, C, Heyward, S, Unadkat, JD, and Prasad, B. (2018). Targeted LC-MS/MS Proteomics-Based Strategy To Characterize in Vitro Models Used in Drug Metabolism and Transport Studies [Research-article]. *Anal. Chem.*, 90(20), 11873–11882.

Yang, J, Jamei, M, Yeo, KR, Tucker, GT, and Rostami-Hodjegan, A. (2007). Prediction of intestinal first-pass drug metabolism. *Curr. Drug Metab.*, 8(7), 676–684.

Younis, IR, Robert Powell, J, Rostami-Hodjegan, A, Corrigan, B, Stockbridge, N, Sinha, V, Zhao, P, Jadhav, P, Flamion, B, and Cook, J. (2017). Utility of Model-Based Approaches for Informing Dosing Recommendations in Specific Populations: Report From the Public AAPS Workshop. *J. Clin. Pharmacol.*, 57(1), 105–109.

Zhang, H, Cui, D, Wang, B, Han, Y-H, Balimane, P, Yang, Z, Sinz, M, and Rodrigues, AD. (2007). Pharmacokinetic Drug Interactions Involving 17α-Ethinylestradiol. *Clin. Pharmacokinet.*, 46(2), 133–157.

Zhu, J-Y. (1999). Measurement of liver volume and its clinical significance in cirrhotic portal hypertensive patients. *World J. Gastroenterol.*, 5(6), 525.

4.7. Supplementary Material

Supplementary Table 4.1. Previous studies that reported scaling fraction protein to original tissue in cirrhosis and their limitations

Study	Software platform	Scaling factor 1	Scaling factor 2	Limitations
Prasad et al., 2018	Simcyp	Healthy S9PPGL (120.8 mg/g)	Functional liver mass (61% of normal for CP-C)	Recovery factors and efficiency of the process of S9 preparation were not considered
Johnson et al., 2010	Simcyp	Healthy MPPGL (39.8 mg/g)	Functional liver mass (81, 65, 53% of normal for CP-A to C, respectively)	Similar enzymatic activity and microsomal yield were assumed in viable diseased cells and healthy cells (i.e. intact cell theory)
Edginton et al., 2008	PK-Sim	$f_{enz.act}$	Functional liver mass (69, 55, 28% of normal for CP-A to C, respectively)	As $f_{enz.act}$ have been determined in cirrhosis tissues, the scaling method accounted for the impact of fibrous tissue on clearance twice, leading to underestimation of clearance in the disease group

S9PPGL, S9 protein content per gram liver; MPPGL, microsomal protein per gram liver; $f_{enz.act}$, fraction of specific enzyme activity in disease relative to healthy livers, a variable parameter with disease severity; CP-A, -B, -C, mild, moderate, and severe Child-Pugh grades of cirrhosis.

Supplementary Table 4.2. Demographic and clinical data for individual donors of control samples

Sample ID	Date of surgery	Age	sex	PT (sec)	Albumin level (g/L)	Weight (Kg) *	Height (m) *	Total bilirubin (µmol/L)	General diagnosis
2759	12/12/16	81	M	11.3	34	82	1.72	11	CRC
2721	06/12/16	36	M	11.5	39	61.5	1.696	18	CRC
2841	28/12/16	57	M	12.3	40	84	1.74	9	CRC
0103	16/01/17	81	M	21.6	38	75	1.67	16	CRC
2847	30/12/16	48	F	12.2	43	67.8	1.619	10	SCC
0044	09/01/17	83	F	10.6	39	62.3	1.637	6	CRC
761	20/04/17	73	M	12.7	35	94.9	1.638	6	HCC
713	13/04/17	57	F	12.1	42	65.9	1.73	9	CRC
502	14/03/17	77	M	11.9	38	112.5	1.71	9	CRC
0125	19/01/17	62	M	10.9	38	69.7	1.7	7	CRC
0336	16/02/17	71	F	10.5	34	76	1.53	8	GIST
484	13/03/17	80	M	21.9	24	71	1.81	28	CRC
0322	14/02/17	71	M	10.8	43	93.6	1.715	11	CRC

PT, prothrombin time; * measured at time of surgery; HCC, hepatocellular carcinoma; CRC, colorectal cancer; SCC, squamous cell carcinoma; GIST, gastrointestinal stromal tumour.

Supplementary Table 4.3. Demographic and clinical data for individual donors of cirrhosis liver samples and Child-Pugh classification

Sample ID	Date of surgery D/M/Y	Age	sex	PT (sec)	Albumin level (g/L)	Total bilirubin (µmol/L)	Weight (Kg) [a]	Height (m) [a]	Ascites volume[b]	HE grade [c]	General diagnosis	CP class (Score)
0974	19/05/17	56	M	18.1	37	8	117.5	1.75	Severe	1-2	SH	B(9)
0549	22/03/17	59	M	18.8	28	53	89.2	1.72	Mild	1-2	NAFLD	C(10)
0355	17/02/17	67	F	17.9	26	81	82.2	1.64	Moderate	None	NAFLD	C(11)
0863	08/05/17	51	F	19.8	23	78	89.2	1.6	Mild	None	NAFLD	C(11)
2728	07/12/16	66	F	24.9	32	29	82.6	1.6	Moderate	1-2	NAFLD	C(10)
1982	17/08/16	63	F	18	25	30	70.7	1.57	Mild	1-2	NAFLD	B(9)
1571	11/06/16	46	F	14.7	25	51	78.6	1.58	Mild	1-2	NAFLD	C(11)
1545	09/06/16	69	F	20.9	50	44	62.7	1.55	Moderate	None	Alcoholic SH	B(9)
1963	13/08/16	68	M	13.6	27	28	113.45	1.77	None	1-2	HCC& alcoholic injury	B(8)
1745	14/07/16	67	M	15.2	27	46	92	1.7	Mild	None	HCC& NAFLD	B(9)
2431	27/10/16	69	M	15.7	28	30	95	1.79	None	None	HCC& HCV	A(6)
2408	22/10/16	51	M	18.9	31	44	88.5	1.85	Mild	None	HCC& HCV	B(8)
1926	10/08/16	63	M	17	33	97	82.3	1.74	None	1-2	HCC& NAFLD	B(9)
997	21/04/16	59	M	19.7	13	63	100.8	1.82	Severe	1-2	CHOL.	C(14)
0746	19/04/17	67	M	13.7	24	58	76.4	1.6	None	1-2	PBC	C(10)

0147	25/01/17	57	M	15.3	19	243	72.3	1.74	Mild	1-2	CHOL.	C(11)
2682	02/12/16	56	F	15.2	40	75	67.3	1.62	Severe	1-2	CHOL.	C(11)
2500	07/11/16	63	F	11.9	30	82	80.15	1.64	Mild	1-2	PBC	C(10)
2306	11/10/16	60	M	16.9	22	326	83.2	1.76	Mild	1-2	PSC	C(11)
2159	15/09/16	39	M	14.2	30	49	80.8	1.90	Mild	None	PSC	B(8)
2136	12/09/16	54	M	19.1	30	484	79.7	1.75	Moderate	1-2	PSC	C(12)
1684	11/07/16	69	F	15.4	28	102	78.6	1.67	Mild	1-2	CHOL.&PBC	C(10)
1570	10/06/16	62	F	16.6	32	26	72.1	1.52	Moderate	1-2	NAFLD	B(9)
0955	18/05/17	63	M	15	36	18	89.2	1.73	None	None	HCC& alcoholic SH	A(5)
1429	18/07/17	57	M	15.2	37	37	69	1.75	Mild	None	PSC	B(7)
0544	21/03/17	70	M	13.3	30	25	87.8	-	None	1-2	PSC	B(7)
2403	21/10/16	57	M	14.4	29	16	89	1.803	None	None	HCC& HCV	A(6)
2020	24/08/16	59	F	15.9	29	26	43.95	1.5	Severe	None	PBC	B(9)
3688	12/11/15	65	F	13.8	40	14	84	1.63	None	None	HCC& alcoholic SH	A(5)
1509	04/06/16	57	M	14.4	33	18	74.95	1.75	Moderate	1-2	Alcoholic SH	B(9)
1228	06/12/17	55	F	14.3	29	13	78.6	1.62	None	None	HCC	A(6)
0819	05/02/17	75	M	13.2	41	18	79.5	1.6	None	None	CHOL.	A(5)

PT, prothrombin time; CP; Child-Pugh; HCC, hepatocellular carcinoma; NAFLD, non-alcoholic fatty liver disease; CHOL, cholestasis; PBC, primary biliary cirrhosis; PSC, primary sclerosing cholangitis, SH, Steatohepatitis; [a] measured at time of surgery; [b] controlled with diuretics recorded as Mild ascites, [c] controlled with rifaximin / lactulose recorded as grade 1-2.

Supplementary Table 4.4. NADPH-P450 reductase activity (Units/mg of liver tissue) in both homogenate and microsomal fractions from control and cirrhosis samples

	Sample ID	NADPH-P450 reductase activity in homogenate sample (unit/mg of tissue)	NADPH-P450 activity in microsomes (unit/mg of tissue)
Control group	2759	2.133	0.506
	2721	3.981	0.995
	2841	2.938	0.336
	103	3.341	0.889
	2847	5.829	1.616
	44	3.697	0.74
	761	1.991	0.914
	713	4.763	2.464
	502	2.085	0.932
	125	3.555	2.445
	336	3.299	1.449
	484	2.37	1.065
	322	4.171	2.137
	Mean	**3.4**	**1.27**
	SD	**1.13**	**0.7**
Mild cirrhosis	2431	2.133	1.128
	955	2.085	1.316
	2403	1.991	1.656
	3688	2.285	1.757
	1228	2.903	1.781
	819	2.53	0.827
	Mean	**2.32**	**1.41**
	SD	**0.34**	**0.39**
Moderate cirrhosis	974	2.169	0.735
	1982	1.836	1.404
	1545	2.178	1.175
	1963	2.444	1.852
	1745	3.988	2.336
	2408	1.28	0.669
	1926	2.52	2.2
	2159	2.23	0.732
	1570	2.559	1.137
	1509	2.148	1.175

	1429	4.756	2.656
	544	3.377	1.477
	2020	3.434	1.991
	Mean	**2.69**	**1.5**
	SD	**0.95**	**0.65**
Severe cirrhosis	549	2.133	1.347
	355	1.873	1.185
	863	1.871	1.297
	2728	1.493	0.682
	1571	1.536	0.704
	997	1.441	0.7
	746	1.045	0.804
	147	1.919	1.195
	2682	3.689	1.895
	2500	2.342	1.263
	2306	1.876	0.812
	2136	2.708	0.931
	1684	2.073	1.078
	Mean	**2**	**1.07**
	SD	**0.66**	**0.35**

Supplementary Table 4.5. Study design, doses, and demographic data from the clinical studies used for simulating alfentanil, metoprolol, and midazolam concentration- time profiles in cirrhosis populations.

Drug	**Route**	**Dose**	**Child-Pugh score**	**N**	**Age range**	**Weight range**	**% females**	**Reference**
Alfentanil	i.v. bolus	0.05 mg/kg	A (1), B (7), C (3)	11	39-69	--	45%	(Ferrier, et al., 1985)
Metoprolol	i.v. infusion over 10 min	20 mg metoprolol tartarate	No information	10	(50-66)	(47-117)	45%	(Regårdh, et al., 1981)
Midazolam	i.v. bolus & oral	7.5 mg (i.v.) & 15 mg (oral)	B (5) C (2)	7	B (30-58) C (66-67)	B (71-108) C (74-87)	0%	(Pentikäinen, et al., 1989)

i.v.; intravenous

Supplementary Table 4.6. PBPK parameters for midazolam, metoprolol, alfentanil, and ethinylestradiol used for the simulations

Physicochemical and Blood Binding										
Parameter	**Midazolam [a]**		**Metoprolol [a]**		**Alfentanil [b]**		**Ethinylestradiol [c]**			
Mol Weight (g/mol)	**325.8**		**267.4**		**416.52**		**296.4**			
log P	**3.53**		**1.88**		**2.16**		**3.81**			
Compound Type	**Monoprotic Base**		**Monoprotic Base**		**Monoprotic Base**		**Diprotic acid**			
pKa	**6**		**9.75**		**6.5**		**10.2, 13.1**			
B/P	**0.603**		**1.15**		**0.63**		**1**			
Haematocrit	**45**		**45**		**45**		**45**			
Fu	**0.032**		**0.88**		**0.104**		**0.015**			
Absorption										
Absorption Model	**1st order**						**1st order**			
Fa	**1 (CV= 30%)**						**0.96 (Predicted)**			
ka (1/h)	**3 (CV=30%)**						**1.17 (Predicted)**			
Q(Gut) (L/h)	**16.18 (Predicted)**						**11.74 (Predicted)**			
Peff,man Cap (10-4 cm/s)	**12**						**2.68 (Predicted)**			
Permeability Assay	**PCaco-2**						**PSA 42.7 (Å^2)** **HBD 2**			
Distribution										
Distribution Model	**Minimal PBPK Model**		**Minimal PBPK Model**		**Full PBPK Model**		**Minimal PBPK Model**			
SAC kin (1/h)	**0.2**		**0**				**0.287**			
SAC kout (1/h)	**0.25**		**0**				**0.096**			
Volume [Vsac] (L/kg)	**0.23**		**1.00E-05**				**2**			
Vss (L/kg)	**0.88**		**3.19**		**0.37 [d]**		**4.06**			
Kp Scalar					**0.567 [d]**					
Elimination										
Clearance Type	**Enzyme Kinetics**									
Pathway	**Vmax pmol/min/pmol**	**Km (µM)**	**CLint µl/min/pmol**	**Fumic**	**CLint µl/min/pmol**	**Fumic**	**Vmax pmol/min/pmol**	**Km (µM)**	**CLint µl/min/pmol**	**fuinc**
(Recombinant in vitro system)										
Enzyme										
•CYP 3A4										
Pathway 1	**5.23**	**2.16**	**0.02**	**1**	**0.559**	**1**			**0.51**	**1**
Pathway 2	**5.2**	**31.8**								
•CYP 3A5										
Pathway 1	**19.7**	**4.16**								

Pathway 2	**4.03**	**34.8**								
•CYP 2D6			**3.61**	**1**						
•CYP2C9									**0.51**	**1**
•CYP1A2									**0.51**	**1**
•CYP2C8									**0.13**	**1**
•UGT1A4	**445**	**40.3**								
•UGT1A1 (HLM)							**408.5**	**19.22**		
•Additional (HLM) µl/min/mg protein					**5.76**	**1**				
•Additional (HLC) µl/min/mg protein									**56[e]**	**1[e]**
•Additional intestine (HIC) µl/min/mg protein									**43.92**	**1**
CL R (L/h)	**0.085**		**5.23**		**0.07**		**2.079**			

[a] Provided with Simcyp Simulator v18 R1
[b] As reported by (Abduljalil, et al., 2020).
[c] Adapted from model file provided with Simcyp Simulator v18 R1 that reported by (Ezuruike, et al., 2018) to account for cytosolic metabolism.
[d] Predicted using Rodgers & Rowland method (2006) with tissue-plasma partition coefficient (Kp) scalar (applied to Kp for all tissues) was set to 0.567 as reported by (Abduljalil, et al., 2020).
[e] calculated from the additional HLM CL_{int} provided by the simulator after accounting for the relative MPPGL and CPPGL for the healthy population and assuming all the remaining metabolism is due to sulfation by SULT1E1.
B/P; Blood to plasma ratio.
Fu; Fraction unbound to plasma proteins.
Fa; the fraction of dose entering the cellular space of the enterocytes (variability is shown in parentheses but values were not allowed to exceed 1).
ka; first order rate constant, Qgut; A nominal flow in gut model (Yang, et al., 2007).
Peff,man; Human effective permeability.
SAC Kin and SAC Kout; first order rate constants which act upon the masses of drug within respectively, the Systemic compartment and the Single Adjusting Compartment (SAC).
VSAC; The apparent volume associated with the SAC.
Vss; volume of distribution at steady state.
CL R; Renal clearance.
CV: coefficient of variation for Fa and ka (these values does not exceed 1).

Dug distribution models used for the investigated drugs

Minimal PBPK distribution model was adopted in the files of the three compounds; midazolam, metoprolol, and ethinylestradiol. It is a 'lumped' PBPK model and, in its simplest form, has only four compartments, predicting only the systemic, portal vein and liver concentration (Rowland Yeo, et al., 2010) . The SAC (Single Adjusting Compartment) is an additional non-physiological compartment which permits adjustment to the drug concentration profile in the

Systemic compartment, where the latter represents a lump of all tissues excluding the liver and portal vein (Ando, et al., 2008). The full PBPK distribution model was used for alfentanil; the model was reported and verified previously in healthy adults (Abduljalil, et al., 2020), which allowed better recovery of the initial phase of the plasma-concentration time curve in subjects with normal liver function. The full-PBPK model simulates the concentrations in various organ compartments—the blood (plasma), adipose, bone, brain, gut, heart, kidney, liver, lung, muscle, pancreas, skin and spleen. Inter-individual variability is introduced through tissue volume predictions using age, sex, weight and height as covariates through a Monte Carlo sampling that takes into account correlations between these covariates (Abduljalil, et al., 2020).

Supplementary Table 4.7. Mean and standard deviation of protein concentrations (µg/µl) of different fractions (microsomes, homogenate, cytosol) for each individual sample (normal and cirrhotic).

	Microsomal fraction		**Homogenate**		**Cytosol**	
Normal	**Mean of 3 readings**	**SD**	**Mean of 3 readings**	**SD**	**Mean of 3 readings**	**SD**
2759	6.90	0.48	9.29	0.11	1.67	0.05
2721	8.71	0.40	9.09	0.14	7.52	0.45
2841	3.32	0.43	9.85	0.10	2.18	0.10
0103	8.95	0.10	14.69	0.88	3.00	0.14
2847	15.20	0.59	10.10	8.70	4.72	0.24
0044	5.68	0.14	9.25	0.21	1.23	0.06
761	28.48	4.82	10.21	0.23	4.17	0.20
713	21.16	0.66	22.13	0.31	6.02	0.21
502	13.88	0.46	12.86	0.29	4.11	0.16
0125	20.77	0.43	12.34	0.39	5.02	0.21
0336	13.54	0.33	11.68	0.47	3.33	0.14
484	16.22	0.87	11.07	0.99	3.32	0.17
0322	15.97	0.34	11.06	0.15	5.08	0.09
Cirrhosis						
974	9.42	0.36	8.65	0.16	5.70	0.27
549	15.94	0.95	10.05	0.32	5.53	0.29
355	14.09	0.73	8.67	0.37	4.48	0.29
863	12.78	0.13	8.13	0.36	3.52	0.24
2728	13.59	0.13	10.86	0.13	3.29	0.13
1982	13.55	0.05	9.24	0.55	4.69	0.28

1570	14.04	0.52	9.04	0.21	4.33	0.17
1571	14.38	0.41	7.23	0.12	2.86	0.08
1545	14.98	0.21	10.12	0.21	3.70	0.05
1509	14.83	0.43	9.45	0.31	4.38	0.12
1745	19.25	0.44	11.02	0.13	6.88	0.19
3688	18.47	0.11	11.29	0.22	8.16	0.30
1926	18.11	0.39	10.71	0.29	6.82	0.16
1429	22.53	0.24	13.10	0.24	8.08	0.03
544	17.48	0.48	10.61	0.31	5.35	0.31
2020	17.88	0.25	11.16	0.10	6.16	0.63
997	12.40	0.38	8.30	0.06	5.28	0.22
746	13.75	0.19	7.89	0.06	4.74	0.28
147	16.57	0.73	8.71	0.16	5.64	0.11
2682	15.01	0.10	6.48	0.22	4.95	0.21
2500	16.74	0.86	11.82	0.51	6.32	0.34
2306	16.51	1.36	8.97	0.51	5.27	0.14
2159	12.80	0.21	9.93	0.27	5.07	0.13
2136	13.75	0.10	10.87	0.41	4.90	0.08
1684	15.49	0.51	10.24	0.23	6.16	0.25
2408	7.85	0.15	8.55	0.33	4.47	0.20
2403	9.37	0.27	11.43	0.15	5.45	0.23
2431	10.66	0.31	8.89	0.47	5.69	0.24
1963	15.73	0.12	9.06	0.96	5.25	0.26
955	16.97	0.47	13.48	0.67	4.97	0.28
1228	12.08	0.27	12.66	0.12	3.45	0.15
0819	8.32	0.14	13.66	0.13	1.30	0.07

Supplementary Table 4.8. Median protein content per gram tissue for each fraction in the control, mild, moderate, and severe cirrhosis groups without correction for the loss due to centrifugation.

Fraction	Control (mg/g)	Mild CP-A (mg/g)	Moderate CP-B (mg/g)	Severe CP-C (mg/g)
Microsomes	15.6 (3.5-28.4)	14.5 (11.8-21.2)	17.5 (8.8-27.4)	16.5 (13.6-20.1)
Cytosol	75.4 (57.4-94.7)	81.8 (61.4-105.5)	67.9 (56.7-85.5)	75.4 (57.4-94.7)
Homogenate	129.8 (72.9-216.4)	89.8 (56.7-191.2)	94.2 (32.5-135.3)	96.6 (56.4-190.7)

Data are presented as median (range). Units: mg protein/g liver

Supplementary Table 4.9. Physiological differences between healthy volunteers and patients with liver cirrhosis population within Simcyp Simulator V18*

Liver condition	Healthy Control	Mild Impairment	Moderate Impairment	Severe Impairment
Simcyp-population	HV	CP-A	CP-B	CP-C
Albumin/α1-AG/HCT (ratio to HV, male)	1/1/1	0.8/0.9/0.9	0.7/0.8/0.8	0.6/0.6/0.8
Enzymes abundances (pmol/mg) • **Liver CYP3A4/5** • **Gut CYP3A4/5** • **Liver CYP2C9/1A2/2C8** • **Liver UGT1A4**	 137 65.4 73/52/24 52	 108 65.4 50.4/32.9/16.6 52	 56 39.9 38/13.6/12.5 52	 31.7 23.6 24.09/6.14/7.92 52
Liver Volume (L)	1.65	1.47	1.17	1.0
Liver Q (Arterial/Portal), (% cardiac output)	6.5/19	9.2/17.3	10.6/13.6	12.5/10.5

*Source: (Johnson, et al., 2010) + Population library in the simulator; HCT, Haematocrit.

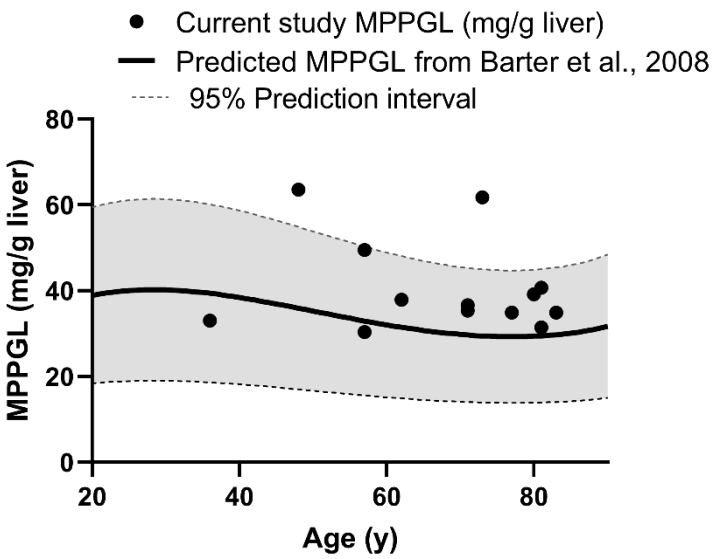

Supplementary Figure 4.1. Comparing current study MPPGL values for the control group corresponding to each patient age with the predicted MPPGL from the equation by (Barter, et al., 2008) with 95% confidence interval lines from the same study.

5 Chapter Five

Quantitative Mass Spectrometry-Based Proteomics in the Era of Model-Informed Drug Development: Applications in Translational Pharmacology and Recommendations for Best Practice

Declaration

This chapter constitutes a published article.

El-Khateeb, E., Vasilogianni, A. M., Alrubia, S., Al-Majdoub, Z. M., Couto, N., Howard, M., Barber, J., Rostami-Hodjegan, A., & Achour, B. **(2019**). Quantitative mass spectrometry-based proteomics in the era of model-informed drug development: applications in translational pharmacology and recommendations for best practice. *Pharmacology & Therapeutics*, 203, 107397 (online publication).

The manuscript was written equally by the first three authors who share the first-authorship. Dr Zubida M. Al-Majdoub, Dr Narciso Couto, Dr Martyn Howard, Dr Jill Barber, Prof Amin Rostami-Hodjegan provided guidance and suggested edits to the manuscript. Dr Brahim Achour outlined the structure of the review, edited the manuscript, and retained editorial control through the journal's invitation.

5.1. Abstract

Quantitative translation of the fate and action of a drug in the body is facilitated by models that allow extrapolation of *in vitro* measurements (such as the rate of metabolism, active transport across membranes, inhibition of enzymes and receptor occupancy) to *in vivo* consequences (intensity and duration of drug effects). These models use various physiological parameters, including data that describe the expression levels of pharmacologically relevant enzymes, transporters and receptors in tissues and *in vitro* systems. Immunoquantification approaches have traditionally been used to determine protein expression levels, generally providing relative quantification data with compromised selectivity and reproducibility. More recently, the development of several quantitative proteomic techniques, fuelled by advances in state-of-the-art mass spectrometry, has led to generating a wealth of qualitative and quantitative data. These data are currently used for various quantitative systems pharmacology applications, with the ultimate goal of conducting virtual clinical trials to inform clinical studies, especially when assessments are difficult to conduct on patients. In this review, we explore available quantitative proteomic methods, discuss their main applications in translational pharmacology and offer recommendations for selecting and implementing proteomic techniques.

5.2. Introduction

Translational pharmacology requires extrapolation of *in vitro* observations to predict the outcome of therapy *in vivo* using various scaling factors measured in tissues and relevant *in vitro* systems (Rostami-Hodjegan, 2012). When extrapolating measurements made *in vitro* (e.g. Km, Vmax, Jmax), functional data may be used as scalars when selective probes are available, for example in the case of several cytochrome P450 (CYP) (Walsky & Obach, 2004) and uridine 5′-diphospho-glucuronosyltransferase (UGT) enzymes (Achour, et al., 2017b; Walsky, et al., 2012). However, owing to a lack of specific substrates for many enzymes and for the majority of transporters and receptors, the use of abundance data remains the preferred approach for *in vitro-in vivo* extrapolation (IVIVE), facilitated by analytical methods that can quantify the levels of individual proteins in heterogeneous biological matrices. Over the past two decades, quantitative proteomics based on liquid chromatography in conjunction with mass spectrometry (LC-MS) has replaced traditional immunoquantitative methods, such as Western blotting and enzyme-linked immunosorbent assays (ELISA) (Aebersold, et al., 2013), mainly because traditional techniques require purified protein standards and specific antibodies for each target, which are not always available.

Pharmacologically active enzymes and transporters tend to have high sequence homology and most of these proteins are found at very low amounts within the membranes of tissues and cellular systems (Vildhede, et al., 2015). Highly selective and sensitive mass spectrometry techniques are therefore ideal for implementation in pharmacology applications (Al Feteisi, et al., 2015b; Heikkinen, et al., 2015). LC-MS analysis offers various other advantages including reproducibility, high throughput and the ability to multiplex measurements. This allows simultaneous detection and quantification of dilute amounts of a large number of proteins (hundreds to thousands) in complex biological systems (Ong & Mann, 2005). Quantitative proteomic techniques have therefore been implemented by different laboratories worldwide for

various pharmacology applications, leading to improved extrapolation of drug pharmacokinetics (Doki, et al., 2018; Kumar, et al., 2018) and better understanding of the effects various factors, including age (Ladumor, et al., 2019; van Groen, et al., 2018), ethnicity (Kawakami, et al., 2011; Ladumor, et al., 2019; Peng, et al., 2015), and genetics (Bhatt, et al., 2019; Peng, et al., 2015; Prasad, et al., 2014a) on the expression of enzymes and transporters.

The typical aim of a proteomic experiment is to characterise the entire set of proteins expressed in a particular system (global proteomics) or to target a specified set of proteins for quantification (targeted proteomics) (Gillet, et al., 2016). These two types of proteomic analysis require specific considerations for robust analysis to be achieved (Prasad, et al., 2019). In this review, we explore state-of-the-art mass spectrometry-based proteomic methods, both global and targeted, used for the characterisation of drug-metabolising and transporting proteins as well as drug targets, and discuss their advantages, limitations, caveats for implementation and their main applications in translational pharmacokinetics (PK) and pharmacodynamics (PD).

5.3. Overview of a typical quantitative proteomic experiment

The quantitative proteomic workflow can be customised for the type of biological sample and the target proteins to be quantified; however, routinely applied bottom-up methods tend to follow generally similar steps (Figure 5.1 A). A biological sample (tissues, cell lines or biofluids) is processed by cell lysis or homogenisation, often followed by enrichment of specific fractions (e.g. microsomes, cytosol, S9, plasma membrane, mitochondrial fraction) (Figure 5.1 B) prior to protein solubilisation and digestion (Drozdzik, et al., 2014; Harwood, et al., 2014; Wiśniewski, et al., 2016b). The variable array of available samples requires consideration of the effects of the type of sample and subsequent processing on end-point protein abundance (Bhatt & Prasad, 2018).

Whole cell lysates or tissue homogenates can be used for the quantification of various pharmacologically relevant proteins (Wegler, et al., 2017). When enriched systems are required, the localisation of the target protein is critical to the decision of which fraction to use (Wiśniewski, et al., 2016b). Cytosolic proteins (e.g. alcohol/aldehyde dehydrogenases, sulfotransferases) are best quantified in cytosol or S9 fractions (Prasad, et al., 2018). Membrane-bound reticular proteins (e.g. CYPs and UGTs) are enriched in microsomal membrane fractions (Chen, et al., 2016). Enzymes localised in the reticular lumen (e.g. carboxylesterases) can be quantified in microsomes; however, a proportion of these proteins is expected to be lost into the cytosol during sample processing and therefore these proteins are quantified more accurately in S9 fractions (consisting of microsomes and cytosol) provided the target proteins are sufficiently abundant (Prasad, et al., 2018; Wang, et al., 2019). Transporters and PD-relevant targets, such as receptors, protein phosphatases and kinases, can be found in the plasma membrane (Batth, et al., 2018; Ohtsuki, et al., 2012), and therefore cell membrane-enriched fractions can be used for these applications. Detailed sub-cellular location information can be found in various databases, including Gene Ontology (www.geneontology.org) and UniProt (www.uniprot.org).

Bottom-up proteomic techniques rely on quantitative analysis of unique (proteotypic) peptides used as surrogates for target proteins (Gillet, et al., 2016). Sample proteins are digested using specific proteases, typically trypsin or lysyl endopeptidase (LysC), independently or in combination (Achour & Barber, 2013; Wiśniewski & Mann, 2012a). Other proteases, such as chymotrypsin, can be used for specific applications, such as increased depth and reproducibility of analysis (Wiśniewski, et al., 2019). Sample digestion can be done in gel, in solution or using filter-aided sample preparation (FASP) (Fallon, et al., 2008; Langenfeld, et al., 2009; Wiśniewski, et al., 2009). Complementary data are expected to be generated when several protein preparation workflows are used (Al Feteisi, et al., 2018; Choksawangkarn, et al., 2012).

After digestion, peptides are desalted, enriched, separated by liquid chromatography (LC) and analysed using mass spectrometry (MS). Additional separation prior to mass spectrometry can be performed using ion mobility (Achour, et al., 2017a; Distler, et al., 2014). Multiple quantitative MS and data acquisition approaches can be used (Figure 5.1 C), depending on the aim of the experiment and the availability of instrumentation (Smith, et al., 2019). Targeted and global methodologies are routinely used to identify and quantify expression levels of pharmacologically-relevant proteins. Standards are added at different stages of the proteomic workflow (Figure 5.1 A). Data acquisition is followed by data analysis and interpretation, often facilitated by vendor or open-source software. Assessment of the performance of various software packages used for targeted and global proteomics was previously reported (Cox & Mann, 2008; Röst, et al., 2014; Tommi, et al., 2018)

Several quality control (QC) steps are required at certain stages of the experiment. Assessment of the quality of sample processing during homogenisation and fractionation is required to ensure maximum recovery of protein, normally using colorimetric/fluorometric protein assays. Assessment of the digestion efficiency is done before LC-MS analysis; this is achieved by evaluating time-dependent release of peptides in targeted experiments or by monitoring the rate of missed cleavage in global experiments. Finally, the reliability of the proteomic quantification technique depends on the performance of the LC-MS system, which can be assessed using internal standards and well-characterised QC samples (Bhatt, et al., 2018; Prasad, et al., 2019).

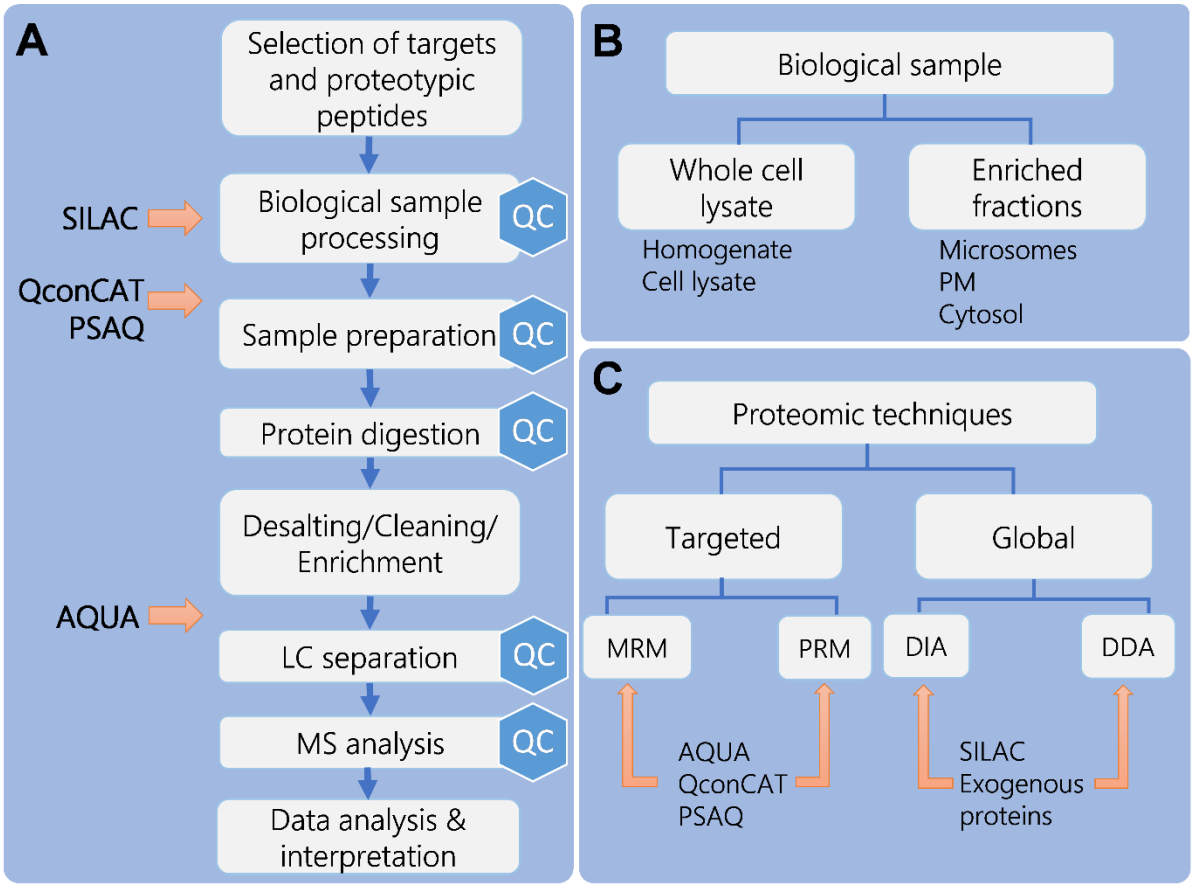

Figure 5.1. Overview of the experimental quantitative proteomic workflow. A. Basic proteomic strategy starting from selection of targets and sample preparation, followed by LC-MS analysis, and finally data analysis/interpretation. Protein digestion relies on proteases, such as trypsin and lysyl endopeptidase (LysC), and can be done in solution, in gel or using filter-aided sample preparation (FASP). Standards are added at different stages of sample preparation. SILAC mixtures represent isotopically labelled proteomes; QconCAT and PSAQ protein standards are added to samples prior to protein digestion; AQUA peptide standards are added before LC-MS analysis. Several quality control (QC) steps are required throughout the workflow. B. The two main types of samples used to generate proteomic data, whole cell lysates (cell and tissue homogenates) and enriched fractions (e.g. microsomes, plasma membrane, cytosol, mitochondrial fractions or S9 fractions). C. The main types of proteomic techniques (targeted and global) and data acquisition methods (MRM/PRM for

targeted proteomics and DDA/DIA for global proteomics). Red arrows show the steps where standards are introduced. Abbreviations: AQUA, absolute quantification peptide standards; DDA, data-dependent acquisition; DIA, data-independent acquisition; MRM; multiple reaction monitoring; QC, quality control; QconCAT, quantitative concatemers; PM, plasma membrane; PRM, parallel reaction monitoring; PSAQ, protein standards for absolute quantification; SILAC, stable isotope labelling by amino acids in cell culture.

5.4. Targeted quantitative proteomic methods

Targeted methods are in many ways superior to global methods for the quantification of specific proteins of interest that are known to be expressed in a particular system. The use of targeted proteomics with enriched fractions (e.g. plasma membrane, microsomes) offers highly reproducible measurements of proteins expressed at low levels. The workflow of quantification using these methods starts with identifying the target proteins of interest, followed by selection of proteotypic peptides used as surrogates to quantify the selected targets. These methods require stable isotope labelled (SIL) internal standards for absolute quantification. Generally, MS platforms used for targeted techniques include triple quadrupole (QqQ), quadrupole/time-of-flight (Q-TOF) and hybrid Orbitrap mass spectrometers. Table 5.1 summarises the advantages and limitations of targeted proteomic methods. The types of targeted acquisition methods are discussed below.

Table 5.1. The overall aims, advantages and limitations of various proteomic data acquisition methods: targeted (MRM, PRM), global data-dependent acquisition (DDA) and data-independent acquisition (DIA) techniques

Method	Advantages	Disadvantages
Targeted techniques (MRM, PRM) **Aim:** Robust quantification of a selected set of proteins, known to be expressed in a particular system	• High sensitivity and reproducibility • Simple data analysis • Allows relative and absolute quantification; SIL standards address matrix effects • High resolution instruments are not required for MRM • High selectivity with PRM	• Limited resolution and selectivity with MRM • Limited number of target proteins (10-50 targets per single analysis) • Requirement of prior knowledge of target proteins • Requirement for synthesis of internal standards • Targeted methods cannot be used for discovery of novel targets or pathways
Global data-dependent acquisition (DDA) techniques **Aim:** discovery proteomics and proteome-wide quantification	• Simple method setup • High proteome coverage • Internal SIL standards are not needed • Allows relative and absolute quantification (with spiked standards or TPA approach) • PTMs can be characterised using global data • Data can provide guidance for targeted quantification	• Bias toward highly expressed proteins and compromised reproducibility for low abundance proteins • Sensitive to changes in LC-MS conditions due to longer runs required • Absolute quantification is relatively less reliable than targeted methods • Requirement of instrument with high-end specifications • Selectivity and sensitivity are compromised
Global data-independent acquisition (DIA) techniques **Aim:** discovery proteomics and proteome-wide quantification. In the case of sequential window methods (SWATH), the aim can also be set to	• Moderate/high precision of peptide quantification. • Wide breadth of peptide identification and quantification leading to high target coverage (typically higher than DDA) • Amenable to discovery and quantitative applications	• Complex and convoluted data • SWATH requires multiple steps to compile spectral libraries, with many parameters to optimise • Requirement of instrument with high-end specifications • Requirement for specialist software and high computational power for analysis

the quantification of a limited number of target proteins	• Provides rich data for targeted methods, including peptide information, fragment information, PTMs and potentially SNPs	

PTM, post-translational modifications; SNP, single-nucleotide polymorphism; TPA, total protein approach

5.4.1. Selected/multiple reaction monitoring (SRM/MRM)

Selected or multiple reaction monitoring (SRM/MRM) is the most commonly used targeted proteomic method in biological and pharmacological research (Gillette & Carr, 2013; Kitteringham, et al., 2009). In MRM, a peptide and a selected set of its fragment ions (transitions) are monitored by mass filtering on a triple quadrupole instrument (Carr, et al., 2014). The technique is routinely used with internal SIL standards, and heavy (standard) and light (analyte) ions are analysed simultaneously. This technique offers several advantages including multiplexed analysis, high throughput, reproducibility, sensitivity and wide dynamic range (Aebersold, et al., 2013; Carr, et al., 2014). The sensitivity achieved by this method makes it ideal when samples are small, e.g. biopsies (Vrana, et al., 2017). The limitations of targeted techniques include the requirement for extensive method development and the selection of suitable targets. Low abundance analyte proteins are not accurately quantifiable and interference can occur due to the use of pre-defined mass filters and low resolution mass analysers (Gillette, et al., 2013; Kitteringham, et al., 2009).

Several applications of this technique have been reported including determination of inter-individual variability in drug-metabolising enzymes and transporters (Gröer, et al., 2014; Kumar, et al., 2015; Margaillan, et al., 2015), prediction of variability in clearance (Vildhede, et al., 2016) and drug-drug interactions (DDIs) (Doki, et al., 2018), determination of inter-species differences of transporter expression at the blood-brain barrier (Al Feteisi, et al., 2018; Hoshi, et al., 2013), characterisation of various hepatocyte-based in vitro systems (Kumar, et al., 2019; Schaefer, et al., 2012), region-specific transporter expression in the brain (Billington, et al., 2019), kidney (Prasad, et al., 2016b) and intestine (Drozdzik, et al., 2014), region-specific enzyme expression in the kidney (Knights, et al., 2016), quantification of biomarkers in biological fluids, such as plasma and urine (Abbatiello, et al., 2015) and assessment of the

effects of disease on different organs (Al-Majdoub, et al., 2019; Billington, et al., 2018; Prasad, et al., 2018).

5.4.2. Parallel reaction monitoring (PRM)

Parallel reaction monitoring (PRM) is a recently introduced targeted method with higher specificity than MRM (Gallien, et al., 2013; Schiffmann, et al., 2014) because of the use of high-end mass spectrometers, such as Orbitrap (Gallien, et al., 2012; Peterson, et al., 2012) and quadrupole/time-of-flight (Schilling, et al., 2015) platforms, offering high resolution and high mass accuracy. The principle of PRM is based on simultaneous monitoring of all (precursor ion/fragment ion) transitions of a targeted peptide arising from both standard and sample, in parallel at the MS and tandem MS (MS/MS) levels. By contrast, the MRM approach monitors only pre-defined fragments. The combination of full scan mode, high resolution and high mass accuracy makes PRM a very attractive method, especially for the analysis of complex biological matrices. PRM requires less time for method development and is less prone to interference than MRM owing to the availability of a higher number of quantifiable fragments (Gallien, et al., 2014; Ronsein, et al., 2015). Because of the large number of monitored transitions, the sensitivity of PRM is sometimes reduced relative to MRM, and the requirement of high resolving power makes the technique less widely applicable (Gallien, et al., 2014). Comparable performance by MRM and PRM has recently been demonstrated (Nakamura, et al., 2016; Ronsein, et al., 2015). Reported applications of PRM-MS include plasma biomarker analysis (Kim, et al., 2015), quantification of enzyme variants (Shi, et al., 2018), and characterisation of liver, kidney and intestine pools (Nakamura, et al., 2016).

5.4.3. Accurate mass and retention time (AMRT)

Quantification (relative or absolute) based on accurate mass and retention time (AMRT) is a simple and rapid method (Silva, et al., 2005). This method is less widely used than MRM and PRM techniques and relies on measurement of precursor ion intensity of analyte and standard

peptides at a predefined mass (*m/z* ratio) and retention time. Confirmation of the peptides identities is carried out after fragmentation at the MS/MS level. This method can be used in conjunction with global proteomic methods to quantify selected targets in proteome-wide analyses. Because AMRT relies on the parent ion intensity in the MS scan, its efficiency is dependent on reproducible peptide separation (by LC) and the use of high resolution mass analysers (MS). In addition, only a limited number of moderate to high abundance proteins can be quantified. This technique was applied to measuring protein abundance in human serum (Silva, et al., 2005) and assessment of disease perturbations in the expression of transporters at the blood-brain barrier (Al-Majdoub, et al., 2019).

5.5. Standards for targeted proteomics

Absolute quantification is typically achieved by targeted techniques that use SIL peptides or proteins as standards or calibrants (Calderón-Celis, et al., 2018). These standards represent heavy versions of the surrogate peptides selected to quantify the target proteins. Standards are synthesised chemically or biologically and incorporate a heavy isotope (^{13}C, ^{15}N), which allows distinction between analyte (light) and standard (heavy) by mass spectrometry. The types of standards routinely used in targeted quantitative proteomics include absolute quantification (AQUA) peptides, quantitative concatemers (QconCAT) and protein standards for absolute quantification (PSAQ). A summary of the characteristics of these standards is shown in Table 5.2.

Table 5.2. Characteristics of standards used in targeted proteomic methods (AQUA, QconCAT and PSAQ) and their analytical performance

	AQUA	QconCAT	PSAQ
Description	Chemically synthesised isotope labelled peptides	Biologically synthesised sequence of isotope labelled peptides	Intact isotopically labelled recombinant protein
Commercial availability	Available	Available	Available
Digestion evaluation	Necessary	Necessary	Not Necessary but desirable
Number of target proteins	One for each standard	Up to 50 per standard protein	One for each standard
Cost	Low, depending on the number of targets	Moderate	High
Considerations for synthesis	Subject to stability issues during the chemical synthesis	Subject to failure of expression	Subject to failure of expression
Addition in the experimental workflow	Post-digestion	Before solubilisation and digestion	Before solubilisation and digestion
Compatible proteomic techniques	MRM PRM	MRM PRM	MRM PRM

		AMRT	
Performance of targeted methods	Highly reproducible Multiplexed	Highly reproducible Multiplexed Ideal for stoichiometric analysis	Highly reproducible Accurate
SNP and stoichiometric analysis	Possible; requires QC	Yes	No
Analysis of PTMs	Yes	No	No

AMRT, accurate mass and retention time mass spectrometry; MRM, multiple reaction monitoring; PRM, parallel reaction monitoring; PTM, post-translational modifications; QC, quality control; SNP, single-nucleotide polymorphism

The selection of standard peptide sequences is a critical step and follows previously reported criteria (Kamiie, et al., 2008). These criteria can also be applied to select surrogate peptides in global proteomic methods (Prasad, et al., 2019). Generally accepted requirements include:

- **Proteotypic sequence:** unique to the protein of interest with distinct mass (*m/z*) and fragmentation pattern (MS/MS); isobaric and isomeric sequences are avoided.
- **Cleavable by proteases used in quantitative proteomics:** the sequence should not be mapped to transmembrane domains; absence of closely occurring cleavage sites in the target protein sequence (e.g. arginine (R) and lysine (K) in the case of trypsin).
- **Detectable by LC-MS:** optimal hydrophobicity (LC) and ionisability (MS); absence of known single nucleotide polymorphism (SNP) and post-translational modification (PTM); optimal length (7-25 amino acids depending on the MS platform).
- **Stable:** not susceptible to chemical modification during storage and handling including oxidation of methionine (M) and deamidation of asparagine/glutamine (N/Q).

These general selection criteria can be customised for different biological applications. For example, peptides with known PTMs and SNPs are targeted if the biological question requires such stoichiometric analysis. Allele-specific protein quantification was demonstrated recently for the assessment of significant genetic variations in CYP and UGT enzymes (Russell, et al., 2013; Shi, et al., 2018).

5.5.1. Absolute quantification (AQUA) peptide standards

SIL peptides or AQUA standards are chemically synthesised isotope labelled standard peptides with sequences specific to the target proteins. High quality and high purity peptides are available commercially in isotopically labelled form, making them easily accessible for large scale studies (Kettenbach, et al., 2011; Kirkpatrick, et al., 2005). A known amount of the AQUA peptide is introduced into the sample at a late stage of sample preparation, usually after

protein digestion. AQUA standards can be applied with MRM or PRM techniques, making these targeted techniques very useful when screening a specific protein in a large number of samples as a clinical test or when the quantification of a small set of proteins is desirable (Smith, et al., 2019). AQUA can also be applied to the elucidation of PTMs, such as phosphorylation (Kettenbach, et al., 2011). However, synthesis and quantification of standards for large scale studies is expensive and time-consuming (Al Feteisi, et al., 2015a). The need to store peptides can be limiting as they tend to precipitate during long-term storage and lead to inconsistent quantification (Mirzaei, et al., 2008). AQUA peptides are normally added to the sample directly before LC-MS analysis and the accuracy of quantification by the AQUA method can therefore be affected by analyte peptide loss during sample preparation (Havliš & Shevchenko, 2004). We recommend addition of standards to the samples before pre-fractionation and desalting so that equal loss of standard and analyte peptides is incurred from the mixture.

The AQUA-MRM approach is the most widely used quantification method in pharmacokinetic research and has been used to quantify various enzymes and transporters in different human tissues. Quantified enzymes include CYP and UGT enzymes in liver (Cieślak, et al., 2016; Fallon, et al., 2013; Hansen, et al., 2019; Ohtsuki, et al., 2012; Prasad, et al., 2018; Sato, et al., 2012, 2014; Weiß, et al., 2018), intestine (Drozdzik, et al., 2018; Gröer, et al., 2014; Harbourt, et al., 2012; Sato, et al., 2014) and Kidney (Harbourt, et al., 2012; Knights, et al., 2016; Sato, et al., 2014). In brain, the AQUA-MRM workflow was used to quantify CYPs, glutathione S-transferases (GSTs) and catechol O-methyltransferase (COMT) (Shawahna, et al., 2011). Non-CYP and non-UGT drug-metabolising enzymes quantified by this method include liver flavin-containing monooxygenases (FMOs), sulfotransferases (SULTs), aldehyde oxidase 1 and alcohol and aldehyde dehydrogenases (Bhatt, et al., 2017; Chen, et al., 2016; Fu, et al., 2013; Yoshitake, et al., 2017). In additions, drug transporters were successfully quantified using this

quantitative strategy in various tissues, including liver (Prasad, et al., 2014a; Wegler, et al., 2017), intestine (Drozdzik, et al., 2014; Gröer, et al., 2013), kidney (Prasad, et al., 2016b), brain (Billington, et al., 2019; Shawahna, et al., 2011; Uchida, et al., 2011) and lung (Fallon, et al., 2018).

5.5.2. Quantitative concatemers (QconCAT)

QconCAT is a concatenated set of peptides expressed recombinantly from an artificial gene. The host organism is usually *E. coli* grown in culture media, supplemented with labelled amino acids, usually $^{13}C_6$-lysine and $^{13}C_6$-arginine. QconCATs are available commercially but can also be expressed in-house at relatively reasonable costs (Russell, et al., 2013). The QconCAT protein is added to the sample at a known concentration (estimated using an unlabelled peptide corresponding to a standard peptide within the QconCAT) prior to digestion and can be used with several targeted techniques (MRM, PRM, AMRT). A single QconCAT can be designed to quantify several proteins (up to 50), making it amenable to multiplexing and achieving higher coverage of protein targets. QconCAT ensures a strict 1:1 stoichiometry making it particularly advantageous in determining polymorphisms (Russell, et al., 2013; Shi, et al., 2018) and establishing protein-protein inter-correlations (Achour, et al., 2014b). The development of QconCAT constructs is time-consuming and most worthwhile when a significant number of proteins (10-50) are to be quantified in a large number of samples. The QconCAT-MRM workflow has been successfully used to quantify hepatic drug-metabolising enzymes (Achour, et al., 2014b; Shi, et al., 2018; Wang, et al., 2015, 2019) as well as transporters in liver (Wegler, et al., 2017), intestine (Harwood, et al., 2016a, 2015) and brain microvessels (Al-Majdoub, et al., 2019; Al Feteisi, et al., 2018).

Complete cleavage of peptides in the digestion process is, of course, essential, and there has been some interest in the use of 'flanking' sequences to make the environment of the peptides more analyte-like so that incomplete digestion will better resemble digestion efficiency of the

target proteins (Cheung, et al., 2015; Kito, et al., 2007). Although this idea is attractive in theory, the claim of comparable digestion efficiency between standard and analyte proteins is yet to be tested. We have preferred to optimise the digestion process so that there is complete release of peptides from the QconCAT and as far as possible of the target proteins (Achour, et al., 2015; Al-Majdoub, et al., 2014).

There is always the possibility of expression failure of a QconCAT, and this has been addressed in several ways (Achour, et al., 2015; Russell, et al., 2013). Experience indicates that smaller QconCATs are generally expressed more efficiently than larger constructs and ideally QconCATs should be below 100 kDa in size (Brownridge, et al., 2011). The use of a small, insoluble tag, such as a ribosomal construct (Al-Majdoub, et al., 2014) can force a QconCAT to express in insoluble form in inclusion bodies, from which it may be readily isolated (Russell et al, 2013). More radically, to address the issue of low yield and expression failure of larger QconCATs, multiplexed efficient expression of recombinant QconCATs (MEERCAT) was recently introduced to serve as standard for large scale protein quantification. The QconCATs are expressed in cell-free medium, with advantages such as expression efficiency, cost-effectiveness and ability to monitor the number of expressed QconCATs (Takemori, et al., 2017).

5.5.3. Protein standards for absolute quantification (PSAQ)

A PSAQ standard is similar in concept to a QconCAT, but consists of an intact isotopically labelled recombinant protein added at a known concentration to the sample under investigation early in the sample preparation workflow. When a PSAQ standard is employed to quantify an unmodified protein, it can control for solubilisation efficiency, digestion and LC-MS conditions; digestion discrepancies are avoided as PSAQ conserves the native context of the target peptides (Chen, et al., 2017). This approach is particularly advantageous when quantifying low abundance, soluble targets in clinical samples (Adrait, et al., 2012; Dupuis, et

al., 2008). However, PSAQ is only applicable to a small number of proteins; the development of such standards is prohibitively expensive and requires rigorous quality control (Al Feteisi, et al., 2015a). This technique is not useful for assessing PTMs, identifying inter-correlations or multiplexed quantification of a large number of targets (Smith, et al., 2019). The application of PSAQ in the quantification of drug-metabolising enzymes and drug transporters in human tissue is yet to be reported. In biomarker research, this method was successfully used to quantify enzymes useful as indicators of cardiovascular disease (Huillet, et al., 2012) and acute kidney injury (Gilquin, et al., 2017) in biological fluids.

5.6. Global quantitative proteomic methods

Global untargeted proteomic approaches are routinely used for assessment of protein expression profiles, biomarker discovery, and identification and quantification of a large number of target proteins. Global approaches offer a wide dynamic range and broad proteome coverage while targeted approaches offer higher precision and accuracy. Proteome-wide quantification by global methods is routinely performed either by stable isotope labelling of sample proteins or peptides, e.g. stable isotope labelling by amino acids in cell culture (SILAC) and isobaric tags for relative and absolute quantitation (iTRAQ) (Ong, et al., 2002; Wiese, et al., 2007), or by label-free analysis of the entire identifiable proteome (Silva, et al., 2006; Vildhede, et al., 2015).

In metabolic labelling methods, such as SILAC, samples are labelled with amino acids (e.g. arginine, lysine or leucine) carrying a stable isotope label (^{13}C, ^{15}N) and pooled before further sample processing, thus minimising bias due to handling. The ratios of light to heavy peptide signals at defined retention times are used to relatively quantify protein expression differences between control and treatment conditions. Recent developments in labelling technology increased the ability of SILAC to multiplex from 2 samples to 6 samples (Merrill, et al., 2014). SILAC is best suited for induction studies, elucidation of drug effects on protein expression

(Kurokawa, et al., 2019; Zhang, et al., 2017), and analysis of post-translational modifications, such as relative quantification of phosphorylated proteins and identification of novel phosphorylation sites (Ibarrola, et al., 2003). In addition, SILAC has been used to prepare labelled standard mixtures for targeted proteomics (Geiger, et al., 2010). These labelled standards are added to analyte samples before protein digestion (Figure 5.1 A), demonstrating similar performance to AQUA standards (Prasad & Unadkat, 2014b). Metabolic labelling of whole animals, such as rodents, represents a recent extension of SILAC, with various applications in pharmacology research, such as the direct quantification of liver drug-metabolising enzymes (MacLeod, et al., 2015).

Chemical labelling methods, such as iTRAQ and tandem mass tags (TMT), are used at the peptide level after proteolytic digestion of sample proteins. Chemical tags react with amine groups and unique reporter ions are released upon fragmentation in MS/MS analysis (Ross, et al., 2004). Unlike SILAC, chemical labelling can be used to analyse up to 8 samples and 11 samples in the same pool using iTRAQ and TMT reagents, respectively. Chemical labelling methods in conjunction with global proteomics demonstrated comparable performance to targeted AQUA-MRM methodology (Vildhede, et al., 2018). Applications of chemical labelling include quantification of hepatic drug-metabolising enzymes and drug transporters (Vildhede, et al., 2018), characterisation of plasma proteins in acute renal rejection (Freue, et al., 2010), biomarker identification for breast cancer (Meiqun, et al., 2011), eye disease (Linghu, et al., 2017) and gum disease (Tsuchida, et al., 2013), and relative quantification of proteins in Alzheimer's disease (Morales, et al., 2017). It is worth noting that proteome-wide labelling methods (SILAC/iTRAQ/TMT) are more aligned with applications that require relative quantification.

In label-free methods, normalisation of measurements uses either unlabelled exogenous protein references or the total protein approach (TPA). Exogenous proteins include various protein

standards distinct from the target proteome; for example, quantification of human enzymes can employ bovine serum albumin or yeast alcohol dehydrogenase at known concentrations (Silva, et al., 2006). The TPA method uses the total intensity of peptide peaks belonging to a certain protein relative to the total intensity of all quantifiable peptides in the proteome (Wiśniewski, et al., 2012b). Both methods have previously been used to quantify human liver enzymes and transporters (Achour, et al., 2017a; Couto, et al., 2019; Vildhede, et al., 2015).

Global proteomic techniques are generally carried out using Q-TOF or Orbitrap instruments. To correct for changes in MS conditions over long analyses, sophisticated correction and chromatographic alignment procedures are used to compensate for retention time shifts and to avoid mismatching peptide peaks across runs (Ludwig, et al., 2018). Data acquisition methods used in global proteomics include data-dependent acquisition (DDA) and data-independent acquisition (DIA). DDA represents the standard shotgun approach widely used for whole-proteome analysis (Geromanos, et al., 2009). On the other hand, the more recent DIA approach can generate more depth of analysis and broader proteome coverage, especially when window acquisition approaches, such as sequential window acquisition of all theoretical fragment mass spectra (SWATH), are used (Hu, et al., 2016; Smith, et al., 2019). A summary of the advantages and limitations of global proteomic methods is presented in Table 5.1.

5.6.1. Data-dependent acquisition (DDA)

In DDA, the initial scan of peptide peaks is used for the selection of peptides for fragmentation depending on their ion intensity, with the most abundant ions being selected preferentially. The main advantages of DDA are its flexibility and broad proteome coverage compared to targeted methods. DDA proteomics can identify thousands of proteins and provide reliable relative quantification across samples (Hu, et al., 2016). DDA can also be used for absolute quantification using suitable exogenous protein standards (Silva, et al., 2006). However, this method is less precise in comparison with targeted quantitative methods as low abundance

peptides are not detected reproducibly, leading to bias toward high abundance proteins (Hu, et al., 2016; Michalski, et al., 2011; Wegler, et al., 2017). The performance of this method declines as sample complexity increases (Bilbao, et al., 2015; Geromanos, et al., 2009).

Q-TOF or Orbitrap mass analysers are normally used and data are interpreted using software packages, such as MaxQuant, Progenesis or Peaks. DDA data analysis can be performed either by spectral counting or by ion abundance/intensity (Ishihama, et al., 2005; Silva, et al., 2006), with ion intensity preferred owing to its higher accuracy and reproducibility (Distler, et al., 2014; Prasad, et al., 2019). Importantly, to ensure robust quantification, consistency in sample preparation and stability of LC-MS conditions are required. DDA shotgun methodology was successfully used for the quantification of transporters and receptors at the blood-brain barrier (Al-Majdoub, et al., 2019) and for profiling various enzymes and transporters in liver tissue (Couto, et al., 2019; Vildhede, et al., 2015, 2018; Wegler, et al., 2017; Wiśniewski, et al., 2019) and hepatocyte-based *in vitro* systems (Vildhede, et al., 2015; Wiśniewski, et al., 2016a).

5.6.2. Data-independent acquisition (DIA)

DIA was proposed to address the limitations of DDA in relation to limited depth of analysis and biased quantification. In DIA, all precursor ions within a selected mass range are fragmented and analysed (Hu, et al., 2016). Theoretically, this method identifies all detectable peptides within the selected mass range and is therefore less biased towards high abundance proteins. However, the generated data tend to be highly complex and specialised software is required for data deconvolution post-acquisition (Ludwig, et al., 2018). DIA combines the advantage of broad proteome coverage offered by DDA methods and highly reproducible quantification, typically achieved by targeted techniques (Gillet, et al., 2016; Hu, et al., 2016). The most widely used DIA approaches include MS^E (Distler, et al., 2014; Silva, et al., 2006) and SWATH (Gillet, et al., 2012). MS^E is a collision energy alternation method that uses a

range of collision energies over a *m/z* window, leading to high- and low-energy fragmentation (Distler, et al., 2014). The deconvoluted spectra are searched against a protein database for identification, while quantification can be done using an unlabelled standard protein. The applications of MS^E include relative and absolute label-free quantification of proteins (Bilbao, et al., 2015). For example, this method was successfully used for quantitative profiling of various drug-metabolising enzymes in human liver (Achour, et al., 2017a).

In methods that use fragmentation windows, such as SWATH-MS, instead of fragmenting the entire set of precursor ions in a particular scan, small *m/z* windows can be selected for fragmentation and acquisition (Gillet, et al., 2012). This potentially reduces the complexity of data and theoretically improves analytical depth and coverage. SWATH is widely applied using Q-TOF and Orbitrap mass analysers, and data are processed by sophisticated pipelines, such as the open-source, cross-platform software OpenSWATH (Röst, et al., 2014). The main advantages of SWATH are its compatibility with the analysis of low abundance sub-proteomes and PTMs, such as acetylation and glycosylation (Keller, et al., 2016), and its high reproducibility and consistency owing to peptide-centric scoring analysis (Ludwig, et al., 2018). SWATH is therefore particularly applicable when wide proteome coverage, high consistency and accurate quantification are required. Post-acquisition interrogation of selected data yields high quality quantification of target proteins comparable to targeted MRM analyses (Gillet, et al., 2012). SWATH has only recently been introduced and therefore it has not been widely used in pharmacology research; reported applications include profiling of hepatic drug-metabolising enzymes (Jamwal, et al., 2017) and quantification of enzymes and transporters in pooled liver, intestine and kidney microsomes (Nakamura, et al., 2016). Importantly, the utility of SWATH has recently been demonstrated in digital biobanking of tissue proteomic maps in health and disease (Guo, et al., 2015).

5.7. Key pharmacology applications of proteomic data

The interaction between various intrinsic and extrinsic factors that affect patient populations can result in variability in the expression levels of PK-relevant proteins and PD targets, leading to variations in drug exposure and response profiles (Figure 5.2 A). Proteomic methods are used to assess the effects of these factors, including age (Bhatt, et al., 2019; Boberg, et al., 2017; Prasad, et al., 2016a; van Groen, et al., 2018), disease (Al-Majdoub, et al., 2019; Billington, et al., 2018; Margaillan, et al., 2015; Prasad, et al., 2018; Wang, et al., 2016), ethnicity (Kawakami, et al., 2011; Peng, et al., 2015) and genetics (Bhatt, et al., 2019; Peng, et al., 2015; Prasad, et al., 2014a), individually or in combination, on protein expression profiles. Changes in abundance associated with perturbed systems relative to control are then used to predict effects on the fate of drugs (Figure 5.2 B) (Bi, et al., 2013; Ishida, et al., 2018; Prasad, et al., 2018; Vildhede, et al., 2014, 2018; Wang, et al., 2016).

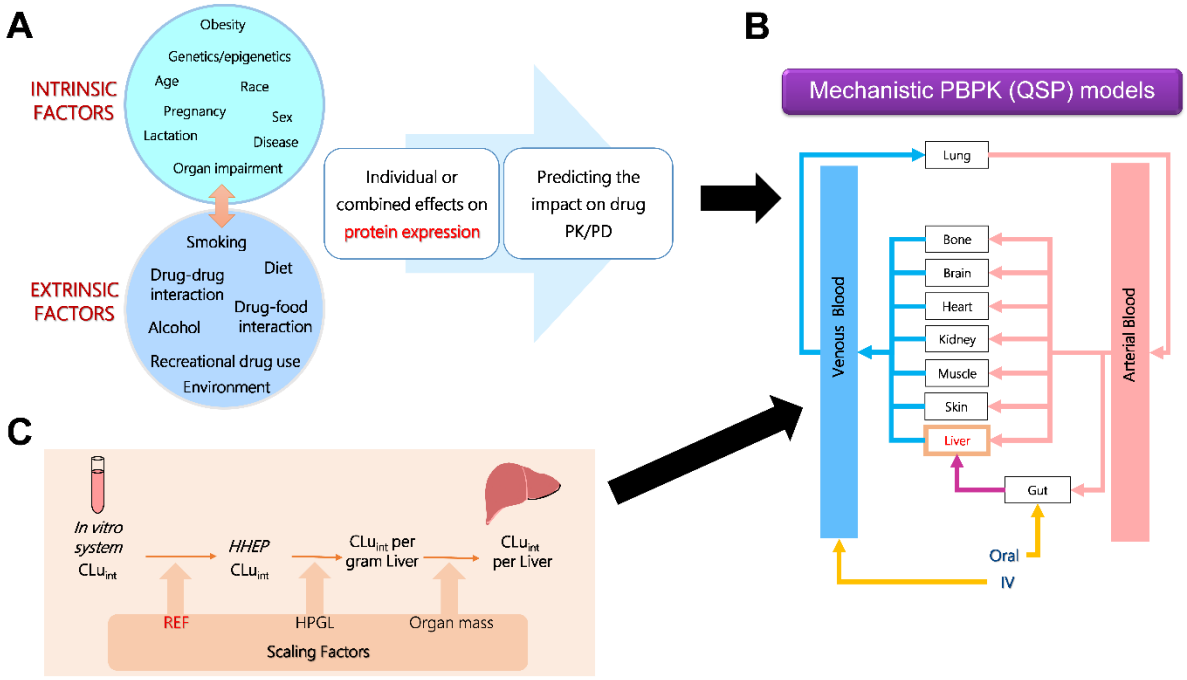

Figure 5.2. The use of proteomic data in PBPK prediction of drug exposure. A. Several intrinsic and extrinsic factors can affect the abundance of proteins which in turn can affect drug PK and PD. B. Effects of intrinsic and extrinsic factors can be simulated using QSP

(PBPK) models that incorporate physiological parameters (e.g. abundance) and drug data. C. The process of extrapolation from in vitro measurements in hepatocytes to the prediction of clearance in human liver; the process of IVIVE is used in combination with PBPK (or QSP) models (B) to predict drug PK (or PD) in a population of interest. Scaling factors used in IVIVE from hepatocytes are REF = Abundance in tissue/Abundance in the in vitro system, HPGL and liver mass. Abbreviations: CLu_{int}, intrinsic clearance of unbound drug; HHEP, human hepatocytes; HPGL, hepatocytes per gram liver; IV, intra-venous administration; PBPK, physiology-based pharmacokinetics; PD, pharmacodynamics; PK, pharmacokinetics; QSP, quantitative systems pharmacology; REF, relative expression factor measured using abundance data.

Ideally, measurement of the effects on abundance and activity of functional proteins should be carried out and used to achieve robust predictions; however, specific substrates and optimised functional assays are still lacking for enzymes and transporters, with the exception of several CYP and UGT enzymes (den Braver-Sewradj, et al., 2017; Walsky, et al., 2012, 2004). Abundance is commonly used as a surrogate for activity; correlation between protein abundance and activity was demonstrated for various hepatic and renal drug-metabolising enzymes, such as CYPs, UGTs, carboxylesterase 1, aldehyde oxidase 1, flavin-containing monooxygenases and sulfotransferases (Achour, et al., 2017b; Chen, et al., 2016; Fu, et al., 2013; Knights, et al., 2016; Margaillan, et al., 2015; Ohtsuki, et al., 2012; Venkatakrishnan, et al., 2000; Wang, et al., 2019; Xie, et al., 2017). This was also demonstrated for certain transporters, such as P-gp and BCRP (Harwood, et al., 2016c; Kumar, et al., 2015). *In vitro* measurements are therefore routinely extrapolated to *in vivo* activity (IVIVE) using scaling factors that rely on abundance measurements (C) (Barter, et al., 2007; Harwood, et al., 2016a). In addition to scaling, measuring the abundance of pharmacologically relevant proteins also allows evaluation of the sources of variability in activity rates; inter-individual variation is

driven by variability in the level of expression, alterations in intrinsic protein activity, or a combination of these factors (Zhang, et al., 2016). Below is a brief account of the main pharmacology applications of proteomic data. Each application requires a different level of proteomic analysis (absolute quantification, relative quantification or discovery/identification) as illustrated in Figure 5.3.

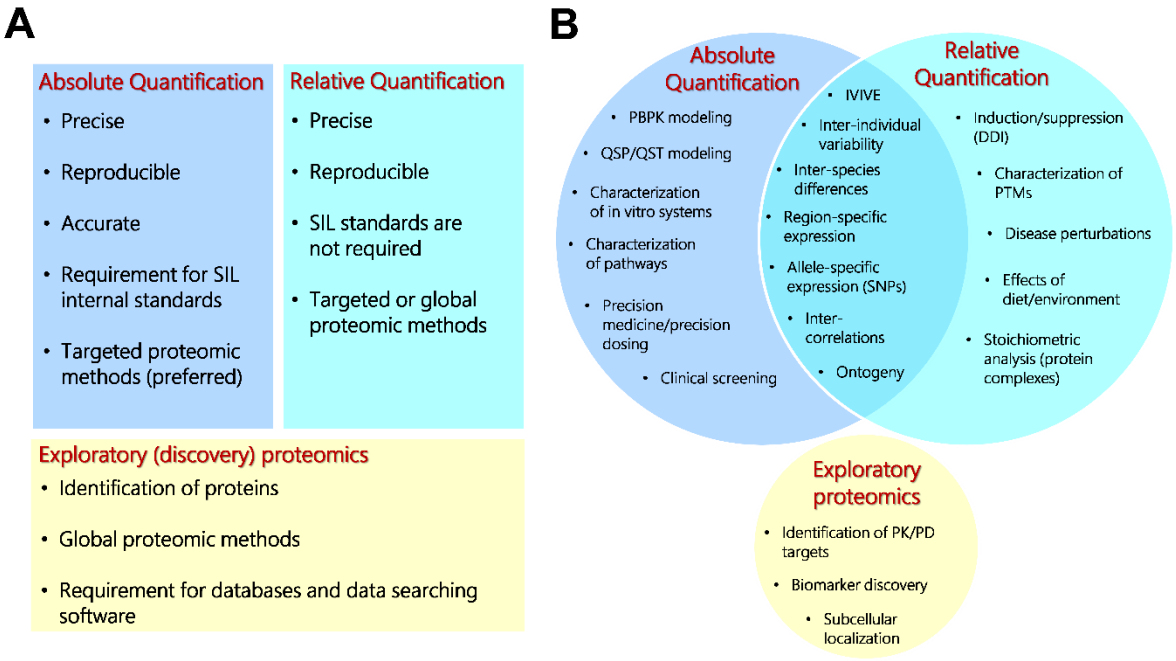

Figure 5.3. The characteristics and applications of absolute quantification, relative quantification and discovery proteomic approaches. A. The requirements and characteristics of different levels of quantitative proteomic analysis. Absolute quantification requires assays that are accurate and precise; relative quantification requires reproducibility. B. Applications of data generated using absolute quantification, relative quantification and exploratory proteomics in translational PK and PD research. Several applications overlap between absolute and relative quantification. Abbreviations: DDI, drug-drug interaction; PBPK, physiology-based pharmacokinetics; PD, pharmacodynamics; PK, pharmacokinetics; PTM, post-translational modification; QSP, quantitative systems pharmacology; QST, quantitative systems toxicology; SIL, stable isotope label; SNP, single nucleotide polymorphism.

5.7.1. Physiology-based pharmacokinetic (PBPK) modelling and IVIVE

The use of PBPK models has now become firmly embedded in practices within the pharmaceutical industry and evidence from these models is used in different phases of drug development (Huang, et al., 2013; Jamei, 2016). PBPK modelling has gained wide acceptance with regulatory agencies (Rowland, et al., 2015), with PBPK data being used in the labels of 21% of new drug applications approved by US Food and Drug Administration (FDA) in 2015 (Marsousi, et al., 2017). Modelling is commonly used for prediction of human pharmacokinetic parameters and evaluation of the effects of factors affecting a patient population, such as genetics and lifestyle (Heikkinen, et al., 2015; Prasad, et al., 2017). PBPK models are built by integrating drug profiles with physiological data, including blood flow, organ size, protein binding, and abundances of enzymes and transporters (Figure 5.2) (Jones & Rowland-Yeo, 2013). Various commercial and non-commercial platforms, e.g. Simcyp, GastroPlus, and PK-Sim, have facilitated the use of PBPK modelling (Kuepfer, et al., 2016), but all require data describing protein abundance and population variability, and such data are still in short supply (Heikkinen, et al., 2015). Key areas where PBPK models suffer from limited data include non-CYP and non-UGT metabolic pathways, extra-hepatic drug-metabolism and disposition, effects of differences in special populations (e.g. hepatically/renally-impaired, paediatric and geriatric patients) and inter-species variability. These limitations have started to be addressed in recent years mainly because of increased availability of (biopsy and surgical) tissue samples, advances in sample preparation methods and increased application of LC-MS proteomic techniques.

The use of IVIVE has extended the utility of PBPK modelling and made biosimulation more widely usable by linking modelling to *in vitro* studies using animal and human systems (Sager, et al., 2015). The application of IVIVE-PBPK requires integration of absolute abundance data in tissue relative to the *in vitro* system and system-specific scaling factors (e.g. microsomal

protein content or hepatocellularity) with various patient-derived physiological parameters (Barter, et al., 2007) to predict pharmacokinetic profiles and account for metabolic differences among specific populations (Rostami-Hodjegan, 2012). A recent systematic survey of the literature showed that the majority of PBPK models are used for the assessment of clinical pharmacokinetics and DDIs (Sager, et al., 2015). Recently reported PBPK models that used proteomic data were developed for an array of applications, such as the prediction of variability in clearance (Harwood, et al., 2016b; Kumar, et al., 2018; Vildhede, et al., 2018), variability in DDIs (Doki, et al., 2018), impact of formulation (Johnson, et al., 2014), effects of liver disease (Prasad, et al., 2018; Wang, et al., 2016) and kidney impairment (Zhao, et al., 2012) on drug pharmacokinetics, and predicting drug kinetics in paediatrics (Jiang, et al., 2013; Johnson, et al., 2014; Ladumor, et al., 2019), older patients (Polasek, et al., 2013) and during pregnancy (Gaohua, et al., 2012; Ke, et al., 2013, 2014). In addition to these applications, PBPK models represent a valuable tool for learning and internal decision making in the pharmaceutical industry as well as storing and integrating compound-specific information throughout drug discovery and development.

5.7.2. Quantitative systems pharmacology (QSP) models

Models with broader pharmacological applications include QSP models which represent new tools for drug development (Danhof, 2016), with several applications, including prediction of the effects of therapeutic agents, mechanisms of interaction between therapeutic targets and elucidating the biological processes underlying disease and resistance to drugs (Dimitrova, et al., 2017; Kirouac, 2018; Kirouac, et al., 2015). The US FDA has recently adopted the use of these models and the first case was the assessment of a novel parathyroid hormone replacement biologic (Peterson & Riggs, 2015). The use of QSP models for supporting new drug submissions is therefore expected to increase (Niu, et al., 2019). In particular, a promising application of QSP models is the assessment of pharmacodynamics DDI potential by probing

the mechanisms of interaction of a drug combination in the system and exploring the outcomes of target perturbations, as reported recently for the interaction between glibenclamide and the glucose-insulin-glucagon system in Type 2 diabetes (Choy, et al., 2013). The requirement for multi-omics data is emphasised for building pharmacology and toxicology models with the essential role of pharmaco- and toxico-proteomics in identifying and quantifying critical proteins in pathways affected by drug, chemical and environmental exposure (Wetmore & Merrick, 2004). This normally follows a strategy consisting of a discovery method followed by robust targeted quantification (Gillet, et al., 2016). Proteomic data were previously used as the basis for developing QSP models to predict the effects of drugs, such as gemcitabine and birinapant in pancreatic cancer (Zhu, et al., 2018) and 5-flurouracil in colorectal cancer (Hector, et al., 2012).

5.7.3. Disease perturbation

Disease perturbation models are QSP models that aim to simulate disease progression and assess the effects of different drug regimens on a diseased population. Modelling disease perturbations requires relative abundance data for the diseased tissue compared to a healthy set of samples used as control. Disease-scale models have been applied to several disease states, including cirrhosis and different types of cancer. Cirrhosis is a disease of the liver that significantly affects drug metabolism and disposition and hence disease modelling can help with tailoring dosage regimens that are both safe and efficacious. Liver fibrosis generally leads to a reduction in expression of phase I and phase II enzymes (including CYPs, UGTs and sulfotransferases), and consequently, progressive decline in their abundance and activity is observed as the disease advances (Fisher, et al., 2009; Hardwick, et al., 2013). Proteomic evidence of changes in the abundance of CYPs, UGTs and other hepatic enzymes was reported in cirrhotic livers and was shown to be dependent on the cause of cirrhosis (Prasad, et al., 2018). Phase I metabolising enzymes are reported to be more influenced by disease progression than

phase II pathways which can be attributed to shortage in blood supply reaching the scarred tissue (Yang, et al., 2003). Incorporating proteomic data into disease-scale PBPK models has led to improved model performance in cirrhosis as reported for zidovudine, morphine (Prasad, et al., 2018), repaglinide, bosentan, telmisartan, valsartan and olmesartan (Li, et al., 2015; Wang, et al., 2016).

Applications of disease models have also been highlighted for different malignancies, including breast cancer (Hodgkinson, et al., 2012) and colon cancer (Hector, et al., 2012). These models were mainly used to predict the prognosis in certain populations and assess the effect of anti-cancer regimens at different stages of the disease. Because of the difficulty in recruiting cancer patient populations in clinical studies and the ethical issues related to the exposure of healthy subjects to toxic anti-cancer drugs, PBPK models are better accepted in oncology drug development compared to other disease states (Yoshida, et al., 2017). There is currently a lack of abundance data in cancer, and LC-MS proteomics is set to address this gap by providing quantitative measurements of enzymes and transporters from biopsies and archived surgical samples (Prasad, et al., 2017).

5.7.4. Protein inter-correlations

Inter-individual variation in drug PK and PD can largely be predicted by integration of known sources of variability, including demographic factors (e.g. age and ethnicity) and physiological parameters (e.g. blood flow, levels of enzymes and transporters) (Jamei, et al., 2009). *In silico* approaches, such as PBPK models, can simulate the interaction between different covariates, such as changes in enzyme/transporter abundance, and predict their effects on clearance and DDIs (Doki, et al., 2018; Melillo, et al., 2019). Considering the inter-correlation between the expression levels of pharmacologically active proteins, and indeed between other physiological parameters (e.g. liver size and blood flow), can lead to more plausible parameter combinations when sampling from a population distribution (Tsamandouras, et al., 2015). Multiplexed

quantitative proteomics can measure multiple enzymes and transporters in individual biological samples simultaneously, allowing robust assessment of inter-correlations between these proteins (Achour, et al., 2014a; Prasad, et al., 2019). Due to the nature of correlation analysis, technical bias can in some cases lead to apparent relationships in protein expression and therefore caution should be exercised in order to use only verified biological inter-correlations in modelling applications (Heikkinen, et al., 2015).

While various inter-correlations between drug-metabolising enzymes and transporters have been confirmed both at the RNA (Izukawa, et al., 2009; Wortham, et al., 2007; Zhang, et al., 2016) and protein levels (Achour, et al., 2014b; Cheung, et al., 2019; Couto, et al., 2019; Mooij, et al., 2016), the quantitative impact of such relationships on pharmacokinetic outcomes has only recently started to be explored, with models incorporating inter-correlations outperforming those that do not (Barter, et al., 2010; Doki, et al., 2018). It is expected that the use of more realistic combinations of physiological parameters will be widely practiced in PK and PD modelling and simulation (Melillo, et al., 2019).

5.7.5. Precision dosing

Model-informed precision dosing (MIPD) aims to predict the right dose of a drug for a specific patient based on individual characteristics. This is expected to lead to improved efficacy and reduced toxicity and pave the way to individualised therapy (Darwich, et al., 2017). This approach is most applicable to drugs with a narrow therapeutic index and for special populations, such as paediatrics, geriatrics and patients with hepatic and renal impairment (Polasek, et al., 2018). Multi-omic approaches and recent developments in ‘liquid biopsy’ assays (Rowland, et al., 2019) are expected to facilitate the construction of ‘virtual twins’ as a useful strategy to enable precision dosing. A ‘virtual twin’ is an *in silico* model that represents an individual patient, created by integrating system parameters (i.e. demographic, clinical and enzyme/transporter abundance data) from the patient in order to simulate individualised drug

response (Patel, et al., 2018). This requires collection of absolute and relative expression data (Polasek, et al., 2018) measured in individual patients using innovative sampling techniques, such as the use of biofluids (Boukouris & Mathivanan, 2015).

5.7.6. Ontogeny

The process of growth and maturation is thought to be the main contributor to observed differences in drug PK profiles across the paediatric population age range and when compared to adult populations (Fernandez, et al., 2011). For example, physiological changes, such as gastric pH and emptying and intestinal motility that occur from birth to adulthood affect the rate of drug absorption. This is particularly evident in neonates in which absorption is generally delayed (Batchelor & Marriott, 2015; Lu & Rosenbaum, 2014). In addition, the ontogeny of drug-metabolising enzymes, such as CYPs and UGTs, and transporter proteins within the liver and other organs contributes to variable rates of drug metabolism and excretion (Badée, et al., 2019; Bhatt, et al., 2017, 2019; Boberg, et al., 2017; van Groen, et al., 2018), with consequences for toxicity and efficacy profiles (Batchelor, et al., 2015; Elmorsi, et al., 2016).

Current drug dosing regimens for paediatrics are based on allometric scaling from adult populations or reliant on local guidance and clinician experience because of lack of data from clinical trials (Calvier, et al., 2017). Regulators are increasingly supportive of mechanistic PBPK models to inform drug labels in lieu of clinical trials in paediatric applications (Jones, et al., 2015; Miller, et al., 2019). There is still, however, a paucity of data to feed these paediatric models, in large part because paediatric samples are obtained opportunistically (Howard, et al., 2018; Templeton, et al., 2018).

Despite the difficulties of sample collection, there is consensus that the abundance and function of the majority of enzyme and transporter proteins are comparatively low in foetal and neonatal samples, increasing at varying rates as a function of age toward adult equivalent levels (Badée,

et al., 2019; Chen, et al., 2016; Cheung, et al., 2019; Upreti & Wahlstrom, 2016). For example, CYP3A4, UGT2B7 and P-gp are present in small amounts in neonatal samples, increasing toward or surpassing adult equivalent levels by 1-3 years of age (Bhatt, et al., 2019; Mehrotra, et al., 2015; van Groen, et al., 2018). Conversely, CYP3A7 abundance is relatively high in foetal and neonatal samples, decreasing rapidly toward adult equivalent levels within 1 year (Leeder & Meibohm, 2016; Mehrotra, et al., 2015). Incorporation of ontogeny profiles with *in silico* models led to useful pharmacokinetic predictions for several drugs, such as theophylline (Ginsberg, et al., 2004), propofol (Michelet, et al., 2018), tramadol (T'jollyn, et al., 2015) and valproic acid (Ogungbenro & Aarons, 2014), in children.

5.7.7. Characterisation of polymorphisms

Most drug-metabolising enzymes, particularly CYPs, and transporters, such as organic anion transporting polypeptides, are polymorphic with a range of clinical consequences (Oswald, 2019; Zhou, et al., 2017). Various genetic polymorphisms are non-synonymous and can be characterised at the protein level, while polymorphisms occurring in the regulatory region of a gene can affect gene expression and mRNA stability in a particular tissue but do not result in modifications to the protein sequence. The effect of polymorphism becomes significant when it causes variability to an extent that necessitates a change in the administered dose of a specific drug (Gentry, et al., 2002); a case in point is CYP2C9 polymorphism and its effects on the required dose of the anti-coagulant warfarin. Our group has previously developed an allele-specific proteomic workflow that can distinguish different polymorphic variants of CYP2B6 (Achour, et al., 2014b; Russell, et al., 2013). Shi et al. (2018) showed applicability of this approach to UGT2B15 with the aim of elucidating the regulatory mechanisms of UGT expression. Although relative quantification is as applicable to studying polymorphisms as absolute quantification, this application requires accurate and reproducible assessment of the

stoichiometry of target enzymes (or transporters), and therefore targeted proteomic methods that employ a QconCAT standard are especially suitable (Achour, et al., 2019).

5.7.8. Disease biomarker discovery

Identification of biomarkers assists in understanding the pathophysiology of a disease and its progression, as well as monitoring patient response during therapy (Hector, et al., 2012; O'Dwyer, et al., 2011). This is applicable not only to traditional drugs but also to testing the efficacy of new candidates and comparing them to already available therapeutic agents. Often more than one biomarker is necessary to characterise a disease state, where the synergy between several targets in the same (or related) disease pathway makes a composite test more effective than monitoring a single biomarker of disease (Russell, et al., 2017). A rigorous discovery proteomics workflow should consist of a preliminary discovery phase using global proteomics, such as shotgun DDA or SWATH profiling, followed by verification or validation of target proteins using more quantitative targeted techniques, such as MRM or PRM. The settings of the targeted experiment will depend on information collected in the discovery phase (Prasad et al., 2019).

The initial step can be performed on a small set of well-characterised samples from patients with the relevant disease state relative to control with the aim of identifying differentially expressed proteins (Gillet, et al., 2016; O'Dwyer, et al., 2011). Global proteomics has led to the discovery of various diagnostic biomarkers, such as proteins related to resistance to cancer chemotherapy, and biomarkers for monitoring treatment (Russell, et al., 2016; Srivastava & Creek, 2019). These biomarkers are normally associated with critical cell function pathways, such as survival, proliferation (Shruthi, et al., 2016), apoptosis (Hector, et al., 2012) and post-translational modification of proteins (Held, et al., 2010). After conclusive identification of a set of biomarkers, targets are quantified in samples from different populations, such as patients

at different stages of the disease, and a healthy cohort (Elschenbroich, et al., 2011; Sjöström, et al., 2015).

A promising application of global proteomics showed differences in expression profiles between Crohn's disease and ulcerative colitis, which are symptomatically very similar but require entirely different treatment regimens (Starr, et al., 2017). In cancer, a wide range of signalling pathways can be perturbed, including the function of protein kinases and phosphatases, which can be monitored as disease biomarkers and targeted by novel drug therapies (Bhullar, et al., 2018; Bollu, et al., 2017). Recently characterised cancer biomarkers for the assessment of prognosis and therapy-related considerations include HER2 for decision-making in cancer treatment (Kirouac, et al., 2015), cAMP-CREB1 axis as a key mechanism associated with resistance to platinum-based therapy (Dimitrova, et al., 2017), caspase networks associated with prognosis of colorectal cancer (Hector, et al., 2012), Stathmin-1 in relation to cell migration in colon cancer metastasis (Tan, et al., 2012), and protein Z as an early biomarker for the detection of ovarian cancer (Russell, et al., 2016).

5.8. Recommendations for best practice in applying proteomic techniques

With the recent expansion in the use of proteomic techniques in clinical and pharmacology research, robust guidelines have become crucially required for choosing the most appropriate method for a specific application. The decision-making process tends to be complex and will depend on multiple factors including the biological question, the type of sample, the number of samples, the number of targets, and the available budget. Figure 5.4 shows a simplified decision tree intended to guide the choice of proteomic methods used for pharmacology applications. In the same line, a workshop was recently held by the International Society for the Study of Xenobiotics (ISSX), with the aim of reaching a consensus on the use of proteomics in translational pharmacology research. Various recommendations for the choice and

application of different techniques were proposed but a general consensus was not achieved (Prasad, et al., 2019).

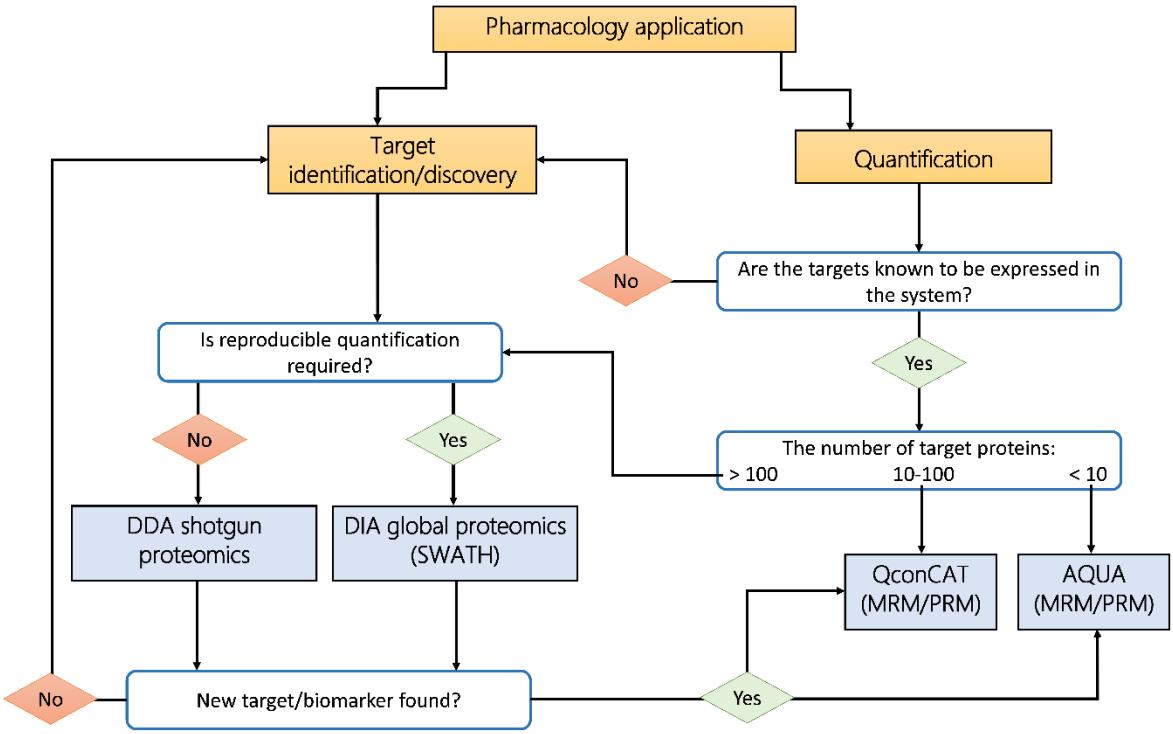

Figure 5.4. Decision tree for choosing suitable proteomic techniques intended for pharmacology applications. A typical number of samples (~30) is used as input for the decision tree. The application can be hypothesis-driven and focused on quantification or hypothesis-generating and intended for discovery. If the application is focused on discovery, global proteomics are most suitable, with preference for data-independent acquisition when reproducible quantification of differential expression is required. When a target or a biomarker is discovered, more accurate quantification is achieved with targeted proteomics. If the target proteins are known to be expressed in the system and are well-defined, targeted proteomics are preferred. If the number of targets is small (< 10), AQUA-based methods (in conjunction with MRM or PRM techniques) are cost-effective. When the number of targets is higher (10-100), QconCAT methodology is preferred. Quantification of larger numbers of targets (> 100) and characterization of proteomes is better achieved using global proteomics. Orange boxes denote applications and blue boxes represent proteomic methods.

Considerations for choosing a technique will generally differ for targeted and global proteomic methods. In targeted analysis, isotopically labelled standards are used to improve precision and accuracy of measurements and reduce bias caused by variations in sample preparation and matrix effects (Bhatt, et al., 2018). This is desirable when accurate quantification of inter-individual variability is required for QSP models and MIPD. Techniques recommended for these applications include MRM applied on triple quadrupole instruments and PRM conducted on higher resolution platforms, such as Orbitraps and Q-TOF instruments. Both methods can be used for multiplexed quantification and they offer a wide dynamic range, typically two orders of magnitude, and therefore spiking of standards should be guided by the range of targeted proteins. One of the main advantages of targeted analysis is possibly its unparalleled sensitivity achieved even in the presence of a complex biological matrix (Holman, et al., 2012). Therefore, recommended practice is to quantify protein expressed at very low abundance in a targeted manner. MRM is currently the 'gold standard' in clinical and pharmacological research (Carr, et al., 2014), and recent guidelines by the Clinical Proteomic Tumour Analysis Consortium (CPTAC) provides recommendations and standard operating procedures (SOPs) for the development, application and reporting of MRM assays (Abbatiello, et al., 2017; Whiteaker, et al., 2014). Large-scale cross-laboratory assessment of plasma proteins showed improved quantification when harmonised SOPs are followed (Abbatiello, et al., 2015). Triple quadrupole instruments used for MRM are less expensive than higher resolution mass spectrometers and the use of scheduled MRM improves the reproducibility of the data and increases the number of peptides that can be analysed in one experiment (Oswald, et al., 2013), thus reducing the cost and time of analysis. PRM methodology offers advantages in selectivity, resolution and sensitivity while requiring a lower level of method development compared to MRM (Peterson, et al., 2012). Orbitrap and Q-TOF instruments tend to be expensive but they

represent versatile platforms capable of targeted (PRM) and global analyses (Peterson, et al., 2012; Schilling, et al., 2015).

Targeted techniques rely on the use of labelled standards and the choice of suitable standards depends on the type of experiment and available budget and expertise. Isotope-labelled internal standards tends to be expensive, but they provide better quality quantification (higher precision and accuracy) than label-free methods. AQUA peptides are ideal for screening applications where a small number of proteins (< 10) are monitored in a large number of samples. QconCATs are more applicable when higher numbers of proteins are targeted and for applications that require strict stoichiometry, such as allele-specific proteomics (Achour, et al., 2019; Shi, et al., 2018). QconCAT standards have the advantage of sustainability and transferability across laboratories (Russell, et al., 2013); a plasmid can be shared by different groups with access to protein expression facilities. We have previously developed a cost-benefit framework to assess the use of quantitative proteomic methods based on cost and application (Al Feteisi, et al., 2015a). This assessment showed that the high cost of PSAQ standards hinders their application when a considerable set of proteins are targeted.

For applications that aim to identify novel proteins or quantify a large number of targets (> 100 proteins), the method of choice is global proteomics. Shotgun global proteomics, in conjunction with the TPA approach, can be cheaper than targeted methods because they do not require the use of labelled standards. This method is applied with Q-TOF and Orbitrap instruments and has a wide range of hypothesis-generating applications, including proteome-wide analysis, assessment of disease perturbations and biomarker discovery. Data-independent methods, such as SWATH, offer increased depth of analysis and quantitative reproducibility (Gillet, et al., 2012), making them very suitable for generating protein network data for systems pharmacology applications. Their use is however still restricted to core facilities, and sophisticated bioinformatics tools are required for data analysis and interpretation (Distler, et

al., 2014; Röst, et al., 2014). A combined discovery-quantification strategy is recommended when characterising a novel target or disease pathway (Gillet, et al., 2016). This requires using global analysis (e.g. SWATH) on well-defined (disease and control) samples followed by targeted (MRM or PRM) quantification.

The concept of a 'proteomic map of disease' has recently been proposed (Guo, et al., 2015; Xu, et al., 2019), supported by highly reproducible sample preparation and global proteomic workflows. We recommend that major academic centres should conduct harmonised efforts to generate and share similar proteomic maps in health and disease for available biopsy and surgical samples from different tissues, as demonstrated recently (Uhlen, et al., 2015). This will likely require the use of highly reproducible methods capable of wide proteome coverage, such as SWATH-MS (Gillet, et al., 2012), and these digital maps can be interrogated retrospectively by various groups for future applications.

5.9. Conclusion

Quantitative proteomic measurements can make a significant contribution to the advance of quantitative systems pharmacology and can be relatively quickly translated into the clinic, where they directly benefit patients. These measurements are powerful, providing selectivity and sensitivity unparalleled by other protein-level techniques. The disadvantage of the unparalleled sensitivity is that independent orthogonal verification of a measurement is often challenging. Further, the cost of these experiments and small sample sizes preclude extensive sample sharing and cross-laboratory analyses. Prasad et al. (2019) have highlighted the difficulty in obtaining consensus as to appropriate protocols for different measurements, especially as the most thorough approaches are beyond the budgets of many laboratories.

We can however make a number of broad observations. Firstly, targeted methods are preferred where a specific, poorly expressed set of proteins is to be quantified, whereas global methods are better adapted to gaining a general picture of the functional proteome in a cell. Secondly,

while there is merit in terms of accuracy in analysing unfractionated samples, the loss of precision and sensitivity compared with the use of fractions is often critical. Thirdly, neither QconCAT proteins nor AQUA peptides are ideal as standards for targeted proteomics; QconCATs are favourable where large numbers of similar samples are to be analysed for several proteins, whereas AQUA peptides are effective for small numbers of target proteins. When a decision is made, the minimal requirement is that the use of a particular quantitative proteomic technique should be 'fit for purpose'. Ultimately, the selected method and the level of proteomic quantification will have a substantial impact on the quality and validity of model-informed predictions.

5.10. References

Abbatiello, SE, Ackermann, BL, Borchers, C, Bradshaw, RA, Carr, SA, Chalkley, R, Choi, M, Deutsch, E, Domon, B, Hoofnagle, AN, Keshishian, H, Kuhn, E, Liebler, DC, MacCoss, M, MacLean, B, Mani, D, Neubert, H, … Zimmerman, L. (2017). New Guidelines for Publication of Manuscripts Describing Development and Application of Targeted Mass Spectrometry Measurements of Peptides and Proteins. *Mol. Cell. Proteomics*, 16(3), 327–328.

Abbatiello, SE, Schilling, B, Mani, DR, Zimmerman, LJ, Hall, SC, MacLean, B, Albertolle, M, Allen, S, Burgess, M, Cusack, MP, Gosh, M, Hedrick, V, Held, JM, Inerowicz, HD, Jackson, A, Keshishian, H, Kinsinger, CR, … Carr, SA. (2015). Large-Scale Interlaboratory Study to Develop, Analytically Validate and Apply Highly Multiplexed, Quantitative Peptide Assays to Measure Cancer-Relevant Proteins in Plasma. *Mol. Cell. Proteomics*, 14(9), 2357–2374.

Achour, B, Al-Majdoub, ZM, Al Feteisi, H, Elmorsi, Y, Rostami-Hodjegan, A, and Barber, J. (2015). Ten years of QconCATs: Application of multiplexed quantification to small medically relevant proteomes. *Int. J. Mass Spectrom.*, 391, 93–104.

Achour, B, Al Feteisi, H, Lanucara, F, Rostami-Hodjegan, A, and Barber, J. (2017a). Global Proteomic Analysis of Human Liver Microsomes: Rapid Characterization and Quantification of Hepatic Drug-Metabolizing Enzymes. *Drug Metab. Dispos.*, 45(6), 666–675.

Achour, B, and Barber, J. (2013). The activities of Achromobacter lysyl endopeptidase and Lysobacter lysyl endoproteinase as digestive enzymes for quantitative proteomics. *Rapid Commun. Mass Spectrom.*, 27(14), 1669–1672.

Achour, B, Barber, J, and Rostami-Hodjegan, A. (2014a). Expression of hepatic drug-metabolizing cytochrome p450 enzymes and their intercorrelations: a meta-analysis. *Drug Metab. Dispos.*, 42(8), 1349–1356.

Achour, B, Dantonio, A, Niosi, M, Novak, JJ, Fallon, JK, Barber, J, Smith, PC, Rostami-Hodjegan, A, and Goosen, TC. (2017b). Quantitative Characterization of Major Hepatic UDP-Glucuronosyltransferase Enzymes in Human Liver Microsomes: Comparison of Two Proteomic Methods and Correlation with Catalytic Activity. *Drug Metab. Dispos.*, 45(10), 1102–1112.

Achour, B, Rostami-Hodjegan, A, and Barber, J. (2019). Response to "Determining Allele-Specific Protein Expression (ASPE) Using a Novel Quantitative Concatamer Based Proteomics Method". *J. Proteome Res.*, 18(1), 574.

Achour, B, Russell, MR, Barber, J, and Rostami-Hodjegan, A. (2014b). Simultaneous quantification of the abundance of several cytochrome P450 and uridine 5'-diphospho-glucuronosyltransferase enzymes in human liver microsomes using multiplexed targeted proteomics. *Drug Metab. Dispos.*, 42(4), 500–510.

Adrait, A, Lebert, D, Trauchessec, M, Dupuis, A, Louwagie, M, Masselon, C, Jaquinod, M, Chevalier, B, Vandenesch, F, Garin, J, Bruley, C, and Brun, V. (2012). Development of a Protein Standard Absolute Quantification (PSAQ^{TM}) assay for the quantification of Staphylococcus aureus enterotoxin A in serum. *J. Proteomics*, 75(10), 3041–3049.

Aebersold, R, Burlingame, AL, and Bradshaw, RA. (2013). Western blots versus selected

reaction monitoring assays: time to turn the tables? *Mol. Cell. Proteomics*, 12(9), 2381–2382.

Al-Majdoub, ZM, Al Feteisi, H, Achour, B, Warwood, S, Neuhoff, S, Rostami-Hodjegan, A, and Barber, J. (2019). Proteomic quantification of human blood–brain barrier SLC and ABC transporters in healthy individuals and dementia patients. *Mol. Pharm.*, 16(3), 1220–1233.

Al-Majdoub, ZM, Carroll, KM, Gaskell, SJ, and Barber, J. (2014). Quantification of the Proteins of the Bacterial Ribosome Using QconCAT Technology. *J. Proteome Res.*, 13(3), 1211–1222.

Al Feteisi, H, Achour, B, Barber, J, and Rostami-Hodjegan, A. (2015a). Choice of LC-MS Methods for the Absolute Quantification of Drug-Metabolizing Enzymes and Transporters in Human Tissue: a Comparative Cost Analysis. *AAPS J.*, 17(2), 438–446.

Al Feteisi, H, Achour, B, Rostami-Hodjegan, A, and Barber, J. (2015b). Translational value of liquid chromatography coupled with tandem mass spectrometry-based quantitative proteomics for in vitro – in vivo extrapolation of drug metabolism and transport and considerations in selecting appropriate techniques. *Expert Opin. Drug Metab. Toxicol.*, 11(9), 1357–1369.

Al Feteisi, H, Al-Majdoub, ZM, Achour, B, Couto, N, Rostami-Hodjegan, A, and Barber, J. (2018). Identification and quantification of blood-brain barrier transporters in isolated rat brain microvessels. *J. Neurochem.*, 146(6), 670–685.

Badée, J, Fowler, S, de Wildt, SN, Collier, AC, Schmidt, S, and Parrott, N. (2019). The Ontogeny of UDP-glucuronosyltransferase Enzymes, Recommendations for Future Profiling Studies and Application Through Physiologically Based Pharmacokinetic Modelling. *Clin. Pharmacokinet.*, 58(2), 189–211.

Barter, ZE, Bayliss, M, Beaune, P, Boobis, A, Carlile, D, Edwards, R, Brian Houston, J, Lake, B, Lipscomb, J, Pelkonen, O, Tucke, G, and Rostami-Hodjegan, A. (2007). Scaling Factors for the Extrapolation of In Vivo Metabolic Drug Clearance From In Vitro Data: Reaching a Consensus on Values of Human Micro-somal Protein and Hepatocellularity Per Gram of Liver. *Curr. Drug Metab.*, 8(1), 33–45.

Barter, ZE, Perrett, HF, Yeo, KR, Allorge, D, Lennard, MS, and Rostami-Hodjegan, A. (2010). Determination of a quantitative relationship between hepatic CYP3A5*1/*3 and CYP3A4 expression for use in the prediction of metabolic clearance in virtual populations. *Biopharm. Drug Dispos.*, 31(8–9), 516–532.

Batchelor, HK, and Marriott, JF. (2015). Paediatric pharmacokinetics: key considerations. *Br. J. Clin. Pharmacol.*, 79(3), 395–404.

Batth, TS, Papetti, M, Pfeiffer, A, Tollenaere, MAX, Francavilla, C, and Olsen, J V. (2018). Large-Scale Phosphoproteomics Reveals Shp-2 Phosphatase-Dependent Regulators of Pdgf Receptor Signaling. *Cell Rep.*, 22(10), 2784–2796.

Bhatt, DK, Gaedigk, A, Pearce, RE, Leeder, JS, and Prasad, B. (2017). Age-dependent protein abundance of cytosolic alcohol and aldehyde dehydrogenases in human liver. *Drug Metab. Dispos.*, 45(9), 1044–1048.

Bhatt, DK, Mehrotra, A, Gaedigk, A, Chapa, R, Basit, A, Zhang, H, Choudhari, P, Boberg, M, Pearce, RE, Gaedigk, R, Broeckel, U, Leeder, JS, and Prasad, B. (2019). Age- and

Genotype-Dependent Variability in the Protein Abundance and Activity of Six Major Uridine Diphosphate-Glucuronosyltransferases in Human Liver. *Clin. Pharmacol. Ther.*, 105(1), 131–141.

Bhatt, DK, and Prasad, B. (2018). Critical Issues and Optimized Practices in Quantification of Protein Abundance Level to Determine Interindividual Variability in DMET Proteins by LC-MS/MS Proteomics. *Clin. Pharmacol. Ther.*, 103(4), 619–630.

Bhullar, KS, Lagarón, NO, McGowan, EM, Parmar, I, Jha, A, Hubbard, BP, and Rupasinghe, HPV. (2018). Kinase-targeted cancer therapies: progress, challenges and future directions. *Mol. Cancer*, 17(1), 48.

Bi, Y, Qiu, X, Rotter, CJ, Kimoto, E, Piotrowski, M, Varma, M V, Ei-Kattan, AF, and Lai, Y. (2013). Quantitative assessment of the contribution of sodium-dependent taurocholate co-transporting polypeptide (NTCP) to the hepatic uptake of rosuvastatin, pitavastatin and fluvastatin. *Biopharm. Drug Dispos.*, 34(8), 452–461.

Bilbao, A, Varesio, E, Luban, J, Strambio-De-Castillia, C, Hopfgartner, G, Müller, M, and Lisacek, F. (2015). Processing strategies and software solutions for data-independent acquisition in mass spectrometry. *Proteomics*, 15(5–6), 964–980.

Billington, S, Ray, AS, Salphati, L, Xiao, G, Chu, X, Humphreys, WG, Liao, M, Lee, CA, Mathias, A, Hop, CECA, Rowbottom, C, Evers, R, Lai, Y, Kelly, EJ, Prasad, B, and Unadkat, JD. (2018). Transporter Expression in Noncancerous and Cancerous Liver Tissue from Donors with Hepatocellular Carcinoma and Chronic Hepatitis C Infection Quantified by LC-MS/MS Proteomics. *Drug Metab. Dispos.*, 46(2), 189–196.

Billington, S, Salphati, L, Hop, CECA, Chu, X, Evers, R, Burdette, D, Rowbottom, C, Lai, Y, Xiao, G, Humphreys, WG, Nguyen, TB, Prasad, B, and Unadkat, JD. (2019). Interindividual and Regional Variability in Drug Transporter Abundance at the Human Blood–Brain Barrier Measured by Quantitative Targeted Proteomics. *Clin. Pharmacol. Ther.*, 106(1), 228–237.

Boberg, M, Vrana, M, Mehrotra, A, Pearce, RE, Gaedigk, A, Bhatt, DK, Leeder, JS, and Prasad, B. (2017). Age-dependent absolute abundance of hepatic carboxylesterases (CES1 and CES2) by LC-MS/MS proteomics: Application to PBPK modeling of oseltamivir in vivo pharmacokinetics in infants. *Drug Metab. Dispos.*, 45(2), 216–223.

Bollu, LR, Mazumdar, A, Savage, MI, and Brown, PH. (2017). Molecular pathways: Targeting protein tyrosine phosphatases in cancer. *Clin. Cancer Res.*, 23(9), 2136–2142.

Boukouris, S, and Mathivanan, S. (2015). Exosomes in bodily fluids are a highly stable resource of disease biomarkers. *Proteomics - Clin. Appl.*, 9(3–4), 358–367.

Brownridge, P, Holman, SW, Gaskell, SJ, Grant, CM, Harman, VM, Hubbard, SJ, Lanthaler, K, Lawless, C, O'Cualain, R, Sims, P, Watkins, R, and Beynon, RJ. (2011). Global absolute quantification of a proteome: Challenges in the deployment of a QconCAT strategy. *Proteomics*, 11(15), 2957–2970.

Calderón-Celis, F, Encinar, JR, and Sanz-Medel, A. (2018). Standardization approaches in absolute quantitative proteomics with mass spectrometry. *Mass Spectrom. Rev.*, 37(6), 715–737.

Calvier, EAM, Krekels, EHJ, Välitalo, PAJ, Rostami-Hodjegan, A, Tibboel, D, Danhof, M, and Knibbe, CAJ. (2017). Allometric Scaling of Clearance in Paediatric Patients: When

Does the Magic of 0.75 Fade? *Clin. Pharmacokinet.*, 56(3), 273–285.

Carr, SA, Abbatiello, SE, Ackermann, BL, Borchers, C, Domon, B, Deutsch, EW, Grant, RP, Hoofnagle, AN, Huttenhain, R, Koomen, JM, Liebler, DC, Liu, T, MacLean, B, Mani, D, Mansfield, E, Neubert, H, Paulovich, AG, … Weintraub, S. (2014). Targeted Peptide Measurements in Biology and Medicine: Best Practices for Mass Spectrometry-based Assay Development Using a Fit-for-Purpose Approach. *Mol. Cell. Proteomics*, 13(3), 907–917.

Chen, B, Liu, L, Ho, H, Chen, Y, Yang, Z, Liang, X, Payandeh, J, Dean, B, Hop, CECA, and Deng, Y. (2017). Strategies of Drug Transporter Quantitation by LC-MS: Importance of Peptide Selection and Digestion Efficiency. *AAPS J.*, 19(5), 1469–1478.

Chen, Y, Zane, NR, Thakker, DR, and Wang, MZ. (2016). Quantification of Flavin-containing Monooxygenases 1, 3, and 5 in Human Liver Microsomes by UPLC-MRM-Based Targeted Quantitative Proteomics and Its Application to the Study of Ontogeny. *Drug Metab. Dispos.*, 44(7), 975–983.

Cheung, CSF, Anderson, KW, Wang, M, and Turko, I V. (2015). Natural Flanking Sequences for Peptides Included in a Quantification Concatamer Internal Standard. *Anal. Chem.*, 87(2), 1097–1102.

Cheung, KWK, Groen, BD, Spaans, E, Borselen, MD, Bruijn, ACJM, Simons-Oosterhuis, Y, Tibboel, D, Samsom, JN, Verdijk, RM, Smeets, B, Zhang, L, Huang, S, Giacomini, KM, and Wildt, SN. (2019). A Comprehensive Analysis of Ontogeny of Renal Drug Transporters: mRNA Analyses, Quantitative Proteomics, and Localization. *Clin. Pharmacol. Ther.*, 106(5), 1083–1092.

Choksawangkarn, W, Edwards, N, Wang, Y, Gutierrez, P, and Fenselau, C. (2012). Comparative study of workflows optimized for In-gel, In-solution, and on-filter proteolysis in the analysis of plasma membrane proteins. *J. Proteome Res.*, 11(5), 3030–3034.

Choy, S, Hénin, E, van der Walt, J-S, Kjellsson, MC, and Karlsson, MO. (2013). Identification of the primary mechanism of action of an insulin secretagogue from meal test data in healthy volunteers based on an integrated glucose-insulin model. *J. Pharmacokinet. Pharmacodyn.*, 40(1), 1–10.

Cieślak, A, Kelly, I, Trottier, J, Verreault, M, Wunsch, E, Milkiewicz, P, Poirier, G, Droit, A, and Barbier, O. (2016). Selective and sensitive quantification of the cytochrome P450 3A4 protein in human liver homogenates through multiple reaction monitoring mass spectrometry. *Proteomics*, 16(21), 2827–2837.

Couto, N, Al-Majdoub, ZM, Achour, B, Wright, PC, Rostami-Hodjegan, A, and Barber, J. (2019). Quantification of Proteins Involved in Drug Metabolism and Disposition in the Human Liver Using Label-Free Global Proteomics. *Mol. Pharm.*, 16(2), 632–647.

Cox, J, and Mann, M. (2008). MaxQuant enables high peptide identification rates, individualized p.p.b.-range mass accuracies and proteome-wide protein quantification. *Nat. Biotechnol.*, 26(12), 1367–1372.

Danhof, M. (2016). Systems pharmacology – Towards the modeling of network interactions. *Eur. J. Pharm. Sci.*, 94, 4–14.

Darwich, AS, Ogungbenro, K, Vinks, AA, Powell, JR, Reny, J-L, Marsousi, N, Daali, Y,

Fairman, D, Cook, J, Lesko, LJ, McCune, JS, Knibbe, CAJ, de Wildt, SN, Leeder, JS, Neely, M, Zuppa, AF, Vicini, P, … Rostami-Hodjegan, A. (2017). Why Has Model-Informed Precision Dosing Not Yet Become Common Clinical Reality? Lessons From the Past and a Roadmap for the Future. *Clin. Pharmacol. Ther.*, 101(5), 646–656.

den Braver-Sewradj, SP, den Braver, MW, Baze, A, Decorde, J, Fonsi, M, Bachellier, P, Vermeulen, NPE, Commandeur, JNM, Richert, L, and Vos, JC. (2017). Direct comparison of UDP-glucuronosyltransferase and cytochrome P450 activities in human liver microsomes, plated and suspended primary human hepatocytes from five liver donors. *Eur. J. Pharm. Sci.*, 109, 96–110.

Dimitrova, N, Nagaraj, AB, Razi, A, Singh, S, Kamalakaran, S, Banerjee, N, Joseph, P, Mankovich, A, Mittal, P, Difeo, A, and Varadan, V. (2017). InFlo: A novel systems biology framework identifies cAMP-CREB1 axis as a key modulator of platinum resistance in ovarian cancer. *Oncogene*, 36(17), 2472–2482.

Distler, U, Kuharev, J, Navarro, P, Levin, Y, Schild, H, and Tenzer, S. (2014). Drift time-specific collision energies enable deep-coverage data-independent acquisition proteomics. *Nat. Methods*, 11(2), 167–170.

Doki, K, Darwich, AS, Achour, B, Tornio, A, Backman, JT, and Rostami-Hodjegan, A. (2018). Implications of intercorrelation between hepatic CYP3A4-CYP2C8 enzymes for the evaluation of drug-drug interactions: a case study with repaglinide. *Br. J. Clin. Pharmacol.*, 84(5), 972–986.

Drozdzik, M, Busch, D, Lapczuk, J, Müller, J, Ostrowski, M, Kurzawski, M, and Oswald, S. (2018). Protein Abundance of Clinically Relevant Drug-Metabolizing Enzymes in the Human Liver and Intestine: A Comparative Analysis in Paired Tissue Specimens. *Clin. Pharmacol. Ther.*, 104(3), 515–524.

Drozdzik, M, Gröer, C, Penski, J, Lapczuk, J, Ostrowski, M, Lai, Y, Prasad, B, Unadkat, JD, Siegmund, W, and Oswald, S. (2014). Protein Abundance of Clinically Relevant Multidrug Transporters along the Entire Length of the Human Intestine. *Mol. Pharm.*, 11(10), 3547–3555.

Dupuis, A, Hennekinne, J-A, Garin, J, and Brun, V. (2008). Protein Standard Absolute Quantification (PSAQ) for improved investigation of staphylococcal food poisoning outbreaks. *Proteomics*, 8(22), 4633–4636.

Elmorsi, Y, Barber, J, and Rostami-Hodjegan, A. (2016). Ontogeny of Hepatic Drug Transporters and Relevance to Drugs Used in Pediatrics. *Drug Metab. Dispos.*, 44(7), 992–998.

Elschenbroich, S, Ignatchenko, V, Clarke, B, Kalloger, SE, Boutros, PC, Gramolini, AO, Shaw, P, Jurisica, I, and Kislinger, T. (2011). In-Depth Proteomics of Ovarian Cancer Ascites: Combining Shotgun Proteomics and Selected Reaction Monitoring Mass Spectrometry. *J. Proteome Res.*, 10(5), 2286–2299.

Fallon, JK, Harbourt, DE, Maleki, SH, Kessler, FK, Ritter, JK, and Smith, PC. (2008). Absolute quantification of human uridine-diphosphate glucuronosyl transferase (UGT) enzyme isoforms 1A1 and 1A6 by tandem LC-MS. *Drug Metab. Lett.*, 2(3), 210–222.

Fallon, JK, Houvig, N, Booth-Genthe, CL, and Smith, PC. (2018). Quantification of membrane transporter proteins in human lung and immortalized cell lines using targeted quantitative proteomic analysis by isotope dilution nanoLC-MS/MS. *J. Pharm. Biomed. Anal.*, 154,

150–157.

Fallon, JK, Neubert, H, Hyland, R, Goosen, TC, and Smith, PC. (2013). Targeted quantitative proteomics for the analysis of 14 UGT1As and -2Bs in human liver using NanoUPLC-MS/MS with selected reaction monitoring. *J. Proteome Res.*, 12(10), 4402–4413.

Fernandez, E, Perez, R, Hernandez, A, Tejada, P, Arteta, M, and Ramos, JT. (2011). Factors and mechanisms for pharmacokinetic differences between pediatric population and adults. *Pharmaceutics*, 3(1), 53–72.

Fisher, CD, Lickteig, AJ, Augustine, LM, Ranger-Moore, J, Jackson, JP, Ferguson, SS, and Cherrington, NJ. (2009). Hepatic Cytochrome P450 Enzyme Alterations in Humans with Progressive Stages of Nonalcoholic Fatty Liver Disease. *Drug Metab. Dispos.*, 37(10), 2087–2094.

Freue, GVC, Sasaki, M, Meredith, A, Günther, OP, Bergman, A, Takhar, M, Mui, A, Balshaw, RF, Ng, RT, Opushneva, N, Hollander, Z, Li, G, Borchers, CH, Wilson-McManus, J, McManus, BM, Keown, PA, and McMaster, WR. (2010). Proteomic Signatures in Plasma during Early Acute Renal Allograft Rejection. *Mol. Cell. Proteomics*, 9(9), 1954–1967.

Fu, C, Di, L, Han, X, Soderstrom, C, Snyder, M, Troutman, MD, Obach, RS, and Zhang, H. (2013). Aldehyde Oxidase 1 (AOX1) in Human Liver Cytosols: Quantitative Characterization of AOX1 Expression Level and Activity Relationship. *Drug Metab. Dispos.*, 41(10), 1797–1804.

Gallien, S, Bourmaud, A, Kim, SY, and Domon, B. (2014). Technical considerations for large-scale parallel reaction monitoring analysis. *J. Proteomics*, 100, 147–159.

Gallien, S, Duriez, E, Crone, C, Kellmann, M, Moehring, T, and Domon, B. (2012). Targeted Proteomic Quantification on Quadrupole-Orbitrap Mass Spectrometer. *Mol. Cell. Proteomics*, 11(12), 1709–1723.

Gallien, S, Duriez, E, Demeure, K, and Domon, B. (2013). Selectivity of LC-MS/MS analysis: Implication for proteomics experiments. *J. Proteomics*, 81, 148–158.

Gaohua, L, Abduljalil, K, Jamei, M, Johnson, TN, and Rostami-Hodjegan, A. (2012). A pregnancy physiologically based pharmacokinetic (p-PBPK) model for disposition of drugs metabolized by CYP1A2, CYP2D6 and CYP3A4. *Br. J. Clin. Pharmacol.*, 74(5), 873–885.

Geiger, T, Cox, J, Ostasiewicz, P, Wisniewski, JR, and Mann, M. (2010). Super-SILAC mix for quantitative proteomics of human tumor tissue. *Nat. Methods*, 7(5), 383–385.

Gentry, PR, Hack, CE, Haber, L, Maier, A, and Clewell Harvey J., III. (2002). An Approach for the Quantitative Consideration of Genetic Polymorphism Data in Chemical Risk Assessment: Examples with Warfarin and Parathion. *Toxicol. Sci.*, 70(1), 120–139.

Geromanos, SJ, Vissers, JPC, Silva, JC, Dorschel, CA, Li, G, Gorenstein, M V, Bateman, RH, and Langridge, JI. (2009). The detection, correlation, and comparison of peptide precursor and product ions from data independent LC-MS with data dependant LC-MS/MS. *Proteomics*, 9(6), 1683–1695.

Gillet, LC, Leitner, A, and Aebersold, R. (2016). Mass Spectrometry Applied to Bottom-Up Proteomics: Entering the High-Throughput Era for Hypothesis Testing. *Annu. Rev. Anal. Chem.*, 9(1), 449–472.

Gillet, LC, Navarro, P, Tate, S, Röst, H, Selevsek, N, Reiter, L, Bonner, R, and Aebersold, R. (2012). Targeted Data Extraction of the MS/MS Spectra Generated by Data-independent Acquisition: A New Concept for Consistent and Accurate Proteome Analysis. *Mol. Cell. Proteomics*, 11(6), O111.016717.

Gillette, MA, and Carr, SA. (2013). Quantitative analysis of peptides and proteins in biomedicine by targeted mass spectrometry. *Nat. Methods*, 10(1), 28–34.

Gilquin, B, Louwagie, M, Jaquinod, M, Cez, A, Picard, G, El Kholy, L, Surin, B, Garin, J, Ferro, M, Kofman, T, Barau, C, Plaisier, E, Ronco, P, and Brun, V. (2017). Multiplex and accurate quantification of acute kidney injury biomarker candidates in urine using Protein Standard Absolute Quantification (PSAQ) and targeted proteomics. *Talanta*, 164, 77–84.

Ginsberg, G, Hattis, D, Russ, A, and Sonawane, B. (2004). Physiologically based pharmacokinetic (PBPK) modeling of caffeine and theophylline in neonates and adults: implications for assessing children's risks from environmental agents. *J. Toxicol. Environ. Heal. Part A*, 67(4), 297–329.

Gröer, C, Brück, S, Lai, Y, Paulick, A, Busemann, A, Heidecke, CD, Siegmund, W, and Oswald, S. (2013). LC-MS/MS-based quantification of clinically relevant intestinal uptake and efflux transporter proteins. *J. Pharm. Biomed. Anal.*, 85, 253–261.

Gröer, C, Busch, D, Patrzyk, M, Beyer, K, Busemann, A, Heidecke, CD, Drozdzik, M, Siegmund, W, and Oswald, S. (2014). Absolute protein quantification of clinically relevant cytochrome P450 enzymes and UDP-glucuronosyltransferases by mass spectrometry-based targeted proteomics. *J. Pharm. Biomed. Anal.*, 100, 393–401.

Guo, T, Kouvonen, P, Koh, CC, Gillet, LC, Wolski, WE, Röst, HL, Rosenberger, G, Collins, BC, Blum, LC, Gillessen, S, Joerger, M, Jochum, W, and Aebersold, R. (2015). Rapid mass spectrometric conversion of tissue biopsy samples into permanent quantitative digital proteome maps. *Nat. Med.*, 21(4), 407–413.

Hansen, J, Palmfeldt, J, Pedersen, KW, Funder, AD, Frost, L, Hasselstrøm, JB, and Jornil, JR. (2019). Postmortem protein stability investigations of the human hepatic drug-metabolizing cytochrome P450 enzymes CYP1A2 and CYP3A4 using mass spectrometry. *J. Proteomics*, 194, 125–131.

Harbourt, DE, Fallon, JK, Ito, S, Baba, T, Ritter, JK, Glish, GL, and Smith, PC. (2012). Quantification of human uridine-diphosphate glucuronosyl transferase 1A isoforms in liver, intestine, and kidney using nanobore liquid chromatography-tandem mass spectrometry. *Anal. Chem.*, 84(1), 98–105.

Hardwick, RN, Ferreira, DW, More, VR, Lake, AD, Lu, Z, Manautou, JE, Slitt, AL, and Cherrington, NJ. (2013). Altered UDP-Glucuronosyltransferase and Sulfotransferase Expression and Function during Progressive Stages of Human Nonalcoholic Fatty Liver Disease. *Drug Metab. Dispos.*, 41(3), 554–561.

Harwood, MD, Achour, B, Neuhoff, S, Russell, MR, Carlson, G, and Warhurst, G. (2016a). In Vitro-In Vivo Extrapolation Scaling Factors for Intestinal P-Glycoprotein and Breast Cancer Resistance Protein: Part I: A Cross-Laboratory Comparison of Transporter-Protein Abundances and Relative Expression Factors in Human Intestine and Caco-2 Cells. *Drug Metab. Dispos.*, 44(3), 297–307.

Harwood, MD, Achour, B, Neuhoff, S, Russell, MR, Carlson, G, Warhurst, G, and Rostami-Hodjegan, A. (2016b). In Vitro-In Vivo Extrapolation Scaling Factors for Intestinal P-

glycoprotein and Breast Cancer Resistance Protein: Part II. The Impact of Cross-Laboratory Variations of Intestinal Transporter Relative Expression Factors on Predicted Drug Disposition. *Drug Metab. Dispos.*, 44(3), 476–480.

Harwood, MD, Achour, B, Russell, MR, Carlson, GL, Warhurst, G, and Rostami-Hodjegan, A. (2015). Application of an LC-MS/MS method for the simultaneous quantification of human intestinal transporter proteins absolute abundance using a QconCAT technique. *J. Pharm. Biomed. Anal.*, 110, 27–33.

Harwood, MD, Neuhoff, S, Rostami-Hodjegan, A, and Warhurst, G. (2016c). Breast Cancer Resistance Protein Abundance, but Not mRNA Expression, Correlates With Estrone-3-Sulfate Transport in Caco-2. *J. Pharm. Sci.*, 105(4), 1370–1375.

Harwood, MD, Russell, MR, Neuhoff, S, Warhurst, G, and Rostami-Hodjegan, A. (2014). Lost in centrifugation: Accounting for transporter protein losses in quantitative targeted absolute proteomics. *Drug Metab. Dispos.*, 42(10), 1766–1772.

Havliš, J, and Shevchenko, A. (2004). Absolute quantification of proteins in solutions and in polyacrylamide gels by mass spectrometry. *Anal. Chem.*, 76(11), 3029–3036.

Hector, S, Rehm, M, Schmid, J, Kehoe, J, McCawley, N, Dicker, P, Murray, F, McNamara, D, Kay, EW, Concannon, CG, Huber, HJ, and Prehn, JHM. (2012). Clinical application of a systems model of apoptosis execution for the prediction of colorectal cancer therapy responses and personalisation of therapy. *Gut*, 61(5), 725–733.

Heikkinen, AT, Lignet, F, Cutler, P, and Parrott, N. (2015). The role of quantitative ADME proteomics to support construction of physiologically based pharmacokinetic models for use in small molecule drug development. *PROTEOMICS - Clin. Appl.*, 9(7–8), 732–744.

Held, JM, Danielson, SR, Behring, JB, Atsriku, C, Britton, DJ, Puckett, RL, Schilling, B, Campisi, J, Benz, CC, and Gibson, BW. (2010). Targeted quantitation of site-specific cysteine oxidation in endogenous proteins using a differential alkylation and multiple reaction monitoring mass spectrometry approach. *Mol. Cell. Proteomics*, 9(7), 1400–1410.

Hodgkinson, VC, Agarwal, V, ELFadl, D, Fox, JN, McManus, PL, Mahapatra, TK, Kneeshaw, PJ, Drew, PJ, Lind, MJ, and Cawkwell, L. (2012). Pilot and feasibility study: comparative proteomic analysis by 2-DE MALDI TOF/TOF MS reveals 14-3-3 proteins as putative biomarkers of response to neoadjuvant chemotherapy in ER-positive breast cancer. *J. Proteomics*, 75(9), 2745–2752.

Holman, SW, Sims, PFG, and Eyers, CE. (2012). The use of selected reaction monitoring in quantitative proteomics. *Bioanalysis*, 4, 1763–1786.

Hoshi, Y, Uchida, Y, Tachikawa, M, Inoue, T, Ohtsuki, S, and Terasaki, T. (2013). Quantitative Atlas of blood-brain barrier transporters, receptors, and tight junction proteins in rats and common marmoset. *J. Pharm. Sci.*, 102(9), 3343–3355.

Howard, M, Barber, J, Alizai, N, and Rostami-Hodjegan, A. (2018). Dose adjustment in orphan disease populations: the quest to fulfill the requirements of physiologically based pharmacokinetics. *Expert Opin. Drug Metab. Toxicol.*, 14(12), 1315–1330.

Hu, A, Noble, WS, and Wolf-Yadlin, A. (2016). Technical advances in proteomics: new developments in data-independent acquisition. *F1000Research*, 5, 419.

Huang, S-M, Abernethy, DR, Wang, Y, Zhao, P, and Zineh, I. (2013). The Utility of Modeling

and Simulation in Drug Development and Regulatory Review. *J. Pharm. Sci.*, 102(9), 2912–2923.

Huillet, C, Adrait, A, Lebert, D, Picard, G, Trauchessec, M, Louwagie, M, Dupuis, A, Hittinger, L, Ghaleh, B, Le Corvoisier, P, Jaquinod, M, Garin, J, Bruley, C, and Brun, V. (2012). Accurate Quantification of Cardiovascular Biomarkers in Serum Using Protein Standard Absolute Quantification (PSAQ^{TM}) and Selected Reaction Monitoring. *Mol. Cell. Proteomics*, 11(2), M111.008235.

Ibarrola, N, Kalume, DE, Gronborg, M, Iwahori, A, and Pandey, A. (2003). A Proteomic Approach for Quantitation of Phosphorylation Using Stable Isotope Labeling in Cell Culture. *Anal. Chem.*, 75(22), 6043–6049.

Ishida, K, Ullah, M, Tóth, B, Juhasz, V, and Unadkat, JD. (2018). Successful Prediction of In Vivo Hepatobiliary Clearances and Hepatic Concentrations of Rosuvastatin Using Sandwich-Cultured Rat Hepatocytes, Transporter-Expressing Cell Lines, and Quantitative Proteomics. *Drug Metab. Dispos.*, 46(1), 66–74.

Ishihama, Y, Oda, Y, Tabata, T, Sato, T, Nagasu, T, Rappsilber, J, and Mann, M. (2005). Exponentially Modified Protein Abundance Index (emPAI) for Estimation of Absolute Protein Amount in Proteomics by the Number of Sequenced Peptides per Protein. *Mol. Cell. Proteomics*, 4(9), 1265–1272.

Izukawa, T, Nakajima, M, Fujiwara, R, Yamanaka, H, Fukami, T, Takamiya, M, Aoki, Y, Ikushiro, SS -i., Sakaki, T, and Yokoi, T. (2009). Quantitative analysis of UGT1A and UGT2B expression levels in human livers. *Drug Metab. Dispos.*, 37(8), 1759–1768.

Jamei, M. (2016). Recent Advances in Development and Application of Physiologically-Based Pharmacokinetic (PBPK) Models: a Transition from Academic Curiosity to Regulatory Acceptance. *Curr. Pharmacol. Reports*, 2(3), 161–169.

Jamei, M, Dickinson, GL, and Rostami-Hodjegan, A. (2009). A Framework for Assessing Inter-individual Variability in Pharmacokinetics Using Virtual Human Populations and Integrating General Knowledge of Physical Chemistry, Biology, Anatomy, Physiology and Genetics: A Tale of 'Bottom-Up' vs 'Top-Down' Recognition . *Drug Metab. Pharmacokinet.*, 24(1), 53–75.

Jamwal, R, Barlock, BJ, Adusumalli, S, Ogasawara, K, Simons, BL, and Akhlaghi, F. (2017). Multiplex and Label-Free Relative Quantification Approach for Studying Protein Abundance of Drug Metabolizing Enzymes in Human Liver Microsomes Using SWATH-MS. *J. Proteome Res.*, 16(11), 4134–4143.

Jiang, X-L, Zhao, P, Barrett, JS, Lesko, LJ, and Schmidt, S. (2013). Application of Physiologically Based Pharmacokinetic Modeling to Predict Acetaminophen Metabolism and Pharmacokinetics in Children. *CPT Pharmacometrics Syst. Pharmacol.*, 2(10), e80.

Johnson, TN, Zhou, D, and Bui, KH. (2014). Development of physiologically based pharmacokinetic model to evaluate the relative systemic exposure to quetiapine after administration of IR and XR formulations to adults, children and adolescents. *Biopharm. Drug Dispos.*, 35(6), 341–352.

Jones, H, and Rowland-Yeo, K. (2013). Basic Concepts in Physiologically Based Pharmacokinetic Modeling in Drug Discovery and Development. *CPT Pharmacometrics Syst. Pharmacol.*, 2(8), e63.

Jones, HM, Chen, Y, Gibson, C, Heimbach, T, Parrott, N, Peters, SA, Snoeys, J, Upreti, V V., Zheng, M, and Hall, SD. (2015). Physiologically based pharmacokinetic modeling in drug discovery and development: a pharmaceutical industry perspective. *Clin. Pharmacol. Ther.*, 97(3), 247–262.

Kamiie, J, Ohtsuki, S, Iwase, R, Ohmine, K, Katsukura, Y, Yanai, K, Sekine, Y, Uchida, Y, Ito, S, and Terasaki, T. (2008). Quantitative Atlas of membrane transporter proteins: Development and application of a highly sensitive simultaneous LC/MS/MS method combined with novel in-silico peptide selection criteria. *Pharm. Res.*, 25(6), 1469–1483.

Kawakami, H, Ohtsuki, S, Kamiie, J, Suzuki, T, Abe, T, and Terasaki, T. (2011). Simultaneous Absolute Quantification of 11 Cytochrome P450 Isoforms in Human Liver Microsomes by Liquid Chromatography Tandem Mass Spectrometry with In Silico Target Peptide Selection. *J. Pharm. Sci.*, 100(1), 341–352.

Ke, AB, Nallani, SC, Zhao, P, Rostami-Hodjegan, A, Isoherranen, N, and Unadkat, JD. (2013). A Physiologically Based Pharmacokinetic Model to Predict Disposition of CYP2D6 and CYP1A2 Metabolized Drugs in Pregnant Women. *Drug Metab. Dispos.*, 41(4), 801–813.

Ke, AB, Nallani, SC, Zhao, P, Rostami-Hodjegan, A, and Unadkat, JD. (2014). Expansion of a PBPK model to predict disposition in pregnant women of drugs cleared via multiple CYP enzymes, including CYP2B6, CYP2C9 and CYP2C19. *Br. J. Clin. Pharmacol.*, 77(3), 554–570.

Keller, A, Bader, SL, Kusebauch, U, Shteynberg, D, Hood, L, and Moritz, RL. (2016). Opening a SWATH Window on Posttranslational Modifications: Automated Pursuit of Modified Peptides. *Mol. Cell. Proteomics*, 15(3), 1151–1163.

Kettenbach, AN, Rush, J, and Gerber, SA. (2011). Absolute quantification of protein and post-translational modification abundance with stable isotope–labeled synthetic peptides. *Nat. Protoc.*, 6(2), 175–186.

Kim, YJ, Gallien, S, El-Khoury, V, Goswami, P, Sertamo, K, Schlesser, M, Berchem, G, and Domon, B. (2015). Quantification of SAA1 and SAA2 in lung cancer plasma using the isotype-specific PRM assays. *Proteomics*, 15(18), 3116–3125.

Kirkpatrick, DS, Gerber, SA, and Gygi, SP. (2005). The absolute quantification strategy: a general procedure for the quantification of proteins and post-translational modifications. *Methods*, 35(3), 265–273.

Kirouac, DC. (2018). How Do We "Validate" a QSP Model? *CPT Pharmacometrics Syst. Pharmacol.*, 7(9), 547–548.

Kirouac, DC, Lahdenranta, J, Du, J, Yarar, D, Onsum, MD, Nielsen, UB, and McDonagh, CF. (2015). Model-Based Design of a Decision Tree for Treating HER2+ Cancers Based on Genetic and Protein Biomarkers. *CPT Pharmacometrics Syst. Pharmacol.*, 4(3), e00019.

Kito, K, Ota, K, Fujita, T, and Ito, T. (2007). A synthetic protein approach toward accurate mass spectrometric quantification of component stoichiometry of multiprotein complexes. *J. Proteome Res.*, 6(2), 792–800.

Kitteringham, NR, Jenkins, RE, Lane, CS, Elliott, VL, and Park, BK. (2009). Multiple reaction monitoring for quantitative biomarker analysis in proteomics and metabolomics. *J. Chromatogr. B*, 877(13), 1229–1239.

Knights, KM, Spencer, SM, Fallon, JK, Chau, N, Smith, PC, and Miners, JO. (2016). Scaling

factors for the in vitro - in vivo extrapolation (IV-IVE) of renal drug and xenobiotic glucuronidation clearance. *Br. J. Clin. Pharmacol.*, 81(6), 1153–1164.

Kuepfer, L, Niederalt, C, Wendl, T, Schlender, J-F, Willmann, S, Lippert, J, Block, M, Eissing, T, and Teutonico, D. (2016). Applied Concepts in PBPK Modeling: How to Build a PBPK/PD Model. *CPT Pharmacometrics Syst. Pharmacol.*, 5(10), 516–531.

Kumar, V, Prasad, B, Patilea, G, Gupta, A, Salphati, L, Evers, R, Hop, CECA, and Unadkat, JD. (2015). Quantitative transporter proteomics by liquid chromatography with tandem mass spectrometry: Addressing methodologic issues of plasma membrane isolation and expression-activity relationship. *Drug Metab. Dispos.*, 43(2), 284–288.

Kumar, V, Salphati, L, Hop, CECA, Xiao, G, Lai, Y, Mathias, A, Chu, X, Humphreys, WG, Liao, M, Heyward, S, and Unadkat, JD. (2019). A Comparison of Total and Plasma Membrane Abundance of Transporters in Suspended, Plated, Sandwich-Cultured Human Hepatocytes Versus Human Liver Tissue Using Quantitative Targeted Proteomics and Cell Surface Biotinylation. *Drug Metab. Dispos.*, 47(4), 350–357.

Kumar, V, Yin, J, Billington, S, Prasad, B, Brown, CDA, Wang, J, and Unadkat, JD. (2018). The Importance of Incorporating OCT2 Plasma Membrane Expression and Membrane Potential in IVIVE of Metformin Renal Secretory Clearance. *Drug Metab. Dispos.*, 46(10), 1441–1445.

Kurokawa, N, Kishimoto, T, Tanaka, K, Kondo, J, Takahashi, N, and Miura, Y. (2019). New approach to evaluating the effects of a drug on protein complexes with quantitative proteomics, using the SILAC method and bioinformatic approach. *Biosci. Biotechnol. Biochem.*, 83(11), 2034–2048.

Ladumor, MK, Bhatt, DK, Gaedigk, A, Sharma, S, Thakur, A, Pearce, RE, Leeder, JS, Bolger, MB, Singh, S, and Prasad, B. (2019). Ontogeny of Hepatic Sulfotransferases and Prediction of Age-Dependent Fractional Contribution of Sulfation in Acetaminophen Metabolism. *Drug Metab. Dispos.*, 47(8), 818–831.

Langenfeld, E, Zanger, UM, Jung, K, Meyer, HE, and Marcus, K. (2009). Mass spectrometry-based absolute quantification of microsomal cytochrome P450 2D6 in human liver. *Proteomics*, 9(9), 2313–2323.

Leeder, JS, and Meibohm, B. (2016). Challenges and opportunities for increasing the knowledge base related to drug biotransformation and pharmacokinetics during growth and development. *Drug Metab. Dispos.*, 44(7), 916–923.

Li, R, Barton, H, and Maurer, T. (2015). A Mechanistic Pharmacokinetic Model for Liver Transporter Substrates Under Liver Cirrhosis Conditions. *CPT Pharmacometrics Syst. Pharmacol.*, 4(6), 338–349.

Linghu, D, Guo, L, Zhao, Y, Liu, Z, Zhao, M, Huang, L, and Li, X. (2017). iTRAQ-based quantitative proteomic analysis and bioinformatics study of proteins in pterygia. *PROTEOMICS – Clin. Appl.*, 11(7–8), 1600094.

Lu, H, and Rosenbaum, S. (2014). Developmental pharmacokinetics in pediatric populations. *J. Pediatr. Pharmacol. Ther.*, 19(4), 262–276.

Ludwig, C, Gillet, L, Rosenberger, G, Amon, S, Collins, BC, and Aebersold, R. (2018). Data-independent acquisition-based SWATH-MS for quantitative proteomics: a tutorial. *Mol. Syst. Biol.*, 14(8), e8126.

MacLeod, AK, Fallon, PG, Sharp, S, Henderson, CJ, Wolf, CR, and Huang, JT-J. (2015). An enhanced in vivo stable isotope labeling by amino acids in cell culture (SILAC) model for quantification of drug metabolism enzymes. *Mol. Cell. Proteomics*, 14(3), 750–760.

Margaillan, G, Rouleau, M, Fallon, JK, Caron, P, Villeneuve, L, Turcotte, V, Smith, PC, Joy, MS, and Guillemette, C. (2015). Quantitative profiling of human renal UDP-glucuronosyltransferases and glucuronidation activity: a comparison of normal and tumoral kidney tissues. *Drug Metab. Dispos.*, 43(4), 611–619.

Marsousi, N, Desmeules, JA, Rudaz, S, and Daali, Y. (2017). Usefulness of PBPK Modeling in Incorporation of Clinical Conditions in Personalized Medicine. *J. Pharm. Sci.*, 106(9), 2380–2391.

Mehrotra, A, Boberg, M, Vrana, M, Gaedigk, A, Pearce, RE, Leeder, S, and Prasad, B. (2015). Age-dependent Expression Analysis of Major Drug Metabolizing Enzymes in Human Liver. *FASEB J.*, 30(1 Supplement), 713.11.

Meiqun, C, Zifan, G, Kehuan, S, and Zhengzhi, W. (2011). Application of iTRAQ quantitative proteomics in identification of serum biomarkers in breast cancer. *4th Int. Conf. Biomed. Eng. Informatics*, 1658–1663.

Melillo, N, Darwich, AS, Magni, P, and Rostami-Hodjegan, A. (2019). Accounting for inter-correlation between enzyme abundance: a simulation study to assess implications on global sensitivity analysis within physiologically-based pharmacokinetics. *J. Pharmacokinet. Pharmacodyn.*, 46(2), 137–154.

Merrill, AE, Hebert, AS, MacGilvray, ME, Rose, CM, Bailey, DJ, Bradley, JC, Wood, WW, El Masri, M, Westphall, MS, Gasch, AP, and Coon, JJ. (2014). NeuCode labels for relative protein quantification. *Mol. Cell. Proteomics*, 13(9), 2503–2512.

Michalski, A, Cox, J, and Mann, M. (2011). More than 100,000 detectable peptide species elute in single shotgun proteomics runs but the majority is inaccessible to data-dependent LC-MS/MS. *J. Proteome Res.*, 10(4), 1785–1793.

Michelet, R, Van Bocxlaer, J, Allegaert, K, and Vermeulen, A. (2018). The use of PBPK modeling across the pediatric age range using propofol as a case. *J. Pharmacokinet. Pharmacodyn.*, 45(6), 765–785.

Miller, NA, Reddy, MB, Heikkinen, AT, Lukacova, V, and Parrott, N. (2019). Physiologically Based Pharmacokinetic Modelling for First-In-Human Predictions: An Updated Model Building Strategy Illustrated with Challenging Industry Case Studies. *Clin. Pharmacokinet.*, 58(6), 727–746.

Mirzaei, H, McBee, JK, Watts, J, and Aebersold, R. (2008). Comparative evaluation of current peptide production platforms used in absolute quantification in proteomics. *Mol. Cell. Proteomics*, 7(4), 813–823.

Mooij, MG, van de Steeg, E, van Rosmalen, J, Windster, JD, de Koning, BAE, Vaes, WHJ, van Groen, BD, Tibboel, D, Wortelboer, HM, and de Wildt, SN. (2016). Proteomic Analysis of the Developmental Trajectory of Human Hepatic Membrane Transporter Proteins in the First Three Months of Life. *Drug Metab. Dispos.*, 44(7), 1005–1013.

Morales, AG, Lachén-Montes, M, Ibáñez-Vea, M, Santamaría, E, and Fernández-Irigoyen, J. (2017). Application of Isobaric Tags for Relative and Absolute Quantitation (iTRAQ) to Monitor Olfactory Proteomes During Alzheimer's Disease Progression. In *Current*

Proteomic Approaches Applied to Brain Function (pp. 29–42).

Nakamura, K, Hirayama-Kurogi, M, Ito, S, Kuno, T, Yoneyama, T, Obuchi, W, Terasaki, T, and Ohtsuki, S. (2016). Large-scale multiplex absolute protein quantification of drug-metabolizing enzymes and transporters in human intestine, liver, and kidney microsomes by SWATH-MS: Comparison with MRM/SRM and HR-MRM/PRM. *Proteomics*, 16(15–16), 2106–2117.

Niu, J, Straubinger, RM, and Mager, DE. (2019). Pharmacodynamic Drug–Drug Interactions. *Clin. Pharmacol. Ther.*, 105(6), 1395–1406.

O'Dwyer, D, Ralton, LD, O'Shea, A, and Murray, GI. (2011). The proteomics of colorectal cancer: identification of a protein signature associated with prognosis. *PLoS One*, 6(11), e27718.

Ogungbenro, K, and Aarons, L. (2014). A physiologically based pharmacokinetic model for Valproic acid in adults and children. *Eur. J. Pharm. Sci.*, 63, 45–52.

Ohtsuki, S, Schaefer, O, Kawakami, H, Inoue, T, Liehner, S, Saito, A, Ishiguro, N, Kishimoto, W, Ludwig-Schwellinger, E, Ebner, T, and Terasaki, T. (2012). Simultaneous Absolute Protein Quantification of Transporters, Cytochromes P450, and UDP-Glucuronosyltransferases as a Novel Approach for the Characterization of Individual Human Liver: Comparison with mRNA Levels and Activities. *Drug Metab. Dispos.*, 40(1), 83–92.

Ong, S-E, Blagoev, B, Kratchmarova, I, Kristensen, DB, Steen, H, Pandey, A, and Mann, M. (2002). Stable isotope labeling by amino acids in cell culture, SILAC, as a simple and accurate approach to expression proteomics. *Mol. Cell. Proteomics*, 1(5), 376–386.

Ong, S-E, and Mann, M. (2005). Mass spectrometry-based proteomics turns quantitative. *Nat. Chem. Biol.*, 1(5), 252–262.

Oswald, S. (2019). Organic Anion Transporting Polypeptide (OATP) transporter expression, localization and function in the human intestine. *Pharmacol. Ther.*, 195, 39–53.

Oswald, S, Gröer, C, Drozdzik, M, and Siegmund, W. (2013). Mass spectrometry-based targeted proteomics as a tool to elucidate the expression and function of intestinal drug transporters. *AAPS J.*, 15(4), 1128–1140.

Patel, N, Wiśniowska, B, Jamei, M, and Polak, S. (2018). Real Patient and its Virtual Twin: Application of Quantitative Systems Toxicology Modelling in the Cardiac Safety Assessment of Citalopram. *AAPS J.*, 20(1), 6.

Peng, K, Bacon, J, Zheng, M, Guo, Y, and Wang, MZ. (2015). Ethnic variability in the expression of hepatic drug transporters: absolute quantification by an optimized targeted quantitative proteomic approach. *Drug Metab. Dispos.*, 43(7), 1045–1055.

Peterson, AC, Russell, JD, Bailey, DJ, Westphall, MS, and Coon, JJ. (2012). Parallel Reaction Monitoring for High Resolution and High Mass Accuracy Quantitative, Targeted Proteomics. *Mol. Cell. Proteomics*, 11(11), 1475–1488.

Peterson, MC, and Riggs, MM. (2015). FDA advisory meeting clinical pharmacology review utilizes a quantitative systems pharmacology (QSP) model: A watershed moment? *CPT Pharmacometrics Syst. Pharmacol.*, 4(3), 189–192.

Polasek, TM, Patel, F, Jensen, BP, Sorich, MJ, Wiese, MD, and Doogue, MP. (2013). Predicted

metabolic drug clearance with increasing adult age. *Br. J. Clin. Pharmacol.*, 75(4), 1019–1028.

Polasek, TM, Shakib, S, and Rostami-Hodjegan, A. (2018). Precision dosing in clinical medicine: present and future. *Expert Rev. Clin. Pharmacol.*, 11(8), 743–746.

Prasad, B, Achour, B, Artursson, P, Hop, CECA, Lai, Y, Smith, PC, Barber, J, Wisniewski, JR, Spellman, D, Uchida, Y, Zientek, MA, Unadkat, JD, and Rostami-Hodjegan, A. (2019). Toward a Consensus on Applying Quantitative Liquid Chromatography-Tandem Mass Spectrometry Proteomics in Translational Pharmacology Research: A White Paper. *Clin. Pharmacol. Ther.*, 106(3), 525–543.

Prasad, B, Bhatt, DK, Johnson, K, Chapa, R, Chu, X, Salphati, L, Xiao, G, Lee, C, Hop, CECA, Mathias, A, Lai, Y, Liao, M, Humphreys, WG, Kumer, SC, and Unadkat, JD. (2018). Abundance of Phase 1 and 2 Drug-Metabolizing Enzymes in Alcoholic and Hepatitis C Cirrhotic Livers: A Quantitative Targeted Proteomics Study. *Drug Metab. Dispos.*, 46(7), 943–952.

Prasad, B, Evers, R, Gupta, A, Hop, CECA, Salphati, L, Shukla, S, Ambudkar, S V., and Unadkat, JD. (2014a). Interindividual Variability in Hepatic Organic Anion-Transporting Polypeptides and P-Glycoprotein (ABCB1) Protein Expression: Quantification by Liquid Chromatography Tandem Mass Spectroscopy and Influence of Genotype, Age, and Sex. *Drug Metab. Dispos.*, 42(1), 78–88.

Prasad, B, Gaedigk, A, Vrana, M, Gaedigk, R, Leeder, JS, Salphati, L, Chu, X, Xiao, G, Hop, C, Evers, R, Gan, L, and Unadkat, JD. (2016a). Ontogeny of Hepatic Drug Transporters as Quantified by LC-MS/MS Proteomics. *Clin. Pharmacol. Ther.*, 100(4), 362–370.

Prasad, B, Johnson, K, Billington, S, Lee, C, Chung, GW, Brown, CDA, Kelly, EJ, Himmelfarb, J, and Unadkat, JD. (2016b). Abundance of Drug Transporters in the Human Kidney Cortex as Quantified by Quantitative Targeted Proteomics. *Drug Metab. Dispos.*, 44(12), 1920–1924.

Prasad, B, and Unadkat, JD. (2014b). Comparison of Heavy Labeled (SIL) Peptide versus SILAC Protein Internal Standards for LC-MS/MS Quantification of Hepatic Drug Transporters. *Int. J. Proteomics*, 2014, 1–11.

Ronsein, GE, Pamir, N, von Haller, PD, Kim, DS, Oda, MN, Jarvik, GP, Vaisar, T, and Heinecke, JW. (2015). Parallel reaction monitoring (PRM) and selected reaction monitoring (SRM) exhibit comparable linearity, dynamic range and precision for targeted quantitative HDL proteomics. *J. Proteomics*, 113, 388–399.

Ross, PL, Huang, YN, Marchese, JN, Williamson, B, Parker, K, Hattan, S, Khainovski, N, Pillai, S, Dey, S, Daniels, S, Purkayastha, S, Juhasz, P, Martin, S, Bartlet-Jones, M, He, F, Jacobson, A, and Pappin, DJ. (2004). Multiplexed Protein Quantitation in *Saccharomyces cerevisiae* Using Amine-reactive Isobaric Tagging Reagents. *Mol. Cell. Proteomics*, 3(12), 1154–1169.

Röst, HL, Rosenberger, G, Navarro, P, Gillet, L, Miladinoviä, SM, Schubert, OT, Wolski, W, Collins, BC, Malmström, J, Malmström, L, and Aebersold, R. (2014). OpenSWATH enables automated, targeted analysis of data-independent acquisition MS data. *Nat. Biotechnol.*, 32(3), 219–223.

Rostami-Hodjegan, A. (2012). Physiologically based pharmacokinetics joined with in vitro-in vivo extrapolation of ADME: A marriage under the arch of systems pharmacology. *Clin.*

Pharmacol. Ther., 92(1), 50–61.

Rowland, A, Ruanglertboon, W, Dyk, M, Wijayakumara, D, Wood, LS, Meech, R, Mackenzie, PI, Rodrigues, AD, Marshall, J-C, and Sorich, MJ. (2019). Plasma extracellular nanovesicle (exosome)-derived biomarkers for drug metabolism pathways: a novel approach to characterize variability in drug exposure. *Br. J. Clin. Pharmacol.*, 85(1), 216–226.

Rowland, M, Lesko, L, and Rostami-Hodjegan, A. (2015). Physiologically Based Pharmacokinetics Is Impacting Drug Development and Regulatory Decision Making. *CPT Pharmacometrics Syst. Pharmacol.*, 4(6), 313–315.

Russell, MR, Achour, B, McKenzie, EA, Lopez, R, Harwood, MD, Rostami-Hodjegan, A, and Barber, J. (2013). Alternative fusion protein strategies to express recalcitrant QconCAT proteins for quantitative proteomics of human drug metabolizing enzymes and transporters. *J. Proteome Res.*, 12(12), 5934–5942.

Russell, MR, Graham, C, D'Amato, A, Gentry-Maharaj, A, Ryan, A, Kalsi, JK, Ainley, C, Whetton, AD, Menon, U, Jacobs, I, and Graham, RLJ. (2017). A combined biomarker panel shows improved sensitivity for the early detection of ovarian cancer allowing the identification of the most aggressive type II tumours. *Br. J. Cancer*, 117(5), 666–674.

Russell, MR, Walker, MJ, Williamson, AJK, Gentry-Maharaj, A, Ryan, A, Kalsi, J, Skates, S, D'Amato, A, Dive, C, Pernemalm, M, Humphryes, PC, Fourkala, E-O, Whetton, AD, Menon, U, Jacobs, I, and Graham, RLJ. (2016). Protein Z: A putative novel biomarker for early detection of ovarian cancer. *Int. J. Cancer*, 138(12), 2984–2992.

Sager, JE, Yu, J, Ragueneau-Majlessi, I, and Isoherranen, N. (2015). Physiologically Based Pharmacokinetic (PBPK) Modeling and Simulation Approaches: A Systematic Review of Published Models, Applications, and Model Verification. *Drug Metab. Dispos.*, 43(11), 1823–1837.

Sato, Y, Nagata, M, Kawamura, A, Miyashita, A, and Usui, T. (2012). Protein quantification of UDP-glucuronosyltransferases 1A1 and 2B7 in human liver microsomes by LC-MS/MS and correlation with glucuronidation activities. *Xenobiotica*, 42(9), 823–829.

Sato, Y, Nagata, M, Tetsuka, K, Tamura, K, Miyashita, A, Kawamura, A, and Usui, T. (2014). Optimized methods for targeted peptide-based quantification of human uridine 59-diphosphate-glucuronosyltransferases in biological specimens using liquid chromatography-tandem mass spectrometry. *Drug Metab. Dispos.*, 42(5), 885–889.

Schaefer, O, Ohtsuki, S, Kawakami, H, Inoue, T, Liehner, S, Saito, A, Sakamoto, A, Ishiguro, N, Matsumaru, T, Terasaki, T, and Ebner, T. (2012). Absolute quantification and differential expression of drug transporters, cytochrome P450 enzymes, and UDP-glucuronosyltransferases in cultured primary human hepatocytes. *Drug Metab. Dispos.*, 40(1), 93–103.

Schiffmann, C, Hansen, R, Baumann, S, Kublik, A, Nielsen, PH, Adrian, L, von Bergen, M, Jehmlich, N, and Seifert, J. (2014). Comparison of targeted peptide quantification assays for reductive dehalogenases by selective reaction monitoring (SRM) and precursor reaction monitoring (PRM). *Anal. Bioanal. Chem.*, 406(1), 283–291.

Schilling, B, MacLean, B, Held, JM, Sahu, AK, Rardin, MJ, Sorensen, DJ, Peters, T, Wolfe, AJ, Hunter, CL, MacCoss, MJ, and Gibson, BW. (2015). Multiplexed, Scheduled, High-Resolution Parallel Reaction Monitoring on a Full Scan QqTOF Instrument with

Integrated Data-Dependent and Targeted Mass Spectrometric Workflows. *Anal. Chem.*, 87(20), 10222–10229.

Shawahna, R, Uchida, Y, Declèves, X, Ohtsuki, S, Yousif, S, Dauchy, S, Jacob, A, Chassoux, F, Daumas-Duport, C, Couraud, P-O, Terasaki, T, and Scherrmann, J-M. (2011). Transcriptomic and Quantitative Proteomic Analysis of Transporters and Drug Metabolizing Enzymes in Freshly Isolated Human Brain Microvessels. *Mol. Pharm.*, 8(4), 1332–1341.

Shi, J, Wang, X, Zhu, H, Jiang, H, Wang, D, Nesvizhskii, A, and Zhu, H-J. (2018). Determining Allele-Specific Protein Expression (ASPE) Using a Novel Quantitative Concatamer Based Proteomics Method. *J. Proteome Res.*, 17(10), 3606–3612.

Shruthi, BS, Vinodhkumar, P, and Selvamani, M. (2016). Proteomics: A new perspective for cancer. *Adv. Biomed. Res.*, 5, 67.

Silva, JC, Denny, R, Dorschel, CA, Gorenstein, M, Kass, IJ, Li, GZ, McKenna, T, Nold, MJ, Richardson, K, Young, P, and Geromanos, S. (2005). Quantitative proteomic analysis by accurate mass retention time pairs. *Anal. Chem.*, 77(7), 2187–2200.

Silva, JC, Gorenstein, M V., Li, G-Z, Vissers, JPC, and Geromanos, SJ. (2006). Absolute Quantification of Proteins by LCMSE: a virtue of parallel MS acquisition. *Mol. Cell. Proteomics*, 5(1), 144–156.

Sjöström, M, Ossola, R, Breslin, T, Rinner, O, Malmström, L, Schmidt, A, Aebersold, R, Malmström, J, and Niméus, E. (2015). A Combined Shotgun and Targeted Mass Spectrometry Strategy for Breast Cancer Biomarker Discovery. *J. Proteome Res.*, 14(7), 2807–2818.

Smith, BJ, Martins-de-Souza, D, and Fioramonte, M. (2019). A Guide to Mass Spectrometry-Based Quantitative Proteomics. *Methods Mol. Biol.*, 1916, 3–39.

Srivastava, A, and Creek, DJ. (2019). Discovery and Validation of Clinical Biomarkers of Cancer: A Review Combining Metabolomics and Proteomics. *Proteomics*, 19(10), 1700448.

Starr, AE, Deeke, SA, Ning, Z, Chiang, CK, Zhang, X, Mottawea, W, Singleton, R, Benchimol, EI, Wen, M, Mack, DR, Stintzi, A, and Figeys, D. (2017). Proteomic analysis of ascending colon biopsies from a paediatric inflammatory bowel disease inception cohort identifies protein biomarkers that differentiate Crohn's disease from UC. *Gut*, 66(9), 1573–1583.

T'jollyn, H, Vermeulen, A, Michelet, R, Van, BJ, Boussery, K, Snoeys, J, Cuyckens, F, Mannens, G, Van, PA, Annaert, P, and Allegaert, K. (2015). Physiologically Based Pharmacokinetic Predictions of Tramadol Exposure Throughout Pediatric Life: an Analysis of the Different Clearance Contributors with Emphasis on CYP2D6 Maturation. *AAPS J.*, 17(6), 1376–1387.

Takemori, N, Takemori, A, Tanaka, Y, Endo, Y, Hurst, JL, Gómez-Baena, G, Harman, VM, and Beynon, RJ. (2017). MEERCAT: Multiplexed Efficient Cell Free Expression of Recombinant QconCATs For Large Scale Absolute Proteome Quantification. *Mol. Cell. Proteomics*, 16(12), 2169–2183.

Tan, HT, Wu, W, Ng, YZ, Zhang, X, Yan, B, Ong, CW, Tan, S, Salto-Tellez, M, Hooi, SC, and Chung, MCM. (2012). Proteomic analysis of colorectal cancer metastasis: Stathmin-1 revealed as a player in cancer cell migration and prognostic marker. *J. Proteome Res.*,

11(2), 1433–1445.

Templeton, IE, Jones, NS, and Musib, L. (2018). Pediatric Dose Selection and Utility of PBPK in Determining Dose. *AAPS J.*, 20(2), 31.

Tommi, V, Suomi, T, and Elo, LL. (2018). A comprehensive evaluation of popular proteomics software workflows for label-free proteome quantification and imputation. *Brief. Bioinform.*, 19(6), 1344–1355.

Tsamandouras, N, Wendling, T, Rostami-Hodjegan, A, Galetin, A, and Aarons, L. (2015). Incorporation of stochastic variability in mechanistic population pharmacokinetic models: handling the physiological constraints using normal transformations. *J. Pharmacokinet. Pharmacodyn.*, 42(4), 349–373.

Tsuchida, S, Satoh, M, Kawashima, Y, Sogawa, K, Kado, S, Sawai, S, Nishimura, M, Ogita, M, Takeuchi, Y, Kobyashi, H, Aoki, A, Kodera, Y, Matsushita, K, Izumi, Y, and Nomura, F. (2013). Application of quantitative proteomic analysis using tandem mass tags for discovery and identification of novel biomarkers in periodontal disease. *Proteomics*, 13(15), 2339–2350.

Uchida, Y, Ohtsuki, S, Katsukura, Y, Ikeda, C, Suzuki, T, Kamiie, J, and Terasaki, T. (2011). Quantitative targeted absolute proteomics of human blood-brain barrier transporters and receptors. *J. Neurochem.*, 117(2), 333–345.

Uhlen, M, Fagerberg, L, Hallstrom, BM, Lindskog, C, Oksvold, P, Mardinoglu, A, Sivertsson, A, Kampf, C, Sjostedt, E, Asplund, A, Olsson, I, Edlund, K, Lundberg, E, Navani, S, Szigyarto, CA-K, Odeberg, J, Djureinovic, D, … Ponten, F. (2015). Tissue-based map of the human proteome. *Science (80-.).*, 347(6220), 1260419–1260419.

Upreti, V V, and Wahlstrom, JL. (2016). Meta-analysis of hepatic cytochrome P450 ontogeny to underwrite the prediction of pediatric pharmacokinetics using physiologically based pharmacokinetic modeling. *J. Clin. Pharmacol.*, 56(3), 266–283.

van Groen, BD, van de Steeg, E, Mooij, MG, van Lipzig, MMH, de Koning, BAE, Verdijk, RM, Wortelboer, HM, Gaedigk, R, Bi, C, Leeder, JS, van Schaik, RHN, van Rosmalen, J, Tibboel, D, Vaes, WH, and de Wildt, SN. (2018). Proteomics of human liver membrane transporters: A focus on fetuses and newborn infants. *Eur. J. Pharm. Sci.*, 124, 217–227.

Venkatakrishnan, K, von Moltke, LL, Court, MH, Harmatz, JS, Crespi, CL, and Greenblatt, DJ. (2000). Comparison between cytochrome P450 (CYP) content and relative activity approaches to scaling from cDNA-expressed CYPs to human liver microsomes: ratios of accessory proteins as sources of discrepancies between the approaches. *Drug Metab. Dispos.*, 28(12), 1493–1504.

Vildhede, A, Karlgren, M, Svedberg, EK, Wisniewski, JR, Lai, Y, Norén, A, and Artursson, P. (2014). Hepatic uptake of atorvastatin: influence of variability in transporter expression on uptake clearance and drug-drug interactions. *Drug Metab. Dispos.*, 42(7), 1210–1218.

Vildhede, A, Mateus, A, Khan, EK, Lai, Y, Karlgren, M, Artursson, P, and Kjellsson, MC. (2016). Mechanistic Modeling of Pitavastatin Disposition in Sandwich-Cultured Human Hepatocytes: A Proteomics-Informed Bottom-Up Approach. *Drug Metab. Dispos.*, 44(4), 505–516.

Vildhede, A, Nguyen, C, Erickson, BK, Kunz, RC, Jones, R, Kimoto, E, Bourbonais, F, Rodrigues, AD, and Varma, MVS. (2018). Comparison of Proteomic Quantification

Approaches for Hepatic Drug Transporters: Multiplexed Global Quantitation Correlates with Targeted Proteomic Quantitation. *Drug Metab. Dispos.*, 46(5), 692–696.

Vildhede, A, Wiśniewski, JR, Norén, A, Karlgren, M, and Artursson, P. (2015). Comparative Proteomic Analysis of Human Liver Tissue and Isolated Hepatocytes with a Focus on Proteins Determining Drug Exposure. *J. Proteome Res.*, 14(8), 3305–3314.

Vrana, M, Whittington, D, Nautiyal, V, and Prasad, B. (2017). Database of Optimized Proteomic Quantitative Methods for Human Drug Disposition-Related Proteins for Applications in Physiologically Based Pharmacokinetic Modeling. *CPT Pharmacometrics Syst. Pharmacol.*, 6(4), 267–276.

Walsky, RL, Bauman, JN, Bourcier, K, Giddens, G, Lapham, K, Negahban, A, Ryder, TF, Obach, RS, Hyland, R, and Goosen, TC. (2012). Optimized assays for human UDP-glucuronosyltransferase (UGT) activities: Altered alamethicin concentration and utility to screen for UGT inhibitors. *Drug Metab. Dispos.*, 40(5), 1051–1065.

Walsky, RL, and Obach, RS. (2004). Validated assays for human cytochrome P450 activities. *Drug Metab. Dispos.*, 32(6), 647–660.

Wang, H, Zhang, H, Li, J, Wei, J, Zhai, R, Peng, B, Qiao, H, Zhang, Y, and Qian, X. (2015). A new calibration curve calculation method for absolute quantification of drug metabolizing enzymes in human liver microsomes by stable isotope dilution mass spectrometry. *Anal. Methods*, 7(14), 5934–5941.

Wang, L, Collins, C, Kelly, EJ, Chu, X, Ray, AS, Salphati, L, Xiao, G, Lee, C, Lai, Y, Liao, M, Mathias, A, Evers, R, Humphreys, W, Hop, CECA, Kumer, SC, and Unadkat, JD. (2016). Transporter expression in liver tissue from subjects with alcoholic or hepatitis C cirrhosis quantified by targeted quantitative proteomics. *Drug Metab. Dispos.*, 44(11), 1752–1758.

Wang, X, Shi, J, and Zhu, H-J. (2019). Functional Study of Carboxylesterase 1 Protein Isoforms. *Proteomics*, 19(4), 1800288.

Wegler, C, Gaugaz, FZ, Andersson, TB, Wiśniewski, JR, Busch, D, Gröer, C, Oswald, S, Norén, A, Weiss, F, Hammer, HS, Joos, TO, Poetz, O, Achour, B, Rostami-Hodjegan, A, Van De Steeg, E, Wortelboer, HM, and Artursson, P. (2017). Variability in Mass Spectrometry-based Quantification of Clinically Relevant Drug Transporters and Drug Metabolizing Enzymes. *Mol. Pharm.*, 14(9), 3142–3151.

Weiß, F, Hammer, HS, Klein, K, Planatscher, H, Zanger, UM, Norén, A, Wegler, C, Artursson, P, Joos, TO, and Poetz, O. (2018). Direct Quantification of Cytochromes P450 and Drug Transporters—A Rapid, Targeted Mass Spectrometry-Based Immunoassay Panel for Tissues and Cell Culture Lysates. *Drug Metab. Dispos.*, 46(4), 387–396.

Wetmore, BA, and Merrick, BA. (2004). Invited Review: Toxicoproteomics: Proteomics Applied to Toxicology and Pathology. *Toxicol. Pathol.*, 32(6), 619–642.

Whiteaker, JR, Halusa, GN, Hoofnagle, AN, Sharma, V, MacLean, B, Yan, P, Wrobel, JA, Kennedy, J, Mani, DR, Zimmerman, LJ, Meyer, MR, Mesri, M, Rodriguez, H, Abbatiello, SE, Boja, E, Carr, SA, Chan, DW, … Paulovich, AG. (2014). CPTAC Assay Portal: a repository of targeted proteomic assays. *Nat. Methods*, 11(7), 703–704.

Wiese, S, Reidegeld, KA, Meyer, HE, and Warscheid, B. (2007). Protein labeling by iTRAQ: a new tool for quantitative mass spectrometry in proteome research. *Proteomics*, 7(3),

340–350.

Wiśniewski, JR, and Mann, M. (2012a). Consecutive Proteolytic Digestion in an Enzyme Reactor Increases Depth of Proteomic and Phosphoproteomic Analysis. *Anal. Chem.*, 84(6), 2631–2637.

Wiśniewski, JR, Ostasiewicz, P, Duś, K, Zielińska, DF, Gnad, F, and Mann, M. (2012b). Extensive quantitative remodeling of the proteome between normal colon tissue and adenocarcinoma. *Mol. Syst. Biol.*, 8, 611.

Wiśniewski, JR, Vildhede, A, Norén, A, and Artursson, P. (2016a). In-depth quantitative analysis and comparison of the human hepatocyte and hepatoma cell line HepG2 proteomes. *J. Proteomics*, 136, 234–247.

Wiśniewski, JR, Wegler, C, and Artursson, P. (2016b). Subcellular fractionation of human liver reveals limits in global proteomic quantification from isolated fractions. *Anal. Biochem.*, 509, 82–88.

Wiśniewski, JR, Wegler, C, and Artursson, P. (2019). Multiple-Enzyme-Digestion Strategy Improves Accuracy and Sensitivity of Label- and Standard-Free Absolute Quantification to a Level That Is Achievable by Analysis with Stable Isotope-Labeled Standard Spiking. *J. Proteome Res.*, 18(1), 217–224.

Wiśniewski, JR, Zougman, A, Nagaraj, N, and Mann, M. (2009). Universal sample preparation method for proteome analysis. *Nat. Methods*, 6(5), 359–362.

Wortham, M, Czerwinski, M, He, L, Parkinson, A, and Wan, YJY. (2007). Expression of constitutive androstane receptor, hepatic nuclear factor 4α, and P450 oxidoreductase genes determines interindividual variability in basal expression and activity of a broad scope of xenobiotic metabolism genes in the human liver. *Drug Metab. Dispos.*, 35(9), 1700–1710.

Xie, C, Yan, T, Chen, J, Li, X, Zou, J, Zhu, L, Lu, L, Wang, Y, Zhou, F, Liu, Z, and Hu, M. (2017). LC-MS/MS quantification of sulfotransferases is better than conventional immunogenic methods in determining human liver SULT activities: implication in precision medicine. *Sci. Rep.*, 7(1), 3858.

Xu, J, Patassini, S, Rustogi, N, Riba-Garcia, I, Hale, BD, Phillips, AM, Waldvogel, H, Haines, R, Bradbury, P, Stevens, A, Faull, RLM, Dowsey, AW, Cooper, GJS, and Unwin, RD. (2019). Regional protein expression in human Alzheimer's brain correlates with disease severity. *Commun. Biol.*, 2(1), 43.

Yang, LQ, Li, SJ, Cao, YF, Man, XB, Yu, WF, Wang, HY, and Wu, MC. (2003). Different alterations of cytochrome P450 3A4 isoform and its gene expression in livers of patients with chronic liver diseases. *World J. Gastroenterol.*, 9(2), 359–363.

Yoshida, K, Budha, N, and Jin, J. (2017). Impact of Physiologically Based Pharmacokinetic Models on Regulatory Reviews and Product Labels: Frequent Utilization in the Field of Oncology. *Clin. Pharmacol. Ther.*, 101(5), 597–602.

Yoshitake, S, McKay-Daily, M, Tanaka, M, and Huang, Z. (2017). Quantification of Sulfotransferases 1A1 and 1A3/4 in Tissue Fractions and Cell Lines by Multiple Reaction Monitoring Mass Spectrometry. *Drug Metab. Lett.*, 11(1), 35–47.

Zhang, F, Xiao, Y, and Wang, Y. (2017). SILAC-Based Quantitative Proteomic Analysis Unveils Arsenite-Induced Perturbation of Multiple Pathways in Human Skin Fibroblast

Cells. *Chem. Res. Toxicol.*, 30(4), 1006–1014.

Zhang, H-F, Wang, H-H, Gao, N, Wei, J-Y, Tian, X, Zhao, Y, Fang, Y, Zhou, J, Wen, Q, Gao, J, Zhang, Y-J, Qian, X-H, and Qiao, H-L. (2016). Physiological Content and Intrinsic Activities of 10 Cytochrome P450 Isoforms in Human Normal Liver Microsomes. *J. Pharmacol. Exp. Ther.*, 358(1), 83–93.

Zhao, P, Vieira, M de LT, Grillo, JA, Song, P, Wu, T-C, Zheng, JH, Arya, V, Berglund, EG, Atkinson, AJ, Sugiyama, Y, Pang, KS, Reynolds, KS, Abernethy, DR, Zhang, L, Lesko, LJ, and Huang, S-M. (2012). Evaluation of Exposure Change of Nonrenally Eliminated Drugs in Patients With Chronic Kidney Disease Using Physiologically Based Pharmacokinetic Modeling and Simulation. *J. Clin. Pharmacol.*, 52(S1), 91S-108S.

Zhou, Y, Ingelman-Sundberg, M, and Lauschke, VM. (2017). Worldwide Distribution of Cytochrome P450 Alleles: A Meta-analysis of Population-scale Sequencing Projects. *Clin. Pharmacol. Ther.*, 102(4), 688–700.

Zhu, X, Shen, X, Qu, J, Straubinger, RM, and Jusko, WJ. (2018). Multi-Scale Network Model Supported by Proteomics for Analysis of Combined Gemcitabine and Birinapant Effects in Pancreatic Cancer Cells. *CPT Pharmacometrics Syst. Pharmacol.*, 7(9), 549–561.

6 Chapter Six

Design, Expression, and Characterisation of Non-Cytochrome P450 and Non-Uridine Diphosphate Glucuronosyltransferase QconCAT (NuncCAT)

Declaration

Elkhateeb, E., Al-Majdoub, Z., Achour, B., Rostami-Hodjegan, A., and Barber, J.

I carried out the literature search, generation and analysis of the data and wrote the manuscript. Dr Zubida Al-Majdoub and Dr Brahim Achour were consulted on experimental methodology. Prof. Amin Rostami-Hodjegan and Dr Jill Barber provided guidance on the study design.

6.1. Abstract

QconCAT is a tool for quantitative proteomics, consisting of an artificial protein, expressed from an artificial gene. This protein is made up of a concatenated string of proteotypic peptides selected from the proteins under study. Isotopically labelled QconCAT, usually containing $^{13}C_6$-arginine and $^{13}C_6$-lysine, provides a standard for each proteotypic peptide included in its sequence. A novel QconCAT (NuncCAT) was constructed in this article for enzymes other than Cytochromes P450 and Uridine 5'-diphospho-glucuronosyltransferase enzymes. The need for such QconCAT, criteria for peptides selection, construct, expression, and quality control tests were presented. The designed and expressed NuncCAT showed good purity, high labelling efficiency (above 98% for all peptides), high coverage (93% of the sequence), and its concentration was measured to allow its use as internal standard with the biological sample of interest. This QconCAT construct is ideal for quantitative experiments that use FASP digestion protocols.

6.2. Introduction

6.2.1. Overview on internal standards

Determination of the absolute abundance of proteins in biological samples can be laborious using western blotting and ELISA. Mass spectrometry enables the simultaneous analysis of multiple proteins, but the mass spectrometry signal does not reflect the absolute amount of the underlying protein. Therefore stable isotope labelled (SIL) peptides or proteins can be used as a standard or reference. These standards include heavy surrogate peptides (contain heavy isotopes (^{13}C, ^{15}N) that are synthesised either chemically or biologically) to quantify target proteins that are present in the biological sample (analyte) in a light form (^{12}C, ^{14}N). The added standards can be either small peptides; absolute quantification (AQUA) peptides for small number of targets, concatenated larger peptides; quantitative concatemers (QconCAT) for

relatively larger number of targets up to 20, or protein standards for absolute quantification (PSAQ) for a single protein target (El-Khateeb et al., 2019).

6.2.2. Concatenated labelled internal standards for proteins involved in drugs metabolism

For modelling approaches in systems biology and drug metabolism, measuring the absolute abundances of different drug-metabolising enzymes and proteins is essential. One way to gain this knowledge is through the use of QconCATs which are synthetic proteins consisting of proteotypic peptides derived from the target proteins to be quantified. This QconCAT technology delivers heavy isotope labelled reference standards that involve signature or surrogate peptides for each target protein of interest. Usually, a known concentration of these purified synthetic concatenated peptides, previously expressed in E.coli is spiked with the analyte or the sample of interest. When both the sample and the QconCAT are simultaneously digested, surrogate peptides from the QconCAT will be released. The ratio of heavy peptide (from the QconCAT) to the light peptide (from the analyte) can be used for the quantification of the protein of interest within the sample. However, the selection and the order of these surrogate peptides have some criteria to be applicable for global proteomic methods (Prasad et al., 2019). These criteria are essential for the optimal cleavage by proteolytic enzymes used in the analyte digestion, in order to completely release the surrogate peptides with high flyability, ionisability, and detectability by Liquid Chromatography-tandem mass spectrometry (LC-MS/MS). These peptides also need to be stable and less liable to modifications or interaction with the analyte.

Several QconCATs have been designed by our group for that purpose. Each QconCAT is considered as an internal standard for the quantification of a specific number of drug-

metabolising enzymes and transporters (DME&T). Each target protein is represented in the QconCAT as one, and preferably, two, or three specific/unique peptides to that target.

The first two QconCATs, which covered most of the drug-metabolising enzymes (either for phase I or II metabolism) and drug transporters in the tissue fraction sample, are the MetCAT (Achour, et al., 2015), and TransCAT (Russell, et al., 2013), respectively.

6.2.3. The Need for Non-Cytochrome P450 and Non-Uridine Diphosphate Glucuronosyltransferase QconCAT (NuncCAT).

The MetCAT included most human liver cytochrome P450 (CYP450) and uridine diphosphate glucuronosyltransferases (UGTs). However, there are lots of compounds with high lipophilicity, low aqueous solubility, low microsomal turnover, and are not mainly CYPs or UGT substrates. These compounds or substances are usually metabolised by other oxidases, reductases, estrases, and sulfotransferase enzymes (Table 6.1). Therefore, there was an urgent need to design another QconCAT that can help in the absolute quantification and hence filling the gap for absolute abundance data for these critical enzymes.

Although the criteria of designing the QconCATs have been published before by our group (Achour, et al., 2015), this internal standard design is target-specific and requires experience in selecting the most promising peptides that are most likely to be specific and with the highest possible expected flyability in the LC-MS/MS.

Table 6.1. Tissue harbouring NuncCAT enzymes, examples of their endogenous and xenobiotic/drug substrates

Serial	Enzyme	Tissue with high expression*	Substrate	Reference
1	**CES1**	Mainly liver, small intestine, but also in kidney, and lungs	Methylphenidate, oseltamivir, clopidogrel, dabigatran etexilate, enalapril, and other ACEs, Simvastatin, lovastatin, clofibrate, fenofibrate, oseltamivir, methylphenidate, cocaine, meperidine, flumazenil, mycophenolate mofetil, ciclesonide, Capecitabine	(Laizure, et al., 2014; Merali, et al., 2014)
2	**CES2**	Mainly liver, small intestine, but also in kidney, and lungs	Prasugrel, aspirin, candesartan citexetil, olmesartan medoxomil, azilsartan medoxomil, tenofovir ester, adefovir ester, valacuclovir, cocaine, Heoin, 6-monoacetylmorphine, methylprednisolone, irinotecan	(Casey Laizure, et al., 2013)
3	**FMO3**	Liver	Sulfer containing drugs such as albendazole, ethionamide, methimazole, phenothiazine, cimetidine, ranitidine, tazarotenic acid, and sulindac. Nitrogen containing drugs such as amfetamine, benzydamine, clozapine, dapsone, itopride, methamfetamine, olopatadine, sulfamethoxazole, and tamoxifen	(Krueger & Williams, 2005)
4	**FMO5**	liver, stomach, pancreas, small intestine and foetal tissues	S-methyl esonarimod, E7016 anticancer, MRX-I antibacterial, phosphosulindac, ranitidine	(Phillips & Shephard, 2017)
5	**EPHX1**	Liver and brain	Endogenous steroids, and xenobiotics such as arene oxides and aflatoxin epoxide, detoxifies certain carcinogenic compounds, e.g., butadiene, benzene, and styrene, it can also activate procarcinogens such as polycyclic aromatic hydrocarbons	(Václavíková, et al., 2015)
6	**POR**	Liver, brain, thyroid, intestine, brain, placenta, skin	Zidovudine, mitomycin C, tacrolimus, and warfarin	(Fayz & Inaba, 1998; Kandel & Lampe, 2014)
7	**MGST1**	Mainly in the liver, and kidney but also in adrenal glands and adipose tissue	Detoxification of epoxide intermediates of glyceryl trinitrate, Aflatoxin B1 chlorambucil, melphalan, carmustine, doxorubicin and cisplatin Activates prodrugs as : doxorubicin derivatives	(Johansson, et al., 2006; Morgenstern, et al., 2011)
8	**MGST 2**	Liver, intestine, placenta.	Metabolise different toxic chemicals, drugs, and environmental pollutants, detoxify some of the toxic carbonyl-, peroxide-, and epoxide-containing metabolites.	(Hayes & Pulford, 1995)
9	**MGST 3**	Adrenal glands, intestine, kidney and lower levels in the liver.		
10	**UGT 2B17**	liver, intestine, kidney, testis, uterus, placenta, mammary gland, adrenal gland, skin, and prostate	Numerous endogenous steroids, including testosterone (T), dihydrotestosterone (DHT), androstane-3-α, 17-β-diol (3-α-diol), androsterone and estradiol, and xenobiotics (e.g., 17-dihydroexemestane, vorinostat, lorcaserin)	(Bhatt, et al., 2018)

11	**ADH1A**	Liver, intestine	Ethanol, retinol, other aliphatic alcohols, hydroxysteroids, and lipid peroxidation products	(Duester, et al., 1999)
12	**ADH1B**	Liver, intestine, adipose tissue		
13	**ADH1C**	Liver, intestine, kidney		
14	**ALDH1A1**	Liver, kidney, red blood cells, skeletal muscle, lung, breast, lens, stomach, brain, pancreas, testis, prostate, ovary	Oxazaphosphorines anticancers, acetaldehyde, cyclophosphamide, and 4-hydroperoxycyclophosphamide	(Tomita, et al., 2016)
15	**AOX1**	Adrenal glands, liver, testis, kidney	6-Mercaptopurine, vitamin B6 or pyridoxal , citalopram, zebularine, caffeine, nicotine, brimonidine, vanillin, phthalazine and N1-methylnicotinamide, zaleplon, methotrexate and ziprasidone, and tamoxifen	(Garattini & Terao, 2012; Kücükgöze & Leimkühler, 2018)
16	**NAT1**	Testis, liver, thyroid, adrenal gland, intestine, kidney, placenta	Acetylates isoniazid (treatment for tuberculosis), hydralazine, procainamide, dapsone, aminoglutethimide, and sulfamethazine	(Meisel, 2002)
17	**NAT2**	Lung, intestine, liver, kidney, testis		
18	**SULT1E1**	Intestine, liver	Endogenous and synthetic oestrogens, and acetaminophen	(Barbosa, et al., 2019)
19	**SULT1A1**	Intestine, liver	Several phenolic compounds, iodothyronine, and acetaminophen	(Gamage, et al., 2006; Yamamoto, et al., 2015)
20	**SULT1A2**	Intestine, liver	Several phenolic compounds	
21	**SULT2A1**	Adrenal gland, liver, intestine	Dehydroepiandrosterone (DHEA), testosterone, abiraterone, and acetaminophen	
22	**TPMT**	Thyroid, kidney, skin, intestine, liver, testis, placenta.	Aromatic thiol compounds such as thiophenol, thiosalicylic acid, azathioprine, mercaptopurine and thioguanine	(Lennard, 1998)
23	**EPHX2**	Mainly in the liver but also in kidney and adipose tissue	Trans-Stilbene oxide, leukotriene A4, and metabolises the biologically active epoxyalcohol metabolites of arachidnoic acid, hepoxilin A3 & B3	(Gautheron & Jéru, 2020)

*The Human Protein Atlas https://www.proteinatlas.org/

6.3. Methods

6.3.1. Design and Synthesis of the NuncCAT.

A. Tools used:

- Uniprot human to find the ID number of the protein, the cellular location and the transmembrane sequence (The UniProt Consortium, 2019).
- Protein Prospector (MS Digest) for the theoretical digestion (http://prospector.ucsf.edu/).
- Peptide uniqueness checker to find the unique peptides in the human proteome (https://www.nextprot.org/tools/peptide-uniqueness-checker).
- Expasy peptide mass to check the post-translational modifications (https://www.expasy.org/).
- Isoelectric point (pI) and the molecular weight (Mwt) calculators to determine the pI and Mwt for each peptide (http://isoelectric.org/calculate.php).
- Phobius to find the transmembrane peptides (https://phobius.sbc.su.se/; double-checked with Uniprot https://www.uniprot.org/)

Firstly, a list has been created for the pharmacologically important liver enzymes/targets that are not included in the MetCAT and TransCAT. Then, a full protein sequence was obtained from Uniprot database search. Using protein prospector, the whole protein was theoretically digested using "Trypsin P" as the digestive enzyme. The produced peptides' list was then introduced into the peptide uniqueness checker to select only the unique peptides for this specific target protein.

A new shorter list was created for which the peptide masses and lengths were calculated. Subsequently, the following criteria have been applied to each peptide of which the first three criteria were considered essential conditions while others were preferable.

B. Criteria:

1) Uniqueness
2) Not including M (methionine-prone to oxidation) and C (cysteine-prone to alkylation) in its sequence.
3) Not a transmembrane peptide
4) Length – ideal 6 to 10 (Peptides up to 20 amino acids length were included if there was no other shorter alternative)
5) N (asparagine-prone to glycosylation) was considered as a disadvantage.
6) Aspartate followed directly by Glutamate (DE) in the peptide sequence or the reverse (ED) were considered as disadvantages (prone to missed cleavages). These peptides were completely excluded if this occurred at the beginning of the peptide.
7) Dibasic or tribasic forms of K (lysine), R (arginine), H (histidine) (e.g. KK, HK, RR, KH, KR, HK, HR, RK, RH, etc) were avoided.
8) No Q (Glutamine) at the start of the peptide sequence (N-terminus)
9) Peptides with Asparagine followed by Glycine (NG), Aspartate followed by Proline (DP), Lysine followed by Proline (KP), or Asparagine followed by Glutamine (NQ) were avoided (prone to deamidation and missed cleavage)
10) Liability to post-translational modifications was checked
11) Avoid C- and N-terminal peptides in the protein/enzyme sequence
12) pI up to 6 was considered appropriate.
13) R or K amino-acids before or after the sequence of the peptide of interest was avoided (prone to missed cleavage)
14) Usually peptides ending at -R were preferred

After applying these criteria, each target was represented by one to three peptides. Peptides that have been used as AQUA standards for the quantification of the same targets in the literature were also preferred if they matched most of the above criteria (Bhatt, et al., 2017; Chen, et al.,

2016; Dubaisi, et al., 2019; Prasad, et al., 2018; Sato, et al., 2014; Song, et al., 2015). The ribosomal core 30S was added to the QconCAT structure to improve its expression in E.coli bacteria as reported by (Al-Majdoub, et al., 2014). His_6-affinity tag, "His-tag", was added to the C-terminus to enable purification. The final molecular weight and pI of the whole QconCAT after adding the His-tag was determined and sent to PolyQuant GmbH, Germany for expression and synthesis.

C. NuncCAT structure

Twenty-three targets have been represented in the QconCAT structure that represent metabolising enzymes other than those included in the MetCAT. Apart from UGT2B17, they were all non-CYPs and non-UGTs enzymes. The newly designed QconCAT was given the name of "NuncCAT" referring to **N**on-**U**GT, **N**on-**C**YP Qcon**CAT**. Two other protein targets (CYP1A2 and ABCB1) were added to the targets list. CYP1A2 is a common enzyme with the MetCAT, and ABCB1 is a common transporter with TransCAT, but they are represented here by unique peptides other than the selected ones in the MetCAT and TransCAT. They were used for quality control within the sample. Out of the 25 targets included in the NuncCAT, 11 targets were microsomal, 1 plasma membrane, and 13 were cytosolic enzymes (Table 6.2). The list of 25 total NuncCAT's targets with their representative peptides, and the main cellular fraction harbouring these targets is shown in the table below. Two non-naturally occurring peptides (NNOPs) were used along with one bacterial/nonhuman peptide for the quantification of the NuncCAT.

D. Expression and synthesis

The designed sequence of the NuncCAT was sent to PolyQuant® for expression and synthesis. The expression protocol is similar to that described previously (Al-Majdoub, et al., 2014; Pratt, et al., 2006).

In short, the QconCAT was synthesised and cloned into a bacterial expression vector namely E.coli. The vector was transformed and a clone with high expression of the QconCAT protein was selected. The labelled QconCAT was produced by culturing the selected clone in ^{13}C-K/R labelling-medium containing ampicillin for selection. QconCAT protein was extracted from the bacterial pellet and purified using nickel-nitrilotriacetic acid resin (Ni-NTA) beads. The eluted QconCAT protein was dialysed against 0.1% formic acid as a storage buffer.

6.3.2. Quality control checks

A. Purity

The presence and the purity of the designed and expressed NuncCAT was assessed using One-dimensional sodium dodecyl sulphate-polyacrylamide gel electrophoresis (1DSDS-PAGE). Two different volumes of the NuncCAT (3µl and 6µl) along with the molecular weight marker (Precision Plus Protein^{TM} Standards) were loaded onto a stacking gel (acryl-bisacrylamide 37.5:1 5%; Tris-HCl 0.2 M, pH 6.8; SDS 1%; ammonium persulfate 1%; and TEMED 1 µl/ml) overlaid on a resolving gel (acryl-bisacrylamide 37.5:1 12%; Tris-HCl 0.375 M, pH 8.8; SDS 0.1%; ammonium persulfate 0.1%; and TEMED 0.4 µl/ml) and resolved with a mini-Protean 3 system (Bio-Rad). Gels were run at a constant voltage 100 V until the dye front penetrated the resolving gel. The voltage was then elevated to 160 V and the run was terminated when the dye front reached the bottom of the gel. The gels were stained overnight with 0.1 % Coomassie Brilliant Blue (Sigma, UK) in 40% methanol, 10% acetic acid. Stained gels were then developed in 45% methanol and 10% acetic acid (de-staining solution) until clear protein bands appeared and the background staining was removed.

B. *Peptides detection and identification*

The protein concentration of the NuncCAT was firstly measured using Bradford assay (ThermoFisher Scientific, Hemel Hempstead, UK). A volume equivalent to 10 µg proteins was

prepared for LC-MS/MS analysis using the filter-aided sample preparation (FASP) (Wiśniewski, et al., 2009) as previously described with minor modifications (Al Feteisi, et al., 2018; Couto, et al., 2019).

The sample was solubilised by incubation with sodium deoxycholate (10% w/v final volume), 1,4-dithiothreitol (DTT) was added at a final concentration of 100 mM, and the protein mixture was incubated at room temperature for 10 min. Reduction of protein disulfide bonds was carried out by incubation at 56°C for 40 min. Amicon Ultra 0.5 ml centrifugal filters, 3 kDa molecular weight cut-off, (Millipore, Nottingham, UK) were conditioned by briefly centrifuging 400 µl of 0.1 M Tris of pH 8.5 at 14000*g* at room temperature. The QconCAT sample was then transferred to the conditioned filter units, followed by centrifugation at 14000*g* at room temperature for 30 min. The sample was then incubated with 100 µl of 50 mM iodoacetamide in the dark for 30 min at room temperature. After alkylation, deoxycholate removal was performed by buffer exchange using two successive washes with 8 M urea in 100 mM Tris-HCl (pH 8.5), 200 µl each. To reduce urea concentration, three additional washes were performed using 1 M urea in 50 mM ammonium bicarbonate (pH 8.5). Protein digestion was achieved using LysC twice (LysC: protein ratio 1:50, 2 hours each, at 30°C), then trypsin digestion was carried out (trypsin: protein ratio 1:25) for 12 hours at 37°C and another equivalent treatment for an extra 6-hour incubation. Peptides were recovered from the filter by centrifugation (14000*g*, 20 min), followed by a second collection using 0.5 M sodium chloride. The collected peptides were lyophilised using a vacuum concentrator at 30 ºC and with vacuum in aqueous mode. Lyophilised peptides were reconstituted in 20% (v/v) acetonitrile in water, acidified with 2% (v/v) trifluoroacetic acid, then desalted using C18 spin columns according to the manufacturer's instructions (Nest group, USA). The peptides were lyophilised and stored at −80°C until mass spectrometric analysis.

Liquid chromatography and tandem mass spectrometry (LC-MS/MS)

Lyophilised peptides were re-suspended in either 10 µl of 3% (v/v) acetonitrile in water with 0.1% (v/v) formic acid. Digested NuncCAT sample was analysed by LC-MS/MS using an UltiMate® 3000 Rapid Separation LC (RSLC, Dionex Corporation, Sunnyvale, CA) coupled to a Q Exactive HF Hybrid Quadrupole-Orbitrap mass spectrometer (Thermo Fisher Scientific, Waltham, MA) mass spectrometer. Mobile phase A was 0.1% formic acid in water and mobile phase B was 0.1% formic acid in acetonitrile, and peptides were eluted on CSH C18 analytical column (75 mm x 250 µm inner diameter, 1.7 µm particle size) (Waters, UK). A 1 µl aliquot of the sample was transferred to a 5 µl loop and loaded onto the column at a flow rate of 300 nl/min for 5 min at 5% B. The loop was then taken out of line and the flow was reduced from 300 nl/min to 200 nl/min in 0.5 min. Peptides were separated using a gradient from 5% to 18% B in 63.5 min, then from 18% to 27% B in 8 min, and finally from 27% B to 60% B in 1 min. The column was washed at 60% B for 3 min before re-equilibration to 5% B in 1 min. At 85 min, the flow was increased to 300 nl/min until the end of the run at 90 min. Mass spectrometry data were acquired in a data-dependent manner for 90 min in positive mode. Peptides were selected for fragmentation automatically by data dependent analysis on a basis of the top 12 peptides with *m/z* between 300 to 1750 Th and a charge state of 2+, 3+, and 4+ with dynamic exclusion set at 15 sec. The MS resolution was set at 120,000 with an AGC target of 3E6 and a maximum fill time set at 20 ms. The MS2 resolution was set to 30,000, with an AGC target of 2E5, a maximum fill time of 45 ms, isolation window of 1.3 Th and a collision energy of 28 eV.

MaxQuant 1.6.1.0 was used for data analysis. The number of surrogate peptides identified was reported. The retention time for each peptide was also defined using Skyline v20.1.0.31.

C. Percent coverage

In order to make sure that the expression was successful and nearly all the sequence have been covered, the percent coverage of the detected peptides to the overall sequence was also calculated. This was achieved by counting the number of amino acids in the detected peptides relative to the number of amino acids in the whole sequence.

D. Incorporation/labelling efficiency of heavy lysine and arginine residues

The efficiency of incorporating heavy labels to every R and K amino acids within the NuncCAT sequence is called incorporation or labelling efficiency. Incorporation efficiency was determined by triple-quadrupole mass spectrometry of trypsin/Lys C digests of the labelled QconCAT proteins followed by the determination of the intensity ratios of the residual unlabelled (Light) to labelled (Heavy) peptide peaks for a set of peptides. It was calculated and reported for each set of peptides, ending with either R or K amino acids.

E. NuncCAT LC-MS/MS quantification

Another 10 µg sample was prepared for analysis as previously described for peptides identification. However in the reconstitution step and before the LC-MS/MS analysis, 52.7 pmoles of the light/unlabelled form of the NNOP peptide (AEGVNDNEEGFFSAR) were added and the volume was completed up to 10 µl with 3% (v/v) acetonitrile in water with 0.1% (v/v) formic acid.

The concentration of the QconCAT in µg/µl was calculated using Equation (1)

$$\text{The concentration of the NuncCAT in } (\mu g/\mu l) = \frac{(H/L)\times NNOP\ amount\ in\ pmol * Mwt}{V\times 10^6 \times LE} \quad (1)$$

Where; H/L is the ratio of the intensities of both heavy form of the NNOP from the NuncCAT to the light form from both the sample and the unlabelled fraction of the NuncCAT, *Mwt* is the molecular weight of the NuncCAT in Daltons, *V* is the starting digested volume of the NuncCAT, *LE* is the labelling efficiency fraction of the peptide (from Section D above).

6.4. Results

6.4.1. Design and synthesis

Using the criteria mentioned above in the Methods, a list of the best peptides for each target was generated to be included in the NuncCAT structure (Table 6.2).

Table 6.2. NuncCAT target protein with their representative peptides and the main cellular location.

Target	Peptides	Reference study if used as AQUA	Main cellular location
CES1	**EGYLQIGANTQAAQK**	(Prasad, et al., 2018)	**Microsomes**
	FLSLDLQGDPR	Current study search	
CES2	**ADHGDELPFVFR**	(Prasad, et al., 2018)	**Microsomes**
	SFFGGNYIK	Current study search	
	TTHTGQVLGSLVHVK	(Prasad, et al., 2018)	
FMO3	**LVGPGQWPGAR**	(Prasad, et al., 2018)	**Microsomes**
	NNLPTAISDWLYVK	Current study search	
FMO5	**WATQVFK**	(Chen, et al., 2016)	**Microsomes**
	TDDIGGLWR	(Chen, et al., 2016)	
	LTHFIWK	(Chen, et al., 2016)	
EPHX1	**IIPLLTDPK**	(Song, et al., 2015)	**Microsomes**
	FSTWTNTEFR	(Song, et al., 2015)	
POR	**QYELVVHTDIDAAK**	Current study search	**Microsomes**
	YYSIASSSK	Current study search	
	IQTLTSSVR	Current study search	
MGST1	**VFANPEDCVAFGK**	(Song, et al., 2015)	**Microsomes**
	IYHTIAYLTPLPQPNR	(Song, et al., 2015)	
MGST 2	**HLYFWGYSEAAK**	(Song, et al., 2015)	**Microsomes**
MGST 3	**IASGLGLAWIVGR***	(Song, et al., 2015)	**Microsomes**
	VLYAYGYYTGEPSK	(Song, et al., 2015)	
UGT 2B17	**WTYSISK**	(Sato, et al., 2014)	**Microsomes**
	GHEVIVLTSSASILVNASK*	Current study search	
	SVINDPIYK	(Prasad, et al., 2018)	
CYP 1A2	**IGSTPVLVLSR**	Current study search	**Microsomes**
ABCB1	**IATEAIENFR**	Current study search criteria	**Plasma membrane**
ADH1A	**GAILGGFK**	(Bhatt, et al., 2017; Prasad, et al., 2018)	**Cytosol**
	NDVSNPQGTLQDGTSR	(Bhatt, et al., 2017; Prasad, et al., 2018)	
	KPIHHFLGISTFSQYTVVDENAVAK	(Prasad, et al., 2018)	
ADH1B	**AAVLWEVK**	(Bhatt, et al., 2017; Prasad, et al., 2018)	**Cytosol**
	GAVYGGFK	Current study search	
ADH1C	**FSLDALITNILPFEK***	Current study search	**Cytosol**
ALDH1A1	**IFVEESIYDEFVR**	(Bhatt, et al., 2017; Prasad, et al., 2018)	**Cytosol**
	IFINNEWHDSVSGK	(Bhatt, et al., 2017; Prasad, et al., 2018)	

	TIPIDGNFFTYTR	Current study search	
AOX1	**LILNEVSLLGSAPGGK**	(Prasad, et al., 2018)	**Cytosol**
	GLHGPLTLNSPLTPEK	(Prasad, et al., 2018)	
	VFFGEGDGIIR	Current study search	
NAT1	**DNTDLIEFK**	Current study search	**Cytosol**
	NYIVDAGFGR	Current study search	
NAT2	**TLTEEEVEEVLK**	Current study search	**Cytosol**
	DNTDLVEFK	Current study search	
SULT1E1	**KPSEELVDR**	(Dubaisi, et al., 2019)	**Cytosol**
	NHFTVALNEK	Current study search	
SULT1A1	**VHPEPGTWDSFLEK**	(Dubaisi, et al., 2019)	**Cytosol**
SULT1A2	**VYPHPGTWESFLEK**	(Dubaisi, et al., 2019)	**Cytosol**
SULT2A1	**DEDVIILTYPK**	(Dubaisi, et al., 2019)	**Cytosol**
	TLEPEELNLILK	Current study search	
TPMT	**NQVLTLEEWQDK**	Current study search	**Cytosol**
	TSLDIEEYSDTEVQK	Current study search	
EPHX2	**GLLNDAFQK**	(Prasad, et al., 2018)	**Cytosol**
	WLDSDAR	Current study search	

*peptides that have not been detected after the experimental digestion.

The overall molecular weight of the concatenated and synthesised protein was 93557 Daltons and the isoelectric point (pI) was 4.7. The fasta file of the whole sequence and the order of the chosen peptides within the NuncCAT structure is shown in Figure 6.1.

MGTKTFTAKPETVKRDWYVVDATGKSMALRLANELSDAAENKFGSELLAKVEGDTKPELEL
TLKSDLSADINEHLIVELYSKGVNDNEEGFFSAKLEPGRLEYDPNRSAGTYVQIVARDAQS
ALTVSETTFGRDFNEALVHQVVVAYAAGARLDNVVYRAVVESIQRWTYSISKNHFTVALNE
KGLHGPLTLNSPLTPEKGAILGGFKNQVLTLEEWQDKIYHTIAYLTPLPQPNRNYIVDAGF
GRGLLNDAFQKFSLDALITNILPFEKIFVEESIYDEFVRSVINDPIYKTEGVNDNEEGFFS
ARDNTDLVEFKIFINNEWHDSVSGKYYSIASSSKEGYLQIGANTQAAQKFSTWTNTEFRAD
HGDELPFVFRVLYAYGYYTGEPSKTLEPEELNLILKLVGPGQWPGARHLYFWGYSEAAKWA
TQVFKSLLAVGITEVIGDFRVHPEPGTWDSFLEKIIPLLTDPKFLSLDLQGDPRGHEVIVL
TSSASILVNASKNDVSNPQGTLQDGTSRVFANPEDCVAFGKKPIHHFLGISTFSQYTVVDE
NAVAKNNLPTAISDWLYVKSFFGGNYIKIASGLGLAWIVGRVYPHPGTWESFLEKVFFGEG
DGIIRIQTLTSSVRAAVLWEVKDNTDLIEFKTLTEEEVEEVLKLILNEVSLLGSAPGGKKP
SEELVDRWLDSDARIATEAIENFRQYELVVHTDIDAAKLTHFIWKDEDVIILTYPKTTHTG

QVLGSLVHVKGAVYGGFKTSLDIEEYSDTEVQKIGSTPVLVLSRAEGVNDNEEGFFSARTI
PIDGNFFTYTRTDDIGGLWRSSYVGDEASSKLAAALEHHHHHH

Figure 6.1. NuncCAT fasta file with the 30S ribosomal core (Orange), 2 non-naturally occurring peptides (NNOP) used for the quantification in Green, one bacterial/nonhuman peptide (Blue), and the replical peptide (Red).

6.4.2. Quality control

A. Purity

As the molecular weight of the NuncCAT was designed to be 93557 Daltons, a band in between 75 and 100 Kilo Daltons (according to the marker's bands) was expected in each NucCAT lane of gel electrophoresis.

In Figure 6.2, clear bands were present within the expected molecular weight region and one of them was nearly half of the other which was matching the loaded volumes. No other dominant bands were present in NuncCAT's lanes indicating a purely expressed QconCAT.

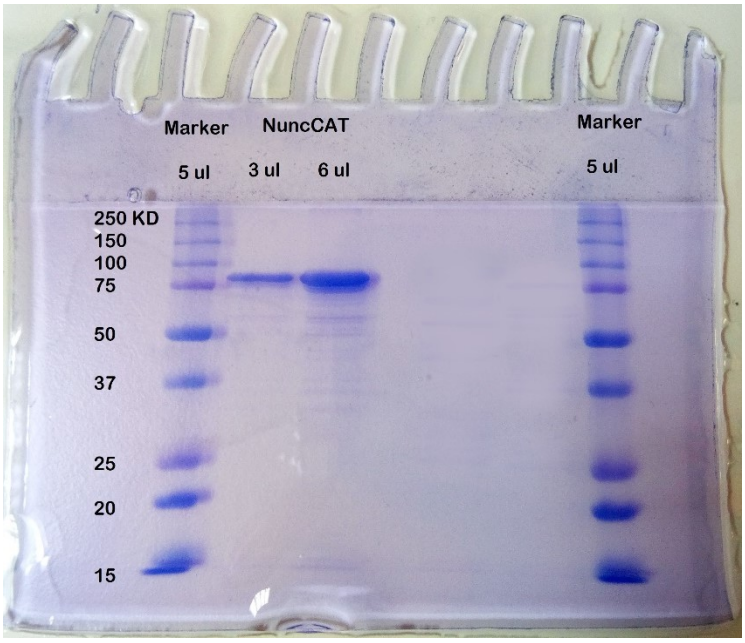

Figure 6.2. SDS-PAGE photo of NuncCAT loaded with two different volumes (3µl and 6µl) along with two different lanes of the molecular weight marker on the right and the left of the QconCAT.

B. Peptides detection and identification

The concentration of NuncCAT protein using Bradford assay was 1.2 µg/µl on average of three readings. A volume equivalent to 10 µg was 12.42 µl and was used for the FASP digestion.

The overall spectrum generated for the digested NuncCAT showed that 48 out of 51 peptides related to the desired targets were identified, in addition to the two NNOPs (AEGVNDNEEGFFSAR, TEGVNDNEEGFFSAR) required for the QconCAT quantification. These peptides have been identified with variable intensities at different retention times (Figure 6.3).

Peptides that have not been detected in the experiment are FSLDALITNILPFEK, GHEVIVLTSSASILVNASK, IASGLGLAWIVGR related to ADH 1C, UGT2B17, and MGST3 enzymes, respectively. 17% of all the detected peptides were miscleaved (198 out of 1142 peptide). Only 15% of these miscleaved peptides are related to the target proteins. Only 35% of the target peptides were miscleaved. The ratio of cleaved to miscleaved peptides ranged from 10 to 770.

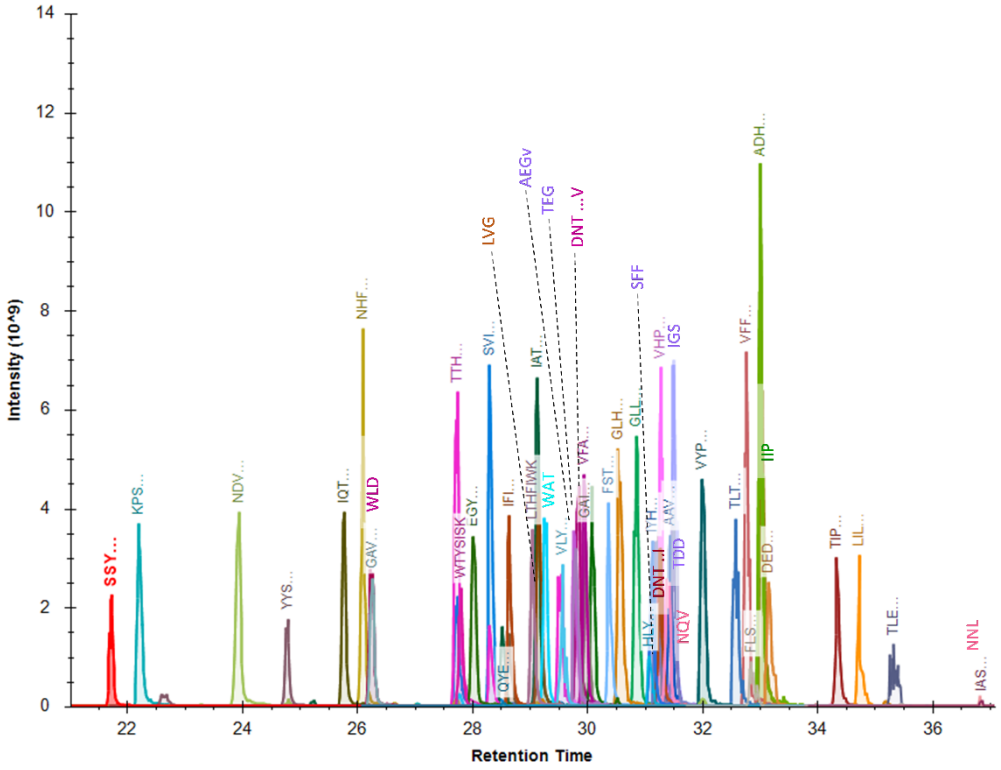

Figure 6.3. The full chromatogram of the NuncCAT peptides showing the retention time at which each peptide was detected. Peptides were annotated with the first three letters and different colours.

C. The percent coverage

The number of amino acids in the whole sequence with the ribosomal core was 836 amino acids and 669 amino acids without the ribosomal core. The number of amino acids that have been detected was 789 and 622 in each case respectively. Therefore, the percent coverage obtained from the analysis was 94% when the ribosomal core was considered, and 93% for sequence without the ribosomal core. The peptides detected are shown in Figure 6.4.

```
1    MGTKTFTAKP  ETVKRDWYVV  DATGKSMALR  LANELSDAAE  NKFGSELLAK
51   VEGDTKPELE  LTLKSDLSAD  INEHLIVELY  SKGVNDNEEG  FFSAKLEPGR
101  LEYDPNRSAG  TYVQIVARDA  QSALTVSETT  FGRDFNEALV  HQVVVAYAAG
151  ARLDNVVYRA  VVESIQRWTY  SISKNHFTVA  LNEKGLHGPL  TLNSPLTPEK
201  GAILGGFKNQ  VLTLEEWQDK  IYHTIAYLTP  LPQPNRNYIV  DAGFGRGLLN
251  DAFQKFSLDA  LITNILPFEK  IFVEESIYDE  FVRSVINDPI  YKTEGVNDNE
301  EGFFSARDNT  DLVEFKIFIN  NEWHDSVSGK  YYSIASSSKE  GYLQIGANTQ
351  AAQKFSTWTN  TEFRADHGDE  LPFVFRVLYA  YGYYTGEPSK  TLEPEELNLI
401  LKLVGPGQWP  GARHLYFWGY  SEAAKWATQV  FKSLLAVGIT  EVIGDFRVHP
451  EPGTWDSFLE  KIIPLLTDPK  FLSLDLQGDP  RGHEVIVLTS  SASILVNASK
501  NDVSNPQGTL  QDGTSRVFAN  PEDCVAFGKK  PIHHFLGIST  FSQYTVVDEN
551  AVAKNNLPTA  ISDWLYVKSF  FGGNYIKIAS  GLGLAWIVGR  VYPHPGTWES
601  FLEKVFFGEG  DGIIRIQTLT  SSVRAAVLWE  VKDNTDLIEF  KTLTEEEVEE
651  VLKLILNEVS  LLGSAPGGKK  PSEELVDRWL  DSDARIATEA  IENFRQYELV
701  VHTDIDAAKL  THFIWKDEDV  IILTYPKTTH  TGQVLGSLVH  VKGAVYGGFK
751  TSLDIEEYSD  TEVQKIGSTP  VLVLSRAEGV  NDNEEGFFSA  RTIPIDGNFF
801  TYTRTDDIGG  LWRSSYVGDE  ASSKLAAALE  HHHHHH
```

Figure 6.4. Segmented fasta sequence of the NuncCAT illustrating parts that have been detected using LC-MS/MS analysis (red). Green parts represent the ribosomal core sequence, while black parts are the undetectable parts in the analysis.

D. The labelling efficiency

Detected peptides have shown high labelling efficiency. The labelling efficiency of K-ending peptides were slightly lower mean ± SD (98.57 ± 0.6%, $n = 29$) than R ending peptides (98.72 ± 0. 5%, $n = 46$) as shown in Figure 6.5.

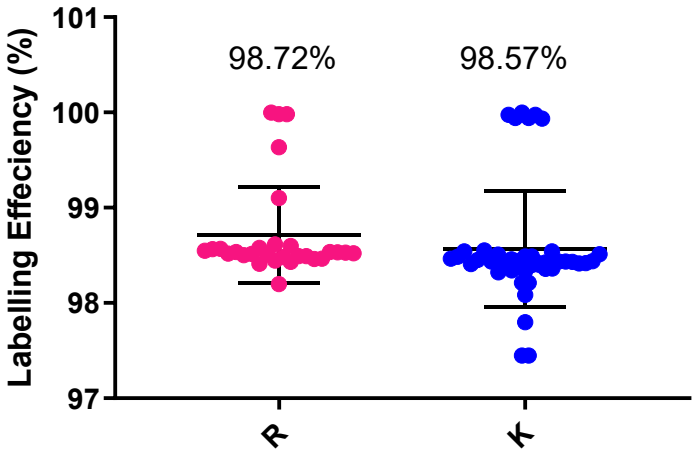

Figure 6.5. Labelling efficiency of both arginine (R) and lysine (K) ending peptides in the NuncCAT. Data are presented as a scatter plot with horizontal lines representing means and standard deviations.

E. NuncCAT quantification

Equation 1 in the Methods section was applied knowing the starting volume of the NuncCAT in the experiment 12.42 µl, the overall molecular weight of 93557, the obtained H/L ratio of 0.707 and the labelling efficiency for an R-ending petide of 0.987. The calculated concentration of the NuncCAT was 0.283 µg/µl which can be used as a standard that is digested at the same time with the biological sample.

6.5. Discussion

Concatenated peptides that are labelled with heavy amino acids are showing increasing usage in targeted proteomics over the last decade (Achour, et al., 2015; Chen & Turko, 2014). They can be spiked at the same time with the biological sample and digested together under the same conditions (El-Khateeb, et al., 2019; Simpson & Beynon, 2012). A QconCAT can be designed for targets in a wide variety of cellular fractions (microsomes, cytosols, S9, or tissue lysate), and for different tissues such as liver, kidney, intestine, or brain (Al-Majdoub, et al., 2019; Al-Majdoub, et al., 2020). Therefore, a prior knowledge of the fraction or the tissue that is rich in the target enzyme under investigation is required for any targeted proteomic experiment.

This methodology allows the absolute quantification and the comparison of target protein levels within a set of samples, as the standard will be digested simultaneously with the sample and released in equimolar stoichiometry under the same conditions (Kito, et al., 2007). However, the choice of surrogate peptides is very critical as different peptides can lead to variable abundance levels (Prasad, et al., 2019). For a new QconCAT, applying the construction criteria explained above increases the probability of generating a successful

standard. However, for targets where the number of unique surrogates is limited, the chance of getting a high quality, best performing peptide is low. This was the case in situations such as VFANPEDCVAFGK (MGST1), KPIHHFLGISTFSQYTVVDENAVAK (ADH1A), and KPSEELVDR (SULT1E1).

The successfully expressed QconCAT should produce detectable, pure, and reliable heavy-labelled peptides upon digestion (Achour, et al., 2015). The QconCAT peptides are designed to incorporate heavy isotope label, in this case $^{13}C_6$-R and $^{13}C_6$-K. The quantification principle here is mainly dependent on the ratio of heavy peptides in the QconCAT to the light peptide within the sample. Therefore, high, consistent, and efficient labelling of all peptides is required to guarantee that the remaining unlabelled fractions from the QconCAT will not greatly interfere with the quantification of the same peptide in the biological sample under investigation (Pratt, et al., 2006). The newly designed NuncCAT showed excellent labelling efficiency for all the resulting peptides. The slightly lower and more variable incorporation of labelled lysine is consistent with the more complex metabolic fate of this amino acid; nevertheless, these levels of incorporation are more than sufficient for the development of quantitative assays using these QconCATs. This was expected and previously reported for other QconCATs (Russell, et al., 2013). When quantification is carried out, quantitative ratios can be corrected for the residual level of unlabelled standard.

The low percentage of miscleavages indicates the efficiency of the sequential digestion protocol using LysC and trypsin. For the miscleaved peptides, the high ratio of cleaved to miscleaved peptides (Over 10 folds) makes the quantification using these peptides still reliable. However, whenever possible, the peptide with complete cleavage is more preferred.

Peptides that have not been detected with the experimental conditions of the current study are long hydrophobic peptides and, therefore, are less readily eluted from the column. They are

considered to be either removed or replaced by other alternatives, when possible, in the second version of the NuncCAT.

In conclusion, the current study offers a novel QconCAT for metabolising enzymes other than CYPs and UGTs (NuncCAT). These enzymes are important for the fate of many drugs within the human body. The NuncCAT showed high performance with regards to the sequence coverage, labelling efficiency, purity, and detectability. Using unique non-naturally occurring peptides in the design of the NuncCAT, it can be quantified at the same time with the digested sample to act as a standard for any protein whose surrogate peptide is included within the QconCAT structure.

6.6. References

Achour, B, Al-Majdoub, ZM, Al Feteisi, H, Elmorsi, Y, Rostami-Hodjegan, A, and Barber, J. (2015). Ten years of QconCATs: Application of multiplexed quantification to small medically relevant proteomes. *Int. J. Mass Spectrom.*, 391, 93–104.

Al-Majdoub, ZM, Al Feteisi, H, Achour, B, Warwood, S, Neuhoff, S, Rostami-Hodjegan, A, and Barber, J. (2019). Proteomic quantification of human blood–brain barrier SLC and ABC transporters in healthy individuals and dementia patients. *Mol. Pharm.*, 16(3), 1220–1233.

Al-Majdoub, ZM, Carroll, KM, Gaskell, SJ, and Barber, J. (2014). Quantification of the Proteins of the Bacterial Ribosome Using QconCAT Technology. *J. Proteome Res.*, 13(3), 1211–1222.

Al-Majdoub, ZM, Achour, B, Couto, N, Howard, M, Elmorsi, Y, Scotcher, D, Alrubia, S, El-Khateeb, E, Vasilogianni, A, Alohali, N, Neuhoff, S, Schmitt, L, Rostami-Hodjegan, A, and Barber, J. (2020). Mass spectrometry-based abundance atlas of ABC transporters in human liver, gut, kidney, brain and skin. *FEBS Lett.*, 594(23), 4134–4150.

Al Feteisi, H, Al-Majdoub, ZM, Achour, B, Couto, N, Rostami-Hodjegan, A, and Barber, J. (2018). Identification and quantification of blood-brain barrier transporters in isolated rat brain microvessels. *J. Neurochem.*, 146(6), 670–685.

Barbosa, ACS, Feng, Y, Yu, C, Huang, M, and Xie, W. (2019). Estrogen sulfotransferase in the metabolism of estrogenic drugs and in the pathogenesis of diseases. *Expert Opin. Drug Metab. Toxicol.*, 15(4), 329–339.

Bhatt, DK, Basit, A, Zhang, H, Gaedigk, A, Lee, S, Claw, KG, Mehrotra, A, Chaudhry, AS, Pearce, RE, Gaedigk, R, Broeckel, U, Thornton, TA, Nickerson, DA, Schuetz, EG, Amory, JK, Leeder, JS, and Prasad, B. (2018). Hepatic Abundance and Activity of Androgen- and Drug-Metabolizing Enzyme UGT2B17 Are Associated with Genotype, Age, and Sex. *Drug Metab. Dispos.*, 46(6), 888–896.

Bhatt, DK, Gaedigk, A, Pearce, RE, Leeder, JS, and Prasad, B. (2017). Age-dependent protein abundance of cytosolic alcohol and aldehyde dehydrogenases in human liver. *Drug Metab. Dispos.*, 45(9), 1044–1048.

Casey Laizure, S, Herring, V, Hu, Z, Witbrodt, K, and Parker, RB. (2013). The Role of Human Carboxylesterases in Drug Metabolism: Have We Overlooked Their Importance? *Pharmacother. J. Hum. Pharmacol. Drug Ther.*, 33(2), 210–222.

Chen, J, and Turko, I V. (2014). Trends in QconCATs for targeted proteomics. *TrAC Trends Anal. Chem.*, 57, 1–5.

Chen, Y, Zane, NR, Thakker, DR, and Wang, MZ. (2016). Quantification of flavin-containing monooxygenases 1, 3, and 5 in human liver microsomes by UPLC-MRM-based targeted quantitative proteomics and its application to the study of ontogeny. *Drug Metab. Dispos.*, 44(7), 975–983.

Couto, N, Al-Majdoub, ZM, Achour, B, Wright, PC, Rostami-Hodjegan, A, and Barber, J. (2019). Quantification of Proteins Involved in Drug Metabolism and Disposition in the Human Liver Using Label-Free Global Proteomics. *Mol. Pharm.*, 16(2), 632–647.

Dubaisi, S, Caruso, JA, Gaedigk, R, Vyhlidal, CA, Smith, PC, Hines, RN, Kocarek, TA, and Runge-Morris, M. (2019). Developmental Expression of the Cytosolic Sulfotransferases in Human Liver. *Drug Metab. Dispos.*, 47(6), 592–600.

Duester, G, Farrés, J, Felder, MR, Holmes, RS, Höög, J-O, Parés, X, Plapp, B V., Yin, S-J, and Jörnvall, H. (1999). Recommended nomenclature for the vertebrate alcohol dehydrogenase gene family. *Biochem. Pharmacol.*, 58(3), 389–395.

El-Khateeb, E, Vasilogianni, A-M, Alrubia, S, Al-Majdoub, ZM, Couto, N, Howard, M, Barber, J, Rostami-Hodjegan, A, and Achour, B. (2019). Quantitative mass spectrometry-based proteomics in the era of model-informed drug development: Applications in translational pharmacology and recommendations for best practice. *Pharmacol. Ther.*, 203, 107397.

Fayz, S, and Inaba, T. (1998). Zidovudine Azido-Reductase in Human Liver Microsomes: Activation by Ethacrynic Acid, Dipyridamole, and Indomethacin and Inhibition by Human Immunodeficiency Virus Protease Inhibitors. *Antimicrob. Agents Chemother.*, 42(7), 1654–1658.

Gamage, N, Barnett, A, Hempel, N, Duggleby, RG, Windmill, KF, Martin, JL, and McManus, ME. (2006). Human Sulfotransferases and Their Role in Chemical Metabolism. *Toxicol. Sci.*, 90(1), 5–22.

Garattini, E, and Terao, M. (2012). The role of aldehyde oxidase in drug metabolism. *Expert Opin. Drug Metab. Toxicol.*, 8(4), 487–503.

Gautheron, J, and Jéru, I. (2020). The Multifaceted Role of Epoxide Hydrolases in Human Health and Disease. *Int. J. Mol. Sci.*, 22(1), 13.

Hayes, JD, and Pulford, DJ. (1995). The Glut athione S-Transferase Supergene Family: Regulation of GST and the Contribution of the lsoenzymes to Cancer Chemoprotection and Drug Resistance Part I. *Crit. Rev. Biochem. Mol. Biol.*, 30(6), 445–520.

Johansson, K, Ahlen, K, Rinaldi, R, Sahlander, K, Siritantikorn, A, and Morgenstern, R. (2006). Microsomal glutathione transferase 1 in anticancer drug resistance. *Carcinogenesis*, 28(2), 465–470.

Kandel, SE, and Lampe, JN. (2014). Role of Protein–Protein Interactions in Cytochrome P450-Mediated Drug Metabolism and Toxicity. *Chem. Res. Toxicol.*, 27(9), 1474–1486.

Kito, K, Ota, K, Fujita, T, and Ito, T. (2007). A synthetic protein approach toward accurate mass spectrometric quantification of component stoichiometry of multiprotein complexes. *J. Proteome Res.*, 6(2), 792–800.

Krueger, SK, and Williams, DE. (2005). Mammalian flavin-containing monooxygenases: structure/function, genetic polymorphisms and role in drug metabolism. *Pharmacol. Ther.*, 106(3), 357–387.

Kücükgöze, G, and Leimkühler, S. (2018). Direct comparison of the four aldehyde oxidase enzymes present in mouse gives insight into their substrate specificities. *PLoS One*, 13(1), e0191819.

Laizure, SC, Parker, RB, Herring, VL, and Hu, Z-Y. (2014). Identification of Carboxylesterase-Dependent Dabigatran Etexilate Hydrolysis. *Drug Metab. Dispos.*, 42(2), 201–206.

Lennard, L. (1998). Clinical Implications of Thiopurine Methyltransferase-Optimization of Drug Dosage and Potential Drug Interactions. *Ther. Drug Monit.*, 20(5), 527–531.

Meisel, P. (2002). Arylamine N-acetyltransferases and drug response. *Pharmacogenomics*, 3(3), 349–366.

Merali, Z, Ross, S, and Paré, G. (2014). The pharmacogenetics of carboxylesterases: CES1 and CES2 genetic variants and their clinical effect. *Drug Metabol. Drug Interact.*, 29(3), 143–151.

Morgenstern, R, Zhang, J, and Johansson, K. (2011). Microsomal glutathione transferase 1: mechanism and functional roles. *Drug Metab. Rev.*, 43(2), 300–306.

Phillips, IR, and Shephard, EA. (2017). Drug metabolism by flavin-containing monooxygenases of human and mouse. *Expert Opin. Drug Metab. Toxicol.*, 13(2), 167–181.

Prasad, B, Achour, B, Artursson, P, Hop, CECA, Lai, Y, Smith, PC, Barber, J, Wisniewski, JR, Spellman, D, Uchida, Y, Zientek, MA, Unadkat, JD, and Rostami-Hodjegan, A. (2019). Toward a Consensus on Applying Quantitative Liquid Chromatography-Tandem Mass Spectrometry Proteomics in Translational Pharmacology Research: A White Paper. *Clin. Pharmacol. Ther.*, 106(3), 525–543.

Prasad, B, Bhatt, DK, Johnson, K, Chapa, R, Chu, X, Salphati, L, Xiao, G, Lee, C, Hop, CECA, Mathias, A, Lai, Y, Liao, M, Humphreys, WG, Kumer, SC, and Unadkat, JD. (2018). Abundance of Phase 1 and 2 Drug-Metabolizing Enzymes in Alcoholic and Hepatitis C Cirrhotic Livers: A Quantitative Targeted Proteomics Study. *Drug Metab. Dispos.*, 46(7), 943–952.

Pratt, JM, Simpson, DM, Doherty, MK, Rivers, J, Gaskell, SJ, and Beynon, RJ. (2006). Multiplexed absolute quantification for proteomics using concatenated signature peptides encoded by QconCAT genes. *Nat. Protoc.*, 1(2), 1029–1043.

Russell, MR, Achour, B, McKenzie, EA, Lopez, R, Harwood, MD, Rostami-Hodjegan, A, and Barber, J. (2013). Alternative fusion protein strategies to express recalcitrant QconCAT proteins for quantitative proteomics of human drug metabolizing enzymes and transporters. *J. Proteome Res.*, 12(12), 5934–5942.

Sato, Y, Nagata, M, Tetsuka, K, Tamura, K, Miyashita, A, Kawamura, A, and Usui, T. (2014). Optimized methods for targeted peptide-based quantification of human uridine 59-diphosphate-glucuronosyltransferases in biological specimens using liquid chromatography-tandem mass spectrometry. *Drug Metab. Dispos.*, 42(5), 885–889.

Simpson, DM, and Beynon, RJ. (2012). QconCATs: design and expression of concatenated protein standards for multiplexed protein quantification. *Anal. Bioanal. Chem.*, 404(4), 977–989.

Song, W, Yu, L, and Peng, Z. (2015). Targeted label-free approach for quantification of epoxide hydrolase and glutathione transferases in microsomes. *Anal. Biochem.*, 478, 8–13.

The UniProt Consortium. (2019). UniProt: a worldwide hub of protein knowledge. *Nucleic Acids Res.*, 47(D1), D506–D515.

Tomita, H, Tanaka, K, Tanaka, T, and Hara, A. (2016). Aldehyde dehydrogenase 1A1 in stem cells and cancer. *Oncotarget*, 7(10), 11018–11032.

Václavíková, R, Hughes, DJ, and Souček, P. (2015). Microsomal epoxide hydrolase 1 (EPHX1): Gene, structure, function, and role in human disease. *Gene*, 571(1), 1–8.

Wiśniewski, JR, Zougman, A, Nagaraj, N, and Mann, M. (2009). Universal sample preparation method for proteome analysis. *Nat. Methods*, 6(5), 359–362.

Yamamoto, A, Liu, M-Y, Kurogi, K, Sakakibara, Y, Saeki, Y, Suiko, M, and Liu, M-C. (2015). Sulphation of acetaminophen by the human cytosolic sulfotransferases: a systematic analysis. *J. Biochem.*, 158(6), 497–504.

7 Chapter Seven

Proteomic Quantification of Changes in Abundance of Drug-Metabolizing Enzymes and Drug Transporters in Human Liver Cirrhosis: Different Methods, Similar Outcomes

Declaration

This chapter constitutes an article submitted for publication to the Drug Metabolism and Disposition Journal

El-Khateeb, E., Al-Majdoub, ZM., Rostami-Hodjegan, A., Barber, J., & Achour, B. (n.d.). Proteomic Quantification of Changes in Abundance of Drug-Metabolizing Enzymes and Drug Transporters in Human Liver Cirrhosis: Different Methods, Similar Outcomes. *Drug Metab. Dispos.*, Under review.

I carried out the literature search, the experiment, generation and analysis of data and wrote the manuscript. Dr Brahim Achour was consulted on the study design, data analysis and edited the manuscript. Dr Zubida Al-Majdoub, Prof Amin Rostami-Hodjegan and Dr Jill Barber were consulted on the study design, and edited the manuscript. I am retaining editorial control.

7.1. Abstract

Model-based assessment of the effects of liver disease on drug pharmacokinetics requires quantification of changes in enzymes and transporters responsible for drug metabolism and disposition. Different proteomic methods are currently used for protein quantification in tissues and *in vitro* systems, each with specific procedures and requirements. The outcome of quantitative proteomic assays from four different methods (one targeted and three label-free), applied to the same sample set, were compared in this study. Three pooled cirrhotic liver microsomal samples, corresponding to cirrhosis with non-alcoholic fatty liver disease, biliary disease or cancer, and a control microsomal pool, were analysed using QconCAT-based targeted proteomics, the total protein approach (TPA), high three (Hi3) ion intensity approach, and intensity-based absolute quantification (iBAQ), to determine the absolute and relative abundance in disease compared with control. The relative abundance data provided a 'disease perturbation factor' (DPF) for each target protein. Absolute and relative abundances generated by standard-based label-free methods (iBAQ and Hi3) showed good agreement with targeted proteomics (limited bias and scatter) but TPA (standard-free method) over-estimated absolute abundances by approximately 2 fold. DPF was consistent between different proteomic methods but varied between enzymes and transporters, indicating discordance of effects of cirrhosis on various ADME proteins. DPF ranged from no change (e.g. for UGT1A6 in NAFLD group) to less than 0.3 (e.g. CES1 in cirrhosis of biliary origin).

7.2. Introduction

The use of liquid chromatography-mass spectrometry (LC-MS) based proteomics for the characterisation of biological samples has become more widespread in recent years. The main advantage of this analytical tool is that it allows sensitive, selective and simultaneous quantification of a large number of proteins in a single assay. Proteomic quantification can be performed either by quantifying all detectable proteins in a global proteomic experiment or by targeting a predefined set of proteins using specific standards (Prasad, et al., 2019). In targeted proteomics, heavy (isotopically-labelled) versions of proteotypic peptides are used to quantify the target proteins. Global proteomics relies on label-free quantification, which is somewhat cheaper, can offer high proteome coverage, and can be employed for absolute quantification through the addition of unlabelled protein standards (Al Feteisi, et al., 2015; El-Khateeb, et al., 2019; Li, et al., 2012; Megger, et al., 2014). In global proteomics, many different data analysis methods have been proposed such as the total protein approach (TPA), high n (Hi-N) ion intensity method, and intensity-based absolute quantification (iBAQ) (Couto, et al., 2019; Fabre, et al., 2014; Wiśniewski, et al., 2019).

Cirrhosis is a liver disease caused by various conditions, including alcoholic and non-alcoholic fatty liver disease, biliary disease, including primary sclerosing cholangitis (PSC) and primary biliary cholangitis (PBC), autoimmune hepatitis, and hepatitis C virus (HCV) infection. Cirrhosis can also progress to primary liver cancer (Schuppan & Afdhal, 2008). Liver disease affects the pharmacokinetics of different drugs, especially compounds that are mainly hepatically extracted, but can also affect renally excreted drugs (Verbeeck, 2008). These effects are normally due to changes in protein binding, hepatic blood flow, and altered expression of different drug-metabolising enzymes (DMEs) and transporters (Edginton & Willmann, 2008; Johnson, et al., 2010). There is, however, no unique and universal measure that can summarise the impact of the cirrhosis on all enzymes and transporters (El-Khateeb, et al. Unpublished)

and not all drugs are affected in the same manner. Therefore, recent FDA guidance encourages performing clinical trials with patients with hepatic impairment for drugs with a narrow therapeutic index if these are mainly eliminated by the liver, and for any other drug if 20% or more of clearance is attributable to the hepatic route (FDA, 2003). Indeed, there has been more demand than before for the inclusion of hepatically-impaired patients in early stage clinical trials in order to be more representative of patients who will receive the drug after approval (FDA, 2020; Lichtman, et al., 2017). The practical determination of a safe and effective dose for those patients is, however, challenging to implement in such clinical trials. Alternative approaches, such as the use of virtual clinical trials based on physiologically based pharmacokinetic (PBPK) modelling and simulation (M&S), to predict the clearance and implement dose adjustment in this population have been suggested and applied for regulatory submission of some drugs (Jamei, 2016). In these models, change in drug clearance in patients is accounted for by administration of selective probes, where available, *in vivo* and subsequent measurement of specific enzyme activity or by using *in vitro* systems and scaling by activity or abundance of relevant enzymes/transporters (Frye, et al., 2006; Johnson, et al., 2010).

Variability in measurements of enzymes and transporters have previously been reported and these can stem from differences in quality and handling conditions of the samples, sample preparation, proteomic methods, data analysis strategies or a combination of these factors (Achour, et al., 2017b; Harwood, et al., 2016; Wegler, et al., 2017). These covariates are especially important when the effect of disease is the focus of the proteomic investigation and increasing the trust in outcome of the predictive PBPK models which rely on the proteomics data as a major input. The aim of this study was therefore to assess the performance of different proteomic methods (targeted and untargeted) in relation to characterisation of the effect of hepatic cirrhosis on the abundance of enzymes and transporters. A strategy to address method-

specific bias is proposed to achieve improved implementation of the generated data in downstream M&S.

7.3. Methods

7.3.1. Human liver samples

Pooled human liver microsomal (HLM) samples represented four sets of samples: histologically normal control group (*n* = 14 individual livers), non-alcoholic fatty liver disease (NAFLD) associated cirrhosis (*n* = 9), biliary disease associated cirrhosis (*n* = 13), and cancer associated cirrhosis (*n* = 9). Individual liver tissue samples were provided by Cambridge University Hospitals Tissue Bank (Cambridge, UK) and HLM fractions were prepared by differential centrifugation, as reported previously (El-Khateeb, et al., 2020). The HLM fractions were pooled for each group separately by mixing 6 µl from each individual sample (corresponding to 6 mg from each liver tissue sample). Anonymised demographic and clinical data for donors are presented in Supplementary Table 7.1 and Supplementary Table 7.2. These samples are covered by ethical approval from the Health Research Authority and Health and Care Research Wales (Research Ethics Committee Approval Reference 18/LO/1969). The samples were prepared and analysed for previous work (El-Khateeb et al., 2020) and the opportunity arose to further use these sets for a comparative investigation of different quantification methods in health and disease.

7.3.2. Sample preparation for proteomics

Protein content in the HLM pooled samples was estimated by the Bradford assay (ThermoFisher Scientific, Hemel Hempstead, UK). Three stable isotope (^{13}C) labelled concatenated standards (QconCATs) (Russell, et al., 2013) were spiked into 70 µg of each pooled sample as internal standards; 0.56 µg of MetCAT (QconCAT standard for the quantification of CYPs and UGTs), 0.45 µg of NuncCAT (QconCAT for the quantification of

non-CYP, non-UGT enzymes), and 0.24 µg of TransCAT (QconCAT for the quantification of transporters), in addition to 0.126 µg of bovine serum albumin (BSA) (as a label-free exogenous protein standard).

Filter-aided sample preparation (FASP) (Wiśniewski, et al., 2009) was used for sample preparation as previously described with minor modifications (Al Feteisi, et al., 2018; Couto, et al., 2019). Sample mixtures were solubilised by incubation with sodium deoxycholate (10% w/v final volume), 1,4-dithiothreitol (DTT) was added at a final concentration of 100 mM, and the protein mixture was incubated at room temperature for 10 min. Reduction of protein disulfide bonds was carried out by incubation at 56°C for 40 min. Amicon Ultra 0.5 mL centrifugal filters, 3 kDa molecular weight cutoff, (Millipore, Nottingham, UK) were conditioned by briefly centrifuging 400 µl of 0.1 M Tris of pH 8.5 at 14000*g* at room temperature. The protein samples were then transferred to the conditioned filter units, followed by centrifugation at 14000*g* at room temperature for 30 min. Alkylation of reduced cysteine was performed by incubation with 100 µl of 50 mM iodoacetamide in the dark for 30 min at room temperature. After alkylation, deoxycholate removal was performed by buffer exchange using two successive washes with 8 M urea in 100 mM Tris-HCl (pH 8.5), 200 µl each. To reduce urea concentration, additional washes (3 x 200 µl were performed using 1 M urea in 50 mM ammonium bicarbonate (pH 8.5). For each wash, solvent (200 µl) was added to the filter, without mixing, centrifuged at 14000*g* at room temperature for 20 min, leaving a volume of approximately 20 µl in the filter. The filtrate containing small molecules such as detergent was discarded. Protein digestion was achieved using LysC twice (LysC: protein ratio 1:50, 2 hours each, at 30°C), then trypsin digestion was carried out (trypsin: protein ratio 1:25) for 12 hours at 37°C and another equivalent treatment for an extra 6 hour incubation. Peptides were recovered from the filter by centrifugation (14000*g*, 20 min); a second collection was achieved by adding 0.5 M sodium chloride (100 µl) to the filter and centrifuged at 14000*g* for another

20 min. The collected peptides were lyophilised to dryness using a vacuum concentrator at 30ºC and with vacuum in aqueous mode; the time required was in the range 1-3 hours and was sample-dependent. Lyophilised peptides were reconstituted in 20% (v/v) acetonitrile in water, acidified with 2% (v/v) trifluoroacetic acid, then desalted using C18 spin columns according to the manufacturer's instructions (Nest group, USA). The peptides were lyophilised and stored at −80°C until mass spectrometric analysis.

7.3.3. Liquid chromatography and tandem mass spectrometry (LC-MS/MS)

Lyophilised peptides were re-suspended in 70 µl 3% (v/v) acetonitrile in water with 0.1% (v/v) formic acid. The samples were analysed by LC-MS/MS using an UltiMate® 3000 Rapid Separation LC (RSLC, Dionex Corporation, Sunnyvale, CA) coupled to a Q Exactive HF Hybrid Quadrupole-Orbitrap mass spectrometer (Thermo Fisher Scientific, Waltham, MA) mass spectrometer. Mobile phase A was 0.1% formic acid in water and mobile phase B was 0.1% formic acid in acetonitrile, and peptides were eluted on CSH C18 analytical column (75 mm x 250 µm inner diameter, 1.7 µm particle size) (Waters, UK). A 1 µl aliquot of the sample was transferred to a 5 µl loop and loaded onto the column at a flow rate of 300 nl/min for 5 min at 5% B. The loop was then taken out of line and the flow was reduced from 300 nl/min to 200 nl/min in 0.5 min. Peptides were separated using a gradient from 5% to 18% B in 63.5 min, then from 18% to 27% B in 8 min, and finally from 27% B to 60% B in 1 min. The column was washed at 60% B for 3 min before re-equilibration to 5% B in 1 min. At 85 min, the flow was increased to 300 nl/min until the end of the run at 90 min. Mass spectrometry data were acquired in a data-dependent manner for 90 min in positive mode. Peptides were selected for fragmentation automatically by data dependent analysis on a basis of the top 12 peptides with *m/z* between 300 to 1750 Th and a charge state of 2+, 3+, and 4+ with dynamic exclusion set at 15 sec. The MS resolution was set at 120,000 with an AGC target of 3E6 and a maximum

fill time set at 20 ms. The MS2 resolution was set to 30,000, with an AGC target of 2E5, a maximum fill time of 45 ms, isolation window of 1.3 Th and a collision energy of 28 eV.

7.3.4. Proteomic data analysis

Proteins were identified by searching peptide MS/MS data against UniProtKB database (http://www.uniprot.org/) using MaxQuant version 1.6.10.43 (Max Planck Institute of Biochemistry, Martinsried, Germany). Processing parameters for both targeted and label-free analysis are summarised in Supplementary Table 7.3. QconCAT-based quantification was carried out as previously described (Achour, et al., 2014; Al-Majdoub, et al., 2019, 2020a) to measure the abundance of 15 CYP and 9 UGT enzymes (MetCAT), in addition to UGT2B17, 22 non-CYP/non-UGT drug-metabolising enzymes (NuncCAT) and 30 transporters (TransCAT). A protein was considered quantifiable in liver microsomal samples if (a) there was evidence of its expression in the liver (Human Protein Atlas, https://www.proteinatlas.org/), (b) it was localised in a membrane (Uniprot, https://www.uniprot.org/), (c) it was identified by at least one razor or one unique peptide, and (c) it was detected in a sufficient number of samples (at least 3/14 samples) and by at least two data analysis methods with priority assigned to the targeted approach. A list of the peptides that constitute these QconCATs is presented in Supplementary Table 7.4. Details of data analysis and quantification approaches are provided below.

- **Method 1. Targeted proteomics**

In targeted analysis, the abundance of each target protein was calculated using the following equation (Achour, et al., 2014; Harwood, et al., 2015).

$$[Protein] = [QconCAT] \times I_{i,L}/I_{i,H} \quad (1)$$

Where $[Protein]$ is the protein abundance based on the surrogate peptide *i*, measured in units of pmol/mg microsomal protein. $I_{i,L}/I_{i,H}$ is the ratio of the intensity of the light (analyte) to the

heavy (QconCAT-derived) surrogate peptide, and [*QconCAT*] is the concentration of the QconCAT standard measured using Equation 2.

$$[QconCAT] = [\mathrm{NNOP}] \times \mathrm{I}_{\mathrm{NNOP,H}}/\mathrm{I}_{\mathrm{NNOP,L}} \quad (2)$$

Where $\mathrm{I}_{\mathrm{NNOP,H}}/\mathrm{I}_{\mathrm{NNOP,L}}$ is the ratio of the intensity of the heavy (QconCAT-derived) to the light (spiked in) non-naturally occurring peptide (NNOP) standard, and [NNOP] is the concentration of the NNOP standard expressed in units of pmol/mg microsomal protein analysed by mass spectrometry. The intensity ratios were corrected for isotope labelling efficiency prior to use in the equations (Achour, et al., 2018; Russell, et al., 2013). Unlabelled NNOP peptides, EGVNDNEEGFFSAR, GVNDNEEGFFSAR and AEGVNDNEEGFFSAR were added to the pooled samples at 38, 125 and 350 fmol, respectively, to quantify the TransCAT, MetCAT and NuncCAT, respectively.

- **Method 2: HiN or Hi3 method**

In label-free analysis with the HiN method, quantification was performed using the averaged intensity of the three most abundant unique peptides based on the acquired MS/MS data for the protein of interest and the standard protein (Achour, et al., 2017a; Al-Majdoub, et al., 2019). The selection of peptides was according to previously published criteria (Achour, et al., 2018). The following equation was applied.

$$[Protein] = [Standard] \times \left(\sum_{i=1}^{n} \mathrm{I}_{rank\,(i)}/n\right) \Big/ \left(\sum_{j=1}^{m} \mathrm{I}_{rank\,(j)}/m\right) \quad (3)$$

Where [*Protein*] represents the abundance of a target protein, [*standard*] represents the abundance of the standard protein, both expressed in units of pmol/mg microsomal protein, and the fraction refers to the ratio of the averaged intensities of the n highest ion peaks for the target protein relative to the reference (in this case, $n = m = 3$). Peptides used in quantification of the selected proteins were identified as unique using a BLAST search (NCBI,

https://www.ncbi.nlm.nih.gov/). For the pooled samples, BSA at known concentration (26 pmol/mg fraction protein) was used as a standard.

- **Method 3: The total protein approach (TPA)**

In the total protein approach (TPA), peptides were assigned to the proteins of interest and the total signal intensity from a particular protein was used for quantification as follows. Peptides were assigned to proteins from the Uniprot human proteome, with full length characterised sequences being prioritised over truncated, uncharacterised and cDNA sequences. The remaining peptides that did not match any protein were deleted. A best-fit analysis was then run to minimise the number of protein assigned to account for all the peptides (Al-Majdoub, et al., 2020b).

$$[Protein] = \sum_{i=1}^{n} \mathrm{I}_i \Big/ (M \times \sum I_{sample}) \qquad (4)$$

Where the ratio of the sum of intensity of all peptides derived from a protein of interest to the sum of intensity of all peptides in a particular sample (expressed in parts per billion) is converted to an abundance value (pmol/mg) by normalising to the molecular mass of the protein, *M*, in Daltons.

- **Method 4: Intensity-based absolute quantification (iBAQ)**

Intensity-based absolute quantification, iBAQ, relies on normalising protein MS intensity to the total number of observable peptides. The protein concentration is then inferred by comparing the obtained normalised intensity to a similar ratio for an internal protein standard at known concentration, as follows.

$$[Protein] = [Standard] \times \left(\sum_{i=1}^{n} \mathrm{I}_i / T_i\right) \Big/ \left(\sum_{j=1}^{m} \mathrm{I}_j / T_j\right) \qquad (5)$$

Where I is the summed intensity of all peptides from the protein of interest *i* or the standard *j*, and T is the number of theoretically observable peptides from *in silico* digestion of protein *i* or standard *j*. Similar to the Hi3 method, BSA at known concentration was used as a standard.

Absolute abundances in pmol/mg microsomal protein were determined using the four methods discussed above for the set of targets that fit our predefined criteria.

7.3.5. Disease-to-control abundance ratios

For each method, the abundance of target proteins obtained from each cirrhotic pool was normalised to the corresponding value from the control pooled sample. This ratio represents alteration in protein expression due to disease and will henceforth be referred to as disease perturbation factor (DPF). In the context of comparative performance, the absolute abundances and the ratios determined using different quantification methods were compared, and the proportion of values within a 2-fold difference across methods were determined. Targets showing ratios for the cirrhotic pools (relative to control) outside the range of 0.5-2 fold were considered to be affected by the disease.

7.3.6. Statistical analysis

Data analysis was performed using Microsoft Excel 2010 and GraphPad Prism 8.4.3 (La Jolla, CA). Linear regression analysis was performed to assess correlations of data from different quantification methods, both at the level of absolute quantification and the disease-to-control ratios. The deviation from the line of unity (represented by the slope of the line of regression) and goodness of fit (R^2) were used to assess the quality of the correlation. Good correlation was considered for comparisons with correlation coefficients above 0.5. The percentage of data points outside a 2-fold range was used as an overall measure of agreement. Bias specific to each method was assessed using the average fold error (AFE) and scatter of one dataset relative to another was assessed using the absolute average fold error (AAFE) as follows:

$$\mathrm{AFE} = 10^{\left[\frac{\sum_1^n \mathrm{Log}\left(x_{2,i}/x_{1,i}\right)}{n}\right]} \quad (6)$$

$$\mathrm{AAFE} = 10^{\left[\frac{\sum_1^n |\mathrm{Log}\left(x_{2,i}/x_{1,i}\right)|}{n}\right]} \quad (7)$$

Where $x_{1,i}$ and $x_{2,i}$ are data derived for the same target *i* using two different methods. Values different from 1 reflect higher bias and scatter.

7.4. Results

7.4.1. Global proteomics of pooled liver membrane fractions

Pools from normal, NAFLD-cirrhosis, biliary-cirrhosis, and cancer-cirrhosis liver sets were analysed using global and targeted proteomics. The average protein content from three different measurements for each pool (mean ± SD) was 7.11 ± 0.09, 7.03 ± 0.01, 13.78 ± 0.01, 12.19 ± 0.02 μg total protein per mg liver tissue, respectively. Global proteomics identified 18073, 20010, 19482, and 18866 peptides from samples representing the control, NAFLD, biliary disease, and cancer related cirrhotic livers. This translated to 2307, 2587, 2577, and 2530 fraction proteins, respectively.

7.4.2. Effect of surrogate peptide selection on targeted quantification

Two unique peptides representing each protein of interest are routinely included in a QconCAT standard. In this study, absolute abundance values and disease-to-control ratios were calculated using QconCAT peptides detected by LC-MS/MS in the majority of the pooled samples (the control sample and at least one diseased pool). Where quantification from both peptides for each target was possible, the values were compared (Table 7.1). Absolute levels were, in several cases (CYP2A6, 2E1, 3A4, 4F2 and UGT1A1), different from one peptide to another for the same target protein (assay-related bias reaching up to 10 fold difference). It is possible to reconcile these differences by selecting the most appropriate peptide or so-called "best performer" peptide using criteria related to the peptide's amino acid composition (stability and

physicochemical properties), mapping of the sequence (cleavability and proximity to the membrane) and visual MS and MS/MS spectral examination, as we have discussed previously (Achour, et al., 2018). The "best performing" peptides, showing reliable intensity values, for each of these proteins in most of the samples are shown in Table 7.1. Excitingly, however, the impact of disease (represented by disease-to-control ratio) was consistent for these pairs of peptides, even where the absolute quantification was not (Table 7.1).

7.4.3. Quantification of key hepatic enzymes and transporters using global proteomics

For global proteomics, quantification of the targets focused on key proteins involved in pharmacokinetics of xenobiotics and therapeutic drugs. The criteria for selecting the targets followed technical and biological considerations to ascertain that the quantification was reliable. We focused on targets quantifiable by the QconCAT standards to enable head-to-head comparison. A total of 35 drug-metabolising enzymes and drug transporters satisfied the criteria (12 CYPs, 7 UGTs, 7 non-CYP non-UGT enzymes and 9 transporters). The data are presented in Table 7.2.

Table 7.1. The absolute and relative abundances of different proteins using targeted proteomic assays based on two surrogate peptides for each protein.

Target protein	Peptides used for targeted	Absolute abundance (pmol/mg protein)				Disease to control ratio		
		Control	NAFLD	Biliary	Cancer	NAFLD	Biliary	Cancer
CYP1A2	ASGNLIPQEK[$]	19	7.1	5.8	9.0	0.37	0.31	0.48
	YLPNPALQR	18.17	7.1	5.3	7.8	0.39	0.29	0.43
CYP2A6	GTGGANIDPTFFLSR[$]	20.1	20.2	8.2	11.7	1.1	0.41	0.58
	DPSFFSNPQDFNPQHFLNEK	1.6	2	0.7	1.1	1.3	0.45	0.71
CYP2D6	AFLTQLDELLTEHR	68.3	38.1	35.4	44.2	0.56	0.52	0.65
	DIEVQGFR[$]	8.7	5.6	4.2	5.1	0.65	0.48	0.59
CYP2E1	GIIFNNGPTWK	13.9	22	7.2	11.5	1.5	0.51	0.82
	FITLVPSNLPHEATR[$]	37.4	49.4	12.2	30.1	1.3	0.33	0.80
CYP3A4	LSLGGLLQPEK[$]	64	33.4	20.9	20.6	0.52	0.33	0.32
	EVTNFLR	24.9	15.5	9.7	8.4	0.62	0.39	0.34
CYP4F2	HVTQDIVLPDGR[$]	9.6	9.5	4.8	5.1	1.02	0.51	0.54
	FDPENIK	3.1	ND	1.7	ND	ND	0.55	ND
UGT1A1	DGAFYTLK[$]	15.5	22.5	14.5	19.8	1.5	0.93	1.28
	TYPVPFQR	6.5	11.7	6.7	7.5	1.7	1.04	1.2
UGT1A6	VSVWLLR	4.7	5.3	3.5	3.8	1.01	0.74	0.79
	SFLTAPQTEYR[$]	5.9	6.1	3.9	3.8	1.03	0.66	0.65
CES2	ADHGDELPFVFR[$]	23.4	18.2	8.7	8.1	0.78	0.37	0.35
	SFFGGNYIK	17.6	14.5	ND	6.6	0.82	ND	0.37
POR	QYELVVHTDIDAAK[$]	19.8	34.5	ND	7.5	1.7	ND	0.38
	IQTLTSSVR	21.1	31.9	16.4	ND	1.5	0.77	ND
MGST3	IASGLGLAWIVGR[$]	8.1	9.5	5.9	2.1	1.2	0.73	0.26
	VLYAYGYYTGEPSK	6.9	7.7	5.4	2.3	1.1	0.79	0.33
BCRP	SSLLDVLAAR[$]	0.15	0.20	0.16	ND	1.3	1.04	ND
	ENLQFSAALR	0.12	ND	0.13	ND	ND	1.1	ND

Control, NAFLD, Biliary, Cancer denote microsomal samples from histologically normal or cirrhotic liver tissue from patients with non-alcoholic fatty liver disease, cholestasis, and hepatocellular carcinoma at the time of sample collection. ND, The peptide was not detected in the sample. [$] Peptide used for the quantification.

Table 7.2. Quantification of drug-metabolising enzymes and drug transporters in pooled human liver samples from normal and cirrhotic livers with different co-existing conditions using four quantification approaches; QconCAT-based targeted proteomics, Hi3 label-free quantification, the total protein approach (TPA), and intensity-based absolute quantification (iBAQ).

Protein	Method 1 Targeted quantification (pmol/mg protein)				Method 2 Hi3 label-free quantification (pmol/mg protein)				Method 3 TPA (pmol/mg protein)				Method 4 iBAQ (pmol/mg protein)			
	Control	NAFLD	Biliary	Cancer	Control	NAFLD	Biliary	Cancer	Control	NAFLD	Biliary	Cancer	Control	NAFLD	Biliary	Cancer
CYP1A2	19	7.1	5.8	9	25.1	8.8	8.5	11.8	31.5	11.7	16.4	27.9	35.7	10.4	10.1	15.3
CYP2A6	20.1	20.2	8.2	11.7	38.9	31.1	16.6	26.6	43.8	38	28.6	45.3	41.5	28.3	14.7	20.8
CYP2B6	2.8	3.4	1.1	2.4	6.5	6.4	2.2	4.3	3.1	3.1	2.2	4.9	3.3	2.7	1.3	2.6
CYP2C8	25.8	17	7.7	12.6	39.5	22.8	10.6	22	53.7	32.4	26.5	47.8	53.9	25.5	14.4	23.2
CYP2C9	92.5	100.2	42.6	58.3	73	58.1	36.1	51.6	68	59.2	56.7	83.6	82.8	56.6	37.4	49.2
CYP2C18	1.3	0.7	0.7	0.7	1.4	0.6	ND	ND	10.5	7	6.1	10	10.5	5.5	3.3	4.8
CYP2D6	8.7	5.6	4.2	5.1	6.7	3.2	3.8	3.5	13.8	8.1	13.3	22.5	15.5	7.1	8.1	12.2
CYP2E1	37.4	49.4	12.2	30.1	25.4	20.9	6.6	24	28.9	38.5	12	35.3	31.8	33.3	7.2	18.7
CYP3A4	64.0	33.4	20.9	20.6	24.8	13.7	8.7	10	36.7	20.7	20.6	23.8	40.8	18	12.4	12.8
CYP3A5	4.4	ND	2.4	7.3	1.2	ND	0.6	ND	12.3	8.2	9.1	14	14.1	7.4	5.7	7.8
CYP2J2	1.26	0.77	0.6	0.55	0.4	0.2	0.2	0.2	0.29	0.13	0.15	0.21	0.26	0.09	0.07	0.09
CYP4F2	9.6	9.5	4.8	5.1	3.3	2.7	1	2.4	14.4	11	9.7	16.4	15	9	5.5	8.2
UGT1A1	15.5	22.5	14.4	19.8	7.3	14.8	5.6	9.7	4.9	10.2	7	13.4	8.1	13.3	6.3	10.8
UGT1A4	20.8	14.3	14.9	ND	27.7	18.2	22.7	21.5	20.4	14.8	30.3	29.8	25.7	14.6	20.7	18.1

UGT1A6	5.9	6.1	3.9	3.8	7	5.7	4.7	6.6	8.6	7.4	9.1	12.1	9.4	6.3	5.4	6.4
UGT1A9	11.8	10.9	5.5	8.3	9.5	5.1	1.4	7.1	7.5	6.3	5.6	13.2	10.7	7.1	4.4	9.1
UGT2B4	25.4	23.6	14.4	16.7	27.4	23.2	11.3	23	25.7	29.5	33	45.1	30.1	27.2	21	25.5
UGT2B7	61.2	43.4	20	30.6	116.2	62.2	38.7	58.6	54.9	37.6	34.8	50.1	69.9	37.6	24.1	30.8
UGT2B17	8	7.1	3.3	3.1	7.8	ND	ND	3.5	28.4	16.8	17.4	28	33.6	15.6	11.2	16
CES1	303.2	180.6	81.2	88.7	277.4	150	70.4	158.8	584	280.7	245.2	498	574.4	216.9	130.8	236.7
CES2	23.4	18.2	8.7	8.1	31.3	22.6	13.4	19.9	27.8	19.3	15.1	31.2	39.4	21.4	11.6	21.3
FMO3	66.8	53	26.5	22.5	68.4	42.1	24	42.1	118.2	85.5	67.6	109.4	111.6	63.4	34.6	49.9
FMO5	18.1	16.5	8.1	5.3	23.9	14.9	11.7	10.5	34.1	23	25.1	26	35.7	18.9	14.2	13.2
POR	19.8	34.5	13.4	7.5	48.2	46	28.7	30.5	26.6	31.9	35	36.8	27.7	26.2	19.8	18.6
MGST1	45.1	38.2	32	13.3	70.1	67.5	44.8	53.5	137.3	128.8	161	159.2	202.7	149.4	128.9	113.6
MGST3	7.5	8.6	5.7	2.2	5.8	5.5	3.4	4.2	7.1	6.8	8.1	8.6	9.9	7.4	6.1	5.8
BSEP	0.23	0.35	0.34	0.11	0.3	0.3	0.3	0.3	0.07	0.08	0.17	0.15	0.07	0.07	0.1	0.08
MRP3	0.16	0.55	0.27	0.13	ND	0.3	ND	0.3	ND	0.06	ND	0.03	ND	0.07	ND	0.02
MRP6	0.41	0.56	0.29	0.19	0.6	0.5	0.3	0.4	0.11	0.09	0.06	0.18	0.15	0.1	0.04	0.12
ATP1A1	2.52	6.63	2.58	1.82	4.3	8.1	4.5	4.6	6.28	13.63	10.57	11.51	7.93	13.52	7.24	7.02
OCT1	1.53	1.5	0.67	0.82	ND	ND	ND	ND	0.3	0.28	0.13	0.41	0.87	0.66	0.21	0.59
OAT2	0.52	1.16	0.4	0.35	ND	ND	ND	ND	0.08	0.12	0.08	0.15	0.09	0.11	0.05	0.08
OATP1B1	0.42	0.72	0.5	0.22	1.6	1.2	0.9	1.2	0.61	0.46	0.49	0.71	0.65	0.39	0.29	0.37
OATP2B1	1.01	1.22	0.74	0.47	1.2	0.7	0.5	0.6	0.22	0.25	0.22	0.2	0.39	0.35	0.21	0.17
MCT1	1.43	3.21	1.47	0.89	ND	ND	ND	ND	ND	0.33	0.18	ND	ND	0.18	0.07	ND

Normal, NAFLD, biliary, cancer denote microsomal samples from histologically normal or cirrhotic liver tissue from patients with non-alcoholic fatty liver disease, cholestasis, and hepatocellular carcinoma at the time of sample collection. ND, not detected using a particular method.

7.4.4. Comparison of absolute abundances of target proteins quantified by different methods

Absolute abundance values of the targets under investigation were highly correlated for all four methods with R^2 ranging from 0.69 to 0.88 (Supplementary Figure 7.1 A). Standard-based label-free methods, iBAQ and Hi3, showed better agreement with targeted quantification (slopes of 1.58 and 0.85, respectively) than the TPA method (1.80 fold higher on average). Label-free methods (iBAQ, Hi3, and TPA) returned values for 60%, 68%, and 42% of the targets, which were within a 2-fold range relative to the targeted data (Figure 7.1). Using the targeted data as a reference, the Hi3 and iBAQ approach were less biased (AFE = 0.96) than the TPA (AFE = 1.19) methods. The TPA approach was the least precise method (AAFE = 2.55), while the Hi3 and iBAQ approaches reflected lower data scatter (AAFE of 1.85 and 2.21, respectively).

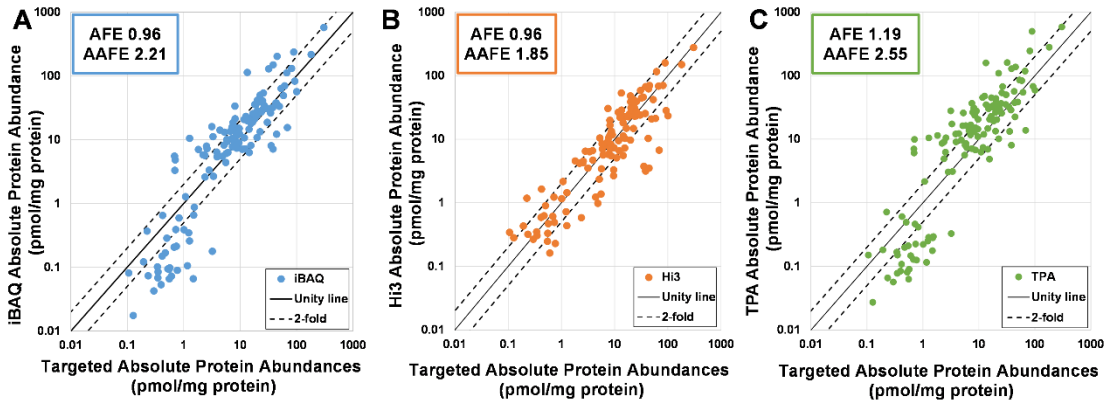

Figure 7.1. Assessment of agreement between absolute abundance data generated using label-free methods (iBAQ, Hi3, and TPA) and targeted proteomics. The AFE and AAFE values reflect bias and scatter of the data. The continuous line is the line of unity and the dashed lines represent the 2-fold range.

7.4.5. Comparison of disease-to-control ratios determined by different proteomic methods

Discrepancies in absolute values in Table 7.1 and Table 7.2 suggest the use of DPF as a way of reconciling differences. We now compared the relative levels of 35 proteins in diseased (with reference to control) samples as determined by four different quantification methods. The ratios obtained by the Hi3 and iBAQ methods showed good correlation with one another and with the targeted approach and TPA data (R^2 range 0.56-0.81). TPA data showed poor correlation to the targeted method with R^2 of only 0.21 (Supplementary Figure 7.1 B). The ratios measured by the iBAQ, Hi3 and TPA label-free methods for 96%, 94%, and 77% of the targets, respectively, were within 2-fold difference from the targeted data. Compared with the absolute abundance values, the scatter of the data was significantly reduced after implementation of the ratio (AAFE of 1.33, 1.31, and 1.62 for iBAQ, Hi3 and TPA, respectively, relative to the targeted data). Bias in the ratio values was low for the Hi3 and iBAQ methods (AFE of 0.95 and 0.87, respectively), but still persisted with the TPA method (AFE of 1.44) (Figure 7.2).

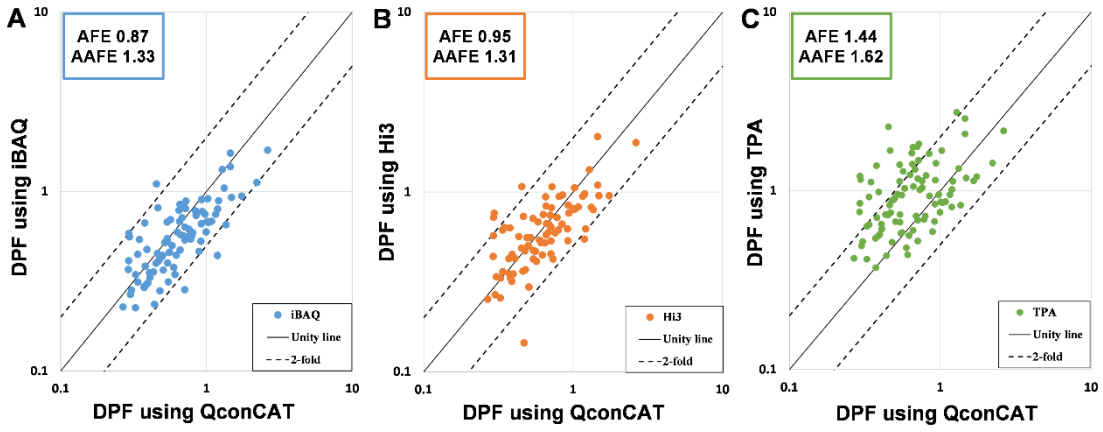

Figure 7.2. Assessment of the agreement between disease-to-control ratios (disease perturbation factor, DPF) generated using label-free methods (iBAQ, Hi3, and TPA) and

targeted proteomics. The AFE and AAFE values reflect bias and scatter of the data. The continuous line is the line of unity and the dashed lines represent the 2-fold range.

7.4.6. Recovering disease-related perturbations in abundance of hepatic enzymes and transporters

Disease effects on the abundances of key drug-metabolising enzymes and drug transporters is shown in Figure 7.3. Based on targeted proteomics, biliary and cancer-related cirrhosis were associated with 2 or more fold reduction in abundance of CYP3A4, 1A2, 2C8, 2J2, UGT2B7, 2B17, CES1, CES2, FMO3 and FMO5. Expression levels of the majority of the remaining enzymes and transporters dropped to less than 50% in cancer-associated cirrhosis compared with control. CYP2A6, 2B6, 2C9, 2E1, and UGT1A9 were significantly downregulated in cholestatic cirrhosis. In this group, BSEP and MRP3 (implicated in transport of bile salts and bile conjugates, respectively) increased by 45 and 70%, respectively, while there was a reduction in OCT1 (by 60%) and OATP2B1 (by 30%). However, for changes that are within a 2-fold cut-off range, disease effects may be masked by analytical or technical variability. Although NAFLD-related cirrhosis had a lower impact on CYPs and UGTs than other types of cirrhosis, this aetiology was associated with increased expression (> 2 fold) of several transporters, including MRP3, OAT2, and MCT1 (Figure 7.3).

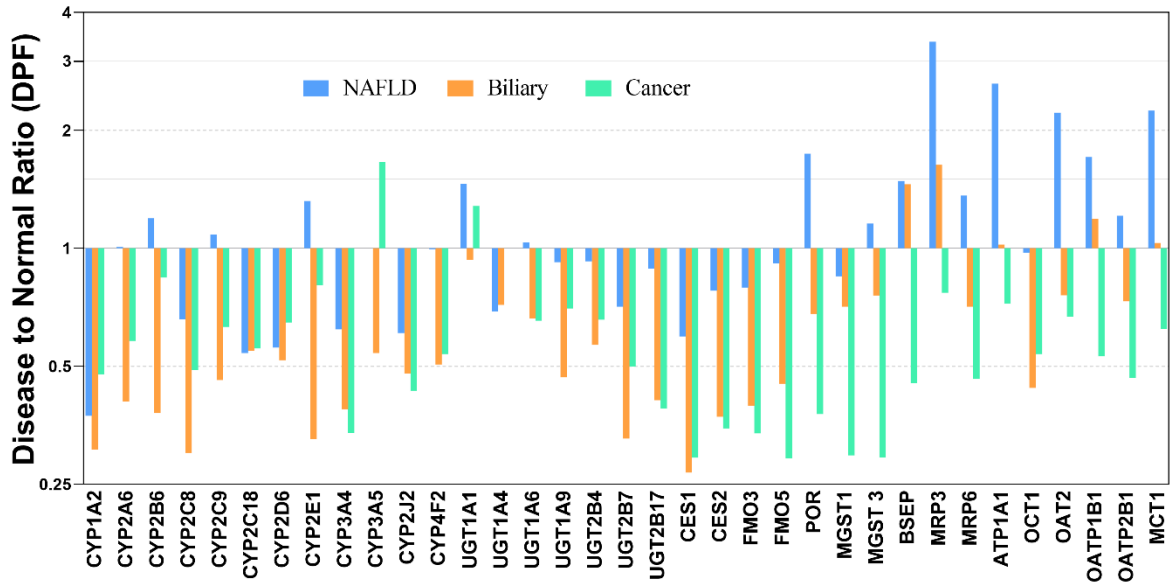

Figure 7.3. Disease-to-control abundance ratios (disease perturbation factor, DPF) for enzymes and transporters measured by targeted (QconCAT) proteomics in three pooled cirrhosis liver samples with concomitant hepatic disease, non-alcoholic fatty liver (NAFLD), cholestasis (biliary), and hepatocellular carcinoma (cancer), relative to histologically normal control liver samples.

7.5. Discussion

This study investigated the performance of targeted and global proteomic methods in measuring the effects of liver disease on expression of hepatic enzymes and transporters. Absolute abundance values of DMEs and transporters measured by targeted and global (Hi3 and iBAQ) methods showed good overall agreement in terms of accuracy and precision. Although the TPA method correlated with the targeted approach, as highlighted previously (Vildhede, et al., 2018), the TPA tended to overestimate consistently by approximately two fold. This emphasises the observation that standard-based methods perform well relative to methods with no standards (such as TPA) when accurate quantification, rather than an estimate, is required. It is not very surprising that the TPA overestimates. The central tenet of this approach is that the total intensity in a sample represents the total amount of protein. In fact,

many proteins fall below the limit of detection, and many others fall below the limit of quantification. Wiśniewski et al (2014) have attempted to overcome this limitation using the protein ruler, allowing a standardisation to internal standards. A further limitation of the classical TPA (used in this study) is that the intensity corresponding to more than one protein (where a peptide is present in more than one protein) is assigned in full to each of those proteins. A modification in the TPA can be performed by assigning such intensity on the basis of the ratio of intensity due to the razor peptides; this modification is more important in limiting overestimation of individual proteins than in addressing the global overestimation (Al-Majdoub, et al., 2020b).

The high correlation between Hi3 and iBAQ methods (R^2 0.87) is in line with findings by Krey et al. (2014). The difference between these two methods is that in the Hi3 method only unique peptides are used for quantification, whereas non-unique peptides may be used in the iBAQ method. This can justify the over-estimation observed in the iBAQ compared to the targeted and the Hi3 using the observed data. There are advantages to both approaches, which have not been fully explored. The elimination of non-unique peptides is arguably more robust; even when their contribution is divided among contributing proteins, the ratio is an estimation. However, their inclusion allows more data to be used in the quantification, and this is important where proteins with few unique peptides are to be quantified.

As previously discussed (Prasad, et al., 2019), absolute quantification is critically dependent on the choice of the surrogate peptides used to quantify each protein. Different peptides behave differently under sample preparation and LC-MS conditions (Chen, et al., 2020). Peptides in close proximity to membrane-spanning domains, those prone to missed cleavage and sequences with hydrophobic amino acids (such as P, V, W) negatively affect proteomic quantification (Achour, et al., 2018). These factors can lead to high variability in the data generated by different laboratories, with differences reaching up to 10 fold in some instances (Chen, et al.,

2020; Prasad & Unadkat, 2014; Wegler, et al., 2017). Our results confirmed previous conclusions of cross-laboratory studies about the impact of peptide choice and analysis method on reported end-point measurements.

This study shows that relative quantification to a control set can lead to greater consistency between quantification methodologies and this might be a useful strategy to offset bias related to surrogate peptides, analytical methods or even different laboratories. Where the aim is to demonstrate the effect of disease, DPF described here, is a useful measure. When the disease to control ratios were compared, they were shown to be more consistent than absolute values across methods and between surrogate peptides. Using the QconCAT approach, the differences in these ratios were within 25% for different targets, which supported the possibility of reconciling inherent technical variability in absolute abundance measurements. In a similar fashion, relative expression factors, REF, extensively used in *in vitro-in vivo* extrapolation, were previously shown to be more consistent when the abundance in tissue and in the *in vitro* system are measured in the same laboratory using the same methodology (Harwood, et al., 2016).

The ability of different quantification methods to define DPF in expression of various drug metabolism proteins was investigated by applying the ratios of expression of each protein in the disease samples relative to histologically normal controls. The ratios should be compatible with reverse translational modelling of drug kinetics and effects of co-morbidities as described previously (Rostami-Hodjegan, 2018). This relies on implementing the DPF into verified models in a healthy population rather than a fully bottom-up approach (Sharma, et al., 2020). Again, the Hi3 and iBAQ label-free methods were able to capture the disease perturbation in agreement with the targeted approach, with much less bias (lower AFE) and scatter in the data (lower AAFE) than the TPA. The reason may well be that this approach does not apply a standard that acts as an anchor to offset the effect of technical variability on measured

abundance. The use of the protein ruler with stable expression in a lysate (Wiśniewski, et al., 2014) together with a principled division of intensities due to non-unique peptides among contributing proteins may bring this in line. The remaining difficulty is to establish a suitable ruler for microsomal samples.

Cirrhosis is a chronic fibrotic liver disease that is known to change the liver architecture and affect the expression of drug-metabolising enzyme and their activities. However, these changes are not fully understood and differences can be related to the enzyme isoform, degree of disease severities and underlying conditions (Elbekai, et al., 2004). Using DPF, the degree of change in expression of hepatic enzymes and transporters among cirrhosis samples of different aetiologies revealed differences in their pathophysiology and confirmed the heterogeneity of cirrhosis as a disease, in line with previous studies (Drozdzik, et al., 2019; El-Khateeb, et al., 2020; Prasad, et al., 2018). In agreement with our findings, Prasad et al. (2018) reported reduced CYP and UGT expression in cirrhosis, although the causes of the disease were different from those explored in the current study. Drozdzik et al., (2019) reported relative changes in the abundance of different transporters in cirrhotic livers with aetiologies associated with alcohol, cholestasis, autoimmune diseases and viral hepatitis compared to normal controls. In their cholestasis group, the reported changes in OCT1, BSEP, and OATP2B1 were in line with findings in the current study. Measuring the effect of disease in the current and previous studies relied on measurements in liver tissue. Non-invasive techniques, such as liquid biopsy (Achour, et al., 2021), might be an avenue for further development to determine the extent and inter-individual variabilities in perturbation, knowing that significant differences exist in the altered values for different pathways, as typical clinical scores of cirrhosis, such as the Child-Pugh system, cannot predict these changes in metabolic capacity (Elmeliegy, et al., 2021; EMA, 2005).

In conclusion, differences were observed in absolute abundances measured by several targeted and untargeted methods. Error inherent to these methods was mitigated by measuring a relative factor that captures the effect of disease on the expression of various hepatic enzymes and transporters. DPF is more consistent than using absolute values, when the same method is employed for the disease and control sample sets. Application of this approach can help in understanding different expression patterns of enzymes and transporters in disease states, such as cirrhosis across different disease aetiologies or severities.

7.6. References

Achour, B, Al-Majdoub, ZM, Grybos-Gajniak, A, Lea, K, Kilford, P, Zhang, M, Knight, D, Barber, J, Schageman, J, and Rostami-Hodjegan, A. (2021). Liquid Biopsy Enables Quantification of the Abundance and Interindividual Variability of Hepatic Enzymes and Transporters. *Clin. Pharmacol. Ther.*, 109(1), 222–232.

Achour, B, Al Feteisi, H, Lanucara, F, Rostami-Hodjegan, A, and Barber, J. (2017a). Global Proteomic Analysis of Human Liver Microsomes: Rapid Characterization and Quantification of Hepatic Drug-Metabolizing Enzymes. *Drug Metab. Dispos.*, 45(6), 666–675.

Achour, B, Dantonio, A, Niosi, M, Novak, JJ, Al-Majdoub, ZM, Goosen, TC, Rostami-Hodjegan, A, and Barber, J. (2018). Data Generated by Quantitative Liquid Chromatography-Mass Spectrometry Proteomics Are Only the Start and Not the Endpoint: Optimization of Quantitative Concatemer-Based Measurement of Hepatic Uridine-5′-Diphosphate–Glucuronosyltransferase Enzymes with Ref. *Drug Metab. Dispos.*, 46(6), 805–812.

Achour, B, Dantonio, A, Niosi, M, Novak, JJ, Fallon, JK, Barber, J, Smith, PC, Rostami-Hodjegan, A, and Goosen, TC. (2017b). Quantitative Characterization of Major Hepatic UDP-Glucuronosyltransferase Enzymes in Human Liver Microsomes: Comparison of Two Proteomic Methods and Correlation with Catalytic Activity. *Drug Metab. Dispos.*, 45(10), 1102–1112.

Achour, B, Russell, MR, Barber, J, and Rostami-Hodjegan, A. (2014). Simultaneous quantification of the abundance of several cytochrome P450 and uridine 5′-diphospho-glucuronosyltransferase enzymes in human liver microsomes using multiplexed targeted proteomics. *Drug Metab. Dispos.*, 42(4), 500–510.

Al-Majdoub, ZM, Al Feteisi, H, Achour, B, Warwood, S, Neuhoff, S, Rostami-Hodjegan, A, and Barber, J. (2019). Proteomic quantification of human blood–brain barrier SLC and ABC transporters in healthy individuals and dementia patients. *Mol. Pharm.*, 16(3), 1220–1233.

Al-Majdoub, ZM, Couto, N, Achour, B, Harwood, MD, Carlson, G, Warhurst, G, Barber, J, and Rostami-Hodjegan, A. (2020a). Quantification of Proteins Involved in Intestinal

Epithelial Handling of Xenobiotics. *Clin. Pharmacol. Ther.*, cpt.2097.

Al-Majdoub, ZM, Achour, B, Couto, N, Howard, M, Elmorsi, Y, Scotcher, D, Alrubia, S, El-Khateeb, E, Vasilogianni, A, Alohali, N, Neuhoff, S, Schmitt, L, Rostami-Hodjegan, A, and Barber, J. (2020b). Mass spectrometry-based abundance atlas of ABC transporters in human liver, gut, kidney, brain and skin. *FEBS Lett.*, 594(23), 4134–4150.

Al Feteisi, H, Achour, B, Rostami-Hodjegan, A, and Barber, J. (2015). Translational value of liquid chromatography coupled with tandem mass spectrometry-based quantitative proteomics for in vitro – in vivo extrapolation of drug metabolism and transport and considerations in selecting appropriate techniques. *Expert Opin. Drug Metab. Toxicol.*, 11(9), 1357–1369.

Al Feteisi, H, Al-Majdoub, ZM, Achour, B, Couto, N, Rostami-Hodjegan, A, and Barber, J. (2018). Identification and quantification of blood-brain barrier transporters in isolated rat brain microvessels. *J. Neurochem.*, 146(6), 670–685.

Chen, Q, Jiang, Y, Ren, Y, Ying, M, and Lu, B. (2020). Peptide Selection for Accurate Targeted Protein Quantification via a Dimethylation High-Resolution Mass Spectrum Strategy with a Peptide Release Kinetic Model. *ACS Omega*, 5(8), 3809–3819.

Couto, N, Al-Majdoub, ZM, Achour, B, Wright, PC, Rostami-Hodjegan, A, and Barber, J. (2019). Quantification of Proteins Involved in Drug Metabolism and Disposition in the Human Liver Using Label-Free Global Proteomics. *Mol. Pharm.*, 16(2), 632–647.

Drozdzik, M, Busch, D, Lapczuk, J, Müller, J, Ostrowski, M, Kurzawski, M, and Oswald, S. (2019). Protein Abundance of Clinically Relevant Drug Transporters in the Human Liver and Intestine: A Comparative Analysis in Paired Tissue Specimens. *Clin. Pharmacol. Ther.*, 105(5), 1204–1212.

Edginton, AN, and Willmann, S. (2008). Physiology-based simulations of a pathological condition: Prediction of pharmacokinetics in patients with liver cirrhosis. *Clin. Pharmacokinet.*, 47(11), 743–752.

El-Khateeb, E, Achour, B, Scotcher, D, Al-Majdoub, ZM, Athwal, V, Barber, J, and Rostami-Hodjegan, A. (2020). Scaling Factors for Clearance in Adult Liver Cirrhosis. *Drug Metab. Dispos.*, 48(12), 1271–1282.

El-Khateeb, E, Darwich, AS, Achour, B, Athwal, V, and Rostami-Hodjegan, A. (n.d.). Time to Revisit Child-Pugh Score as the Basis for Predicting Drug Clearance in Hepatic Impairment. *Aliment. Pharmacol. Ther.*, Submitted.

El-Khateeb, E, Vasilogianni, A-M, Alrubia, S, Al-Majdoub, ZM, Couto, N, Howard, M, Barber, J, Rostami-Hodjegan, A, and Achour, B. (2019). Quantitative mass spectrometry-based proteomics in the era of model-informed drug development: Applications in translational pharmacology and recommendations for best practice. *Pharmacol. Ther.*, 203, 107397.

Elbekai, R, Korashy, H, and El-Kadi, A. (2004). The Effect of Liver Cirrhosis on the Regulation and Expression of Drug Metabolizing Enzymes. *Curr. Drug Metab.*, 5(2), 157–167.

Elmeliegy, M, Yang, DZ, Salama, E, Parivar, K, and Wang, DD. (2021). Discordance Between Child-Pugh and National Cancer Institute Classifications for Hepatic Dysfunction: Implications on Dosing Recommendations for Oncology Compounds. *J. Clin.*

Pharmacol., 61(1), 105–115.

EMA. (2005). Guideline on the Evaluation of the Pharmacokinetics of Medicinal Products in Patients With Impaired Hepatic Function. *Ema*, 1-10 CPMP/EWP/2339/02. https://www.ema.europa.eu/en/documents/scientific-guideline/guideline-evaluation-pharmacokinetics-medicinal-products-patients-impaired-hepatic-function_en.pdf

Fabre, B, Lambour, T, Bouyssié, D, Menneteau, T, Monsarrat, B, Burlet-Schiltz, O, and Bousquet-Dubouch, M-P. (2014). Comparison of label-free quantification methods for the determination of protein complexes subunits stoichiometry. *EuPA Open Proteomics*, 4, 82–86.

FDA. (2003). Pharmacokinetics in patients with impaired hepatic function: study design, data analysis, and impact on dosing and labelling. *FDA Guid.* https://www.fda.gov/regulatory-information/search-fda-guidance-documents/pharmacokinetics-patients-impaired-hepatic-function-study-design-data-analysis-and-impact-dosing-and

FDA. (2020). Enhancing the Diversity of Clinical Trial Populations—Eligibility Criteria, Enrollment Practices, and Trial Designs Guidance for Industry. *Guid. Doc.* https://www.fda.gov/regulatory-information/search-fda-guidance-documents/enhancing-diversity-clinical-trial-populations-eligibility-criteria-enrollment-practices-and-trial

Frye, RF, Zgheib, NK, Matzke, GR, Chaves-Gnecco, D, Rabinovitz, M, Shaikh, OS, and Branch, RA. (2006). Liver disease selectively modulates cytochrome P450-mediated metabolism. *Clin. Pharmacol. Ther.*, 80(3), 235–245.

Harwood, MD, Achour, B, Neuhoff, S, Russell, MR, Carlson, G, Warhurst, G, and Rostami-Hodjegan, A. (2016). In Vitro-In Vivo Extrapolation Scaling Factors for Intestinal P-glycoprotein and Breast Cancer Resistance Protein: Part II. The Impact of Cross-Laboratory Variations of Intestinal Transporter Relative Expression Factors on Predicted Drug Disposition. *Drug Metab. Dispos.*, 44(3), 476–480.

Harwood, MD, Achour, B, Russell, MR, Carlson, GL, Warhurst, G, and Rostami-Hodjegan, A. (2015). Application of an LC-MS/MS method for the simultaneous quantification of human intestinal transporter proteins absolute abundance using a QconCAT technique. *J. Pharm. Biomed. Anal.*, 110, 27–33.

Jamei, M. (2016). Recent Advances in Development and Application of Physiologically-Based Pharmacokinetic (PBPK) Models: a Transition from Academic Curiosity to Regulatory Acceptance. *Curr. Pharmacol. Reports*, 2(3), 161–169.

Johnson, TN, Boussery, K, Rowland-Yeo, K, Tucker, GT, and Rostami-Hodjegan, A. (2010). A semi-mechanistic model to predict the effects of liver cirrhosis on drug clearance. *Clin. Pharmacokinet.*, 49(3), 189–206.

Krey, JF, Wilmarth, PA, Shin, J-B, Klimek, J, Sherman, NE, Jeffery, ED, Choi, D, David, LL, and Barr-Gillespie, PG. (2014). Accurate Label-Free Protein Quantitation with High- and Low-Resolution Mass Spectrometers. *J. Proteome Res.*, 13(2), 1034–1044.

Li, Z, Adams, RM, Chourey, K, Hurst, GB, Hettich, RL, and Pan, C. (2012). Systematic Comparison of Label-Free, Metabolic Labeling, and Isobaric Chemical Labeling for Quantitative Proteomics on LTQ Orbitrap Velos. *J. Proteome Res.*, 11(3), 1582–1590.

Lichtman, SM, Harvey, RD, Damiette Smit, M-A, Rahman, A, Thompson, MA, Roach, N, Schenkel, C, Bruinooge, SS, Cortazar, P, Walker, D, and Fehrenbacher, L. (2017).

Modernizing Clinical Trial Eligibility Criteria: Recommendations of the American Society of Clinical Oncology–Friends of Cancer Research Organ Dysfunction, Prior or Concurrent Malignancy, and Comorbidities Working Group. *J. Clin. Oncol.*, 35(33), 3753–3759.

Megger, DA, Pott, LL, Ahrens, M, Padden, J, Bracht, T, Kuhlmann, K, Eisenacher, M, Meyer, HE, and Sitek, B. (2014). Comparison of label-free and label-based strategies for proteome analysis of hepatoma cell lines. *Biochim. Biophys. Acta - Proteins Proteomics*, 1844(5), 967–976.

Prasad, B, Achour, B, Artursson, P, Hop, CECA, Lai, Y, Smith, PC, Barber, J, Wisniewski, JR, Spellman, D, Uchida, Y, Zientek, MA, Unadkat, JD, and Rostami-Hodjegan, A. (2019). Toward a Consensus on Applying Quantitative Liquid Chromatography-Tandem Mass Spectrometry Proteomics in Translational Pharmacology Research: A White Paper. *Clin. Pharmacol. Ther.*, 106(3), 525–543.

Prasad, B, Bhatt, DK, Johnson, K, Chapa, R, Chu, X, Salphati, L, Xiao, G, Lee, C, Hop, CECA, Mathias, A, Lai, Y, Liao, M, Humphreys, WG, Kumer, SC, and Unadkat, JD. (2018). Abundance of Phase 1 and 2 Drug-Metabolizing Enzymes in Alcoholic and Hepatitis C Cirrhotic Livers: A Quantitative Targeted Proteomics Study. *Drug Metab. Dispos.*, 46(7), 943–952.

Prasad, B, and Unadkat, JD. (2014). Optimized Approaches for Quantification of Drug Transporters in Tissues and Cells by MRM Proteomics. *AAPS J.*, 16(4), 634–648.

Rostami-Hodjegan, A. (2018). Reverse Translation in PBPK and QSP: Going Backwards in Order to Go Forward With Confidence. *Clin. Pharmacol. Ther.*, 103(2), 224–232.

Russell, MR, Achour, B, McKenzie, EA, Lopez, R, Harwood, MD, Rostami-Hodjegan, A, and Barber, J. (2013). Alternative fusion protein strategies to express recalcitrant QconCAT proteins for quantitative proteomics of human drug metabolizing enzymes and transporters. *J. Proteome Res.*, 12(12), 5934–5942.

Schuppan, D, and Afdhal, NH. (2008). Liver cirrhosis. *Lancet*, 371(9615), 838–851.

Sharma, S, Suresh Ahire, D, and Prasad, B. (2020). Utility of Quantitative Proteomics for Enhancing the Predictive Ability of Physiologically Based Pharmacokinetic Models Across Disease States. *J. Clin. Pharmacol.*, 60(S1).

Verbeeck, RK. (2008). Pharmacokinetics and dosage adjustment in patients with hepatic dysfunction. *Eur. J. Clin. Pharmacol.*, 64(12), 1147.

Vildhede, A, Nguyen, C, Erickson, BK, Kunz, RC, Jones, R, Kimoto, E, Bourbonais, F, Rodrigues, AD, and Varma, MVS. (2018). Comparison of Proteomic Quantification Approaches for Hepatic Drug Transporters: Multiplexed Global Quantitation Correlates with Targeted Proteomic Quantitation. *Drug Metab. Dispos.*, 46(5), 692–696.

Wegler, C, Gaugaz, FZ, Andersson, TB, Wiśniewski, JR, Busch, D, Gröer, C, Oswald, S, Norén, A, Weiss, F, Hammer, HS, Joos, TO, Poetz, O, Achour, B, Rostami-Hodjegan, A, Van De Steeg, E, Wortelboer, HM, and Artursson, P. (2017). Variability in Mass Spectrometry-based Quantification of Clinically Relevant Drug Transporters and Drug Metabolizing Enzymes. *Mol. Pharm.*, 14(9), 3142–3151.

Wiśniewski, JR, Hein, MY, Cox, J, and Mann, M. (2014). A “Proteomic Ruler” for Protein Copy Number and Concentration Estimation without Spike-in Standards. *Mol. Cell.*

Proteomics, 13(12), 3497–3506.

Wiśniewski, JR, Wegler, C, and Artursson, P. (2019). Multiple-Enzyme-Digestion Strategy Improves Accuracy and Sensitivity of Label- and Standard-Free Absolute Quantification to a Level That Is Achievable by Analysis with Stable Isotope-Labeled Standard Spiking. *J. Proteome Res.*, 18(1), 217–224.

Wiśniewski, JR, Zougman, A, Nagaraj, N, and Mann, M. (2009). Universal sample preparation method for proteome analysis. *Nat. Methods*, 6(5), 359–362.

7.7. Supplementary Material

Supplementary Table 7.1. Demographic and clinical data for individual donors of control samples

Serial	Sample ID	Date of surgery	Age	sex	PT (sec)	Albumin level (g/L)	Weight (Kg) *	Height (m) *	Total bilirubin (µmol/L)	General diagnosis
1	2759	12/12/16	81	M	11.3	34	82	1.72	11	CRC
2	2721	06/12/16	36	M	11.5	39	61.5	1.696	18	CRC
3	2841	28/12/16	57	M	12.3	40	84	1.74	9	CRC
4	0103	16/01/17	81	M	21.6	38	75	1.67	16	CRC
5	2847	30/12/16	48	F	12.2	43	67.8	1.619	10	SCC
6	0044	09/01/17	83	F	10.6	39	62.3	1.637	6	CRC
7	761	20/04/17	73	M	12.7	35	94.9	1.638	6	HCC
8	713	13/04/17	57	F	12.1	42	65.9	1.73	9	CRC
9	502	14/03/17	77	M	11.9	38	112.5	1.71	9	CRC
10	0125	19/01/17	62	M	10.9	38	69.7	1.7	7	CRC
11	0336	16/02/17	71	F	10.5	34	76	1.53	8	GIST
12	484	13/03/17	80	M	21.9	24	71	1.81	28	CRC
13	0322	14/02/17	71	M	10.8	43	93.6	1.715	11	CRC
14	2809	20/12/16	52	M	10.1	42	88	1.735	6	CRC

PT, prothrombin time; * measured at time of surgery; HCC, hepatocellular carcinoma; CRC, colorectal cancer; SCC, squamous cell carcinoma; GIST, gastrointestinal stromal tumour.

Supplementary Table 7.2. Demographic and clinical data for individual donors of cirrhosis liver samples and Child-Pugh classification

Serial for each group	Sample ID	Date of surgery D/M/Y	Age	sex	PT (sec)	Albumin level (g/L)	Total bilirubin (µmol/L)	Weight (Kg) [a]	Height (m) [a]	Ascites volume[b]	HE grade [c]	General diagnosis	CP class (Score)
1	0974	19/05/17	56	M	18.1	37	8	117.5	1.75	Severe	1-2	SH	B(9)
2	1982	17/08/16	63	F	18	25	30	70.7	1.57	Mild	1-2	NAFLD	B(9)
3	1570	10/06/16	62	F	16.6	32	26	72.1	1.52	Moderate	1-2	NAFLD	B(9)
4	0549	22/03/17	59	M	18.8	28	53	89.2	1.72	Mild	1-2	NAFLD	C(10)
5	0355	17/02/17	67	F	17.9	26	81	82.2	1.64	Moderate	None	NAFLD	C(11)
6	0863	08/05/17	51	F	19.8	23	78	89.2	1.6	Mild	None	NAFLD	C(11)
7	2728	07/12/16	66	F	24.9	32	29	82.6	1.6	Moderate	1-2	NAFLD	C(10)
8	1571	11/06/16	46	F	14.7	25	51	78.6	1.58	Mild	1-2	NAFLD	C(11)
9	0286	10/02/17	48	M	NA	NA	NA	NA	NA	NA	NA	NAFLD	NA
1	2403	21/10/16	57	M	14.4	29	16	89	1.803	None	None	HCC& HCV	A(6)
2	0955	18/05/17	63	M	15	36	18	89.2	1.73	None	None	HCC& alcoholic SH	A(5)
3	1963	13/08/16	68	M	13.6	27	28	113.45	1.77	None	1-2	HCC& alcoholic injury	B(8)
4	1745	14/07/16	67	M	15.2	27	46	92	1.7	Mild	None	HCC& NAFLD	B(9)
5	2431	27/10/16	69	M	15.7	28	30	95	1.79	None	None	HCC& HCV	A(6)
6	2408	22/10/16	51	M	18.9	31	44	88.5	1.85	Mild	None	HCC& HCV	B(8)
7	1926	10/08/16	63	M	17	33	97	82.3	1.74	None	1-2	HCC& NAFLD	B(9)
8	3688	12/11/15	65	F	13.8	40	14	84	1.63	None	None	HCC& alcoholic SH	A(5)
9	1228	06/12/17	55	F	14.3	29	13	78.6	1.62	None	None	HCC	A(6)
1	997	21/04/16	59	M	19.7	13	63	100.8	1.82	Severe	1-2	CHOL.	C(14)
2	0746	19/04/17	67	M	13.7	24	58	76.4	1.6	None	1-2	PBC	C(10)
3	0147	25/01/17	57	M	15.3	19	243	72.3	1.74	Mild	1-2	CHOL.	C(11)

4	2682	02/12/16	56	F	15.2	40	75	67.3	1.62	Severe	1-2	CHOL.	C(11)
5	2500	07/11/16	63	F	11.9	30	82	80.15	1.64	Mild	1-2	PBC	C(10)
6	2306	11/10/16	60	M	16.9	22	326	83.2	1.76	Mild	1-2	PSC	C(11)
7	2159	15/09/16	39	M	14.2	30	49	80.8	1.90	Mild	None	PSC	B(8)
8	2136	12/09/16	54	M	19.1	30	484	79.7	1.75	Moderate	1-2	PSC	C(12)
9	1684	11/07/16	69	F	15.4	28	102	78.6	1.67	Mild	1-2	CHOL.&PBC	C(10)
10	1429	18/07/17	57	M	15.2	37	37	69	1.75	Mild	None	PSC	B(7)
11	0544	21/03/17	70	M	13.3	30	25	87.8	-	None	1-2	PSC	B(7)
12	2020	24/08/16	59	F	15.9	29	26	43.95	1.5	Severe	None	PBC	B(9)
13	0819	05/02/17	75	M	13.2	41	18	79.5	1.6	None	None	CHOL.	A(5)

PT, prothrombin time; HE, Hepatic encephalopathy; CP, Child-Pugh; NA, No data available; HCC, hepatocellular carcinoma; NAFLD, non-alcoholic fatty liver disease; CHOL, cholestasis; PBC, primary biliary cirrhosis; PSC, primary sclerosing cholangitis, SH, Steatohepatitis; [a] measured at time of surgery; [b] controlled with diuretics recorded as Mild ascites, [c] controlled with rifaximin / lactulose recorded as grade 1-2.

Supplementary Table 7.3. MaxQuant main quantification parameters for targeted and label-free quantifications

Parameter description	Label-Free Quantification	Targeted
Label free quantification	Yes	None
Multiplicity	1	2 (Max. Labelled 2 (heavy labels Arg6 &Lys6)
Digestion Enzyme	Trypsin/P	Trypsin/P
Variable Modifications	Oxidation (M) & Deamidation (NQ)	Oxidation (M) & Deamidation (NQ)
Fixed modifications	Carbamidomethyl (C)	Carbamidomethyl (C)
Max number of modifications per peptide	5	5
Max charge	7	7
Main search peptide tolerance	5 ppm	5 ppm
Min pep length	5	5
Min pep length for unspecific search	8	8
Max pep length for unspecific search	25	25
Max peptide mass [Da]	5000 Da	5000 Da
Peptides for quantification	All	All
MS/MS match tolerance	0.5 Da	0.5 Da
False discovery rate (FDR)	1%	1%

Supplementary Table 7.4.Targets and their unique peptides in each QconCAT standard; NuncCAT, MetCAT, and TransCAT

NuncCAT		MetCAT		TransCAT	
Target	**Peptide Sequence**	**Target**	**Peptide Sequence**	**Target**	**Peptide Sequence**
CES1	EGYLQIGANTQAAQK§	**CYP1A2**	ASGNLIPQEK§	**P-gp, MDR1**	FYDPLAGK
	FLSLDLQGDPR		YLPNPALQR		AGAVAEEVLAAIR§
CES2	ADHGDELPFVFR§	**CYP2A6**	DPSFFSNPQDFNPQHFLNEK	**BSEP**	STALQLIQR
	SFFGGNYIK		GTGGANIDPTFFLSR§		AADTIIGFEHGTAVER§
	TTHTGQVLGSLVHVK	**CYP2B6**	ETLDPSAPR	**MDR3**	IATEAIENIR
FMO3	LVGPGQWPGAR§		GYGVIFANGNR§		GAAYVIFDIIDNNPK
	NNLPTAISDWLYVK	**CYP2C18**	GSFPVAEK§	**MRP2**	LTIIPQDPILFSGSLR
			SLTNFSK		
FMO5	WATQVFK	**CYP2C19**	GHFPLAER		YLGGDDLDTSAIR
	TDDIGGLWR	**CYP2C8**	SFTNFSK§		AFEHQQR
	LTHFIWK§	**CYP2C9**	GIFPLAER§	**MRP3**	AEGEISDPFR
EPHX1	IIPLLTDPK		LPPGPTPLPVIGNILQIGIK		IDGLNVADIGLHDLR§
	FSTWTNTEFR	**CYP2D6**	AFLTQLDELLTEHR	**MRP4**	AEAAALTETAK
POR	QYELVVHTDIDAAK§		DIEVQGFR§		APVLFFDR
	YYSIASSSK	**CYP2E1**	FITLVPSNLPHEATR§	**MRP6**	SSLPSALLGELSK
	IQTLTSSVR		GIIFNNGPTWK		APETEPFLR§
MGST1	VFANPEDCVAFGK	**CYP2J2**	FEYQDSWFQQLLK		SSLASGLLR
	IYHTIAYLTPLPQPNR§		VIGQGQQPSTAAR§	**BCRP**	VIQELGLDK

MGST2	HLYFWGYSEAAK	**CYP3A4**	EVTNFLR		SSLLDVLAAR§
MGST 3	IASGLGLAWIVGR§		LSLGGLLQPEK§		ENLQFSAALR
	VLYAYGYYTGEPSK	**CYP3A43**	YIPFGAGPR	**ATP1A1**	IVEIPFNSTNK
UGT2B17	WTYSISK	**CYP3A5**	DTINFLSK§		SPDFTNENPLETR§
	GHEVIVLTSSASILVNASK		YWTEPEEFRPER	**Cadherin-17**	AENPEPLVFGVK
	SVINDPIYK§	**CYP3A7**	FGGLLLTEK		QNSRPGK
ADH1A*	GAILGGFK		FGGLLLTEKPIVLK	**Cadherin-23**	ATDADEGEFGR
	NDVSNPQGTLQDGTSR		FNPLDPFVLSIK		DAYVGALR
	KPIHHFLGISTFSQYTVVDENAVAK	**CYP4F2**	HVTQDIVLPDGR§	**OST-α**	YTADLLEVLK
ADH1B *	AAVLWEVK	**UGT1A1**	DGAFYTLK§		VGYETFSSPDLDLNLK
	GAVYGGFK		TYPVPFQR	**OST-β**	DHNSLNNLR
ADH1C	FSLDALITNILPFEK	**UGT1A3**	HVLGHTQLYFETEHFLK		ETPEVLHLDEAK
ALDH1A1 *	IFVEESIYDEFVR		YLSIPTVFFLR	**OCT1**	MLSLEEDVTEK§
	IFINNEWHDSVSGK	**UGT1A4**	GTQCPNPSSYIPK§		GVALPETMK
	TIPIDGNFFTYTR		YIPCDLDFK		ENTIYLK
AOX1 *	LILNEVSLLGSAPGGK	**UGT1A6**	SFLTAPQTEYR§	**OCT2**	GIALPETVDDVEK
			VSVWLLR		
	GLHGPLTLNSPLTPEK	**UGT1A9**	AFAHAQWK§		FLQGVFGK
	VFFGEGDGIIR		ESSFDAVFLDPFDNCGLIVAK	**OCTN2**	TWNIR
NAT1 *	DNTDLIEFK	**UGT2B4**	ANVIASALAK		DYDEVTAFLGEWGPFQR
	NYIVDAGFGR		FSPGYAIEK§	**OAT2**	WLLTQGHVK
NAT2*	TLTEEEVEEVLK	**UGT2B7**	ADVWLIR§		NVALLALPR§
	DNTDLVEFK		TILDELIQR	**OAT4**	DTLTLEILK
SULT1E1*	KPSEELVDR	**UGT2B10**	GHEVTVLASSASILFDPNDSSTLK		ISLLSFTR
	NHFTVALNEK	**UGT2B11**	GHEVTVLASSASILFDPNDASTLK	**MATE1**	GGPEATLEVR
SULT1A1	VHPEPGTWDSFLEK	**UGT2B15**	SVINDPVYK		DHVGYIFTTDR
SULT1A2	VYPHPGTWESFLEK		ASGNLIPQEK	**OATP1A2**	EGLETNADIIK
SULT2A1 *	DEDVIILTYPK				IYDSTTFR
	TLEPEELNLILK			**OATP1B1**	YVEQQYGQPSSK
TPMT*	NQVLTLEEWQDK				MFLAALSLSFIAK
	TSLDIEEYSDTEVQK				LNTVGIAK§
EPHX2 *	GLLNDAFQK			**OATP1B3**	NVTGFFQSLK
	WLDSDAR				IYNSVFFGR§
				OATP2B1	VLLQTLR
					SSPAVEQQLLVSGPGK§
				OATP4C1	HLPGTAEIQAGK
					SPEPSLPSAPPNVSEEK
					DFPAALK
				NTCP	GIYDGDLK
					GIVISLVLVLIPCTIGIVLK
					AHLWKPK
				PEPT1	GNEVQIK
					TLPVFPK
					HTLLVWAPNHYQVVK
				ASBT	IAGLPWYR
					LWIIGTIFPVAGYSLGFLLAR
				MCT1	SITVFFK
					DLHDANTDLIGR§
				OATP4A1	YEVELDAGVR
					ILGGIPGPIAFGWVIDK

***** Represent targets mainly located in the cytosolic fraction. § Peptides used for the quantification of the targets in the current study

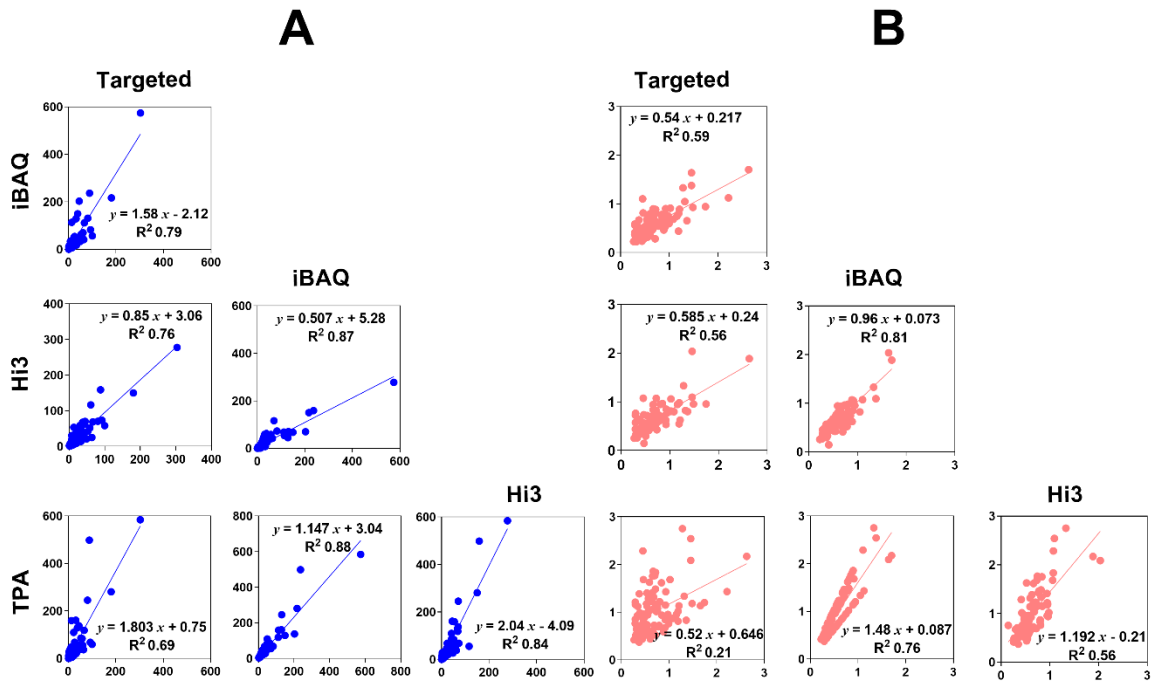

Supplementary Figure 7.1. Linear regression analysis to assess the possible correlations between (A) absolute quantification data and (B) disease-to-control ratios derived from analysis of pooled samples (normal and cirrhotic) using four quantification methods (targeted, Hi3, iBAQ and TPA approaches).

8 Chapter Eight

Proteomic Quantification of Drug-Metabolising Enzymes and Drug Transporters in Human Liver with Different Grades of Cirrhosis and PBPK Modelling of Disease Perturbation

Declaration

Eman El-Khateeb, Brahim Achour, Zubida M. Al-Majdoub, Jill Barber, Amin Rostami-Hodjegan

I carried out the experimental work, and the data analysis, created the graphs, and wrote the manuscript. Dr Brahim Achour was consulted on statistics, data analysis and edited the manuscript. Dr Zubida M. Al-Majdoub was consulted on the experimental methodology. Dr Jill Barber and Prof Amin Rostami-Hodjegan participated in the study design.

8.1. Abstract

Liver cirrhosis is a chronic disease that affects liver structure, protein expression and overall metabolic function. Abundance data for drug-metabolising enzymes and transporters (DMET) across all stages of disease severity are scarce. Levels of these proteins are crucial for the accurate prediction of drug clearance in hepatically-impaired patients using physiologically-based pharmacokinetic (PBPK) models, which can be used to guide the selection of more precise dosing. This study aimed to determine the absolute abundance of 51 DMET proteins in human liver across the three degrees of cirrhosis severity (n = 32; 6 mild, 13 moderate, and 13 severe), compared to histologically-normal controls (n = 14), using QconCAT-based targeted proteomics. The results revealed significant reduction in abundance of the majority of enzymes and transporters, from control, by 30-50% in mild, 40-70% in moderate, and 50-90% in severe cirrhosis groups. Cancer and/or NAFLD-related cirrhosis showed larger deterioration in levels of CYP3A4, 2C8, 2E1, 1A6, UGT2B4/7, CES1, FMO3/5, EPHX1, MGST1/3, BSEP, and OATP2B1 than the cholestasis set. Application of abundance changes in PBPK models of repaglinde, dabigatran etexilate and zidovudine successfully recovered disease-related alterations in drug exposure. The current study demonstrates the utility of proteomics-informed PBPK modelling in predicting the differential effect of the severity of liver cirrhosis on drug metabolism and disposition.

8.2. Introduction

Cirrhosis occurs in late-stage liver fibrosis (scarring) as a result of different types of liver disease, such as hepatitis, cholestasis, cancer, alcoholic and non-alcoholic fatty liver disease (Bataller & Brenner, 2005). It leads to alterations to hepatic architecture, which cause changes in blood flow, protein binding, and expression of drug-metabolising enzymes (DMEs) (Johnson, et al., 2010). These changes lead to variable pharmacokinetics (PK) of many drugs in cirrhotic populations, compared to healthy subjects, through multiple mechanisms, such as a reduction in the absolute number of functioning cells in the liver, changes in abundance and/or activity of enzymes in surviving hepatocytes, and impaired drug and oxygen entry into liver cells (Elbekai, et al., 2004). Therefore, patients with liver disease are liable to decreased capacity of the liver to eliminate drugs and may require specific drug dosage adjustment (FDA, 2003).

In drug development, dedicated PK studies on patients with different degrees of hepatic impairment (HI) are recommended; however, such studies are not conducted for most drugs approved by regulatory agencies, and patients with hepatic impairment currently receive these drugs with no dosage guidance (Jadhav, et al., 2015). Recent FDA guidelines recommended the inclusion of HI patients into the early phases of clinical studies with close monitoring of side effects (FDA, 2020). Implementation of this recommendation may require time, and alternate approaches, such as the use of physiologically-based pharmacokinetic (PBPK) models, are therefore applied for predicting changes in drug exposure and guiding dose adjustment in HI populations (Heimbach, et al., 2020). These HI PBPK models incorporate either *in vitro* abundance data from immunoblotting studies or *in vivo* activity data using selective probe substrates administered to patients with liver disease (Johnson, et al., 2010). The highlighted strategies are limited to protein targets that have specific antibodies or probe substrates. More recently, the use of LC-MS proteomics in the quantification of phase I and II

enzymes as well as transporters has contributed useful data, which have so far been only limited to the severe stage of cirrhosis and do not cover some key aetiologies of the disease (Prasad, et al., 2018; Wang, et al., 2016). Therefore, the aim of this study was to assess the impact of cirrhosis at different degrees of disease severity, classified according to the Child-Pugh (CP) system (Pugh, et al., 1973) (as Mild, CP-A, Moderate, CP-B, and Severe, CP-C). Further, the possible effects of disease aetiologies associated with cirrhosis, such as non-alcoholic fatty liver disease (NAFLD), alcoholic fatty liver, biliary disease and cancer, on the expression of enzymes and transporters were investigated.

8.3. Methods

8.3.1. Liver samples and donor characteristics

Human liver microsomal (HLM) samples ($n = 46$) representing four sets: histologically-normal control group (n = 14, Supplementary Table 8.1) and three cirrhotic groups (n = 32, Supplementary Table 8.2), divided according to the severity of cirrhosis using CP scoring into: CP-A or mild cirrhosis group (n = 6), CP-B or moderate cirrhosis group (n =13), CP-C or severe cirrhosis group (n = 13). These 32 cirrhosis samples are also subdivided according to liver disease associated with cirrhosis into: non-alcoholic fatty liver disease (NAFLD) associated cirrhosis (n = 8), biliary disease associated cirrhosis (n = 13), cancer associated cirrhosis (n = 9), and alcoholic fatty liver disease (n = 2).

Individual liver tissue samples were provided by Cambridge University Hospitals Tissue Bank (Cambridge, UK), and HLM fractions were prepared by differential centrifugation, as reported previously (El-Khateeb, et al., 2020). This study is covered by ethical approval from the Health Research Authority and Health and Care Research Wales (HCRW) (Research Ethics Committee Approval Reference 18/LO/1969). Anonymised demographic and clinical data for the donors were previously reported (El-Khateeb, et al., 2020) and are summarised in

Supplementary Table 8.1 and Supplementary Table 8.2. The average age for the control group was 66 years (range: 36 to 83 years). The average age of cirrhosis patients was 60 years (range: 39 to 70 years). The percentage of female subjects was 29% in the control group and 39% in the cirrhosis group. In addition to individual samples, a pool of normal samples was prepared by mixing 6 µl from each individual HLM fraction and was used to assess the analytical variability between and within batches of samples.

8.3.2. Sample preparation for proteomics

Three stable isotope (^{13}C) labelled concatenated concatemers (QconCATs) (Russell, et al., 2013) were spiked into 70 µg of each individual HLM sample as internal standards: 0.351 µg of MetCAT [QconCAT standard for the quantification of cytochrome P450 enzymes (CYPs) and uridine-5'-diphospho-glucuronosyltransferases (UGTs)], 0.450 µg of NuncCAT [QconCAT for the quantification of non-CYP, non-UGT enzymes] and 0.165 µg of TransCAT [QconCAT for the quantification of transporters]. The samples were also spiked with a mixture of unlabelled exogenous protein standards [0.126 µg bovine serum albumin (BSA), 0.037 µg yeast aldehyde dehydrogenase (ADH) and 0.168 µg horse myoglobin] to monitor experimental conditions and enable label-free quantification of the liver proteome.

Filter-aided sample preparation (FASP) (Wiśniewski, et al., 2009) was used for sample preparation, as previously described with minor modifications (Al Feteisi, et al., 2018; Couto, et al., 2019). Sample mixtures were solubilised by incubation with sodium deoxycholate (10% w/v final volume), 1,4-dithiothreitol (DTT) was added at a final concentration of 100 mM, and the protein mixture was incubated at room temperature for 10 min. Reduction of protein disulfide bonds was carried out by incubation at 56°C for 40 min. Amicon Ultra 0.5 ml centrifugal filters, 3 kDa molecular weight cut-off, (Millipore, Nottingham, UK) were conditioned by brief centrifugation of 400 µl of 0.1 M Tris-HCl, pH 8.5, at 14000*g* at room

temperature. Protein samples were then transferred to the conditioned filter units, followed by centrifugation at 14000*g* at room temperature for 30 min. Alkylation of reduced cysteines was performed by incubation with 100 µl of 50 mM iodoacetamide in the dark for 30 min at room temperature. After alkylation, deoxycholate removal was performed by buffer exchange using two successive washes with 8 M urea in 100 mM Tris-HCl (pH 8.5), 200 µl each. To reduce urea concentration, additional washes (3 x 200 µl) were performed using 1 M urea in 50 mM ammonium bicarbonate (pH 8.5). For each wash, the buffer (200 µl) was added to the filter, without mixing, centrifuged at 14000*g* at room temperature for 20 min, leaving a volume of approximately 20 µl in the filter. The filtrate containing small molecules, such as detergent, was discarded. Protein digestion was achieved using LysC twice (LysC:protein ratio 1:50, 2 hours each, at 30°C), then trypsin digestion was carried out (trypsin:protein ratio 1:25) for 12 hours at 37°C and another equivalent treatment for an extra 6-hour incubation. Peptides were recovered from the filter by centrifugation (14000*g*, 20 min); a second collection was achieved by adding 0.5 M NaCl (100 µl) to the filter and centrifugation at 14000*g* for another 20 min. The collected peptides were lyophilised to dryness using a vacuum concentrator at 30ºC and with vacuum in aqueous mode; the time required was in the range 1-3 hours and was sample-dependent. Lyophilised peptides were reconstituted in 20% (v/v) acetonitrile in water, acidified with 2% (v/v) trifluoroacetic acid, then desalted using C18 spin columns according to the manufacturer's instructions (Nest group, USA). The peptides were lyophilised and stored at −80°C until mass spectrometric analysis.

8.3.3. Liquid chromatography and tandem mass spectrometry (LC-MS/MS)

Lyophilised peptides were re-suspended in 70 µl of 3% (v/v) acetonitrile in water with 0.1% (v/v) formic acid. Digested samples were analysed by LC-MS/MS using an UltiMate® 3000 Rapid Separation LC (RSLC, Dionex Corporation, Sunnyvale, CA) coupled to a Q Exactive HF Hybrid Quadrupole-Orbitrap mass spectrometer (Thermo Fisher Scientific, Waltham, MA)

mass spectrometer. Mobile phase A was 0.1% formic acid in water and mobile phase B was 0.1% formic acid in acetonitrile, and peptides were eluted on CSH C18 analytical column (75 mm x 250 µm inner diameter, 1.7 µm particle size) (Waters, UK). A 1 µl aliquot of the sample was transferred to a 5 µl loop and loaded onto the column at a flow rate of 300 nl/min for 5 min at 5% B. The loop was then taken out of line and the flow was reduced from 300 nl/min to 200 nl/min over 0.5 min. Peptides were separated using a gradient from 5% to 18% B in 63.5 min, then from 18% to 27% B in 8 min, and finally from 27% B to 60% B in 1 min. The column was washed at 60% B for 3 min before re-equilibration to 5% B in 1 min. At 85 min, the flow was increased to 300 nl/min until the end of the run at 90 min. Mass spectrometry data were acquired in a data-dependent manner for 90 min in positive mode. Peptides were selected for fragmentation automatically by data dependent analysis on a basis of the top 12 peptides with *m/z* between 300 to 1750 Th and a charge state of 2+, 3+, and 4+ with dynamic exclusion set at 15 sec. The MS resolution was set at 120,000 with an AGC target of 3E6 and a maximum fill time set at 20 ms. The MS2 resolution was set to 30,000, with an AGC target of 2E5, a maximum fill time of 45 ms, isolation window of 1.3 Th and a collision energy of 28 eV.

8.3.4. Proteomic data analysis

Proteins were identified by searching peptide MS/MS data against UniProtKB database (http://www.uniprot.org/) using MaxQuant version 1.6.10.43 (Max Planck Institute of Biochemistry, Martinsried, Germany). QconCAT-based quantification was carried out as previously described (Achour, et al., 2021; Al-Majdoub, et al., 2019; Harwood, et al., 2015) to measure 15 CYPs and 9 UGTs (MetCAT), in addition to UGT2B17, 22 non-CYP/non-UGT drug-metabolising enzymes (NuncCAT) and 30 transporters (TransCAT). A protein was considered quantifiable in liver microsomal samples if (a) there was evidence of its expression in the liver (Human Protein Atlas, https://www.proteinatlas.org/), (b) it was localised in a membrane (Uniprot, https://www.uniprot.org/), (c) it was identified by at least one razor or one

unique peptide, and (c) it was detected in a sufficient number of samples (at least 3 samples/group). A list of the peptides that constitute the QconCATs used in this study is presented in Supplementary Table 8.3. The abundance of each target protein was calculated using the Equation 1.

$$[Protein] = [QconCAT] \times I_{i,L}/I_{i,H} \quad (1)$$

Where [*Protein*] is the protein abundance based on surrogate peptide *i*, measured in units of pmol/mg microsomal protein. $I_{i,L}/I_{i,H}$ is the ratio of the intensity of the light (analyte) to the heavy (QconCAT-derived) surrogate peptide, and [*QconCAT*] is the concentration of the QconCAT standard measured using Equation 2.

$$[QconCAT] = [\mathrm{NNOP}] \times I_{j,H}/I_{j,L} \quad (2)$$

Where $I_{j,H}/I_{j,L}$ is the ratio of the intensity of the heavy (QconCAT-derived) to the light (spiked in) NNOP standard peptide, and [NNOP] is the concentration of the NNOP peptide standard expressed in units of pmol/mg microsomal protein, analysed by the mass spectrometer. The intensity ratios were corrected for isotope labelling efficiency prior to use in the equations (Achour, et al., 2018; Russell, et al., 2013). Unlabelled NNOP peptides, EGVNDNEEGFFSAR, GVNDNEEGFFSAR and AEGVNDNEEGFFSAR were added to the samples at 376, 700 and 156 fmol, respectively, to quantify the TransCAT, MetCAT and NuncCAT, respectively.

The measured abundance values of each protein were scaled up to their corresponding levels in tissue (pmol/g liver) using individual microsomal protein content per gram of liver (MPPGL) for each sample, as previously reported (El-Khateeb, et al., 2020).

8.3.5. Comparing abundance of enzymes and transporters among sample groups

The absolute abundance values of the quantified liver enzymes and transporters in mild, moderate, severe cirrhosis samples (classified according to CP score) were compared and assessed against abundance in the control group. A secondary aim of the study was to investigate the impact of disease aetiology or associated liver disease on the individual abundance data for each target. For this purpose, the samples were grouped into NAFLD, cancer, and cholestasis related cirrhosis. Targets that were detected in at least 3 samples per group were included in the comparison. Alcohol-related cirrhosis was represented by only 2 samples, and therefore this group was excluded from the comparison. To rule out the confounding effect of disease severity, this comparison was restricted to moderate disease, which was the only disease grade that included a sufficient number of samples in each aetiology.

8.3.6. Assessment of the degree of technical and analytical variability

Nine samples, representing all groups (2 normal, 2 cancer, 1 alcohol, 2 cholestasis, and 2 NAFLD samples), were prepared in triplicate and analysed by LC-MS/MS under the same conditions. The data were used to assess technical variability in quantification. A pool of normal samples (n = 14) was prepared once and analysed twice in each of 5 batches of samples (10 overall runs) to assess intra and inter-batch variability. Technical and batch-to-batch variability was evaluated using the coefficient of variation (CV) of replicates from different analyses in each set and across batches.

8.3.7. Statistical analysis

The samples were classified based on disease severity, using the CP score, and according to the associated disease. Statistical analysis of the data was carried out and graphs were created using GraphPad Prism version 7.0 (La Jolla, California, USA). Shapiro-Wilk normality test

was applied to assess normality of distribution of the data. In the absence of normal distribution, non-parametric statistics was used and the data were presented as median and 95% confidence interval (CI). Equality of variance was assessed by a modified Levene's test (Brown-Forsythe test). Differences in abundance values between the control group and the three levels of disease severity (mild, moderate, and severe) were assessed using Kruskal-Wallis ANOVA test with statistical significance cut-off set at 0.05. If this test indicated statistically significant differences, post-hoc Mann-Whitney test was performed for pairwise comparison. Similar ANOVA analysis with post-hoc tests were used to compare the data for the control group and three disease aetiologies (cancer, cholestasis, and NAFLD) at the same degree of severity of cirrhosis (moderate set). Statistical significance was again considered with a cut-off *p*-value of 0.05 and Bonferroni-corrected for multiple iterations to $p < 0.0085$* and $p < 0.0017$** (six iteration). Correlation between the abundance of hepatic transporters and log-transformed total serum bilirubin for each individual patient was performed using Spearman test (Rs). Correlations were considered significant if Rs was at least 0.5 and the probability was < 0.05.

8.3.8. Application of proteomic data in PBPK models of cirrhosis

Three previously verified PBPK models were used to confirm applicability of the collected proteomic data in the prediction of drug exposure in cirrhosis populations. In this modelling exercise, we used repaglinide (an antidiabetic agent and a substrate for CYP2C8, CPY3A4, and OATP1B1), dabigatran etexilate (a prodrug converted by carboxylesterases CES1 and CES2 to the active anticoagulant dabigatran, which is mainly excreted unchanged in urine), and zidovudine (an antiretroviral drug and a substrate for UGT2B7 and, to a lesser degree, metabolised by CYP/CYP reductase).

For each drug, simulations with virtual cirrhosis populations were performed using the following two methods and the outputs were compared:

1- Prototeomic_sim_cirrhosis method: The disease to normal abundance ratio from the current study was used as a scalar for the intrinsic clearance in each cirrhosis population (CP-A, CP-B, or CP-C). As this ratio was based on enzyme abundance per gram of tissue, changes in MPPGL between diseased samples and normal livers have already been accounted for in this ratio. Therefore, the functional liver volume hypothesised by Johnson et al (2010) was returned back to normal values measured in healthy populations. Physiological changes other than enzyme abundance per g liver tissue and liver size scalar were kept the same as in Simcyp V19 population library, as previously reported by Johnson et al. (2010) and summarised here in Supplementary Table 8.4.
2- Simcyp_cirrhosis method: Default Simcyp V 19 settings in cirrhosis populations were kept the same including abundance data and liver volume scalars presented in Supplementary Table 8.4.

Demographic data for both healthy and cirrhosis individuals were reported previously for repaglinide (Hatorp, et al., 2000), dabigatran etexilate (Stangier, et al., 2008), and zidovudine (Taburet, et al., 1990) and are summarised in Supplementary Table 8.5. Drug-specific input parameters and changes in the intrinsic clearance of the three drugs in cirrhosis populations are presented in Table 8.1. All parameters were derived from the simulator's library unless otherwise stated, as shown in Table 8.1. Simulation trials were set to 10 trials of 10 individuals each. The ratio of the area under the curve predicted by the model (AUC_{pred}) and the observed value (AUC_{obs}) was calculated and considered acceptable if the value was between 0.5 to 2 fold. The ability of the model to predict changes in exposure due to cirrhosis was performed by comparing the ratio of AUC for the diseased population to that for the healthy population (AUCR) in both simulated and observed data. The model's prediction was considered acceptable if the ratio of predicted AUCR to observed AUCR was between 0.5 and 2 fold.

Table 8.1. Input parameters used for physiologically based pharmacokinetic (PBPK) simulations of repaglinide, dabigatran etexilate and zidovudine.

	Repaglinide				Dabigatran etexilate*			Zidovudine				
PBPK Parameter	**Control**	**Cirrhosis**		**Reference**	**Control**	**Cirrhosis**	**Reference**	**Control**	**Cirrhotic**			**Reference**
		CP-B	**CP-C**			**CP-B**			**CP-A**	**CP-B**	**CP-C**	
Molecular mass (g/mol)	452.6			Simcyp library	627.75		Simcyp library	267.2				Simcyp library
LogP	5.18			Simcyp library	3.8		Simcyp library	0.05				Simcyp library
Acid dissociation constant (pKa)	4.18, 6.02			Simcyp library	4, 6.7		Simcyp library	9.7				Simcyp library
Blood-to-plasma ratio	0.566			Simcyp library	1.26		Simcyp library	0.91				Simcyp library
Unbound fraction (F_u)	0.026			(Hatorp, et al., 2000)	0.063		Simcyp library	0.8				Simcyp library
Absorption Model	First order			Simcyp library	ADAM model		Simcyp library	First order				
	Peff,man permeability 4.6 10^{-4} cm/s			Simcyp library	$P_{trans,0}$ permeability 6×10^{-6} cm/s (Mechanistic passive regional permeability predictor)		Simcyp library	Fraction absorbed $F_a = 0.83$				Predicted by advanced dissolution, absorption, and metabolism model (Prasad, et al., 2018)
k_a (h^{-1})	-				-			4.05				(Zhang & Unadkat, 2017)
Distribution model	Full PBPK			Simcyp library	Full PBPK		Simcyp library	Minimal PBPK model				(Zhang, et al., 2017)
Steady-state volume of distribution (V_{ss}, L/kg)	0.226			Predicted by Rodgers & Rowland Method (2007)	15.08		Predicted by Rodgers & Rowland Method (2007)	1.1				(Zhang, et al., 2017)
Renal clearance (L/h)	0.0128			Simcyp library (van Heiningen, et al., 1999)	0			13.2				(Singlas, et al., 1989; Taburet, et al., 1990)
***CL*int,$_{CYP2C8}$** (μl/min per mg protein)	93.01	34 (↓63%)	22.6 (↓75%)	(Varma, et al., 2013), & proteomic data from the current study	-							

	Repaglinide				Dabigatran etexilate*			Zidovudine				
PBPK Parameter	**Control**	**Cirrhosis**		**Reference**	**Control**	**Cirrhosis**	**Reference**	**Control**	**Cirrhotic**			**Reference**
		CP-B	**CP-C**			**CP-B**			**CP-A**	**CP-B**	**CP-C**	
***CL*int,$_{CYP3A4}$** (μl/min per mg protein)	38	8.7 (↓77%)	7.6 (↓80%)		-							
CES1 **Vmax** (pmol/min/mg S9 protein) **Km** (µM) **Fuinc** **Liver scalar** **Intestine scalar** **Kidney scalar**	-				17588 33.5 0.692 1 0.004 0.01	8442.24 (↓72%) 33.5 0.692 1 0.004 0.01	Simcyp library & proteomic data from the current study					
CES2 **Vmax** (pmol/min/mg S9 protein) **Km (µM)** **Fuinc** **Liver scalar** **Intestine scalar** **Kidney scalar**	-				46.2 15.4 0.692 1 10 0	129.36 (↓52%) 15.4 0.692 1 10 0	Simcyp Library & proteomic data from the current study					
***CL*int,$_{UGT2B7}$** (μl/min per mg protein)	-				-			29.5	16.2 (↓45%)	8.85 (↓70%)	4.2 (↓86%)	Estimated from literature (Singlas, et al., 1989; Taburet, et al., 1990) & proteomic data from the current study
Additional clearance $CL_{int,\ P450\ reductase}$ (L/h)	-				-			3.07	1.47 (↓52%)	1.63 (↓47%)	1.1 (↓65%)	Estimated from literature (Stagg, et al., 1992) & proteomic data from the current study
OATP1B1 **CLint,T** µl/min per million cells	838.11	348.39 (↓58%)	248.60 (↓70%)	Simcyp library & proteomic data from the current study	-							

* Dabigatran is the active metabolite that is mainly eliminated by the kidney; the input parameters were kept the same as the default in Simcyp V19 library as no abundance data were required to be modified.

8.4. Results

8.4.1. Quality and scaling of the proteomic data

In this study, we applied QconCAT-based targeted proteomics to investigate changes in protein expression of liver enzymes and transporters across three degrees of cirrhosis severity relative to histologically-normal liver. The targets included 14 CYPs, 9 UGTs, 9 non-CYP and non-UGT enzymes and 19 transporters. Technical and batch-to-batch variabilities were within 30% for 90% and 92% of targets, respectively (Supplementary Figure 8.1). The targets that reflected the highest variability (>30%) were of low abundance and were not detected consistently. The lower limit of quantification (LLOQ) for consistently quantified targets was 0.08 pmol/mg protein (translating to an average tissue content of ~2 pmol/g liver) based on a cut-off technical variability of 20% in quality control samples.

The abundance levels measured in pmol/mg membrane protein were scaled up to tissue levels using MPPGL values for each individual sample. Individual MPPGL values were previously reported for the same set of samples (El-Khateeb, et al., 2020) and are summarised in Supplementary Table 8.6. The median MPPGL for the control group was 37.3 (range 30.4 - 63.6 mg/g), whereas for the cirrhotic samples, it was 30.8 (range 12.9 - 49.1 mg/g). We used the measured tissue levels of enzymes and transporters to compare abundance and model differences in drug exposure between cirrhotic and normal sets of samples.

8.4.2. Abundance of drug-metabolising enzymes and transporters in livers with different severities of cirrhosis

A summary of the abundance of drug-metabolising enzymes and transporters is presented in Supplementary Table 8.8. The data were not normally distributed (Shapiro-Wilk test, $p < 0.05$) and variance within severity groups was homogeneous (Brown-Forsythe test, $p > 0.05$). Accordingly, non-parametric statistics was used to assess differences between groups

(Kruskal-Wallis and post-hoc Mann-Whitney tests). Figure 8.1,Figure 8.2, Figure 8.3, and Figure 8.4 show the individual abundance values of CYP, UGT, non-CYP non-UGT and transporter targets, respectively, with the medians and 95% confidence intervals (CI) in each cirrhosis group, compared to control.

Kruskal-Wallis ANOVA test showed significant differences ($p < 0.05$) for most of the targets of interest, except UGT1A1 ($p = 0.051$), UGT 1A3 ($p = 0.34$), MDR3 ($p = 0.051$), MRP4 ($p = 0.25$), BCRP ($p = 0.78$), ASBT ($p = 0.18$), and OATP1A2 ($p = 0.11$). For targets that showed significant differences, post-hoc Mann-Whitney test with Bonferroni corrected *p*-value was applied for pairwise comparisons. For mild cirrhosis, median abundance was significantly lower than control for only six proteins: CES1 (by 47%, $p = 0.003$*), FMO3 (by 37%, $p < 0.001$**), EPHX1 (by 41%, $p = 0.005$*), MGST3 (by 51%, $p = 0.003$*), MRP2 (54%, $p < 0.001$**) and OATP1B1 (by 54%, $p < 0.001$**). For Moderate cirrhosis group, some targets showed a statistically significant reduction from control, by 40 to 50%, such as MGST1, P-gp, MRP3, OCT3, and ATP1A1. Several targets showed a more significant decline by up to 77% from the control group, including CYP3A4, 1A2, 2C8, 2C9, 2E1, 2D6, 2A6, 2J2, 4F2, UGT1A6/9, 2B4/7, CES1/2, FMO3, EPHX1, MGST3, OAT2/4, OCT1, MRP2/6, BSEP, OATP1B1, OATP2B1, NTCP, and MCT1. The largest reduction was observed with most of the targets in the severe grade of cirrhosis. The level of reduction ranged from 40 to 55% with P-gp, MRP3, ATP1A1, and OCT3, while a decline of 60 to 78% was noted for CYP2C8/9/18, 2D6, 2A6, UGT1A4/6, 2B4, 2B15, 1A9, CES2, FMO5, POR, MGST1/3, BSEP, MRP6, OAT 2/4, OATP1B1, 2B1, NTCP, and MCT1. Further, CYP3A4, 1A2, 2E1, 2J2, 4F2, 2C9/19, UGT2B7, CES1, FMO3, EPHX1, MRP2, and OCT1 showed 80% to 98% reduction in the disease group relative to control. By contrast, CYP2B6 and OATP1B3 did not show statistically significant change in any of the three cirrhosis groups compared to control in spite of showing significant differences across groups with the Kruskal-Wallis ANOVA test

($p < 0.05$). Both CYP2B6 and OATP1B3 have not been consistently detected in the set of samples.

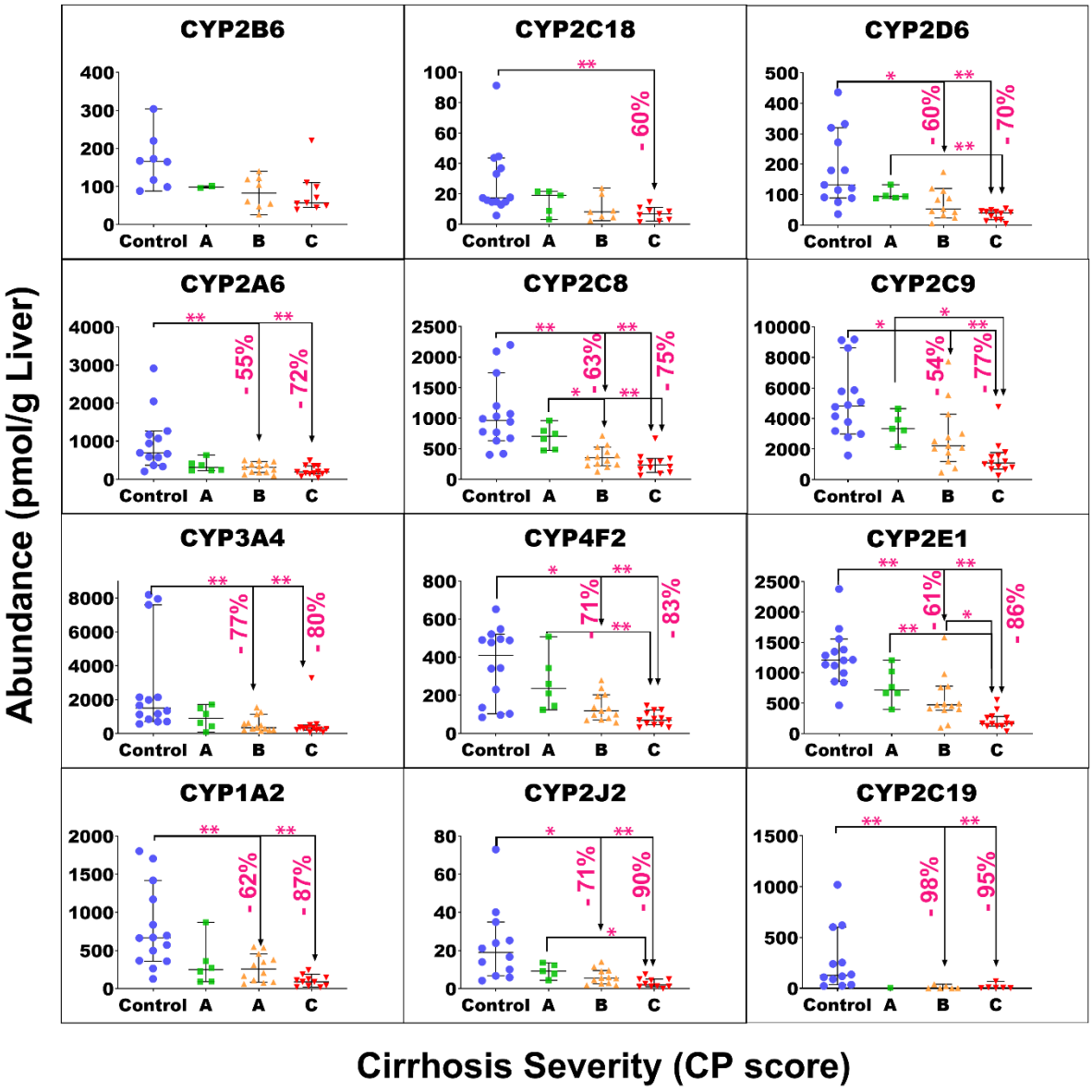

Figure 8.1. Individual abundance values of cytochrome P450 enzymes in pmol per g of liver tissue from normal control compared to different grades of liver cirrhosis stratified using Child-Pugh (CP) score (A: CP-A or mild; B: CP-B or moderate and C: CP-C or severe). Horizontal lines represent medians and error bars are the 95% confidence intervals. Stars represent comparisons with statistical significance (*p < 0.0085 and **p <0.0017), while the percentages represent the degree of change from normal control.

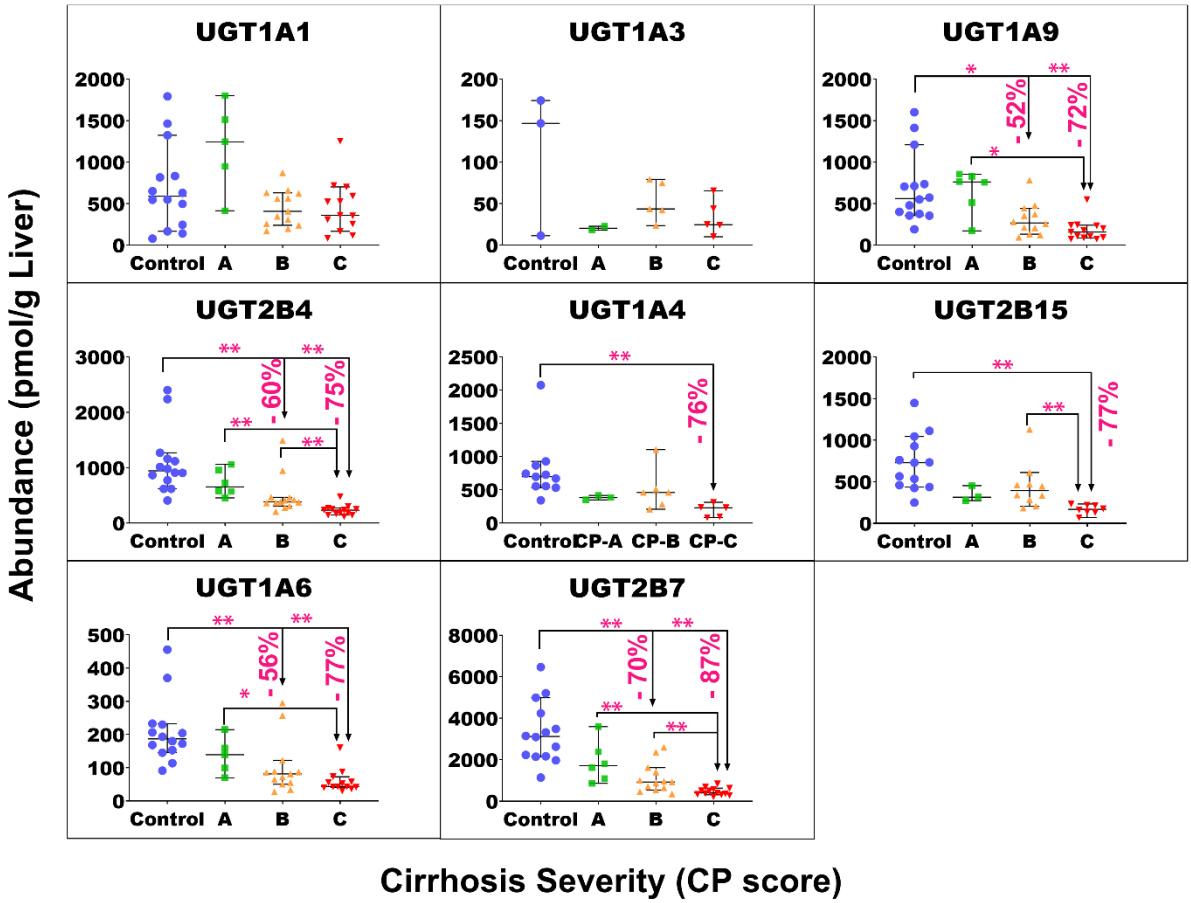

*Figure 8.2. Individual abundance values of uridine-5'-diphospho-glucuronosyltransferase (UGT) enzymes in pmol per g of liver tissue from normal control compared to different grades of liver cirrhosis stratified using Child-Pugh (CP) score (A: CP-A or mild; B: CP-B or moderate and C: CP-C or severe). Horizontal lines represent medians and error bars are the 95% confidence intervals. Stars represent comparisons that are statistically significant (*p < 0.0085 and **p <0.0017), while the percentages represent the degree of change from normal control.*

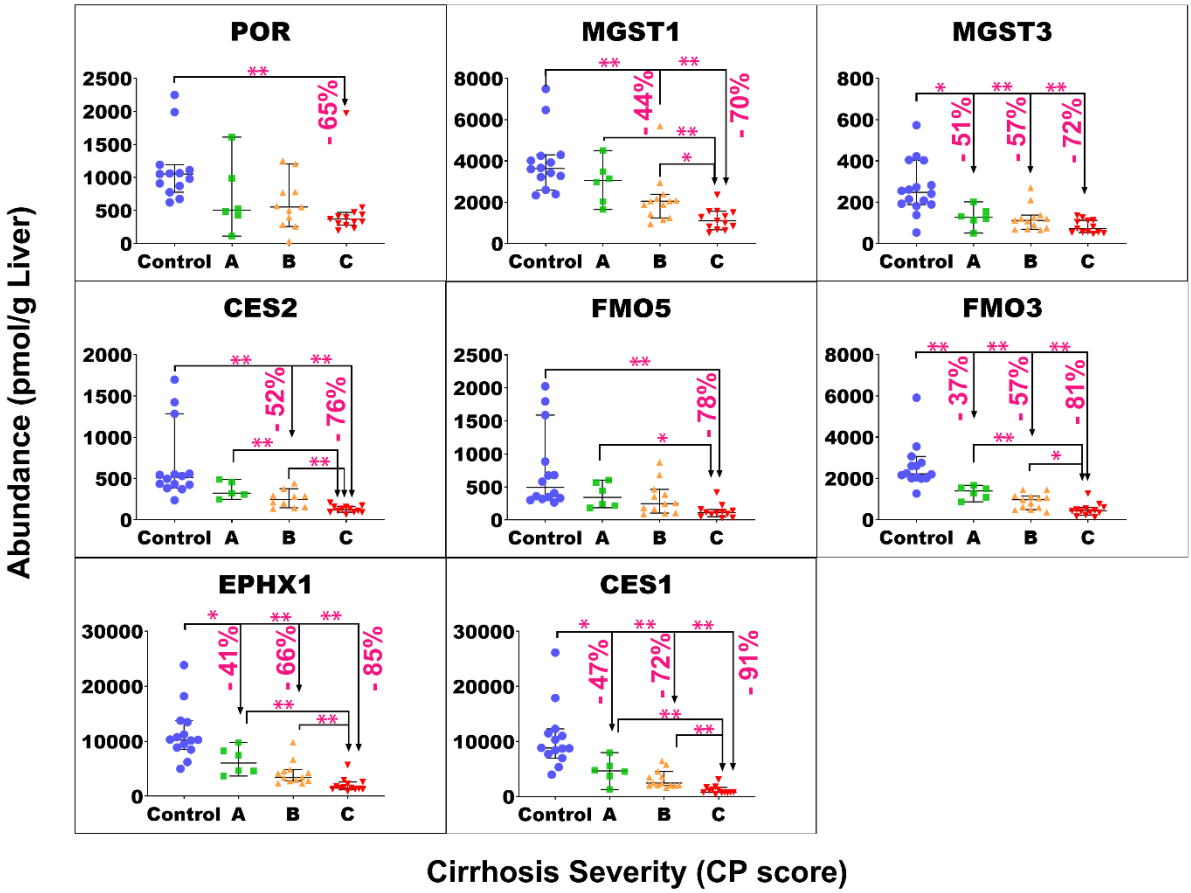

*Figure 8.3. Individual abundance values of non-CYP and non-UGT enzymes in pmol per g of liver tissue from normal control compared to different grades of liver cirrhosis stratified using Child-Pugh (CP) score (A: CP-A or mild; B: CP-B or moderate and C: CP-C or severe). Horizontal lines represent medians and error bars are the 95% confidence intervals. Stars represent comparisons that are statistically significant (*p < 0.0085 and **p <0.0017), while the percentages represent the degree of change from normal control.*

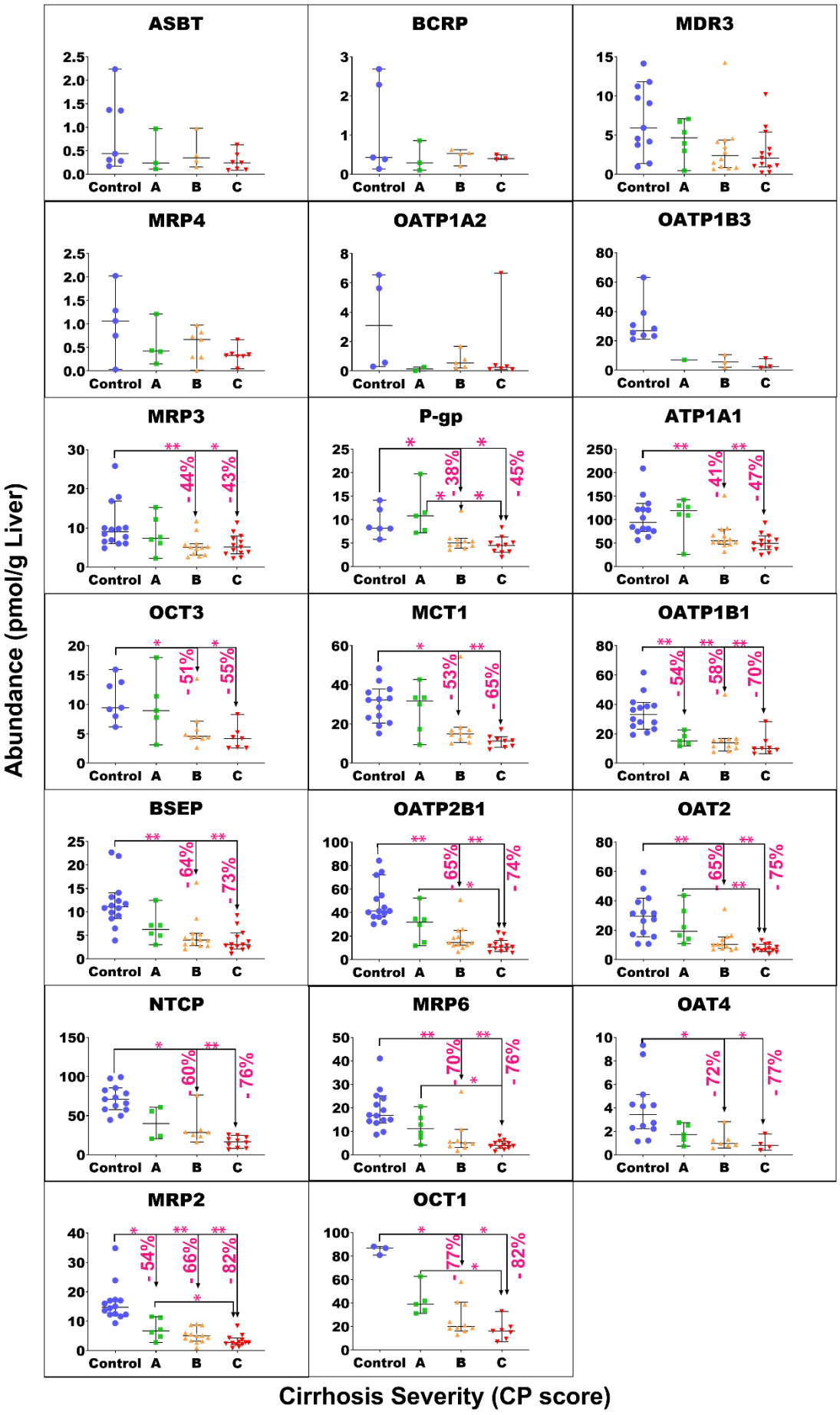
ASBT
BCRP
MDR3
MRP4
OATP1A2
OATP1B3
MRP3
P-gp
ATP1A1
OCT3
MCT1
OATP1B1
BSEP
OATP2B1
OAT2
NTCP
MRP6
OAT4
MRP2
OCT1
Control A B C
- 44%
- 43%
- 38%
- 45%
- 41%
- 47%
- 51%
- 55%
- 53%
- 65%
- 54%
- 58%
- 70%
- 64%
- 73%
- 65%
- 74%
- 65%
- 75%
- 60%
- 76%
- 70%
- 76%
- 72%
- 77%
- 54%
- 66%
- 82%
- 77%
- 82%
Abundance (pmol/g Liver)
Cirrhosis Severity (CP score)

Figure 8.4. Individual abundance values of transporters in pmol per g of liver tissue from normal control compared to different grades of liver cirrhosis stratified using Child-Pugh (CP) score (A: CP-A or mild; B: CP-B or moderate and C: CP-C or severe). Horizontal lines represent medians and error bars are the 95% confidence intervals. Stars represent comparisons that are statistically significant (*p < 0.0085 and **p < 0.0017), while the percentages represent the degree of change from normal control.

8.4.3. Relative distribution of enzymes in cirrhotic liver

The order in abundances of hepatic metabolising enzymes (CYPs, UGTs, and others) was generally similar in cirrhosis compared to control with few exceptions (Supplementary Figure 8.2). CYP2C9 and CYP3A4 were the most abundant CYPs across the normal and cirrhosis groups. CYP2E1 was one of the top 3 highest expressed CYP enzymes in the control, mild and moderate cirrhosis groups; however, it dropped down to the 5th rank in the severe stage of the disease. UGT2B4 and 2B7 were the dominant UGTs in all groups, while UGT1A1 ranked the 5th in the control group and the 2nd in the mild and severe cirrhosis groups. Non-CYP and non-UGT enzymes did not show differences in their relative distribution between control and diseased livers.

8.4.4. Correlations between transporter abundances and total serum bilirubin levels

Increased levels of systemic bilirubin are a common symptom of liver disease. The mean total serum bilirubin level (± SD) was 11 ± 6.1 for the control group, 18.2 ± 6.0 in mild, 36.8 ± 21.7 in moderate, and 132.7 ± 135.3 µmol/L in severe cirrhosis. As transporter abundances were not normally distributed (Shapiro-Wilk test, $p < 0.05$), Spearman correlation analysis was used. Linear regression was used to assess scatter of the data. Correlations between the transporter abundance and log-transformed total bilirubin for liver donors showed moderate correlation (R^2 = 0.3-0.5; Rs = 0.5-0.8, $p < 0.05$), with a declining trend, in the case of bile efflux

transporters: P-gp, BSEP, MRP2, MRP3, and MRP6, and also uptake transporters: NTCP, MCT1, OCT1, OCT3, OATP2B1, OAT2, OAT4, and OATP1B1/1B3 (Supplementary Figure 8.3).

8.4.5. The effect of aetiology of liver cirrhosis on abundance of enzymes and transporters

Changes in the abundance of the targets relative to normal control varied according to liver disease present with or underlying cirrhosis. Considering samples with the same degree of severity (CP-B), cirrhosis associated with cancer and NAFLD showed a more significant reduction in the levels of most targets, relative to control, than cholestasis-related cirrhosis (Figure 8.5). Targets affected only by NAFLD-associated cirrhosis were CYP2C8, MGST1, MGST3, UGT2B4, FMO5, and BSEP, while targets that showed a significant reduction only with cancer-associated cirrhosis were CYP2E1 and UGT1A6. Targets significantly affected by both diseases were CYP3A4, FMO3, UGT2B7, OATP2B1, EPHX1 and CES1. The only target showing a significant reduction in cholestasis-associated cirrhosis was MRP2; expression of this transporter was also reduced with cancer but not with NAFLD. Further, the degree of difference across the disease groups was not statistically significant in the current study (Supplementary Table 8.7).

,

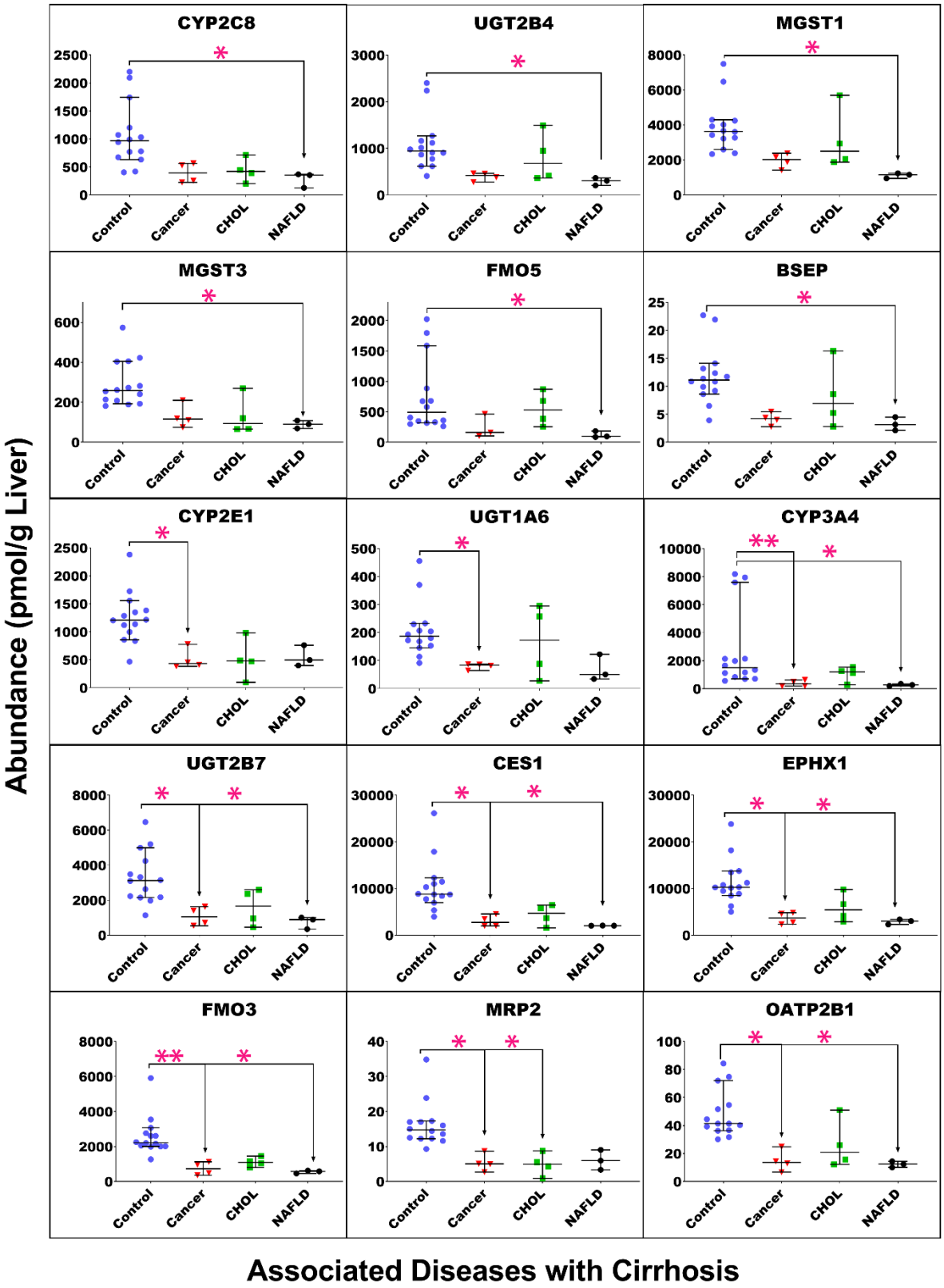

Figure 8.5. Individual abundance values of drug-metabolising enzymes and transporters in moderate cirrhosis groups classified by associated liver disease into cancer; CHOL,

cholestasis; and NAFLD, non-alcoholic fatty liver disease, compared to the control group. Horizontal lines represent medians and error bars are the 95% confidence intervals. Stars represent comparisons that are statistically significant (*p < 0.0085 and **p <0.0017).

8.4.6. The impact of cirrhosis-related changes in abundance on the performance of PBPK models

The proteomic data generated with cirrhosis samples at different grades of severity were applied in PBPK models for repaglinide (in a mixed CP-B&-C population) and dabigatran etexilate (in CP-B population). For dabigatran simulations, the model accounting for proteomic changes in CES1/2 in cirrhosis relative to normal was able to capture drug exposure in cirrhosis and was in agreement with output from Simcyp default settings for cirrhosis populations (<1% difference in AUC_{pred}) (Figure 8.6). For repaglinide, the $AUCR_{pred}$ using proteomic data from the current study was 4.9 compared to 2.8 with default Simcyp population settings (Supplementary Table 8.9). The ratio of the predicted AUCR ($AUCR_{pred}$) to the observed value ($AUCR_{obs}$) was 1.19 using abundance data from the current study and 0.68 using default Simcyp population data, both within 2 fold of the observed exposure change.

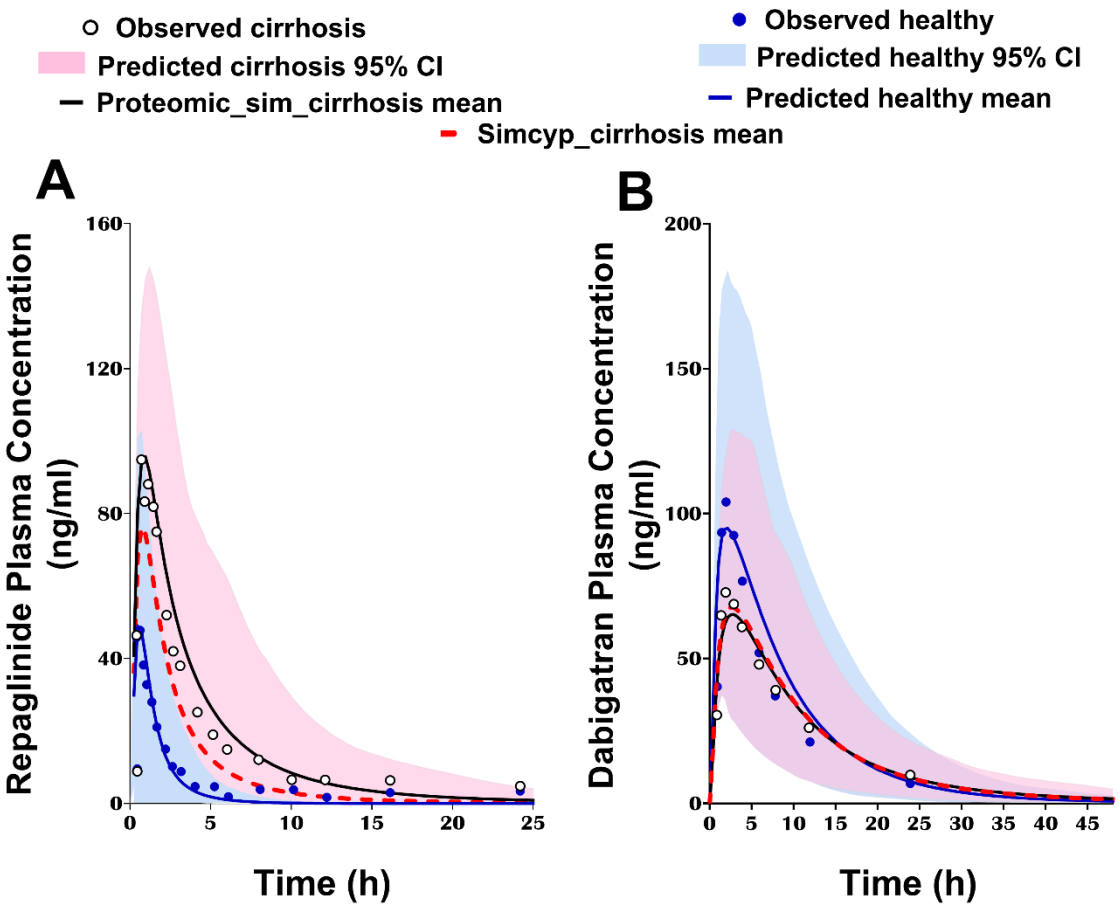

Figure 8.6. Repaglinide (A) and dabigatran (B) simulated plasma concentration-time profiles with changes in the abundance of metabolising enzymes and transporters using proteomic data from the current study (Proteomic_sim_cirrhosis mean; solid black lines), and default settings in Simcyp V19 (Simcyp_cirrhosis mean; dotted red lines) in cirrhosis populations, compared to profiles in a healthy population (blue line). The corresponding observed data are presented for diseased (white circles) and healthy individuals (blue circles). CI, confidence interval around the mean.

For zidovudine, adjusting the intrinsic clearance with proteomic data resulted in $AUCR_{pred}$ of 2.1 in CP-A, 3.4 in CP-B, 5.7 in CP-C (Figure 8.7). The predicted simulations adjusted with proteomic data showed AUC levels within 2 fold of the observed data. Predicted-to-observed AUCR for CP-A, B, and C with proteomic data were 0.62, 0.97, and 1.2, respectively. By

contrast, with default Simcyp abundance data, these values were not within 2 fold (0.38, 0.46, and 0.49, respectively), as shown in Supplementary Table 8.9.

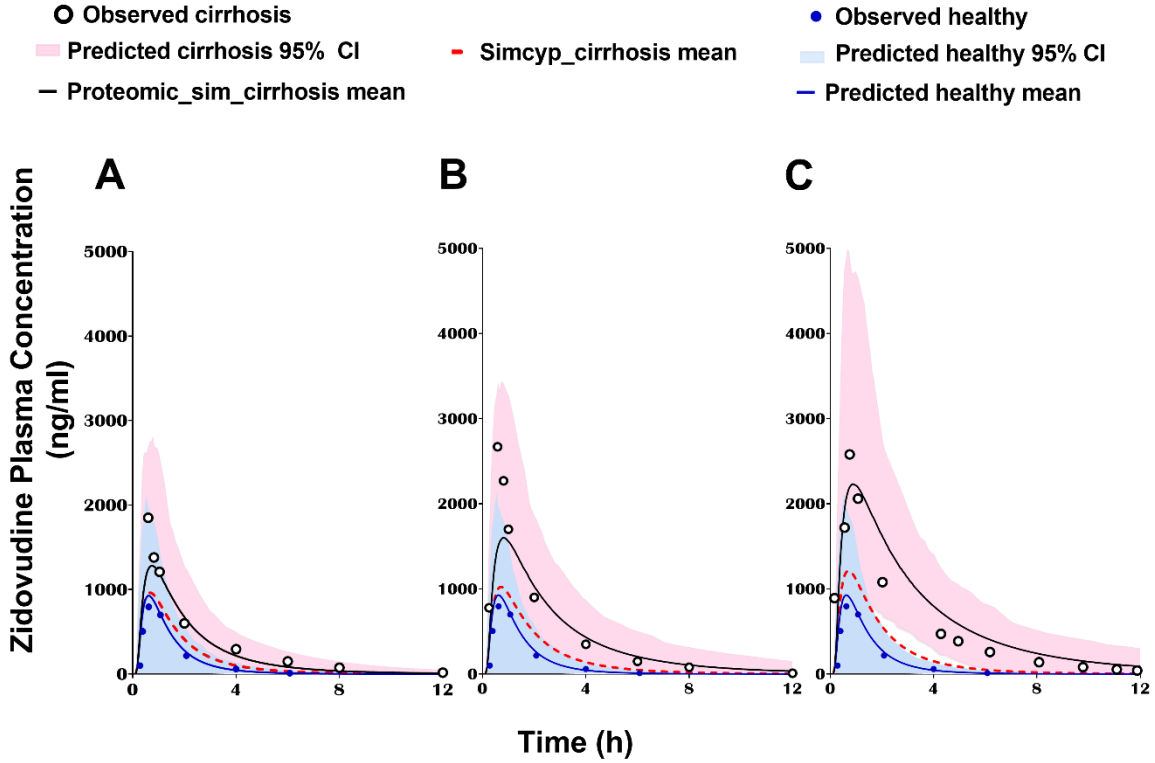

Figure 8.7. Zidovudine simulated plasma concentration-time profile with changes in the abundance of metabolising enzymes and transporters using proteomic data from the current study (Proteomic_sim_cirrhosis mean; solid black lines) and default settings in Simcyp V19 (Simcyp_cirrhosis mean; dotted red lines) in mild (A), moderate (B) and severe (C) cirrhosis populations, compared to the profile in a healthy population (blue line). The corresponding observed data are presented for diseased (white circles) and healthy individuals (blue circles). CI, confidence interval around the mean.

8.5. Discussion

Heterogeneity in chronic liver disease and the degree of change in hepatic metabolic function are a challenge in the selection of effective drug dosing to patients with impaired liver function. Specific alterations in the metabolic pathway by which a drug is eliminated is one of the contributing factors to this issue. This is because not all enzymatic reactions are affected by liver disease equally, even at the same disease severity, which is routinely determined clinically by the CP score. To the best of our knowledge, this study is the first to use quantitative LC-MS proteomics for the characterisation of changes in the expression of enzymes and transporters in three grades (mild, moderate and severe) of liver cirrhosis.

We observed progressive decline in abundance of enzymes and transporters with the severity of cirrhosis relative to control livers. The suppressed expression of enzymes and transporters, as reported in this study, is likely due to exposure to inflammatory cytokines in chronic inflammation and the resulting downregulation of gene expression. This has been reported for several chronic inflammatory diseases, such as cirrhosis, rheumatoid arthritis and cancer (Chung, et al., 2011; Lippitz & Harris, 2016; Prystupa, et al., 2015). The level of inflammatory cytokines, such as IL-6 and TNFα, increases gradually with cirrhosis progression (Tilg, et al., 1992), which supports the theory of inflammatory effect and corroborates the results of the current study.

Further, we assessed changes in relative distribution of enzymes in cirrhotic liver. Distribution pie charts of CYP and UGT protein abundances in the control group were in overall agreement with previous studies (Achour, et al., 2014; Couto, et al., 2019; Ohtsuki, et al., 2012; Prasad, et al., 2018). Notably, CYP2C9 was the most abundant CYP enzyme in control livers, which is in line with findings by Ohtsuki et al., (2012) and Couto et al., (2019). However, other studies had CYP3A4 as the most abundant CYP (Achour, et al., 2014; Prasad, et al., 2018). This

difference may be attributed to the origin of the control samples as ours were excised from histologically-normal samples adjacent to tumours and were not from healthy individuals. Similarly for UGTs, the order of quantified proteins was in agreement with results from previous studies (Izukawa, et al., 2009; Margaillan, et al., 2015; Prasad, et al., 2018). The rate of disease-driven deterioration in the enzyme abundance affects its relative distribution within its family. Most CYP enzymes did not show major differences in rank order with disease progression except for CYP2E1, which had a lower relative abundance in severe cirrhosis. The most abundant UGTs were UGT2B4 and 2B7 in disease and control groups. On the other hand, UGT1A1 relative abundance was higher in mild and severe stages of cirrhosis compared to controls. These changes might be important for drugs cleared by multiple pathways, with expected changes in the relative contribution of each pathway (f_m) with disease progression and the response to metabolic drug-drug interactions (Palatini & De Martin, 2016; Yu, et al., 2017).

The absolute abundance of UGTs in HLM fractions was consistently higher than that reported in post-mitochondrial supernatant (S9 fraction), as reported by Fallon et al., (2013), which is consistent with enrichment data in our samples (El-Khateeb, et al., 2020), leading to more robust measurements (Wang, et al., 2020). We quantified the abundance of CYP2B6 and UGT1A1 for the first time in cirrhotic liver; these proteins were below the limit of quantification achieved by other studies that used non-enriched samples, such as post-mitochondrial supernatant fractions (Prasad et al., 2018). Several targets, such as CYP3A4, 1A2, 2A6, POR, UGT1A4, UGT2B7, showed comparable change in severe cirrhosis from control to those reported by others (Prasad, et al., 2018). On the other hand, CYP2D6, 2E1, 2C8, 2C9, CES1 and CES2 were more affected in our data by severe stages of cirrhosis than reported in previous studies (Prasad, et al., 2018). The change in CYP2D6 was consistent with earlier reports (Frye, et al., 2006; Johnson, et al., 2010). These differences might be attributed not only to differences in disease causes but also to the fact that previous reports did not classify

samples based on full criteria of the CP scoring system (as we have done herein) and only considered transplantation to occur in severe stages of the disease, which is not accurate for some of the cases. Therefore, this could increase the likelihood of including moderately impaired patients, and possibly even mild cases, in the sample donors (Lucey, et al., 1997).

Several reports have claimed that phase II reactions are less affected by HI than oxidative phase I reactions (Hoyumpa & Schenker, 1991; Morgan & McLean, 1995; Park, 1996). Results from the current study show that expression of several UGTs, such as UGT1A6, 1A9, 2B4 and 2B7, was significantly impaired by cirrhosis, especially in moderate to severe stages, which reflected changes at a degree similar to that observed with most of CYP enzymes. For non-CYP and non-UGT metabolising enzymes, the current study quantified nine enzymes, resident in the endoplasmic reticulum membrane, for the first time in cirrhosis, and assess the degree of change in their abundances relative to the control. These include MGST1, MGST3, and FMO5. It is worth noting that changes in sulfotransferases and other cytosolic enzymes such as ADH1, ALDH1A1, AOX, NAT, and EPHX2 (whose surrogate peptides are present in the NuncCAT) were not investigated because we used microsomal fractions in this study.

The current study and previous reports suggest variability in the impact of cirrhosis on expression of transporters according to the disease severity and the underlying pathophysiology (viral, alcoholic and biliary diseases) (Drozdzik, et al., 2020; Taniguchi, et al., 2020; Wang, et al., 2016). The progressive decline in the expression of NTCP, OATP1B1/2B1, OCT1, BSEP, and MRP2 with increasing CP score is in line with previous findings by (Drozdzik, et al., 2020). By contrast to findings by Dorzdzik, et al., (2020) which suggested a lack of change in expression of BSEP, MRP3, OAT2, OCT3, and OATP1B3 in cirrhosis, we demonstrated a progressive decline in abundance of these transporters. This could be due to differences in disease aetiologies in the two set of samples. Although it was reported in previous studies that MRP4 is not normally detectable in healthy livers (Al-Majdoub et al., 2020), it was detectable

in our control group. This can also be attributed to the fact that these control samples are excised from histologically-normal samples adjacent to tumours and were not from healthy individuals.

Bilirubin level is a liver function test and a component of the Child-Pugh scoring system (Talal, et al., 2017). Bilirubin is released into the blood after breakdown of haemoglobin, conjugated in the liver by UGTs, and then excreted into bile by transporters (Méndez-Sánchez, et al., 2017). Elevated levels (above the normal limit of 20.5 μmol/L) occur in different conditions, including liver disease (Shiraishi, et al., 2019). Progressive elevation with disease severity was observed in our data. Correlations between transporter abundances and total serum bilirubin can be explained mechanistically by the role of these transporters in bilirubin disposition as either efflux or uptake transporters. The drop in their expression leads to hyperbilirubinemia, which is common in patients with cirrhosis and can be used as a predictor for poor prognosis (López-Velázquez, et al., 2014). The expression of these transporters also plays a key role in biliary secretion and enterohepatic recycling of various drugs, which when taken into account in PBPK models, can help in predicting their plasma levels, and ultimately, dose adjustment can be facilitated for these drugs in health and disease (Patel, et al., 2016; Thakkar, et al., 2017; Wegler, et al., 2021).

The effect of underlying conditions in the patient cohort were investigated at the same level of severity (moderate cirrhosis). The effects of cholestasis and viral cirrhosis have been investigated previously (Prasad, et al., 2018; Wang, et al., 2016), and the current study is the first investigation of the effects of NAFLD and cancer-associated cirrhosis. NAFLD and cancer-related cirrhosis had a higher impact on expression of enzymes and transporters compared to cholestasis. This difference in impact was previously reported to affect MPPGL in the same samples (El-Khateeb, et al., 2020). In previous reports that examined other causes of cirrhosis (alcoholic and HCV infection) in a larger number of samples (~30 per group), the impact of underlying disease was similar for most targets, and only the degree of change from

the control group showed significant differences (Prasad, et al., 2018; Wang, et al., 2016). The current CP classification system does not distinguish different causes or pathophysiology of cirrhosis.

Although modelling and simulation currently employ protein expression data generated in the past few decades by Western blotting, these data have recently started to be supplanted by state-of-the-art proteomic data, which should lead to improved performance of these models, as demonstrated in this study. We used our data to simulate the impact of changes in the abundance of liver enzymes on exposure of a cirrhotic population to repaglinide, dabigatran etexilate and zidovudine. The choice of the drugs aimed to cover one or more proteins from each group (CYPs, UGTs, non-CYP non-UGT enzymes, and transporters), while prioritising drugs that have clinical data in both healthy and cirrhosis patients and have a verified model that is either available in the simulator's library or is reported in a previous publication. The performance of the adapted models was verified against observed data and compared to the output from Simcyp default cirrhosis settings. The latter were based on a combination of available Western blotting abundance and *in vitro* and *in vivo* activity studies (Johnson, et al., 2010). Differences were not large for repaglinide and dabigatran, either due to similar measure of change in disease used in these models (LC-MS expression data and data implemented into the disease populations from immunoblotting and activity meta-analyses) or because of low sensitivity of drug exposure to changes in expression. By contrast, in the case of zidovudine, the default Simcyp settings did not account for any change in expression and/or activity of UGTs with cirrhosis, and hence proteomic data improved the performance of the model and allowed the predictions to capture the impact of the disease on drug clearance.

In conclusion, this study demonstrated, for the first time, gradual decline in the expression of enzymes and transporters with the progression of cirrhosis severity. The rate of this decline was specific to each target protein. The impact of underlying condition was most significant in

the cases of cancer and NAFLD. Introducing specific proteomic data related to changes due to cirrhosis into the population parameters of PBPK models will improve the predictive performance of these models in hepatic impairment populations.

8.6. References

Achour, B, Al-Majdoub, ZM, Grybos-Gajniak, A, Lea, K, Kilford, P, Zhang, M, Knight, D, Barber, J, Schageman, J, and Rostami-Hodjegan, A. (2021). Liquid Biopsy Enables Quantification of the Abundance and Interindividual Variability of Hepatic Enzymes and Transporters. *Clin. Pharmacol. Ther.*, 109(1), 222–232.

Achour, B, Dantonio, A, Niosi, M, Novak, JJ, Al-Majdoub, ZM, Goosen, TC, Rostami-Hodjegan, A, and Barber, J. (2018). Data Generated by Quantitative Liquid Chromatography-Mass Spectrometry Proteomics Are Only the Start and Not the Endpoint: Optimization of Quantitative Concatemer-Based Measurement of Hepatic Uridine-5′-Diphosphate–Glucuronosyltransferase Enzymes with Ref. *Drug Metab. Dispos.*, 46(6), 805–812.

Achour, B, Russell, MR, Barber, J, and Rostami-Hodjegan, A. (2014). Simultaneous quantification of the abundance of several cytochrome P450 and uridine 5′-diphospho-glucuronosyltransferase enzymes in human liver microsomes using multiplexed targeted proteomics. *Drug Metab. Dispos.*, 42(4), 500–510.

Al-Majdoub, ZM, Al Feteisi, H, Achour, B, Warwood, S, Neuhoff, S, Rostami-Hodjegan, A, and Barber, J. (2019). Proteomic quantification of human blood–brain barrier SLC and ABC transporters in healthy individuals and dementia patients. *Mol. Pharm.*, 16(3), 1220–1233.

Al-Majdoub, ZM, Achour, B, Couto, N, Howard, M, Elmorsi, Y, Scotcher, D, Alrubia, S, El-Khateeb, E, Vasilogianni, A, Alohali, N, Neuhoff, S, Schmitt, L, Rostami-Hodjegan, A, and Barber, J. (2020). Mass spectrometry-based abundance atlas of ABC transporters in human liver, gut, kidney, brain and skin. *FEBS Lett.*, 594(23), 4134–4150.

Al Feteisi, H, Al-Majdoub, ZM, Achour, B, Couto, N, Rostami-Hodjegan, A, and Barber, J. (2018). Identification and quantification of blood-brain barrier transporters in isolated rat brain microvessels. *J. Neurochem.*, 146(6), 670–685.

Bataller, R, and Brenner, DA. (2005). Liver fibrosis. *J. Clin. Invest.*, 115(2), 209–218.

Chung, S-J, Kwon, Y-J, Park, M-C, Park, Y-B, and Lee, S-K. (2011). The Correlation between Increased Serum Concentrations of Interleukin-6 Family Cytokines and Disease Activity in Rheumatoid Arthritis Patients. *Yonsei Med. J.*, 52(1), 113.

Couto, N, Al-Majdoub, ZM, Achour, B, Wright, PC, Rostami-Hodjegan, A, and Barber, J. (2019). Quantification of Proteins Involved in Drug Metabolism and Disposition in the Human Liver Using Label-Free Global Proteomics. *Mol. Pharm.*, 16(2), 632–647.

Drozdzik, M, Szelag-Pieniek, S, Post, M, Zeair, S, Wrzesinski, M, Kurzawski, M, Prieto, J, and Oswald, S. (2020). Protein Abundance of Hepatic Drug Transporters in Patients With Different Forms of Liver Damage. *Clin. Pharmacol. Ther.*, 107(5), 1138–1148.

El-Khateeb, E, Achour, B, Scotcher, D, Al-Majdoub, ZM, Athwal, V, Barber, J, and Rostami-Hodjegan, A. (2020). Scaling Factors for Clearance in Adult Liver Cirrhosis. *Drug Metab. Dispos.*, 48(12), 1271–1282.

Elbekai, R, Korashy, H, and El-Kadi, A. (2004). The Effect of Liver Cirrhosis on the Regulation and Expression of Drug Metabolizing Enzymes. *Curr. Drug Metab.*, 5(2), 157–167.

Fallon, JK, Neubert, H, Hyland, R, Goosen, TC, and Smith, PC. (2013). Targeted quantitative proteomics for the analysis of 14 UGT1As and -2Bs in human liver using NanoUPLC-MS/MS with selected reaction monitoring. *J. Proteome Res.*, 12(10), 4402–4413.

FDA. (2003). Pharmacokinetics in patients with impaired hepatic function: study design, data analysis, and impact on dosing and labelling. *FDA Guid.* https://www.fda.gov/regulatory-information/search-fda-guidance-documents/pharmacokinetics-patients-impaired-hepatic-function-study-design-data-analysis-and-impact-dosing-and

FDA. (2020). Enhancing the Diversity of Clinical Trial Populations—Eligibility Criteria, Enrollment Practices, and Trial Designs Guidance for Industry. *Guid. Doc.* https://www.fda.gov/regulatory-information/search-fda-guidance-documents/enhancing-diversity-clinical-trial-populations-eligibility-criteria-enrollment-practices-and-trial

Frye, RF, Zgheib, NK, Matzke, GR, Chaves-Gnecco, D, Rabinovitz, M, Shaikh, OS, and Branch, RA. (2006). Liver disease selectively modulates cytochrome P450-mediated metabolism. *Clin. Pharmacol. Ther.*, 80(3), 235–245.

Harwood, MD, Achour, B, Russell, MR, Carlson, GL, Warhurst, G, and Rostami-Hodjegan, A. (2015). Application of an LC-MS/MS method for the simultaneous quantification of human intestinal transporter proteins absolute abundance using a QconCAT technique. *J. Pharm. Biomed. Anal.*, 110, 27–33.

Hatorp, V, Walther, KH, Christensen, MS, and Haug-Pihale, G. (2000). Single-Dose Pharmacokinetics of Repaglinide in Subjects with Chronic Liver Disease. *J. Clin. Pharmacol.*, 40(2), 142–152.

Heimbach, T, Chen, Y, Chen, J, Dixit, V, Parrott, N, Peters, SA, Poggesi, I, Sharma, P, Snoeys, J, Shebley, M, Tai, G, Tse, S, Upreti, V V., Wang, Y, Tsai, A, Xia, B, Zheng, M, … Hall, S. (2020). Physiologically-Based Pharmacokinetic Modeling in Renal and Hepatic Impairment Populations: A Pharmaceutical Industry Perspective. *Clin. Pharmacol. Ther.*, cpt.2125.

Hoyumpa, AM, and Schenker, S. (1991). Is glucuronidation truly preserved in patients with liver disease? *Hepatology*, 13(4), 786–795.

Izukawa, T, Nakajima, M, Fujiwara, R, Yamanaka, H, Fukami, T, Takamiya, M, Aoki, Y, Ikushiro, S, Sakaki, T, and Yokoi, T. (2009). Quantitative Analysis of UDP-Glucuronosyltransferase (UGT) 1A and UGT2B Expression Levels in Human Livers. *Drug Metab. Dispos.*, 37(8), 1759–1768.

Jadhav, PR, Cook, J, Sinha, V, Zhao, P, Rostami-Hodjegan, A, Sahasrabudhe, V, Stockbridge, N, and Powell, JR. (2015). A proposal for scientific framework enabling specific population drug dosing recommendations. *J. Clin. Pharmacol.*, 55(10), 1073–1078.

Johnson, TN, Boussery, K, Rowland-Yeo, K, Tucker, GT, and Rostami-Hodjegan, A. (2010). A semi-mechanistic model to predict the effects of liver cirrhosis on drug clearance. *Clin.*

Pharmacokinet., 49(3), 189–206.

Lippitz, BE, and Harris, RA. (2016). Cytokine patterns in cancer patients: A review of the correlation between interleukin 6 and prognosis. *Oncoimmunology*, 5(5), e1093722.

López-Velázquez, JA, Chávez-Tapia, NC, Ponciano-Rodríguez, G, Sánchez-Valle, V, Caldwell, SH, Uribe, M, and Méndez-Sánchez, N. (2014). Bilirubin alone as a biomarker for short-term mortality in acute-on-chronic liver failure: an important prognostic indicator. *Ann. Hepatol.*, 13(1), 98–104.

Lucey, MR, Brown, KA, Everson, GT, Fung, JJ, Gish, R, Keeffe, EB, Kneteman, NM, Lake, JR, Martin, P, McDiarmid, S V., Rakela, J, Shiffman, ML, So, SK, and Wiesner, RH. (1997). Minimal criteria for placement of adults on the liver transplant waiting list: A report of a national conference organized by the American Society of Transplant Physicians and the American Association for the Study of Liver Diseases. *Liver Transplant. Surg.*, 3(6), 628–637.

Margaillan, G, Rouleau, M, Klein, K, Fallon, JK, Caron, P, Villeneuve, L, Smith, PC, Zanger, UM, and Guillemette, C. (2015). Multiplexed targeted quantitative proteomics predicts hepatic glucuronidation potential. *Drug Metab. Dispos.*, 43(9), 1331–1335.

Méndez-Sánchez, N, Vítek, L, Aguilar-Olivos, NE, and Uribe, M. (2017). Bilirubin as a Biomarker in Liver Disease. In Patel V. & Preedy V. (Eds.), *Biomarkers in Disease: Methods, Discoveries and Applications* (pp. 281–304). Springer, Dordrecht.

Morgan, DJ, and McLean, a J. (1995). Clinical pharmacokinetic and pharmacodynamic considerations in patients with liver disease. An update. *Clin. Pharmacokinet.*, 29(5), 370–391.

Ohtsuki, S, Schaefer, O, Kawakami, H, Inoue, T, Liehner, S, Saito, A, Ishiguro, N, Kishimoto, W, Ludwig-Schwellinger, E, Ebner, T, and Terasaki, T. (2012). Simultaneous Absolute Protein Quantification of Transporters, Cytochromes P450, and UDP-Glucuronosyltransferases as a Novel Approach for the Characterization of Individual Human Liver: Comparison with mRNA Levels and Activities. *Drug Metab. Dispos.*, 40(1), 83–92.

Palatini, P, and De Martin, S. (2016). Pharmacokinetic drug interactions in liver disease: An update. *World J. Gastroenterol.*, 22(3), 1260–1278.

Park, GR. (1996). Molecular mechanisms of drug metabolism in the critically ill. *Br. J. Anaesth.*, 77(1), 32–49.

Patel, M, Taskar, KS, and Zamek-Gliszczynski, MJ. (2016). Importance of Hepatic Transporters in Clinical Disposition of Drugs and Their Metabolites. *J. Clin. Pharmacol.*, 56, S23–S39.

Prasad, B, Bhatt, DK, Johnson, K, Chapa, R, Chu, X, Salphati, L, Xiao, G, Lee, C, Hop, CECA, Mathias, A, Lai, Y, Liao, M, Humphreys, WG, Kumer, SC, and Unadkat, JD. (2018). Abundance of Phase 1 and 2 Drug-Metabolizing Enzymes in Alcoholic and Hepatitis C Cirrhotic Livers: A Quantitative Targeted Proteomics Study. *Drug Metab. Dispos.*, 46(7), 943–952.

Prystupa, A, Kiciński, P, Sak, J, Boguszewska-Czubara, A, Toruń-Jurkowska, A, and Załuska, W. (2015). Proinflammatory Cytokines (IL-1 α , IL-6) and Hepatocyte Growth Factor in Patients with Alcoholic Liver Cirrhosis. *Gastroenterol. Res. Pract.*, 2015, 1–7.

Pugh, RNH, Murray-Lyon, IM, Dawson, JL, Pietroni, MC, and Williams, R. (1973). Transection of the oesophagus for bleeding oesophageal varices. *Br. J. Surg.*, 60(8), 646–649.

Rodgers, T, and Rowland, M. (2007). Mechanistic Approaches to Volume of Distribution Predictions: Understanding the Processes. *Pharm. Res.*, 24(5), 918–933.

Russell, MR, Achour, B, McKenzie, EA, Lopez, R, Harwood, MD, Rostami-Hodjegan, A, and Barber, J. (2013). Alternative fusion protein strategies to express recalcitrant QconCAT proteins for quantitative proteomics of human drug metabolizing enzymes and transporters. *J. Proteome Res.*, 12(12), 5934–5942.

Shiraishi, M, Tanaka, M, Okada, H, Hashimoto, Y, Nakagawa, S, Kumagai, M, Yamamoto, T, Nishimura, H, Oda, Y, and Fukui, M. (2019). Potential impact of the joint association of total bilirubin and gamma-glutamyltransferase with metabolic syndrome. *Diabetol. Metab. Syndr.*, 11(1), 12.

Singlas, E, Pioger, JC, Taburet, AM, Colaneri, S, and Fillastre, JP. (1989). Comparative pharmacokinetics of zidovudine (AZT) and its metabolite (G.AZT) in healthy subjects and HIV seropositive patients. *Eur. J. Clin. Pharmacol.*, 36(6), 639–640.

Stagg, MP, Cretton, EM, Kidd, L, Diasio, RB, and Sommadossi, J-P. (1992). Clinical pharmacokinetics of 3′-azido-3′-deoxythymidine (zidovudine) and catabolites with formation of a toxic catabolite, 3′-amino-3′-deoxythymidine. *Clin. Pharmacol. Ther.*, 51(6), 668–676.

Stangier, J, Stähle, H, Rathgen, K, Roth, W, and Shakeri-Nejad, K. (2008). Pharmacokinetics and Pharmacodynamics of Dabigatran Etexilate, an Oral Direct Thrombin Inhibitor, Are Not Affected by Moderate Hepatic Impairment. *J. Clin. Pharmacol.*, 48(12), 1411–1419.

Taburet, A-M, Naveau, S, Zorza, G, Colin, J-N, Delfraissy, J-F, Chaput, J-C, and Singlas, E. (1990). Pharmacokinetics of zidovudine in patients with liver cirrhosis. *Clin. Pharmacol. Ther.*, 47(6), 731–739.

Talal, AH, Venuto, CS, and Younis, I. (2017). Assessment of Hepatic Impairment and Implications for Pharmacokinetics of Substance Use Treatment. *Clin. Pharmacol. Drug Dev.*, 6(2), 206–212.

Taniguchi, T, Zanetti-Yabur, A, Wang, P, Usyk, M, Burk, RD, and Wolkoff, AW. (2020). Interindividual Diversity in Expression of Organic Anion Uptake Transporters in Normal and Cirrhotic Human Liver. *Hepatol. Commun.*, 4(5), 739–752.

Thakkar, N, Slizgi, JR, and Brouwer, KLR. (2017). Effect of liver disease on hepatic transporter expression and function. *J. Pharm. Sci.*, 106(9), 2282–2294.

Tilg, H, Wilmer, A, Vogel, W, Herold, M, Nölchen, B, Judmaier, G, and Huber, C. (1992). Serum levels of cytokines in chronic liver diseases. *Gastroenterology*, 103(1), 264–274.

van Heiningen, PNM, Hatorp, V, Kramer Nielsen, K, Hansen, KT, van Lier, JJ, De Merbel, NC, Oosterhuis, B, and Jonkman, JHG. (1999). Absorption, metabolism and excretion of a single oral dose of 14 C-repaglinide during repaglinide multiple dosing. *Eur. J. Clin. Pharmacol.*, 55(7), 521–525.

Varma, MVS, Lai, Y, Kimoto, E, Goosen, TC, El-Kattan, AF, and Kumar, V. (2013). Mechanistic Modeling to Predict the Transporter- and Enzyme-Mediated Drug-Drug Interactions of Repaglinide. *Pharm. Res.*, 30(4), 1188–1199.

Wang, L, Collins, C, Kelly, EJ, Chu, X, Ray, AS, Salphati, L, Xiao, G, Lee, C, Lai, Y, Liao, M, Mathias, A, Evers, R, Humphreys, W, Hop, CECA, Kumer, SC, and Unadkat, JD. (2016). Transporter expression in liver tissue from subjects with alcoholic or hepatitis C cirrhosis quantified by targeted quantitative proteomics. *Drug Metab. Dispos.*, 44(11), 1752–1758.

Wang, X, He, B, Shi, J, Li, Q, and Zhu, H-J. (2020). Comparative Proteomics Analysis of Human Liver Microsomes and S9 Fractions. *Drug Metab. Dispos.,* 48(1), 31–40.

Wegler, C, Prieto Garcia, L, Klinting, S, Robertsen, I, Wiśniewski, JR, Hjelmesæth, J, Åsberg, A, Jansson-Löfmark, R, Andersson, TB, and Artursson, P. (2021). Proteomics-Informed Prediction of Rosuvastatin Plasma Profiles in Patients With a Wide Range of Body Weight. *Clin. Pharmacol. Ther.*, 109(3), 762–771.

Wiśniewski, JR, Zougman, A, Nagaraj, N, and Mann, M. (2009). Universal sample preparation method for proteome analysis. *Nat. Methods*, 6(5), 359–362.

Yu, M, Zhu, Y, Cong, Q, and Wu, C. (2017). Metabonomics Research Progress on Liver Diseases. *Can. J. Gastroenterol. Hepatol.*, 2017, 1–10.

Zhang, Z, and Unadkat, JD. (2017). Development of a Novel Maternal-Fetal Physiologically Based Pharmacokinetic Model II: Verification of the model for passive placental permeability drugs. *Drug Metab. Dispos.*, 45(8), 939–946.

8.7. Supplementary Material

Supplementary Table 8.1. Demographic and clinical information for the individual donors of control samples.

Serial	Sample ID	Date of surgery	Age	sex	PT (sec)	Albumin level (g/L)	Weight (Kg) *	Height (m) *	Total bilirubin	General diagnosis
1	2759	12/12/16	81	M	11.3	34	82	1.72	11	CRC
2	2721	06/12/16	36	M	11.5	39	61.5	1.696	18	CRC
3	2841	28/12/16	57	M	12.3	40	84	1.74	9	CRC
4	0103	16/01/17	81	M	21.6	38	75	1.67	16	CRC
5	2847	30/12/16	48	F	12.2	43	67.8	1.619	10	SCC
6	0044	09/01/17	83	F	10.6	39	62.3	1.637	6	CRC
7	761	20/04/17	73	M	12.7	35	94.9	1.638	6	HCC
8	713	13/04/17	57	F	12.1	42	65.9	1.73	9	CRC
9	502	14/03/17	77	M	11.9	38	112.5	1.71	9	CRC
10	0125	19/01/17	62	M	10.9	38	69.7	1.7	7	CRC
11	0336	16/02/17	71	F	10.5	34	76	1.53	8	GIST
12	484	13/03/17	80	M	21.9	24	71	1.81	28	CRC
13	0322	14/02/17	71	M	10.8	43	93.6	1.715	11	CRC
14	2809	20/12/16	52	M	10.1	42	88	1.735	6	CRC

PT, prothrombin time; *measured at time of surgery; HCC, hepatocellular carcinoma; CRC, colorectal cancer; SCC, squamous cell carcinoma; GIST, gastrointestinal stromal tumour.

Supplementary Table 8.2. Demographic and clinical information for the individual donors of cirrhosis liver samples with associated Child-Pugh classification.

Serial for each group	Sample ID	Date of surgery DD/MM/YY	Age	sex	PT (sec)	Albumin level (g/L)	Total bilirubin (µmol/L)	Weight (Kg) [a]	Height (m) [a]	Ascites volume[b]	HE grade [c]	General diagnosis	CP class (Score)
1	0974	19/05/17	56	M	18.1	37	8	117.5	1.75	Severe	1-2	SH	B(9)
2	1982	17/08/16	63	F	18	25	30	70.7	1.57	Mild	1-2	NAFLD	B(9)
3	1570	10/06/16	62	F	16.6	32	26	72.1	1.52	Moderate	1-2	NAFLD	B(9)
4	0549	22/03/17	59	M	18.8	28	53	89.2	1.72	Mild	1-2	NAFLD	C(10)
5	0355	17/02/17	67	F	17.9	26	81	82.2	1.64	Moderate	None	NAFLD	C(11)
6	0863	08/05/17	51	F	19.8	23	78	89.2	1.6	Mild	None	NAFLD	C(11)
7	2728	07/12/16	66	F	24.9	32	29	82.6	1.6	Moderate	1-2	NAFLD	C(10)
8	1571	11/06/16	46	F	14.7	25	51	78.6	1.58	Mild	1-2	NAFLD	C(11)
1	2403	21/10/16	57	M	14.4	29	16	89	1.803	None	None	HCC & HCV	A(6)
2	0955	18/05/17	63	M	15	36	18	89.2	1.73	None	None	HCC & alcoholic SH	A(5)
3	1963	13/08/16	68	M	13.6	27	28	113.45	1.77	None	1-2	HCC & alcoholic	B(8)
4	1745	14/07/16	67	M	15.2	27	46	92	1.7	Mild	None	HCC & NAFLD	B(9)
5	2431	27/10/16	69	M	15.7	28	30	95	1.79	None	None	HCC & HCV	A(6)
6	2408	22/10/16	51	M	18.9	31	44	88.5	1.85	Mild	None	HCC & HCV	B(8)
7	1926	10/08/16	63	M	17	33	97	82.3	1.74	None	1-2	HCC & NAFLD	B(9)
8	3688	12/11/15	65	F	13.8	40	14	84	1.63	None	None	HCC & alcoholic SH	A(5)
9	1228	06/12/17	55	F	14.3	29	13	78.6	1.62	None	None	HCC	A(6)
1	997	21/04/16	59	M	19.7	13	63	100.8	1.82	Severe	1-2	CHOL	C(14)
2	0746	19/04/17	67	M	13.7	24	58	76.4	1.6	None	1-2	PBC	C(10)
3	0147	25/01/17	57	M	15.3	19	243	72.3	1.74	Mild	1-2	CHOL	C(11)
4	2682	02/12/16	56	F	15.2	40	75	67.3	1.62	Severe	1-2	CHOL	C(11)
5	2500	07/11/16	63	F	11.9	30	82	80.15	1.64	Mild	1-2	PBC	C(10)
6	2306	11/10/16	60	M	16.9	22	326	83.2	1.76	Mild	1-2	PSC	C(11)

7	2159	15/09/16	39	M	14.2	30	49	80.8	1.90	Mild	None	PSC	B(8)
8	2136	12/09/16	54	M	19.1	30	484	79.7	1.75	Moderate	1-2	PSC	C(12)
9	1684	11/07/16	69	F	15.4	28	102	78.6	1.67	Mild	1-2	CHOL & PBC	C(10)
10	1429	18/07/17	57	M	15.2	37	37	69	1.75	Mild	None	PSC	B(7)
11	0544	21/03/17	70	M	13.3	30	25	87.8	-	None	1-2	PSC	B(7)
12	2020	24/08/16	59	F	15.9	29	26	43.95	1.5	Severe	None	PBC	B(9)
13	0819	05/02/17	75	M	13.2	41	18	79.5	1.6	None	None	CHOL	A(5)
1	1509	04/06/16	57	M	14.4	33	18	74.95	1.75	Moderate	1-2	Alcoholic SH	B(9)
2	1545	09/06/16	69	F	20.9	50	44	62.7	1.55	Moderate	None	Alcoholic SH	B(9)

PT, prothrombin time; CP, Child-Pugh; NA, HCC, hepatocellular carcinoma; NAFLD, non-alcoholic fatty liver disease; CHOL, cholestasis; PBC, primary biliary cirrhosis; PSC, primary sclerosing cholangitis, SH, steatohepatitis; [a] measured at time of surgery; [b] controlled with diuretics recorded as mild ascites, [c] controlled with rifaximin / lactulose recorded as grade 1-2.

Supplementary Table 8.3. Targets and their surrogate peptides in each QconCAT standard, NuncCAT, MetCAT and TransCAT

NuncCAT		MetCAT		TransCAT	
Target	**Peptide Sequence**	**Target**	**Peptide Sequence**	**Target**	**Peptide Sequence**
CES1	EGYLQIGANTQAAQK§	**CYP1A2**	ASGNLIPQEK§	**P-gp, MDR1**	FYDPLAGK§
	FLSLDLQGDPR		YLPNPALQR§		AGAVAEEVLAAIR
CES2	ADHGDELPFVFR	**CYP2A6**	DPSFFSNPQDFNPQHFLNEK	**BSEP**	STALQLIQR
	SFFGGNYIK§		GTGGANIDPTFFLSR§		AADTIIGFEHGTAVER§
	TTHTGQVLGSLVHVK	**CYP2B6**	ETLDPSAPR	**MDR3**	IATEAIENIR
FMO3	LVGPGQWPGAR§		GYGVIFANGNR§		GAAYVIFDIIDNNPK§
	NNLPTAISDWLYVK	**CYP2C18**	GSFPVAEK	**MRP2**	LTIIPQDPILFSGSLR§
			SLTNFSK§		
FMO5	WATQVFK§	**CYP2C19**	GHFPLAER		YLGGDDLDTSAIR
	TDDIGGLWR	**CYP2C8**	SFTNFSK§		AFEHQQR
	LTHFIWK	**CYP2C9**	GIFPLAER§	**MRP3**	AEGEISDPFR
EPHX1	IIPLLTDPK§		LPPGPTPLPVIGNILQIGIK		IDGLNVADIGLHDLR§
	FSTWTNTEFR	**CYP2D6**	AFLTQLDELLTEHR	**MRP4**	AEAAALTETAK
POR	QYELVVHTDIDAAK		DIEVQGFR§		APVLFFDR§
	YYSIASSSK	**CYP2E1**	FITLVPSNLPHEATR	**MRP6**	SSLPSALLGELSK
	IQTLTSSVR§		GIIFNNGPTWK§		APETEPFLR§
MGST1	VFANPEDCVAFGK§	**CYP2J2**	FEYQDSWFQQLLK		SSLASGLLR
	IYHTIAYLTPLPQPNR		VIGQGQQPSTAAR§	**BCRP**	VIQELGLDK
MGST2	HLYFWGYSEAAK	**CYP3A4**	EVTNFLR		SSLLDVLAAR§
MGST 3	IASGLGLAWIVGR§		LSLGGLLQPEK§		ENLQFSAALR
	VLYAYGYYTGEPSK	**CYP3A43**	YIPFGAGPR	**ATP1A1**	IVEIPFNSTNK
UGT2B17	WTYSISK§	**CYP3A5**	DTINFLSK§		SPDFTNENPLETR§
	GHEVIVLTSSASILVNASK		YWTEPEEFRPER	**Cadherin-17**	AENPEPLVFGVK
	SVINDPIYK	**CYP3A7**	FGGLLLTEK§		QNSRPGK
ADH1A*	GAILGGFK		FGGLLLTEKPIVLK	**Cadherin-23**	ATDADEGEFGR
	NDVSNPQGTLQDGTSR		FNPLDPFVLSIK		DAYVGALR
	KPIHHFLGISTFSQYTVVDENAVAK	**CYP4F2**	HVTQDIVLPDGR§	**OST-α**	YTADLLEVLK
ADH1B *	AAVLWEVK	**UGT1A1**	DGAFYTLK§		VGYETFSSPDLDLNLK
	GAVYGGFK		TYPVPFQR	**OST-β**	DHNSLNNLR
ADH1C	FSLDALITNILPFEK	**UGT1A3**	HVLGHTQLYFETEHFLK		ETPEVLHLDEAK
ALDH1A1 *	IFVEESIYDEFVR		YLSIPTVFFLR§	**OCT-1**	MLSLEEDVTEK

	IFINNEWHDSVSGK	**UGT1A4**	GTQCPNPSSYIPK§		GVALPETMK§
	TIPIDGNFFTYTR		YIPCDLDFK		ENTIYLK
AOX1 *	LILNEVSLLGSAPGGK	**UGT1A6**	SFLTAPQTEYR	**OCT-2**	GIALPETVDDVEK
	GLHGPLTLNSPLTPEK		VSVWLLR§		FLQGVFGK
	VFFGEGDGIIR	**UGT1A9**	AFAHAQWK§	**OCTN2**	TWNIR
NAT1 *	DNTDLIEFK		ESSFDAVFLDPFDNCGLIVAK		DYDEVTAFLGEWGPFQR
	NYIVDAGFGR	**UGT2B4**	ANVIASALAK	**OAT2**	WLLTQGHVK
NAT2*	TLTEEEVEEVLK		FSPGYAIEK§		NVALLALPR§
	DNTDLVEFK	**UGT2B7**	ADVWLIR§	**OAT4**	DTLTLEILK
SULT1E1*	KPSEELVDR		TILDELIQR		ISLLSFTR§
	NHFTVALNEK	**UGT2B10**	GHEVTVLASSASILFDPNDSSTLK	**MATE-1**	GGPEATLEVR
SULT1A1	VHPEPGTWDSFLEK	**UGT2B11**	GHEVTVLASSASILFDPNDASTLK		DHVGYIFTTDR
SULT1A2	VYPHPGTWESFLEK	**UGT2B15**	SVINDPVYK	**OATP1A2**	EGLETNADIIK
			ASGNLIPQEK		IYDSTTFR§
SULT2A1*	DEDVIILTYPK		WIYGVSK§	**OATP1B1**	YVEQQYGQPSSK§
	TLEPEELNLILK				MFLAALSLSFIAK
TPMT*	NQVLTLEEWQDK				LNTVGIAK
	TSLDIEEYSDTEVQK			**OATP1B3**	NVTGFFQSLK§
EPHX2 *	GLLNDAFQK				IYNSVFFGR
	WLDSDAR			**OATP2B1**	VLLQTLR
					SSPAVEQQLLVSGPGK§
				OATP4C1	HLPGTAEIQAGK
					SPEPSLPSAPPNVSEEK
					DFPAALK
				NTCP	GIYDGDLK§
					GIVISLVLVLIPCTIGIVLK
					AHLWKPK
				PEPT-1	GNEVQIK
					TLPVFPK
					HTLLVWAPNHYQVVK
				ASBT	IAGLPWYR§
					LWIIGTIFPVAGYSLGFLLAR
				MCT-1	SITVFFK§
					DLHDANTDLIGR
				OATP4A1	YEVELDAGVR
					ILGGIPGPIAFGWVIDK

* Represent targets mainly located in the cytosolic fraction; §Peptides used for the quantification of the targets in the current study

Supplementary Table 8.4. Physiological parameters for healthy individuals and cirrhosis patients within Simcyp Simulator V19.

Liver condition	Healthy Control	Mild Impairment	Moderate Impairment	Severe Impairment
Simcyp-population	HV	CP-A	CP-B	CP-C
Gastric residence time (h) (fasted/fed)/colon transit time	0.4/1.0/12	0.48/1.2/24	0.55/1.38/24	0.6/1.5/24
Albumin/α1-AG/ Haematocrit (ratio to HV, male)	1 / 1/1	0.8 /0.9/0.9	0.7 /0.8/0.8	0.6/0.6/0.8
CYP3A4 abundance in the liver (pmol/mg)	137	108	56	31.7
CYP2C8 abundance in the liver (pmol/mg)	24	16.6	12.5	7.92
OATP1B1 abundance in the liver (pmol/mg)	3.1	3.1	3.1	3.1
CES1/CES2 abundance in the liver (pmol/mg)	ND	ND	ND	ND
CYP3A4 abundance in the intestine (pmol/mg)	65.4	65.4	39.9	23.6
Liver Volume (L)	1.65	1.47	1.17	1.0
Liver Q (Arterial/Portal), (% cardiac output)	6.5/19	9.2/17.3	10.6/13.6	12.5/10.5

ND, No data are available; CP, Child-Pugh score; HV, healthy volunteer; Q, blood flow.

Supplementary Table 8.5. Demographic data of the healthy and cirrhosis subjects used for repaglinide, dabigatran etexilate and zidovudine simulations.

Drug	Parameter	Cirrhosis patients	Healthy subjects	References
Repaglinide	Mean age in years (range)	52.9 (37- 62)	53.2 (42- 62)	(Hatorp, et al., 2000)
	Proportion of females	0	0	
	Weight (kg) ± SD	86.8 ± 13.9	78.5 ± 12	
	Number of participants	12 (9 CP-B, 3 CP-C)	12	
Dabigatran etexilate	Mean age in years (range)	55.2 (41-68)	54.9 (38-66)	(Stangier, et al., 2008)
	Proportion of females	0.417	0.417	
	Weight (kg) ± SD	80.6 ± 17.7	82.3 ± 18.7	
	Number of participants	12 (all are CP-B)	12	
Zidovudine	Mean age in years (range)	CP-A 57 (54-59), CP-B 52 (43-60), CP-C 53 (46-63)	45 (26-62)	(Taburet, et al., 1990)
	Proportion of females	0	0	
	Weight (kg) ± SD	CP-A 71 ± 6, CP-B 73 ± 16, CP-C 63 ± 15	70 ± 10	
	Number of participants	3 (CP-A), 5 (CP-B), 6 (CP-C)	6	

SD, standard deviation; CP-B and CP-C, Child-Pugh grades B (moderate cirrhosis) and C (severe cirrhosis).

Supplementary Table 8.6. MPPGL values for each sample used for scaling up abundances in pmol/mg microsomal protein to pmol/g liver tissue.

Serial	Sample ID	Type [CP class (grade), disease cause]	MPPGL (mg microsomes/g liver)
1	2759	HN	31.4
2	2721	HN	33
3	2841	HN	30.4
4	0103	HN	40.7
5	2847	HN	63.6
6	0044	HN	34.9
7	761	HN	61.8
8	713	HN	49.5
9	502	HN	34.9
10	0125	HN	37.9
11	0336	HN	35.4
12	484	HN	39.2
13	0322	HN	36.6
14	2809	HN	62.7
15	0974	B(9), NAFLD	28.5
16	1982	B(9), NAFLD	30.8
17	1570	B(9), NAFLD	36
18	0549	C(10), NAFLD	25.9
19	0355	C(11), NAFLD	25.1
20	0863	C(11), NAFLD	20.9
21	2728	C(10), NAFLD	20
22	1571	C(11), NAFLD	35
23	2403	A(6), Cancer	39.9
24	0955	A(5), Cancer	32.8
25	1963	B(8), Cancer	22.4
26	1745	B(9), Cancer	12.9
27	2431	A(6), Cancer	30
28	2408	B(8), Cancer	21
29	1926	B(9), Cancer	24.8
30	3688	A(5), Cancer	22
31	1228	A(6), Cancer	25.6
32	997	C(14), CHOL	28.1
33	0746	C(10), CHOL	18.5
34	0147	C(11), CHOL	29.5
35	2682	C(11), CHOL	38.3
36	2500	C(10), CHOL	37.2
37	2306	C(11), CHOL	40.9
38	2159	B(8), CHOL	42.4
39	2136	C(12), CHOL	41.7
40	1684	C(10), CHOL	34
41	1429	B(7), CHOL	49.1
42	0544	B(7), CHOL	44.8
43	2020	B(9), CHOL	35
44	0819	A(5), CHOL	42.2
45	1509	B(9), Alcoholic SH	30.2
46	1545	B(9), Alcoholic SH	32.4

CP, Child-Pugh; HN, histologically normal liver tissue, NAFLD, non-alcoholic fatty liver disease; CHOL, cholestasis; SH, steatohepatitis

Supplementary Table 8.7. Comparison of the impact of disease associated with cirrhosis (cancer, cholestasis, and NAFLD) on the abundance of enzymes and transporters relative to normal control.

Groups / Target proteins	**ANOVA (Control and 3 diseased groups)**	**Control *vs* Cancer-cirrhosis % change in medians (*p*-value)**	**Control *vs* Cholestasis-cirrhosis % change in medians (*p*-value)**	**Control *vs* NAFLD-cirrhosis % change in medians (*p*-value)**	**ANOVA (3 diseased groups)**
CYP2A6	0.012^	-53 (0.018)	-52 (0.039)	-72 (0.017)	0.76
CYP2C8	0.003^	-60 (0.014)	-57 (0.026)	-63 (0.003*)	0.5
CYP2C9	0.013^	-59 (0.019)	+2 (0.9)	-63 (0.01)	0.051
CYP2C18	0.35	-70 (NA)	+26 (NA)	-53 (NA)	0.17
CYP2E1	0.002^	-64 (0.003*)	-60 (0.012)	-59 (0.024)	0.87
CYP3A4	0.003^	-77 (0.001**)	-20 (0.33)	-82 (0.003*)	0.11
CYP4F2	0.026^	-77 (0.017)	-54 (0.37)	-81 (0.02)	0.18
UGT1A1	0.05	-23 (NA)	-27 (NA)	-57 (NA)	0.49
UGT2B15	0.19	-49 (NA)	-39 (NA)	-54 (NA)	0.94
UGT1A6	0.013^	-55 (0.008*)	-7 (0.45)	-73 (0.016)	0.54
UGT1A9	0.023^	-52 (0.013)	-15 (0.92)	-63 (0.03)	0.085
UGT2B4	0.006^	-55 (0.015)	-28 (0.35)	-68 (0.003*)	0.14
UGT2B7	0.003^	-66 (0.008*)	-47 (0.059)	-72 (0.004*)	0.55
CES1	0.001^	-69 (0.002*)	-46 (0.02)	-77 (0.005*)	0.58
FMO3	0.001^	-67 (0.001**)	-51 (0.024)	-74 (0.002*)	0.09
FMO5	0.22^	-67 (0.08)	+8 (0.87)	-80 (0.006*)	0.06
EPHX1	0.001^	-64 (0.003*)	-47 (0.048)	-71 (0.003*)	0.29
MGST1	0.002^	-44 (0.013)	-31 (0.2)	-68 (0.001**)	0.023^ (NS)
MGST3	0.004^	-55 (0.024)	-64 (0.018)	-65 (0.006*)	0.62
POR	0.004^	-60 (0.009)	14 (0.58)	-62 (0.01)	0.046^ (NS)
ABCB11 (BSEP)	0.008^	-62 (0.01)	-38 (0.224)	-72 (0.007*)	0.29
ABCB4 (MDR3)	0.009^	-80 (0.12)	-23 (0.57)	-67 (0.098)	0.023^ (NS)
ABCC2 (MRP2)	0.001^	-66 (0.002*)	-67 (0.002*)	-60 (0.017)	0.74
ABCC3 (MRP3)	0.037^	-45 (0.015)	-44 (0.088)	-62 (0.1)	0.97

ATP1A1	0.032^	-42 (0.021)	-46 (0.039)	-43 (0.093)	0.82
SLC22A7 (OAT2)	0.015^	-65 (0.036)	-74 (0.013)	-64 (0.051)	0.48
SLCO2B1 (OATP2B1)	0.002^	-67 (0.003*)	-50 (0.068)	-70 (0.004*)	0.32

NAFLD, non-alcoholic fatty liver disease; ^, statistically significant difference with Kruskal-Wallis ANOVA test ($p < 0.05$); (-) and (+) signs refer to decreased or increased abundance from control, respectively; *, statistically significant difference in pairwise comparison ($p < 0.008$); **, statistically significant pairwise comparison ($p < 0.0017$); NS, no statistical significance with post hoc test; NA, not applicable pairwise comparison as the ANOVA test showed no statistical significance ($p > 0.05$).

Supplementary Table 8.8. Absolute abundance in pmol/g liver tissue of drug-metabolising enzymes and transporters in normal controls and cirrhosis samples of various severities and causes.

Target	Normal control pmol/mg liver tissue			Mild (CP-A) cirrhosis pmol/mg liver tissue			Moderate (CP-B) cirrhosis pmol/mg liver tissue			Severe (CP-C) cirrhosis pmol/mg liver tissue		
	Mean ± SD	Median [CI]		Mean ± SD	Median [CI]		Mean ± SD	Median [CI]		Mean ± SD	Median [CI]	
CYP1A2	795.8±531	**665.8**	[359-1418]	318.5±289	**248.8**	[90-869]	272.1±180.4	**256.5**	[83-454]	99.7±72.4	**88.4**	[20.6-187]
CYP2A6	987.6±758	**692.9**	[368-1265]	351.9±158	**305.5**	[225-634]	298.8±139.9	**312.2**	[178-465]	221.3±129.6	**191.2**	[146-351]
CYP2B6	166.4±71	**165.9**	[88-304]	98.3±4	**98.3**	[96-101]	84.1±42	**82.4**	[25.5-140]	82.8±57.1	**56.7**	[45-110]
CYP2C18	28±22.8	**17.4**	[14.7-43.7]	14.9±8	**19.1**	[3.2-21.6]	10.4±8.2	**8.2**	[2.4-23.8]	7±4.4	**6.9**	[2.2-11]
CYP2C19	272±312	**126.6**	[34.7-601.8]	4.7±ND	**4.7**	ND	10.5±16.3	**1.3**	[0.1-39.8]	15.5±26	**5.8**	[1.8-68.5]
CYP2C8	1066.6±569	**965.6**	[630-1741]	686.1±188	**702.1**	[473-960]	362.2±165.5	**353**	[224-528]	252.8±163	**234.4**	[112-341]
CYP2C9	5124.3±2402	**4825.4**	[2885-8618]	3450.3±925	**3326.6**	[2139-4638]	2797.3±201	**2216**	[1191-4279]	1409.2±1134	**1091.2**	[680-1780]
CYP2D6	182.9±120.7	**131.9**	[88.6-319.5]	100±19	**94**	[87-133]	70.8±50	**52.7**	[23-120]	32.9±16.3	**39.6**	[17-45.5]
CYP2E1	1250.4±452	**1209.5**	[857-1557]	787.7±287	**718.1**	[397-1207]	571.8±387.7	**471.2**	[384-778]	216.8±136.6	**165.3**	[124-283]
CYP2J2	22.9±19	**18.9**	[6.7-35]	9.4±4	**9.1**	[4.4-13.6]	6.2±4	**5.5**	[2.6-9.5]	2.9±2.4	**1.9**	[1-4.9]
CYP3A4	2719.1±2864	**1498.4**	[704-7597]	917.1±637	**891.6**	[89-1713]	558.4±460.4	**347**	[200-1129]	516.7±841	**306.5**	[200-493]
CYP3A5	973.9±983	**880.1**	[41-2001]	565.3±613	**464.7**	[36-1296]	53.4±25.8	**53.4**	[30.5-89.5]	529.5±470	**508.5**	[37.6-1063]
CYP3A7	ND	**ND**	ND	138.9±56	**142.6**	[8.8-193]	115.6±54.7	**92.3**	[72-224]	70.8±11.4	**68**	[56-87]
CYP4F2	357.5±195	**410.3**	[103-521]	265±143	**235**	[124-508]	136.3±70.7	**118.4**	[72-203]	76.6±37.3	**68.9**	[45.5-123]
UGT1A1	694.7±517	**588.9**	[166.5-1323]	1183.7±534	**1245.1**	[413-1800]	448.2±216.9	**406.9**	[239-630]	458.4±317.9	**360**	[156-701]
UGT1A3	110.7±87	**146.6**	[11.5-174]	20.4±3	**20.4**	[18-23]	52.7±23.6	**43.6**	[23.6-79]	33.6±21.5	**24.7**	[10-65.5]

UGT1A4	790.4±457	**697.1**	[532-928.4]	383.1±33	**383.4**	[350-416]	504.6±316.9	**460.4**	[208-1105]	192.4±98.7	**231.4**	[83.4-312.2]
UGT1A6	208.4±97	**186.7**	[145.5-233]	136.7±56	**139.2**	[70-215]	101.6±81.8	**81.5**	[50.5-122]	58.9±34.1	**43.5**	[40.7-73]
UGT1A9	689.7±425	**561.1**	[357-1209]	648.3±263	**760.5**	[173-855]	310.5±192.9	**267.1**	[132-443]	180.7±128	**156.9**	[89-240]
UGT2B15	725.1±335	**729.7**	[436-1045]	347.4±94	**315.4**	[273-454]	446±273	**392.7**	[205-611]	167.6±54.8	**169.2**	[69-233]
UGT2B4	1091.8±570	**945.5**	[619-1270]	725±238	**653.9**	[454-1059]	497.5±346.2	**382**	[307-466]	227.7±93	**233.3**	[145-272]
UGT2B7	3302.6±1470	**3122.5**	[2148-4993]	1894.5±993	**1715.3**	[863-3594]	1111.3±703.	**927.5**	[540-1623]	464.7±180.6	**406.2**	[318-636]
UGT2B17	137.7±136	**81.6**	[11.7-419.4]	ND	**ND**	ND	48.4±NA	**48.4**	ND	ND	**ND**	ND
ATP1A1	105.8±41	**94.2**	[75-134]	107.7±42	**119**	[26.6-142]	64.8±29.4	**55.3**	[48-79.6]	50.3±18.8	**49.5**	[36-65.4]
CES1	10552.1±5590	**8790.8**	[6964-12270]	4637.8±219	**4648.9**	[1280-7951]	3112.5±157	**2431**	[1999-4533]	1145.1±704.3	**787.3**	[721-1655]
CES2	669.1±449	**513.2**	[384-1283]	363.4±103	**321.4**	[247-488]	252.5±102.3	**246.4**	[145-376]	126.5±41.5	**121.6**	[91.5-159]
EPHX1	11417.6±4814	**10269.2**	[8475-13749]	6395.8±242 9	**6052.1**	[3682-9757]	4182.7±206 8.1	**3452. 7**	[2761-4815]	2002.2±1248. 9	**1506.3**	[1261-2586]
FMO3	2600.5±1100	**2221.8**	[2003-3064]	1323.7±305	**1390.9**	[866-1668]	887.3±366.6	**964.2**	[489-1146]	469.4±298.4	**424.6**	[216.8-601]
FMO5	753.2±602	**492.5**	[317-1587]	375.4±186	**342.3**	[183-603]	323.2±245.8	**248**	[104-463]	129.6±105.8	**107.7**	[49-158]
MGST1	3922.6±1452	**3632.5**	[2596-4294]	2960.4±102 7	**3053.9**	[1647-4503]	2143.2±119 8.6	**2049. 1**	[1235-2380]	1161.6±508.8	**1094**	[664-1558]
MGST3	292.8±115	**258**	[188.8-403]	128.4±50	**126.1**	[49.6-201.5]	120.5±59.5	**111.7**	[69-137]	81.1±31.8	**72.1**	[53.3-112]
POR	1119.1±477	**1051.8**	[775-1191]	690.9±530	**505.7**	[113-1610]	600.2±380.1	**553.8**	[256-1204]	481.3±457.9	**371.1**	[278-470.5]
P-gp, MDR1	9.4±3	**8.2**	[5.8-14]	11.4±5	**10.8**	[7.2-20]	5.6±2.4	**5.1**	[3.9-6]	4.5±1.8	**4.5**	[3-6.3]
BSEP	11.9±5	**11.1**	[8.6-14]	6.7±3	**6.3**	[3-12.5]	5.1±3.7	**4**	[2.8-5.4]	3.8±2.3	**3**	[2.1-5.5]
MDR3	7±4	**5.9**	[1.4-11.8]	4.4±2	**4.7**	[0.5-7]	3.4±3.7	**2.4**	[0.9-4.4]	2.8±2.9	**2.1**	[0.9-5.4]
MRP2	16.2±6	**14.7**	[12.2-17.3]	7.3±3	**6.7**	[2.7-11.5]	5.1±2.5	**5**	[3-8.7]	3.1±2	**2.7**	[2.1-4.3]
MRP3	10.5±6	**9**	[6-17]	8.4±5	**7.3**	[2.2-15]	5.4±2.7	**5**	[3-6]	5.6±2.7	**5.1**	[3.4-7.9]
MRP4	1±0.7	**1.1**	[0.03-2]	0.6±0.1	**0.4**	[0.2-1.2]	0.5±0.3	**0.7**	[0.01-1]	0.9±1.5	**0.3**	[0.05-0.7]
MRP6	19.2±8	**16.8**	[13.5-25]	11.7±6	**11.1**	[4-20.5]	7.5±7.7	**5.1**	[3-11]	4.3±1.9	**4**	[2.9-5.8]
BCRP	1.2±1	**0.4**	[0.14-2.7]	0.4±0.04	**0.3**	[0.1-0.9]	0.5±0.2	**0.5**	[0.2-0.6]	38.4±65.7	**0.4**	[0.38-0.49]
NTCP	71.3±17	**71**	[57.8-85.4]	40.4±21	**39.9**	[20.8-60.9]	33.1±19.7	**28.6**	[16.5-76.5]	16.1±7	**16.7**	[8.2-24.8]
ASBT	0.9±0.8	**0.4**	[0.17-2.2]	0.4±0.03	**0.2**	[0.1-1]	0.5±0.4	**0.3**	[0.15-1]	13.6±37.7	**0.2**	[0.08-0.6]
MCT1	30.2±10	**32.2**	[20.5-37.8]	27.7±12	**31.7**	[9.4-42.8]	18.4±13	**15**	[10.5-18.3]	11.1±3.1	**11.3**	[8-13.4]
OCT1	85.2±4	**86.7**	[80.8-88]	41.7±12	**39.1**	[31.2-62.7]	26.8±14.4	**19.9**	[16.3-40.8]	16.7±8.4	**16**	[7-32.8]
OCT3	10.8±4	**9.4**	[6.2-15.9]	9.8±5	**8.9**	[3.1-18]	5.8±3.4	**4.6**	[4.2-7]	7±9.1	**3.4**	[2.6-8.3]
OAT2	29.3±14	**29.4**	[15.5-41.8]	23.3±13	**19.2**	[10.8-43.6]	12.4±7.7	**10.2**	[7.5-15.4]	7.7±2.7	**7.3**	[5.3-10.3]

OAT4	4±3	**3.4**	[2.2-5.1]	1.8±1	**1.7**	[0.7-2.7]	1.2±0.7	**1**	[0.6-2.8]	0.9±0.6	**0.8**	[0.37-1.8]
OATP1A2	3.3±3	**3.1**	[0.3-6.5]	0.1±0	**0.1**	[0.005-0.28]	0.7±0.6	**0.5**	[0.2-1.7]	1.3±2.6	**0.2**	[0.09-6.7]
OATP1B1	34.2±12	**33.1**	[23.2-41.5]	16.3±4	**15.1**	[11.6-22.7]	15.9±10.7	**13.8**	[8.2-16.8]	11.9±7.1	**9.8**	[6.4-28.3]
OATP1B3	31.8±14	**26.9**	[21-63.1]	7±0	**7.1**	ND	6±4.2	**5.6**	[2-10.5]	3.8±3.4	**2.4**	[1.4-7.7]
OATP2B1	48.5±17	**41.3**	[36.2-72]	29.6±15	**32**	[11.8-52.5]	18.3±11.2	**14.4**	[12.2-24.8]	12±5.5	**10.8**	[7-16.4]

CP, Child-Pugh score; CI, confidence interval around the median; ND, not detected; NA, not applicable

Supplementary Table 8.9. Observed and simulated pharmacokinetic parameters in healthy and cirrhosis populations using either Simcyp V19 default settings or the change in the protein abundance from the current study.

Drug	**AUC_{obs} in healthy ng.h/ml**	**AUC_{obs} in cirrhosis ng.h/ml**	**AUC_{pred} in healthy ng.h/ml**	**AUC_{pred} Proteomic in cirrhosis ng.h/ml**	**AUC_{pred} Simcyp in cirrhosis ng.h/ml**	**AUR_{obs}**	**$AUCR_{pred}$ Proteomics**	**$AUCR_{pred}$ Simcyp**	**$AUCR_{pred/obs}$ Proteomics**	**$AUCR_{pred/obs}$ Simcyp**
Repaglinide	91.6±6.7	368.9±233.4	84.3±66	414±303	236±180	4.1	4.9	2.8	1.19	0.68
Dabigatrane etexilate	937±649	922±965	1014.3±649	879±523	885±526	0.98	0.87	0.87	0.89	0.89
Zidovudine	1388.4±374	CPA: 4714.6±1909 CPB: 4842.1±1289 CPC: 6321.4±1624	1412.4±635	CPA: 3026.4±1456 CPB: 4839.2±2123 CPC: 8078.1±3084.5	CPA: 1867.7±940 CPB: 2196.5±1088 CPC: 2515.7±1228	CPA:3.4 CPB: 3.5 CPC: 4.6	CPA:2.1 CPB:3.4 CPC:5.7	CPA:1.3 CPB:1.6 CPC:1.8	CPA:0.62 CPB:0.97 CPC:1.2	CPA:0.38 CPB:0.46 CPC:0.39

AUC, area under concentration-time profile; AUCR, ratio of AUC in cirrhosis population relative to healthy population; obs, observed data from clinical studies; pred, predicted by the model; Proteomics, predicted data by the model after applying the change in the abundance of protein in cirrhosis population relative to control; Simcyp, predicted data by the model after applying default abundance settings in the Simcyp simulator

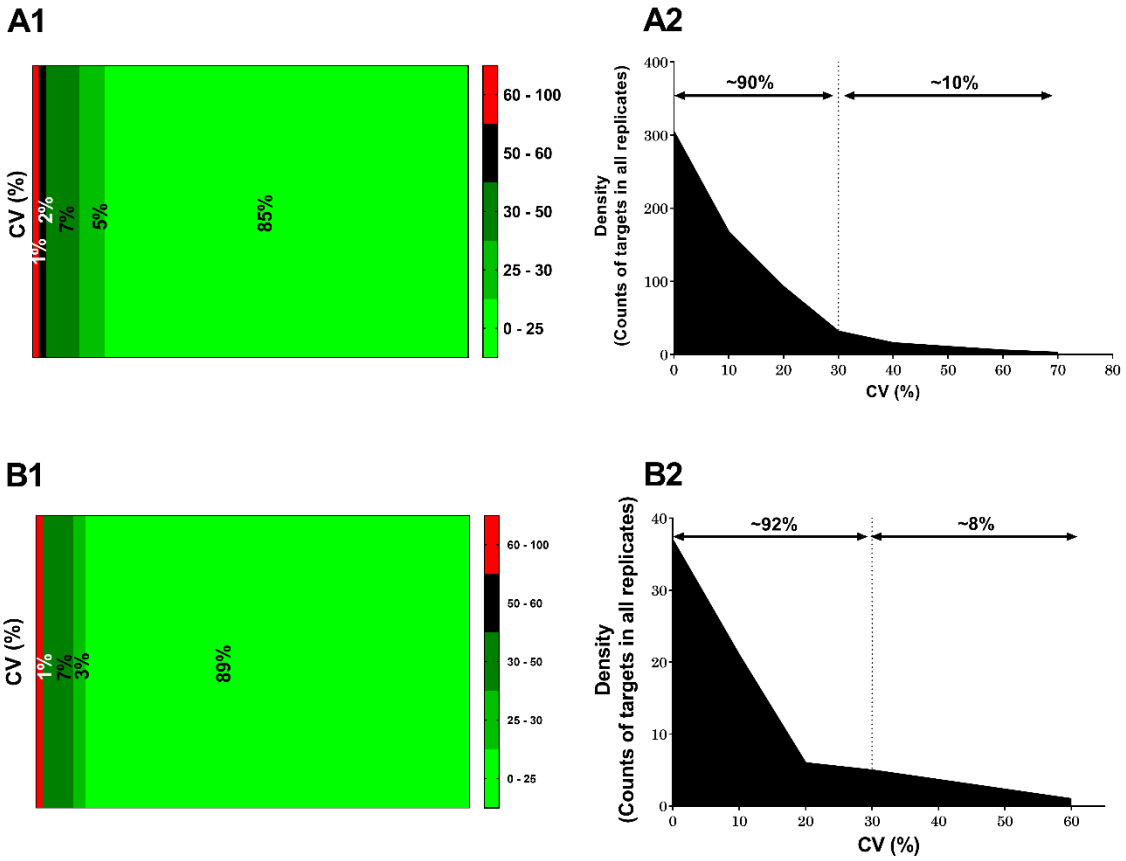

Supplementary Figure 8.1. Technical (A1) and batch-to-batch (B1) variability represented by percent coefficient of variations (%CV) for different targets in a set of QC samples (triplicates of 9 samples for the technical variability and 10 runs of same sample for batch-to-batch variability) and the density of targets at each CV value (A2, B2).

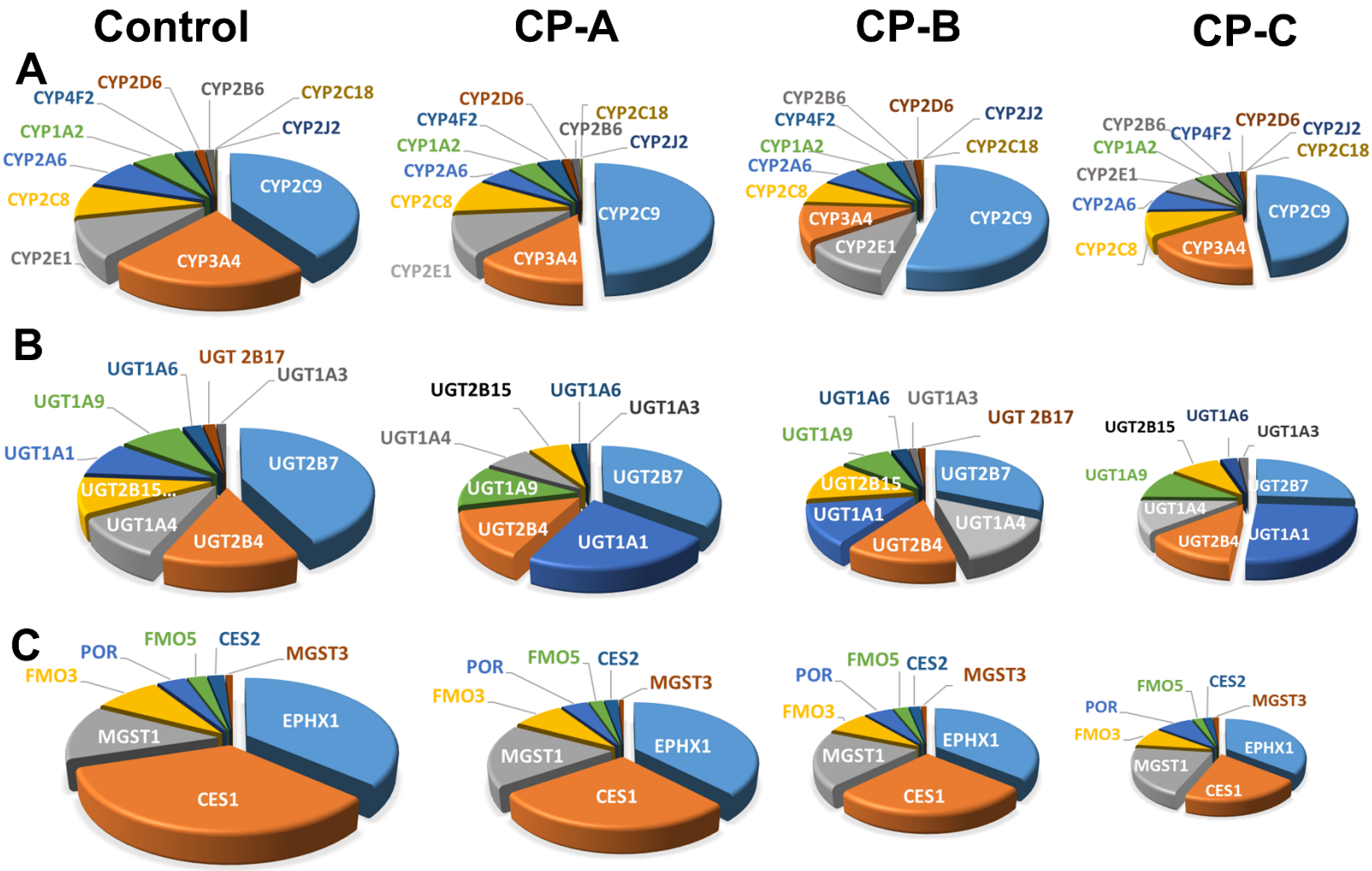

Supplementary Figure 8.2. Pie charts representing relative abundance distribution of CYP enzymes (A), uridine-5'-diphospho-glucuronosyltransferases (B), and other microsomal enzymes (C) per gram of liver tissue from the normal control, mild (CP-A), moderate (CP-B), and severe (CP-C) cirrhosis groups.

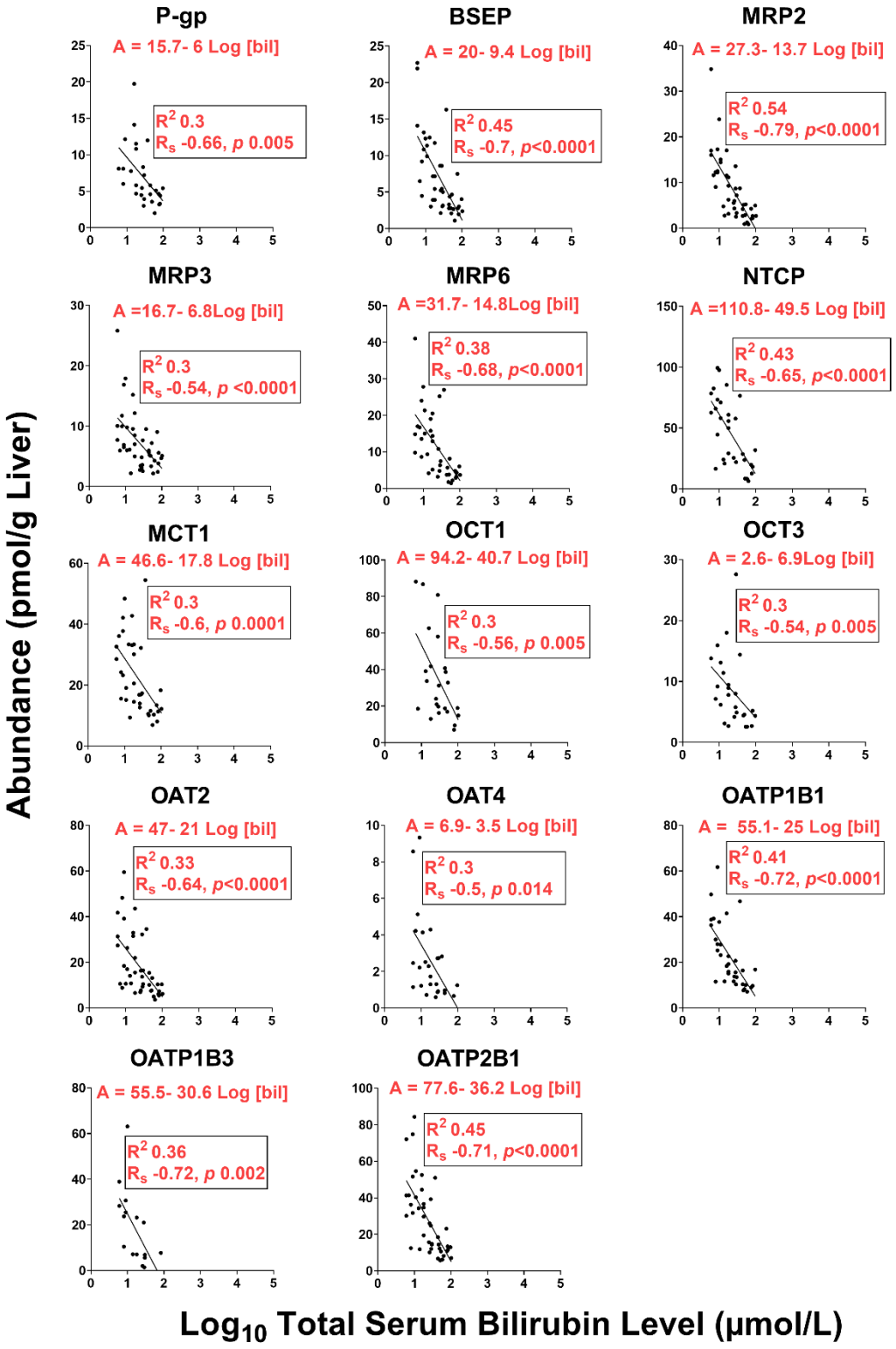

Supplementary Figure 8.3. Correlations between abundance of liver transporters (in pmol/g tissue), and log-transformed total serum bilirubin levels; Log [bil] (µmol/L) in liver donors assessed by Spearman correlation test (Rs) and linear regression (R^2).

9 Chapter Nine

General Discussion

9.1. Starting point and the needs

The liver is an important route of elimination for many drugs and their metabolites. This elimination is either via hepatic metabolism, biliary excretion, or a combination of both, and therefore it is a main contributor to the pharmacokinetic profiles of drugs. Chronic liver diseases such as cirrhosis affect the metabolic capacity of the liver drastically and therefore affects the pharmacokinetics of many hepatically-metabolised or eliminated drugs. In some other instances, it can also affect indirectly the elimination of renally excreted drugs (Verbeeck & Horsmans, 1998). As a progressive illness, the degree of effect of this disease is changing over time and results in high inter-individual variations in drug response (Lauschke & Ingelman-Sundberg, 2016). Based on previous reports and data from current study analysis, many drugs available in the market, that are involved in the treatment of liver cirrhosis patients, skip the dedicated clinical studies in hepatically-impaired patients and hence drug therapy is left to clinician judgment and guess rather than valid evidence (Jadhav, et al., 2015).

In vitro assays and *in vitro-in vivo* extrapolation (IVIVE) approaches have been increasingly used for the prediction of pharmacokinetic parameters, particularly hepatic clearance (Rostami-Hodjegan, 2012). Improved use of these tools over the last two decades has increased the confidence in the models for a number of applications which resulted in a reduction in the attrition rate in drug development for some cases (Kola & Landis, 2004; Waring, et al., 2015). However, generalising this impact on other populations or disease conditions such as liver cirrhosis is still immature and the models work properly for some drugs and do not for others

(Heimbach, et al., 2020). Therefore, more work is still required to reach to a high level of confidence in both drug and system related parameters.

In the current thesis, an extensive literature search was carried out to pick up the current weak points in IVIVE and physiologically-based pharmacokinetic (PBPK) modelling, to allow prediction of drug exposures in cirrhotic patients computationally in more confidence, and to make this area of PBPK applications more trustworthy in drug development. Aspects such as understanding the classification system of cirrhosis, cirrhosis-specific IVIVE scaling factors, changes in metabolising enzymes and transporters expressions with the disease, and application of these multiple parameters together in PBPK models were extensively investigated in this thesis.

9.2. Cirrhosis classification system: from clinical use to drug development

In spite of the availability of different scoring systems in cirrhosis, Child-Pugh (CP) score is the most commonly used clinically for cirrhotic patients. Because of its routine and ease use, it has been applied for stratifying patients in pharmacokinetic studies. However, looking deeply into its validity from drug dosing perspectives, it was evident that it is not completely fitting to that purpose and can be a contributor to the noticed disconnection between predicted and observed clinical data in many situations due to various limitations.

Inclusion of kidney function related parameters, limiting the subjectivity of clinically assessed parameters such as hepatic encephalopathy and ascites scores with more careful criteria, distinguishing patients with or without portal hypertention/ porto-systemic shunting even if they have the same CP score, and the identification of cirrhosis disease aetiology can help in overcoming CP score limitations for the purpose of drug dosing. Coupling CP score with parameters from other scoring systems, imaging information, disease severity index, and the discovery of cirrhosis specific markers that can be detected in the plasma through liquid biopsy

are proposed future solutions and directions to avoid these limitations. However, these proposals require long term as well as prospective studies rather than going retrospectively and gathering data from the literature. It also highlights the need to report all relevant and patient-specific information in future clinical and pharmacokinetic studies to facilitate such investigations, not only the overall CP score for each patient.

9.3. Moving from empirical scaling factors to biologically-relevant and cirrhosis-specific scalars

Any *in vitro* assay such as those used for the determination of intrinsic clearance for specific metabolic pathways in liver microsomes need to be extrapolated to its corresponding values per gram of liver. This is required to estimate the overall hepatic intrinsic clearance which along with other parameters (such as plasma protein binding and liver blood flow) can allow the prediction of drug exposure in any individual. In liver cirrhosis populations, this extrapolation was previously performed empirically using image processing techniques. These techniques provides approximate estimation of the fraction of the non-fibrous (more likely to retain function) part of the liver and assumes that this part is as functioning as healthy liver tissue.

Although the method used for the determination of factors that can scale these in vitro data from any fraction (microsome, cytosol, or hepatocytes) was well-known and was used for healthy livers, it has not been previously applied on adult cirrhotic liver samples. Therefore, the current project has provided experimentally defined values for these scalars in cirrhosis. These values were different from those in the healthy population and were variable according to the pathophysiology of the cirrhotic liver and the associated liver diseases.

9.4. The use of gold standard proteomics for the quantification of key proteins involved in drug metabolism

The key advance in this projects was assessed as an estimation of the abundances of enzymes and transporters in diseased and healthy tissues. This is most conveniently achieved using LC-MS/MS proteomic techniques. Mass spectrometry is extremely sensitive and selective and is powerful for multiplexed measurements. The problem is that the relationship between the size of the signal and the concentration of the analyte is complex. The selection of a peptide whose signal is unique to that specific protein of interest is crucial. Most measurements rely on standards that may be unrelated to the analytes, represent the whole family (not a specific isoform), or, in the best case, are isotopomers of the analytes. In chapter 5, we considered the available proteomic techniques currently in use, and conclude that the QconCAT methodology is the most appropriate single technique for the quantification of the desired number of metabolism related proteins in this study. Support from global (label-free analysis) has been employed in this work to resolve ambiguity and the best workflow may ultimately be a combination of the two approaches or at least to use the other for validation.

NuncCAT standard protein specifically designed in this study for the proteomic quantification of non-CYP non-UGTs enzymes can be used for any tissue known to express these proteins and for other disease states. These proteins are usually dismissed and fewer data are available in the literature for them compared to CYPs and UGTs. Consequently, most models ignore the impact of the disease on these enzymes. Therefore, this work aimed to quantify them and investigate the impact of different grades of disease severities on these enzymes. Data produced in this thesis can be used to refine PBPK models for drugs (covering most of the known metabolic pathways) and to improve the predictability of the model with higher confidence.

One obstacle facing modellers is the availability of different quantitative studies in the literature that might have overlapping or different conclusions and need to be criticised to get the best values that can be populated into their models. Chapter 7 provides a comparison of the most common LC-MS proteomic data analysis methods that might show variabilities in the resulting

absolute quant of the protein of interest. However, when the disease perturbation factor was calculated (the ratio of the abundances in the diseased sample to healthy controls), it reconciled most of these differences and resulted in comparable results irrespective of the data analysis method performed and the used standard. Although we used pooled samples for this exercise, pools are not usually representative of the whole population, and analysis of individual samples is required to assess the disease-perturbation factor more precisely and reduces the impact of outliers that can mask the right conclusion.

Analysis of individual adult human cirrhotic liver samples allowed the investigation - for the first time - of not only the impact of the disease severity on more than 50 ADME protein abundances but also the other contributing factors such as the disease pathology. Most of the drug-metabolising enzymes and transporters showed gradual reductions in the abundance with disease progression. However, the degree of this reduction was protein-specific ranging from no change at all (as in the case of UGT1A1) to more than 90% reduction in the protein level (as for CYP2C19). This can be attributed to the fact that each protein has its specific susceptibility to degradation by inflammatory mediators in chronic inflammatory diseases like cirrhosis. This also suggests that drug dosing should not be empirically based on the disease stage but should consider the pathway in which the drug is metabolised and the degree of enzyme deterioration to ensure efficacy and safety of the treatment. Additionally, we have spotted differences in bile transporters that correlate, in most cases, with the total serum bilirubin levels. Bile transport and solubilisation might be important for lipophilic drug absorption and drugs that undergo enterohepatic recycling. Therefore, accounting for the change in bile transporters' expression with cirrhosis will improve the predictability of the models for these drugs.

9.5. The use of modelling to answer urgent and unmet clinical needs

All these effort to optimise PBPK models for drugs in various populations ultimately aim to help in providing evidence in scenarios where clinical data are scarce or not available, or for less urgent situations, to help in the proper design of these clinical studies. Sometimes, ethical and practical issues limit the numbers of clinical studies that one can feasibly conduct. A clear and urgent application of this approach was the use of PBPK modelling to help during the hardship of the current COVID pandemic. PBPK models were used to study the change in the pharmacokinetics of drugs repurposed for COVID-19 in geriatric patients, different race groups, organ impairment (hepatic and renal impairments), and drug-drug interaction risks (Pilla Reddy, et al., 2021). As we need these drugs to treat COVID-19 in all populations, we realised that there is no enough clinical data that can support their dosing as the case for most of the approved drugs, especially in organ impaired patients. In the presence of complex conditions and the cytokine storm due to the virus infection and the populations' physiological changes, there is an urgent need for individualised therapy. Models verified with the available clinical data were used to predict plasma and lung exposures in these untested scenarios for these drugs to ensure if the current dosing regimen will produce sufficient lung concentrations to eradicate the virus. As most of the repurposed drugs for COVID-19 treatment are primarily metabolised in the liver, it was unsurprising to find that impaired liver function or liver disease impacts the PK of these drugs. PBPK models suggest dosing adjustments for CYP3A4 substrates like ibrutinib, dexamethasone, and acalabrutinib are likely to be necessary (Pilla Reddy, et al., 2021).

9.6. Final Conclusion

This project was an attempt to fill some of the gaps in this area of precision dosing in hepatic impairment, improve some translational aspects of PBPK modelling and simulation approaches in liver cirrhosis populations via the determination of the abundances of key disposition

proteins in cirrhosis populations, and scale them to liver tissue in order to populate models with the resulting data.

The availability of disease-specific and biologically-relevant IVIVE scaling factors increases the confidence in the model and limits the uncertainties for various system and substrate parameters to allow model refinement and improvement. It also highlights the heterogeneity of cirrhosis disease that has different aetiologies with variable pathophysiological mechanisms which can in turns result in different response to drug therapy.

The use of gold standard proteomics can substitute the less reliable mRNA, limited immunoblotting, and empirically corrected *in vivo* data that were restricted to few proteins and depends on the availability of selective and appropriate probe or antibody to only a limited number of target proteins. Whereas using proteomic LC-MS/MS, a large number of proteins can be investigated simultaneously in the sample in a highly sensitive and selective manner. For the quantification of predefined target enzymes and transporters (up to 100 proteins) in a single run, QconCAT-based quantification was concluded to be the best option that can reconcile experimental and analytical bias and allows the determination of not only the absolute levels of each enzyme or transporter, but also the relative change from the control set of samples. The latter can be applied directly to the already verified PBPK models when models in healthy populations were ought to be extrapolated to liver disease populations. Proteomic data from the current study have improved the performance of PBPK for selected drugs that cover several metabolic pathways. However, it is believed that these data are applicable for any other drug for future investigation.

From drug development perspective and as pointed out by Heimbach and co-workers in the IQ consortium, (2020) , building robust PBPK models in hepatic impairment populations can help to inform and optimise the design of hepatic impairment studies, shorten study duration, reduce

the costs, or simulate other scenarios (such as steady-state exposure, different dose, other categories of disease severity different from those previously studied clinically, drug-drug interactions due to enzymes/transporters inhibition, etc.).

The role that hepatic impairment PBPK models can play in drug development may vary depending on the predictive performance of the model and the therapeutic index of the drug. If the model predictions were within bioequivalence range of the observed data, the dedicated trials in hepatic impairment can be restricted to only severe stage of the disease to support drug label and can be delayed from phase II to phase III trials. Whereas, in the presence of a good predictive model and the lack of information on the drug's therapeutic index, models can also help to widen the inclusion list for subjects enrolled in phase II and III trials with less severe stages of the disease with or without dose adjustment. However, if the model predictions were outside the bioequivalence limits, models can still be applied to help in the design of dedicated hepatic impairment studies and assist in supplementing current evidences when clinical data are lacking. Generally, with the current set-up of hepatic impairment model, it was clear that when the model succeeds to predict exposures within the moderate stage of disease severity, it is more likely to predict the exposure in mild and severe stages within 2 fold of the observed data.

The more we understand the physiological changes in hepatic impairment and the higher the confidence the parameters included into mathematical models, the more engagement of PBPK models in drug development and supporting drug labels. While it is still challenging to develop evidence-based and individualised dosing regimens for special patient populations including hepatic impairment, the knowledge and tools to do so are available. Therefore it is mandatory to make safe and effective pharmacotherapy available for these patients. Current efforts in optimising modelling and simulation tools to allow the prediction of drug pharmacokinetics in

hepatic impairment patients (including this thesis work) can help the field of model informed precision dosing (MIPD) to move forward even further.

9.7. Future outlook

For hepatic impairment populations, further studies are recommended to investigate the impact of disease severity on hepatic cytosolic enzymes such as sulfotransferases, alcohol and aldehyde dehydrogenases, N-acetyltransferases, and aldehyde oxidases that could not be quantified in our human liver microsomal fractions.

Although the change in duodenal CYP3A expression in cirrhosis patients has been previously investigated (McConn II, et al., 2009), extrahepatic consequences of cirrhosis on other intestinal enzymes and transporters as well as the change in the expression of these proteins in other intestinal segments need to be further explored.

Application of current study proteomic data results in further PBPK models of various drugs will build confidence and allow more focus on other intrinsic and extrinsic factors that can affect the model performance. This can also be linked to pharmaco-economic studies to investigate how the application of these models in drug development can lead to the cost-effective design of the clinical studies and allow more focusing on necessary and promising trials.

All the liver tissues used herein were derived from the right lobe of the excised livers. Variabilities in the expression of metabolism-related proteins in different lobes and zones of the liver may also be useful. As noted in the first chapter, Child-Pugh scoring was not aimed at stratifying patients according to their liver metabolic capacities. Therefore, classification based on imaging, non-invasive biomarkers, or liquid biopsy might be required.

9.8. References

Heimbach, T, Chen, Y, Chen, J, Dixit, V, Parrott, N, Peters, SA, Poggesi, I, Sharma, P, Snoeys, J, Shebley, M, Tai, G, Tse, S, Upreti, V V., Wang, Y, Tsai, A, Xia, B, Zheng, M, … Hall, S. (2020). Physiologically-Based Pharmacokinetic Modeling in Renal and Hepatic Impairment Populations: A Pharmaceutical Industry Perspective. *Clin. Pharmacol. Ther.*, cpt.2125.

Jadhav, PR, Cook, J, Sinha, V, Zhao, P, Rostami-Hodjegan, A, Sahasrabudhe, V, Stockbridge, N, and Powell, JR. (2015). A proposal for scientific framework enabling specific population drug dosing recommendations. *J. Clin. Pharmacol.*, 55(10), 1073–1078.

Kola, I, and Landis, J. (2004). Can the pharmaceutical industry reduce attrition rates? *Nat. Rev. Drug Discov.*, 3(8), 711–716.

Lauschke, V, and Ingelman-Sundberg, M. (2016). The Importance of Patient-Specific Factors for Hepatic Drug Response and Toxicity. *Int. J. Mol. Sci.*, 17(10), 1714.

McConn II, D, Lin, Y, Mathisen, T, Blough, D, Xu, Y, Hashizume, T, Taylor, S, Thummel, K, and Shuhart, M. (2009). Reduced Duodenal Cytochrome P450 3A Protein Expression and Catalytic Activity in Patients With Cirrhosis. *Clin. Pharmacol. Ther.*, 85(4), 387–393.

Pilla Reddy, V, El-Khateeb, E, Jo, H, Giovino, N, Lythgoe, E, Sharma, S, Tang, W, Jamei, M, and Rastomi-Hodjegan, A. (2021). Pharmacokinetics under the COVID-19 storm. *Br. J. Clin. Pharmacol.*, bcp.14668.

Rostami-Hodjegan, A. (2012). Physiologically based pharmacokinetics joined with in vitro-in vivo extrapolation of ADME: A marriage under the arch of systems pharmacology. *Clin. Pharmacol. Ther.*, 92(1), 50–61.

Verbeeck, RK, and Horsmans, Y. (1998). Effect of hepatic insufficiency on pharmacokinetics and drug dosing. *Pharm. World Sci.*, 20(5), 183–192.

Waring, MJ, Arrowsmith, J, Leach, AR, Leeson, PD, Mandrell, S, Owen, RM, Pairaudeau, G, Pennie, WD, Pickett, SD, Wang, J, Wallace, O, and Weir, A. (2015). An analysis of the attrition of drug candidates from four major pharmaceutical companies. *Nat. Rev. Drug Discov.*, 14(7), 475–486.